Donghoi Kim

Evaluation and Optimization of Processes in the Liquefied Natural Gas (LNG) Value Chain

Donghoi Kim

Doctoral Thesis

NTNU
Norwegian University of
Science and Technology
Faculty of Engineering
Department of Energy and Process Engineering

NTNU
Norwegian University of
Science and Technology

NTNU

NTNU
Norwegian University of
Science and Technology

Donghoi Kim

Evaluation and Optimization of Processes in the Liquefied Natural Gas (LNG) Value Chain

Thesis for the degree of Philosophiae Doctor

Trondheim, March, 2019

Norwegian University of Science and Technology
Faculty of Engineering
Department of Energy and Process Engineering

◉ NTNU
Norwegian University of
Science and Technology

NTNU
Norwegian University of Science and Technology

Thesis for the degree of Philosophiae Doctor

Faculty of Engineering
Department of Energy and Process Engineering

Preface

This thesis is submitted as the result of my Ph.D. project performed at the Norwegian University of Science and Technology (NTNU). The work was carried out at the Department of Energy and Process Engineering with Prof. Truls Gundersen as the main supervisor. Dr. Oddvar Jørstad who is a principal researcher at Equinor was co-supervisor. This research was conducted as the third stage of NTNU-MIT collaboration for LNG process optimization, funded by Equinor, the Faculty of Engineering Science and Technology at NTNU, and the Research Council of Norway.

Abstract

As a cleaner fuel and an intermediate energy source on the way to a carbon-free society, the demand for natural is expected to grow considerably. Consequently, a larger production of liquefied natural gas (LNG) is also required due to its mobility with a high energy density per unit volume. To produce LNG and supply the liquid fuel to end-users, natural gas goes through a series of processes often referred to as the LNG value chain (gas production, pipeline transport of gas, natural gas liquefaction, ship transportation of LNG, regasification of LNG). Thus, a proper evaluation and improvement of systems in the chain is important to reduce the environmental footprints of LNG. Therefore, this thesis optimizes and evaluates various LNG systems to improve both their thermodynamic and economic effectiveness.

For a fair comparison of LNG systems, the SQP algorithm (local solver) has been compared with two different global search algorithms (PSO and DIRECT) for the optimization of the processes. The local solver was found to be proper for any LNG system, while the near-global solvers give sub-optimal solutions for complex processes.

To improve the liquefaction part of the LNG value chain, the different configurations of the dual hydrocarbon mixed refrigerant (DMR) technology have been optimized and compared as a promising base-load LNG process. The results proved that a large number of evaporation pressures for the refrigerants and phase separation of the cold refrigerant give a higher energy efficiency. The DMR process has also been compared with non-flammable liquefaction systems. The highest energy efficiency was still observed for the DMR process even though the non-flammable liquefaction systems have complex structures to improve their inherently low efficiency. However, the non-flammable processes can guarantee a higher safety for floating facilities than the hydrocarbon-based refrigeration systems. Different constraint formulations have also been assessed to make the DMR process more energy efficient. It was observed that the use of relaxed superheating constraints for the two MRs and the use of maximum heat exchanger conductance value constraints with relaxed minimum temperature difference constraints improve the efficiency of DMR processes.

The LNG value chain can also be improved by the systems handling boil-off-gas (BOG) on LNG vessels since the gas is typically wasted after a part of it is being used as fuel for propulsion. This thesis has suggested BOG liquefaction systems based on self-liquefaction processes to prevent the loss of cargo. Economic optimization of the reliquefaction process proves that it can save around 10 % of total annual cost, compared to LNG carriers having only the fuel supply system.

For complex LNG systems, exergy efficiency will be useful to reflect changes in the quality of products (heat, power, chemical materials) since energy efficiency only measures the quantity. Thus, an exergy efficiency (Exergy Transfer Effectiveness - ETE) developed in our research group has been thoroughly extended with general mathematical expressions to cover processes having changes in temperature, pressure, and chemical composition. The extended *ETE* with a proper level of exergy decomposition was proven to be more consistent and accurate for a complex LNG process than other exergy efficiencies.

By using exergy as a post design tool, the integration scheme of an air separation unit (ASU) and the LNG regasification step in the LNG chain has been suggested and evaluated to minimize the loss of LNG cold energy during conventional evaporation. The use of LNG cold energy in air separation was verified to be a proper solution for LNG regasification, increasing the extended *ETE* of the ASU by 13 %. A sensitivity analysis with LNG supply pressure for the ASU system proved that the extended *ETE* could properly reflect the quality changes in the products that occurred by the varying LNG pressure, while energy efficiency fails to do so.

The extended *ETE* has also been tested as objective function for the optimization of the DMR process integrated with NGL extraction. The optimization results indicate that the solutions from the exergy-based objective function give increased quality of products (LNG and NGL) with similar energy consumption as the results from an energy-based objective function. The results from the exergy-based objective function also confirm that upstream NGL extraction is thermodynamically better than the integrated systems unless the two processes are well heat integrated.

Acknowledgements

First, I would like to thank my main supervisor Prof. Truls Gundersen. His support and valuable feedback including thorough proofreading were essential to my Ph.D. project. I was also grateful for the extreme (?) ski training I had during our research group trip to his cabin. It has been a solid foundation for me to survive in Norway during the snowy winters. I will also never forget about the speech he made for my wedding in Korea. I was so pleased that he and his wife Aud could make time to visit Korea for my wedding.

I would like to express my gratitude to my co-supervisor Dr. Oddvar Jørstad from Equinor for the organization of the project. I also want to thank Dr. Jostein Pettersen from Equinor, who guided me to this LNG field. He even gave me thoughtful advice, considering practical issues for the project. I also would like to thank Prof. Paul Barton at the Massachusetts Institute of Technology (MIT) and Dr. Harry Watson for the NTNT-MIT collaboration. The project inspired me to realize the world of process optimization.

During my Ph.D., it was a great experience to visit the Offshore Process Systems Engineering Laboratory at Seoul National University. I would like to thank to Prof. Youngsub Lim and Ph.D. candidate Chulmin Hwang for our collaboration. This research stay allowed me to have different research approaches to offshore LNG systems. Thanks to other lab members for the warm welcome that they showed me.

Special thanks to the administrative staff at the Department of Energy and Process Engineering. They were always supportive whenever I had problems during my project. I deeply appreciate the time they spent for me.

For the last four years, it was a great pleasure to stay in our Process Integration group with Rahul, Chao, Bjørn, Matias, Haoshui, Avinash, and Zhongxuan. They were my academic consultants and friends all the time. I would like to thank to my colleagues at the Department

Table of Contents

List of Figures

List of Tables

xiv

Nomenclature

Abbreviations

AAV	ambient air vaporizer
ASU	air separation unit
BOG	boil-off-gas
BTX	benzene, toluene, and xylene
C_1	methane
C_2	ethane
C_3	propane
C_{5+}	hydrocarbons heavier than pentane
CMR	cold mixed refrigerant
DFDE	dual fuel diesel electric engine
DIRECT	divide a hyper-rectangle
DMR	dual mixed refrigerant
FLNG	floating LNG
GA	genetic algorithm
GCU	gas combustion units
GSP	gas sub-cooled process
HC	hydrocarbon
He	helium
HFC	hydrofluorocarbon
HFO	heavy fuel oil
HHC	heavier hydrocarbon
i-C_4	iso butane
i-C_5	iso pentane
IFV	intermediate fluid vaporizer
IMO	International Maritime Organization
IP	integer program
ISS	industry standard single stage process

JT	Joule-Thomson
KPI	key performance indicator
LB	lower bound
LN2	liquid nitrogen
LNG	liquefied natural gas
LO2	liquid oxygen
LP	linear program
LT	liquid turbine
ME-GI	M-type electronically controlled gas injection engine
MFC	multi fluid cascade
MINLP	mixed integer non-linear programming
MIP	mixed integer program
MR	mixed refrigerant
MTPA	million ton per annum
NBP	normal boiling point
n-C_4	normal butane
n-C_5	normal pentane
NGL	natural gas liquid
NLP	non-linear program
NRU	nitrogen removal unit
ORV	open rack vaporizer
PSO	particle swarm optimization
RSV	recycle split vapor
SCV	submerged combustion vaporizer
SM	sequential modular
SMR	single mixed refrigerant
SQP	sequential quadratic programming
ST	steam turbine
STV	shell and tube exchange vaporize
UB	upper bound
USD	United States dollar
WMR	warm mixed refrigerant
X-DF	extra-long stroke dual fuel engine

Roman symbols

A	capacity of units [varying units]	
$ATCI$	annual total capital investment [$/yr]	
$ATOC$	annual total operating cost [$/yr]	
C	annual cost [$/yr]	
CBC	component by component exergy efficiency [%]	
CEE	coefficient of exergy efficiency [%]	
d	day [-]	
Dt	duty of heat exchanger [kW]	
$\dot{E}$	exergy rate [kW]	
$\bar{e}$	molar exergy [kJ/kmol]	
En	energy consumption [kW]	
ETE	exergy transfer effectiveness [%]	
F	factor [-]	
$\dot{H}$	enthalpy rate [kW]	
i	interest rate [%]	
K	coefficients for cost function	
kts	knots [-]	
L	loss of BOG [$/d]	
Lv	liquid level [%]	
$\dot{m}$	mass flow rate [kg/s]	
MMBtu	million British thermal units [-]	
$\dot{n}$	molar flow rate [kmol/s]	
N	number of cycles [cycle/yr]	
n	service life of LNG vessels [yr]	
p	pressure [bar]	
P	power [kW]	
ppm	parts per million	
Pr	pressure ratio [-]	
$\dot{Q}$	Heat rate [kW]	
R	universal gas constant [8.314 kJ/kmol K]	
r	rate [%/d]	
$\dot{S}$	entropy rate [kW/K]	
$SFOC$	specific fuel oil consumption [kJ/kWh]	
T	temperature [K]	
t	duration [d/cycle]	
TAC	total annual cost [$/yr]	

TCI	total capital investment [\$/yr]	
UA	heat exchanger conductance [MW/K]	
V	volume [m3]	
v	unit price [\$/kJ, \$/kW]	
$\dot{W}$	work [kW]	
$\mathbf{x}$	decision variables	
x	fraction [-]	
yr	year	

Greek symbols

Δp	pressure drop [bar]
ΔT	temperature difference between hot and cold composite curves [°C]
ΔT_{min}	minimum approach temperature [°C]
η	efficiency [%]
ρ	density [kg/m3]

Subscripts and superscripts

0	ambient conditions
BM	bare module costs
BOG	boil-off gas
BOG loss	boil-off gas burned in GCU
BOR	boil-off rate
Ch	chemical exergy
Chem	standard chemical exergy
Comp	compositional exergy
comp	compressor
cons	consumed
Consumed-produced	consumed-produced type exergy efficiency
CTO	correlation from capital cost to operating cost
CW	cooling water
cycle	voyage cycle
D	exergy destruction
engine	DFDE or propulsion engine
exp	expander

Ext	extra expenses
fuel	fuel for the DFDE or propulsion engine
GCU	gas combustion unit
H	hot composite curve
in	inlet
in-out	input-output exergy efficiency
LB	lower bound
LN2	liquid nitrogen
LNG	liquefied natural gas
LO2	liquid oxygen
LT	liquid turbine
m	outlet stream
mixture	multi-component stream
net	net work
NGL	natural gas liquid
out	outlet stream
p	pressure based exergy
P	purchased cost
prod	produced
Pure	pure component
pure	pure component
Q	exergy of heat
Reac	reactional exergy
reb	reboiler
specific	specific consumption
sup	degree of superheating
T	temperature based exergy
tank	LNG storage tanks
TM	thermo-mechanical exergy
total	total compression power
Total	total exergy of a stream
tr	transit exergy
UB	upper bound
vap	vapor
W	work exergy

Chapter 1   Introduction

1.1   Motivation

Liquefied natural gas (LNG) is one of the main sources for energy production due to its mobility with high energy density per volume and less environmental impact than other fossil fuels. With a growing demand for energy in developing countries and tighter restrictions on CO_2 emission, the need for LNG is expected to increase rapidly, making it the primary fuel for energy in the near future. Therefore, more energy efficient procedures are required to produce and distribute LNG in order to minimize the environmental footprints from the entire value chain of LNG.

The LNG value chain is a series of gas processes, including production, pipeline transportation, liquefaction, ship transportation, and regasification. Especially the performance of the latter three processes are highly dependent on their system structures, affecting energy consumption and thus operating cost. Thus, various studies have been conducted to increase energy efficiency of liquefaction processes, boil-off-gas (BOG) liquefaction systems on LNG ships, and regasification systems in LNG import terminals.

In these studies, optimization has been the tool for an objective comparison of different technical solutions by finding the best operating conditions for each alternative. However, there is still a lack of research on the optimization of industry standard liquefaction processes since most published works are based on relatively simple LNG processes such as single mixed refrigerant (SMR) and gas expander based processes. Therefore, thorough optimization is required for more complex LNG systems such as dual mixed refrigerant (DMR) processes.

Although there have been various suggestions for BOG liquefaction systems based on energy analysis, the main concern of LNG carriers (LNGCs) is not energy efficiency, but the economic viability of the refrigeration facility on the vessel. Therefore, the need for economic optimization of BOG handling systems on LNG vessels is another motivation for this thesis to improve the project profitability of the LNG value chain.

One way to improve energy efficiency of the total LNG value chain is to recover LNG cold energy when it is regasified. Since the LNG cold energy is wasted to the environment (seawater or air) during evaporation, using the cold energy in air separation units (ASUs) has been one of the promising methods to improve the energy efficiency of LNG regasification processes. However, development and comparison of ASU systems integrated with LNG regasification has been performed without optimization. Thus, thorough optimization is required for accurate evaluation and objective comparison of the ASU systems.

When evaluating optimized processes (or formulating objective functions), efficiencies based on the first law of thermodynamics are typically used. However, this method does not consider the quality of energy. Unlike this traditional method, exergy analysis is a relatively new way of evaluating processes, which applies both the first and second law of thermodynamics. Exergy is the maximum available work produced by bringing a system to equilibrium with its environment. Exergy analysis also allows identifying where exergy is destroyed in a process, in other words, the location of entropy generation. This gives guidelines to improve efficiency by highlighting units having the largest exergy destruction.

In exergy analysis, there has been various definitions suggested for exergy efficiency. However, most of these efficiencies are defined and formulated for above ambient processes. Thus, a new exergy efficiency referred to as the exergetic transfer effectiveness (ETE) has been developed in our research group by carefully defining exergy sources and sinks. Depending on the operating temperature level of a system, this efficiency thoroughly identifies the components of the exergy sources and sinks by decomposing the physical exergy into temperature and pressure based exergies. As a result, the ETE can be used for any processes operating above, across, and below ambient. However, the ETE is only valid for systems

having changes in temperature and pressure i.e. changes in thermo-mechanical or physical exergy. Thus, the extension of the *ETE* with general mathematical expressions is needed so that it can be applied to processes also having compositional changes, i.e. changes in chemical exergy.

Although exergy efficiency is a better performance indicator compared to energy efficiency, it has not been frequently used as objective function in optimization studies. Thus, a comparison of objective functions based on energy and exergy efficiency has to be conducted for optimization of complex LNG systems.

1.2   Objectives

The main objective of this thesis is to improve the process performance of systems in the LNG value chain. Thus, it is attempted to improve existing concepts for systems in the LNG value chain using mathematical optimization and assess their performances based on energy or costs.

Another target of this thesis is to develop an exergy efficiency, which is applicable to any types of LNG systems. The exergy efficiency is used to evaluate the accurate thermodynamic performance of LNG processes as a post-design tool. The exergy efficiency is also tested as an objective function in the optimization of LNG systems in order to find the most efficient operating conditions.

1.3   Scope

The scope of this thesis is limited by the purpose of this thesis. Thus, only some parts of the LNG value chain are considered such as systems in LNG plants, LNG carriers, and LNG import terminals. An LNG plant consists of several process units. However, the aim of this thesis is to optimize the liquefaction part. Thus, pre-treatment and nitrogen removal processes will not be included as they increase the complexity and difficulty of the optimization problem drastically.

Gas expander, SMR, and DMR processes are the main liquefaction technologies considered in this thesis.

Simulation of an LNGC is also limited to BOG reliquefaction and fuel supply systems since they are the main components affecting the economics of the vessel. Thus, other sub-systems on LNGCs such as LNG tanks, gas combustion units, propulsion engines, and cooling water systems are not considered. In the simulation model of an LNG import terminal, recondensation of boil-off-gas from the storage tanks and other utility systems are not considered. Instead, only regasification of the stored LNG and air separation units are simulated since this thesis for the import terminal part mainly focuses on the utilization of LNG cold energy.

LNG systems are only built as steady-state models. Dynamic simulation to study for example start-up, commissioning, operation, and shutdown is not a concern in this thesis for evaluating and optimizing basic design concepts of LNG systems. In addition, this brings process control issues, which is another domain of optimization. Thermodynamic properties will be modeled using cubic equations of state, such as Peng-Robinson. Detailed equipment modeling of cryogenic heat exchangers, compressors, and expanders are not considered.

Optimization of the simulation models will be conducted by local NLP solvers based on sequential quadratic programming (SQP). This thesis will also use existing global search algorithms in order to compare their performance with the local solver. Thus, development of optimization algorithms will not be part of the scope. LNG processes will be optimized mainly to maximize energy or exergy efficiency and minimizing total costs.

In this thesis, different exergy efficiency definitions will be applied to a DMR process, most of these exergy methodologies are based only on physical exergy. The Exergy Transfer Effectiveness (ETE) mentioned in Section 1.1, originally developed for physical exergy, will be extended to also handle chemical exergy. The extended ETE will be verified for complex LNG and ASU systems having changes both in physical and chemical exergies. The extended ETE will also be tested as objective function for the optimization of NGL extraction systems to be used in the early design phase.

1.4   **Contributions**

The main contributions of this PhD program can be summarised as follows:

- Two types of optimization algorithms (local and global search solvers) have been evaluated and compared for LNG systems. Different penalty functions have also been tested for the global search algorithms to handle constraints. It was found that both type of solvers have similar performance for simple LNG processes. However, better solutions were observed from the local solvers than the global search algorithms for complex LNG processes.

- Different configurations of the DMR process have been optimized and compared. It was observed that DMR systems having a large number of evaporation pressures for the mixed refrigerants and phase separation for the cold mixed refrigerant reduces power consumption.

- Various technical options for non-flammable liquefaction processes, have been optimized and compared with a DMR process. It was found that non-flammable liquefaction processes do not reach the energy efficiency of the DMR process, thus a higher safety for FLNG comes at the expense of energy efficiency.

- Different constraint formulations for DMR processes have been tested. It was found that relaxation of superheating constraints for the inlet streams of refrigerant compressors improves the energy efficiency of the DMR system. Reduced energy consumption of the liquefaction process was also observed when using total UA value constraints with relaxed $\Delta T_{\min}$ constraints.

- New technical solutions using self-liquefaction processes have been suggested for BOG reliquefaction on LNG carriers having high-pressure gas injection engines. Cost optimization verified that a fuel supply system without BOG reliquefaction on an LNG vessel requires a higher total annual cost than using a self-liquefaction based BOG liquefaction facility. Break-even-point of the self-liquefaction system was also found to be around 4 USD based on sensitivity analysis with varying LNG price.

- The ETE, which is an exergy efficiency definition, has been extended with general mathematical expressions for processes having changes in chemical composition. The novel efficiency and other efficiency definitions have also been categorized based on the level of exergy decomposition. The different exergy efficiencies have been compared by applying them to a DMR process. The comparison confirmed that the extended ETE with a detailed level of exergy decomposition gives the most accurate efficiency values for the liquefaction system.

- Various options for integration of single column ASU systems with LNG regasification have been suggested and optimized. The different ASU systems have also been compared based on both energy and exergy analysis. It was found that the use of LNG cold energy for pre-cooling of air and a nitrogen stream gives a higher energy and exergy efficiency than using it in a liquid nitrogen production cycle. In addition, a sensitivity analysis with varying LNG supply pressure has also conducted, verifying that energy performance indicators do not effectively reflect changes in product quality, compared to the extended ETE.

- Different technical solutions for the integration of a DMR process with NGL extraction have been optimized and compared. Two different objective functions (specific energy consumption and the extended ETE) have also been tested for the optimization of the systems. It was observed from the optimization results with energy-based objective function that the LNG process integrated with the NGL extraction using a refluxed column has the smallest specific energy consumption. However, the optimization results with exergy-based objective function verified that upstream NGL extraction has a higher exergy efficiency with an increased quality of products, while maintaining the quantity.

1.5   Thesis structure

This thesis is structured by nine separate chapters to discuss the evaluation and optimization of processes for liquefaction of natural gas (LNG). This thesis has largely two parts: conventional

analysis (Chapter 3 to Chapter 5) and exergy-based analysis (Chapter 6 to Chapter 8) for LNG systems.

- **Chapter 1** is an introductory chapter, including the motivation, scope of work, and contributions of this thesis.
- **Chapter 2** gives the technical background for LNG processes, indicating the general overview of the entire LNG value chain.
- **Chapter 3** makes a comparison of different analysis methods (energy and exergy efficiency) for LNG systems. Various mathematical optimization algorithms are also tested and compared to select a proper solver for LNG systems.
- **Chapter 4** evaluates different configurations of DMR processes to find the most energy efficient system. Non-flammable LNG processes are also compared with a DMR process for FLNG applications. Finally, the effect of optimization formulations for DMR processes is addressed to improve their energy efficiency further.
- **Chapter 5** suggests new systems to manage BOG produced in LNG carriers having gas injection engines in order to minimize both capital and operating costs of the BOG handling system.
- **Chapter 6** extends an exergy efficiency to be suitable for analysis of LNG systems. The novel exergy efficiency is also compared with other exergy efficiency definitions to prove the performance.
- **Chapter 7** proposes technical options to integrate ASU systems with LNG regasification and evaluates them based on the exergy efficiency developed in Chapter 6.
- **Chapter 8** tests the new exergy efficiency as objective function for the optimization of LNG processes integrated with NGL extraction systems. The results are also compared with the solutions from an energy based objective function in order to assess the performance of the exergy efficiency as a tool for the early design phase.
- **Chapter 9** summarizes the studies conducted in this PhD thesis and suggests further work.

1.6   Publications

Full text papers (categorized as Level 2 publication in Norway)

- Kim D, Hwang C, Gundersen T, Lim Y. Process design and economic optimization of boil-off-gas re-liquefaction systems for LNG carriers. Energy (in review).
- Yu H, Kim D, Gundersen T. A study of working fluids for Organic Rankine Cycles (ORCs) operating across and below ambient temperature to utilize Liquefied Natural Gas (LNG) cold energy. Energy. 2019;167:730-9.
- Kim D, Gundersen T. Development and use of exergy efficiency for complex cryogenic processes. Energy Conversion and Management. 2018;171:890-902.
- Kim D, Giametta R, Gundersen T. Optimal Use of Liquefied Natural Gas (LNG) Cold Energy in Air Separation Units. Industrial & Engineering Chemistry Research. 2018;57(17):5914-23.

Shorter papers (categorized as Level 1 publication in Norway)

- Kim D, Gundersen T. Comparison of Liquefaction Processes for FLNG. Proceedings of the 28th International Ocean and Polar Engineering Conference. Sapporo, Japan: International Society of Offshore and Polar Engineers; 2018.
- Kim D, Gundersen T. Constraint Formulations for Optimisation of Dual Mixed Refrigerant LNG Processes. Chemical Engineering Transactions. 2017;61:643-8.
- Watson HAJ, Kim D, Gundersen T, Barton PI. Modeling and simulation of phase change and non-ideality in multistream heat exchangers. Computer Aided Chemical Engineering. 2016;38:505-10.
- Kim D, Gundersen T. Helium Extraction from LNG End-Flash. Chemical Engineering Transactions. 2015;45:595-600.

Conference paper

– Yu H, Kim D, Gundersen T. Cascaded Transcritical/Supercritical $CO2$ Cycles and Organic Rankine Cycles to Recover Low-Temperature Waste Heat and LNG Cold Energy Simultaneously. International Journal of Electrical, Computer, Energetic, Electronic and Communication Engineering. 2018;12(4).

Presentations

o Kim D, Gundersen T, Comparison of Liquefaction Processes for FLNG, 28th International Ocean and Polar Engineering Conference (ISOPE 2018), 10-15 June 2018, Sapporo, Japan. Oral presentation.

o Kim D, Giametta R, Gundersen T, Optimal Use of LNG Cold Energy in Air Separation Units, 2017 AIChE annual meeting, 29 October - 3 November 2017, Minneapolis, USA. Oral presentation.

o Kim D, Gundersen T, Constraint Formulations for Optimisation of Dual Mixed Refrigerant LNG Processes, 20th Conference on Process Integration for Energy Saving and Pollution Reduction (PRES 2017), 21-24 August 2017, Tianjin, China. Oral presentation.

o Kim D, Gundersen T, Development of Exergy Efficiency for Complex LNG Processes, 4th Trondheim Gas Technology Conference (TGTC), 5 December 2016, Trondheim, Norway. Oral presentation.

o Kim D, Gundersen T, Exergy Targeting for Complicated LNG Processes, 2016 AIChE annual meeting, 13-18 November 2016, San Francisco, USA. Oral and poster presentation.

o Kim D, Gundersen T, Application of Exergy Efficiencies in Complicated Cryogenic Processes, 2015 AIChE Annual Meeting, 8-13 November 2015, Salt Lake City, USA. Oral presentation.

o Kim D, Gundersen T, Helium extraction from LNG end-flash, 18th Conference on Process Integration for Energy Saving and Pollution Reduction (PRES 2015), 23-27 August 2015, Kuching, Malaysia. Oral presentation.

Chapter 2   Processes in the LNG value chain

2.1   LNG as a clean fuel

Natural gas is a mixture of lighter hydrocarbon gases that are extracted beneath the surface of the earth. During combustion, natural gas has a lower CO_2 emission than other hydrocarbon fuels such as oil and coal. Thus, the hydrocarbon mixture in gas phase is regarded as an intermediate energy source in the transition to a carbon-free society before renewable and cleaner energies become dominant. Therefore, with tighter regulations about CO_2 emission, only natural gas and renewable energy have been the energy sources experiencing an increase in their share of the total energy market for the last six years [1]. In 2017, natural gas was even the energy source having the largest increase in its demand, accounting for over 23 % of total energy consumption in the world. Although the improvement of energy efficiency reduces the growth rate of fuel consumption, natural gas is also expected to be the primary fuel for energy market in 2040, mainly led by power production and industry sectors [2, 3]. Even in marine transport, more gas-fueled ships are considered to meet the extended restriction on CO_2 emission, which will increase the demand for natural gas [4, 5].

To meet the high demand around the world, natural gas is typically transported either by pipelines or in the form of liquid. Especially, the high energy density per volume allows liquefied natural gas (LNG) to be more suitable for long-distance transport, compared to pipelines [6, 7]. Thus, the production of LNG has increased significantly along with the increase in natural gas demand, accounting for around 10 % of the total gas trade in 2017 [8]. In the early 2020s, the trade of natural gas in liquid form is even expected to be larger than

through inter-regional pipelines [3]. Therefore, the technical development of LNG systems from liquefaction to regasification has been the key issue to meet the huge LNG demand while minimizing environmental footprint of the LNG value chain. Thus, the following chapters will discuss the systems in the LNG value chain (liquefaction, transport, and regasification) and address the technical issues.

2.2   Processes in the LNG value chain

Natural gas is typically extracted from onshore gas reservoirs. However, to meet the huge energy demand, it is essential to exploit unconventional gas, especially from offshore gas fields [9]. Even though there are other types of unconventional gas such as shale gas and tight gas, nearly 45% of the total natural gas reserves are still located in offshore fields [10]. In order to produce LNG from this type of fields, offshore platforms are commonly used. Natural gas from gas reservoirs is extracted and sent to an offshore platform through riser pipelines so that oil and other impurities from the raw gas can be removed on the platform. Then, the pre-treated natural gas is compressed for a long distance transport to land by subsea pipelines. The imported natural gas to an onshore LNG plant is pre-treated before being liquefied and stored in tanks. The LNG in the storage tanks is loaded to an LNG carrier, sailing to an LNG import terminal. Then, the LNG from the vessel is unloaded to storage tanks in the terminal. The stored LNG is gasified and distributed through pipelines for end-users. The combination of processes from gas production to distribution is called the LNG (value) chain as seen in Figure 2.1.

In this LNG chain, the liquefaction section accounts for 30 % of the final LNG supply cost, which is the largest portion compared to other stages [11, 12]. Shipping of LNG via vessels also contribute to the cost by a similar amount as the liquefaction step. Therefore, technical improvement in these two steps (liquefaction and vessel shipping) of the LNG chain will be important to have a better project profitability with the increased energy efficiency of the systems. Although the influence on the LNG supply cost is less than a half of the liquefaction section, the LNG terminal also requires novel methodologies to improve the regasification step,
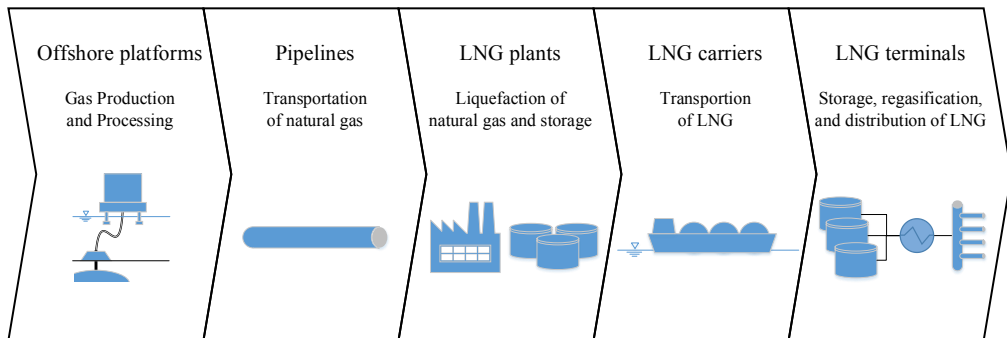
Figure 2.1 LNG chain from gas production to regasification of LNG.

where significant cold energy of LNG is wasted to the environment. Therefore, this thesis mainly focuses on the systems for LNG plants, LNG carriers, and LNG terminals in order to improve the total efficiency of the LNG value chain.

2.2.1 LNG processes and NGL extraction

Natural gas transported through subsea pipelines arrives in an onshore LNG plant to be liquefied by several sub-processes as seen in Figure 2.2. Due to the low temperature of the seabed, the pipeline gas is partially condensed, thus forming liquid slugs. In order to prevent the possible damage to the LNG plant, the inlet gas with slug waves are collected in a reception facility called slug catcher and the liquid is separated as condensate product [13].

Natural gas is then fed to gas cleaning facilities before being liquefied [12, 14, 15]. First, acid gases such as CO_2 and H_2S are removed to a very low level in natural gas. Carbon dioxide in natural gas causes plugging in cryogenic heat exchangers since it is easily solidified at low temperatures. The Hydrogen sulfide is also eliminated to meet the sales specifications of LNG as a toxic substance. Then, the sweetened natural gas is sent to a dehydration unit to remove water content to prevent freeze-out. Finally, mercury is also extracted since it is corrosive to aluminum, which is the main material for cryogenic heat exchangers.
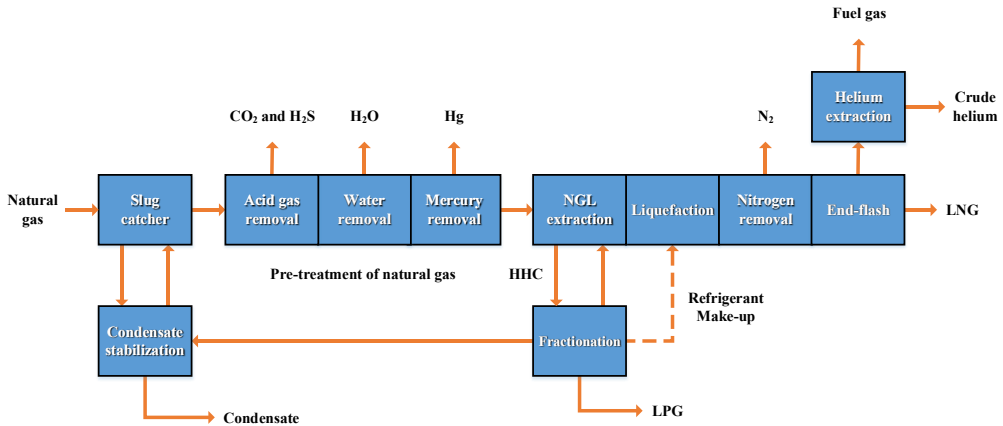
Figure 2.2 Block flow diagram of a LNG plant.

The pre-treated natural gas is fed to the natural gas liquid (NGL) extraction unit to remove heavier hydrocarbons (HHC) from the feed gas to prevent the solidification of HHC in the liquefier and control the heating value of the LNG product [12, 14, 15]. The NGL extraction is performed either upstream or as an integral part of the liquefaction system. The extracted HHC is further treated to produce liquid petroleum gas (LPG). If the liquefaction system uses hydrocarbon refrigerants, the HHC is fractionated to make-up the working fluids.

The lean feed gas is then fully condensed in a liquefaction system. If the LNG product has a high nitrogen content over 1 %, it goes through an N_2 removal system in order to prevent issues during transport in storage tanks such as rollover [16]. The nitrogen vent stream from the N_2 removal system is also restricted to have hydrocarbons lower than 1 mol % to meet the environmental legislation [17].

Finally, the liquefied natural gas is throttled to ambient pressure and phase separated. The liquid stream at around -160 °C is stored in tanks and the vapor stream is used as fuel for utility systems in the LNG plant. If the feed gas contains noble gases such as helium, additional systems will be installed to the end-flash step in order to recover the valuable gases [18].

Table 2.1 Classification of natural gas liquefaction processes.

cycle	Refrigerants			
	Boiling		Gas	
	Pure	Mixed	Pure	Mixed
1	N/A	1 HC mixture [19-21]	N_2 [22-24]	Feed gas [25, 26]
2	R410a-Xe [27]	2 HC mixtures [28-32] C_3H_8-HC mixture [33]	CO_2-N_2 [34] CH_4-N_2 [35]	N/A
3	C_3H_8-C_2H_6-CH_4 [36]	3 HC mixtures [37] 2 HC mixtures-N_2 [38]	CO_2-N_2O-N_2 [39]	(N_2+CH_4+C_2H_6)-(N_2+CH_4+C_2H_6)-N_2 [40]

N/A: Not available, (): a mixture, -: This symbol is inserted between cycles.

Although there are a number of sub-systems to pretreat and liquefy natural gas, the liquefaction section is the main contributor to the total cost of the LNG plant, accounting for 30 % [15, 41]. Consequently, it is natural to put more attention to liquefaction processes in order to improve their energy efficiency, thus improving the total project profitability.

The system performance of liquefaction processes is mainly dependent on the distance between hot (natural gas) and cold (refrigerants) composite curves in cryogenic heat exchangers [15, 42, 43]. If the two curves match closely and have a small gap, entropy generation of the heat exchangers and the system will be minimized, increasing process efficiency. Thus, different types of configurations have been suggested to reduce irreversibilities in cryogenic heat exchangers as seen in Table 2.1.

Liquefaction systems for natural gas are typically categorized based on the type of refrigerants as seen in Table 2.1. Refrigeration cycles for liquefaction of natural gas can either have boiling refrigerants or gas phase refrigerants. Since natural gas is a hydrocarbon mixture, it has a gliding cooling curve during liquefaction. If a refrigerant is phase changed in heat exchangers, it can have a heating curve with varying inclination, resulting in a close match with the cooling curve (natural gas). In contrast, gas phase refrigerants will have almost the same slope for the heating curve in the entire region, increasing the gap from the cooling curve and thus entropy

generation. Therefore, LNG processes with boiling refrigerants tend to have a higher energy efficiency than the systems with gas phase refrigerants [15, 44, 45].

LNG processes can also be classified according to the number of refrigeration cycles used. Although one refrigeration cycle can cover the entire range of cooling temperatures from ambient to -160 °C, using multiple cycles for different temperature ranges will be advantageous to reduce the temperature difference in the cryogenic heat exchangers by selecting the most suitable refrigerant for each range. With multiple refrigeration cycles, LNG processes can be improved further by applying multi-component working fluids for each cycle. The mixed refrigerants (MR) can be customized by changing their compositions to have a better match with the hot composite curve in the heat exchangers.

Thus, the C_3-MR process [33], which has two refrigeration cycles with boiling refrigerants (pure propane and a hydrocarbon MR) has been frequently selected as the technical solution for base-load LNG plants, accounting for 43 % of total liquefaction capacity in the world [8]. Although multi-component refrigerants are not applied, the optimized cascade process from ConocoPhillips [36] is the second most used system (21 % of total liquefaction capacity) followed by the C_3-MR system. The cascade process has three cycles with pure boiling refrigerants, which give a high process performance. In order to maximize the energy efficiency and production capacity of LNG processes, systems using three cycles with MRs from Statoil-Linde [37] and Air Products and Chemicals [38] have also been developed, but being deployed in few plants [8].

The single mixed refrigerant (SMR) process having one cycle with a multi-component working fluid and systems using gas phase refrigerants are typically considered for small scale production of LNG, including offshore applications due to their simplicity [45-49]. However, for large scale LNG plants, the dual mixed refrigerant (DMR) processes have been considered as alternatives to the C_3-MR process [9, 50, 51]. The DMR systems have been applied to some sites since the replacement of the propane refrigeration part in the C_3-MR process with a MR cycle gives better flexibility and efficiency to the two MR systems [8, 47, 52-55]. Therefore,

this thesis will discuss the DMR processes in detail to improve the system performance, considering also NGL extraction.

2.2.2 Boil-off-gas handling during LNG transportation

During the transportation of LNG by vessels, the liquid cargo is evaporated due to heat leaks to the storage containments, generating gas called boil-off-gas (BOG) [56, 57]. Since the production of BOG in the tanks is a loss of cargo, it reduces the economic viability of the entire LNG project. Thus, there have been various methods suggested to handle the valuable cargo on LNG carriers (LNGCs) as seen in Figure 2.3 [58].

BOG handling technologies are largely categorized based on how the BOG is utilized. The gas from storage tanks can either be fully liquefied and returned to the containments or used as fuel for propulsion systems. The former method has only been applied in a limited number of cases, such as Qatar LNG due to the extra fuel (diesel oil) required for propulsion [59-61]. Instead, BOG has been typically used as fuel for the operation of LNGCs [59, 62, 63]. Historically, steam turbines have been selected for the propulsion system of LNG vessels by feeding BOG to the steam boilers [4, 64, 65].

However, the low efficiency of steam turbines resulted in gas-fueled diesel engines to be the market dominator from the 2000s [59, 64, 65]. Consequently, various studies have been performed to develop proper liquefaction systems for the BOG left after being used for the dual fuel diesel engine generators that are running electric motors for propulsion [66-68]. Recently, the loss of power due to the indirect propulsion system using electric motors has led engine manufacturers to launch direct mechanical propulsion systems with the dual fuel engine having different operating conditions (high-pressure or low-pressure fuel) [4, 69]. Thus, further research has been required for BOG reliquefaction processes, which are suitable for the mechanical propulsion to improve the efficiency of the total gas system on LNGCs. Therefore, this thesis will analyze BOG reliquefaction systems especially for high-pressure gas injection engines, considering cost.
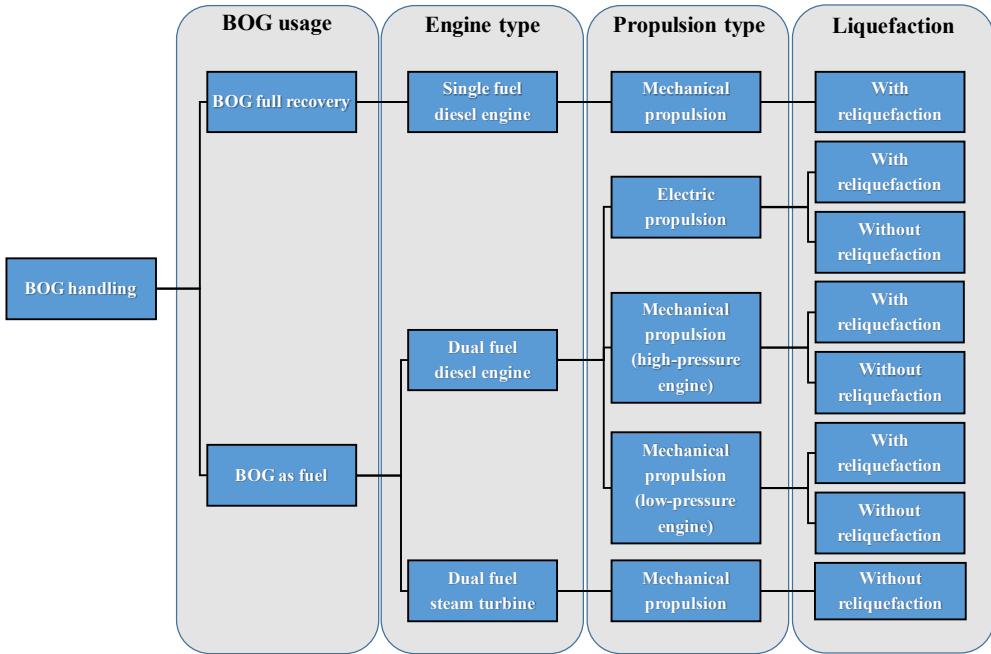
Figure 2.3 Classification of propulsion systems with BOG handling for LNG carriers [58].

2.2.3 LNG regasification in LNG terminals

LNG transported by vessels is typically unloaded to import terminals and stored in tanks. Upon demand from end-users, the stored cold LNG is then regasified and distributed through pipeline networks. The regasification of LNG is performed by heat exchange with seawater, air or other hot streams even produced by combustion energy as seen in Figure 2.4 [14, 70]. Thus, a large amount of cold energy in LNG is wasted in the environment during the regasification [71].

In order to utilize the valuable cold energy, various technologies have been applied to LNG import terminals such as power production, food freezing, space cooling, desalination, and air separation [72-77]. However, most of the applications do not match well with the temperature range of LNG vaporization, thus not fully utilizing the LNG cold energy [73-76]. In contrast, the cold operating temperature of air separation processes below -170 °C allows using the LNG
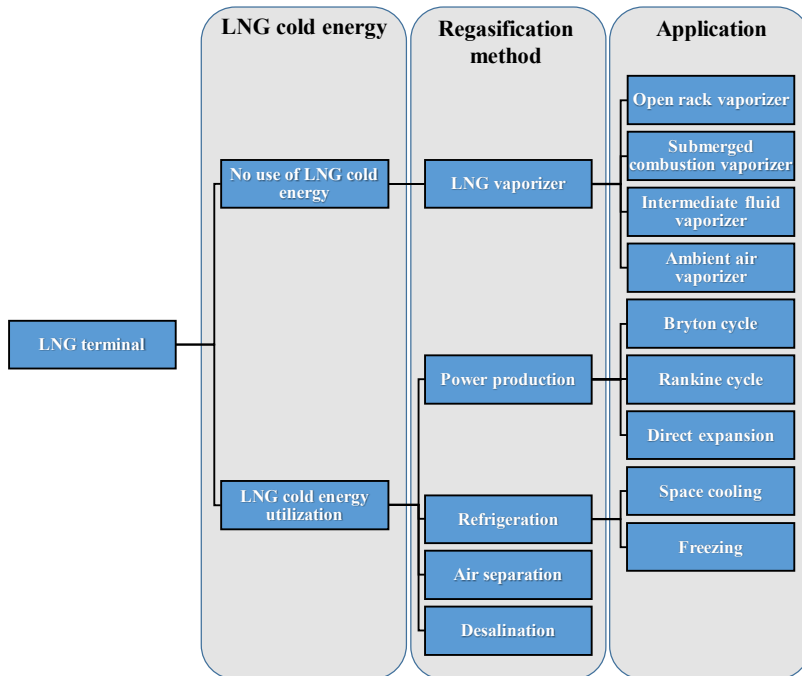
Figure 2.4 Classification of LNG regasification systems [72-77].

cold energy from the beginning of evaporation, which is at around -160 °C. Thus, the heat integration of an air separation unit (ASU) with LNG regasification is regarded as an energy efficient, economical and technically feasible solution for LNG terminals [77, 78]. Therefore, this thesis also study a novel ASU system with a single column integrated with the LNG regasification processes in order to improve the total energy efficiency of the LNG value chain.

Chapter 3   Analysis methods for LNG systems

It is essential to select a proper analysis method to study cryogenic processes in order to deliver comparative and reliable results. Thus, in this chapter, the following questions are given to perform a rigorous study.

- o   What is the proper method for a thermodynamic analysis of LNG systems?
- o   What are the robust optimization algorithms for a fair comparison of LNG systems?

3.1   Energy, exergy, and cost analysis of cryogenic processes

A process is a series of operations to produce useful outputs by consuming inputs. Thus, processes are varied based on their purposes such as using hydrocarbons to produce electricity, heat, or petrochemical products. Such variations in the structure of processes require more general efficiency definitions for the assessment of system performance. An energy performance indicator is one of the possible tools for the evaluation. Regardless of difference in energy forms (e.g. heat and power), energy efficiency is typically defined as follows:

$$\eta_{\text{energy}} = \frac{\sum \text{output energy}}{\sum \text{input energy}} \qquad\qquad (3.1)$$

If a process is designed to focus on the quantity of products, an energy performance index (specific energy consumption) can be defined as given in Eq. (3.2).

$$En_{\text{specific}} = \frac{\sum \text{input energy}}{\sum \dot{m}_{\text{prod}}} \qquad\qquad (3.2)$$

Specific energy consumption (En_{specific}) is a commonly used performance index to evaluate liquefaction and cryogenic distillation systems since the purpose of the processes is to produce valuable products (LNG, NGL, liquid O_2, Helium) while minimizing the energy consumption. In addition, this performance index is often used as objective function in optimization studies for cryogenic systems to improve their thermodynamic efficiency [79-88]. Therefore, in this thesis, specific energy consumption is selected as a performance indicator to measure the efficiency of various systems in the LNG value chain.

However, energy performance indicators do not consider the quality of products such as temperature, pressure, and composition. Besides, heat and power are equally treated in the performance indexes although the thermodynamic value of heat varies based on temperature. Thus, the use of energy performance indicators may result in an inaccurate thermodynamic evaluation of systems having quality changes in input energy and products. Instead, exergy based performance indicators have been applied to various cryogenic processes since exergy

can reflect the quality of products and different energy forms [86, 89-99]. Therefore, in this thesis, exergy efficiency is selected as an alternative to energy performance indicators and used for a thorough thermodynamic evaluation of cryogenic systems. The detailed definition and use of exergy efficiency are addressed from Chapter 6 to Chapter 8.

During analysis and optimization, natural gas liquefaction systems are assumed to have fixed feed and product conditions (temperature, pressure, composition and flowrate) when focusing on the liquefaction part of the processes [42, 80, 81, 100-105]. In this case, only mechanical energy (electricity) and no heat is consumed. Then, exergy efficiency for the liquefaction processes will give the same analysis result as energy performance indicators, since there will not be changes in the quality of the product. Thus, in Chapter 4 where liquefaction is the main topic, only energy efficiency is used to analyze and optimize LNG processes.

To realize systems in the LNG value chain, it is also essential to perform cost analysis in order to evaluate the economic feasibility. By calculating both capital and operating costs, the economic analysis will suggest different optimal operating conditions of the processes, compared to the results from energy and exergy analysis. Thus, there have been various studies conducting economic evaluation of LNG systems [51, 106-111].

Therefore, it would have been preferable to perform both energy/exergy analysis and cost analysis in order to compare the thermodynamic and economic optima of LNG systems. However, it is hard to conduct accurate cost analysis since the actual material, fabrication, site construction, and maintenance costs are typically confidential. Besides, most cost estimation methods, which were developed for standardized process units, will give a large deviation for offshore applications where equipment is often customized [112]. Thus, in this thesis, cost analysis is only applied to the liquefaction systems on LNG carriers in Chapter 5 by collaborating with a research group knowledgeable about the economics of such systems.

3.2   Optimization algorithms used for LNG systems

Liquefaction processes are very energy intensive and there is a strong need to increase their energy efficiency. This can be performed by using mathematical optimization algorithms or applying thermodynamic analysis to improve the process concepts. Due to the diverse design alternatives for LNG systems, it is also important to have a comparative evaluation and comparison in order to select the right process option for a specified condition. Unless all the processes being compared are optimized to the same level, it is hard to achieve an objective comparison, which eventually needs global optimization of each process. Therefore, to deal with such challenges, rigorous process modeling and optimization in combination with advanced thermodynamics and domain knowledge about low temperature (sub-ambient) processes are required.

Solving an optimization problem depends mainly on the characteristics of variables, objective and constraint functions [113]. If variables are only sets of integers, such as {0, 1}, it is a discrete problem and solved by integer programming (IP). Continuous problems can arise if all variables are real numbers. A mixed integer program (MIP) corresponds to a case having both integer and real numbers in the set of variables. Another important criterion is the linearity of objective and constraint functions. If all functions are linear, the problem can be solved by linear programming (LP). A non-linear program (NLP) is used when any of objective and constraint functions are non-linear.

Optimization of LNG processes is generally formulated as NLPs since it contains continuous variables with non-linear objective and constraint functions. Unless developing a superstructure of an LNG process, for example optimizing the number of compression stages, mixed integer non-linear programming (MINLP) models are not considered. When formulating an NLP, it is important to know whether an optimization problem is convex or not. In a convex problem, no more than one solution can be found in a given domain, meaning that any local solutions obtained are always global optima. However, multiple local solutions may appear in

a non-convex problem and this makes it hard to guarantee that the solution found is the global optimum [114].

As optimization of LNG processes represent non-linear and non-convex problems, these have proven to be extremely hard to solve and most algorithms have trouble to converge to a global optimum [104]. The use of multi-component refrigerants, the cyclic nature of these processes and the interaction between cycles are sources of convergence problems as well as the non-linear behavior that results in non-convexities, which prevent the optimizer to identify the global optimum and leads to non-optimal (local optima) solutions. Thus, most of the studies conducted in the area of LNG process optimization have used local solvers and near global solvers [115].

To solve such NLPs, sequential quadratic programming (SQP) and other local solvers have been used as this applies a Newton step and results in a quick convergence [51, 81, 101, 107, 116-121]. Nevertheless, this optimization technique and other local optimization solvers do not guarantee global optima when solving non-convex problems [122]. Rather these methods suggest a solution, which is a minimum within its neighborhood that is not necessarily the lowest value of the objective function in a non-convex problem.

The local solvers rely on accurate gradient information, thus commercial sequential modular (SM) simulation tools such as Aspen HYSYS are not suitable for this problem. To obtain such gradient information, each unit module in a process flowsheet has to provide the partial derivatives based on their inputs and outputs. This is a problem in SM flowsheeting since the unit modules are of a "Black-box" type, which prevents the generation of analytical derivatives. Thus, complex programming is needed to produce approximate gradient information in SM tools. As a result, the derivative information produced is noisy and inaccurate so the optimizer frequently fails to converge [123].

Instead, in recent studies, global search algorithms such as genetic algorithm (GA), particle swarm optimization (PSO), and divide a hyper-rectangle (DIRECT) have been selected as alternative solvers for SM tools since they do not require derivative information [66, 80-82, 86,

103, 106, 108, 117, 124-126]. Besides, these solvers deliver near-global optima by investigating the entire search space. Nevertheless, the derivative-free algorithms are computationally expensive and time consuming compared to the local solvers due to the global search ability.

Therefore, the two different types of solvers (local and near global) are tested in this chapter in order to find the most suitable optimization methods for various LNG systems. Modeling of LNG systems is performed by Aspen HYSYS. The SQP algorithm implemented in Aspen HYSYS is selected as the representative of local solvers. In the category of near global solvers, PSO and DIRECT are chosen since the former is based on a stochastic algorithm and the latter is a deterministic algorithm. PSO is a metaheuristic algorithm using randomly generated initial solutions and particles (potential solutions), which flow through the search space considering best-known solutions nearby [127]. DIRECT is a deterministic algorithm, partitioning the search space by n-dimensional hyper-cubes and evaluating the mid value to find potential solutions [128]. In this chapter, a modified DIRECT algorithm using extra partitioning is applied to have better performance in finding potential solutions located near infeasible regions [81]. Both global search algorithms are implemented in Matlab and connected to Aspen HYSYS where the process models for LNG systems are located.

3.3   Optimization formulation and penalty functions

Unlike SQP, the two global search algorithms (PSO and DIRECT) were originally developed for non-constrained optimization problems. However, actual systems such as LNG processes have various constraints to be considered. A common strategy to handle constraints in the derivative-free algorithms is imposing a penalty on the objective function when constraints are violated [129-131]. Thus, the use of penalty functions results in constrained optimization problems having only a feasible region. However, inappropriate penalty functions can lead the global search algorithms to have solutions stuck in local optima or located in an actually

infeasible region. Therefore, various penalty functions are tested in this chapter to find a proper strategy to handle constrained non-linear optimization problems.

An optimization problem is typically formulated as Eq. (3.3).

$$\min_{\mathbf{x}} F(\mathbf{x})$$

$$\text{subject to} \quad g_i(\mathbf{x}) \leq 0, \qquad i = \{1,2,\dots,m\}.$$

$$h_j(\mathbf{x}) = 0, \qquad j = \{1,2,\dots,n\}$$

$$\mathbf{x}_{LB} \leq \mathbf{x} \leq \mathbf{x}_{UB}$$

$$(3.3)$$

where $F(\mathbf{x})$ is the objective function including a penalty function. $g_i(\mathbf{x})$ and $h_j(\mathbf{x})$ represent inequality and equality constraints. In this chapter, we do not consider equality constraints since they are not used in this thesis. If a potential solution is feasible, $F(\mathbf{x})$ is equal to original objective function $f(\mathbf{x})$.

$$F(\mathbf{x}) = f(\mathbf{x}) \tag{3.4}$$

If a potential solution is infeasible, a penalty function is added to the original objective function $f(\mathbf{x})$. There are two types of penalty functions, stationary and non-stationary. Stationary penalty functions use fixed penalty parameters during optimization, while non-stationary types have varied penalty parameters. Stationary penalty functions can simply be calculated by Eq. (3.5).

$$F_{\text{static1}}(\mathbf{x}) = f(\mathbf{x}) + C_1 \left(\sum_k q_k(\mathbf{x}) \right), \qquad k = \{1,2,\dots,p\} \tag{3.5}$$

where

$$q_k(\mathbf{x}) = \max\{0, g_k(\mathbf{x})\} \tag{3.6}$$

k represents one of the inequality constraints applied in the optimization problem. Thus, the total amount of constraint violations is multiplied by parameter C_1 and added to the original

objective function. This penalty function is referred to as static1. In order to evaluate the effect of the parameter C_1, two values (25 and 50) are selected and tested in Chapter 3.4.

Stationary penalty functions can also consider the total number of constraints violated as seen Eq. (3.7).

$$F_{\text{static2}}(\mathbf{x}) = f(\mathbf{x}) + C_1 \left(\sum_k q_k(\mathbf{x}) \right) + C_2 \times (\text{Number of constraints violated}) \tag{3.7}$$

The second penalty parameter (C_2) for the total number of constraints violated is set to be 25. This penalty is referred to as static2.

An exponential function is another option for the stationary type of penalty functions. As seen in Eq. (3.8), the penalty value is exponentially increased with the total amount of constraint violation.

$$F_{\text{static3}}(\mathbf{x}) = f(\mathbf{x}) + C_3 e^{(\sum_k q_k(\mathbf{x}))} \tag{3.8}$$

In this case, the penalty parameter value (C_3) is 25. This function gives the penalty value to be exponentially proportional to the amount of constraint violations. Thus, the exponential penalty function will be beneficial to find optima located near the infeasible region where the penalty value will be relatively small. This penalty function is referred to as static3.

The most simple way to handle the infeasible region is to give an infinite number to the objective function value as seen in Eq. (3.9).

$$F_{\text{death}}(\mathbf{x}) = f(\mathbf{x}) + \infty \times \left(\sum_k q_k(\mathbf{x}) \right) \tag{3.9}$$

This function is typically called death penalty. The infinite penalty value will make global search algorithms to focus only on the feasible region. However, if solutions are located near the infeasible region, the objective function with the death penalty will struggle to find them.

Unlike stationary type, penalty parameters in non-stationary penalty functions are changed during optimization. Eq. (3.10) shows an annealing type of non-stationary penalty.

$$F_{\text{annealing}}(\mathbf{x}) = f(\mathbf{x}) \times \left(e^{(\Sigma_k q_k(\mathbf{x}))\sqrt{r}}\right) \qquad r = \{1,2, \dots, s\} \tag{3.10}$$

In this equation, r represents the current iteration number during optimization. Thus, the value of the penalty parameter ($\sqrt{r}$) in the function increases with the iteration number. Therefore, the algorithms will have better global search ability since they can explore a wider search space at the beginning of the optimization due to the small penalty imposed on infeasible solutions. Besides, this penalty parameter increases significantly over time, and the algorithms will only focus on the current feasible region, resulting in quick convergence and rigorous results.

Eq. (3.11)-(3.12) indicate another non-stationary penalty function, referred to as dynamic penalty.

$$F_{\text{dynamic}}(\mathbf{x}) = f(\mathbf{x}) + \sqrt{r}\left(\sum_k \alpha\big(q_k(\mathbf{x})\big) q_k(\mathbf{x}) e^{\beta(q_k(\mathbf{x}))}\right) \tag{3.11}$$

where

$$\alpha\big(q_k(\mathbf{x})\big) = \begin{cases} 10 & q_k(\mathbf{x}) \leq 0.1 \\ 20 & 0.1 \leq q_k(\mathbf{x}) \leq 1 \\ 100 & q_k(\mathbf{x}) > 1 \end{cases}$$

$$\beta\big(q_k(\mathbf{x})\big) = \begin{cases} 1 & q_k(\mathbf{x}) < 1 \\ 2 & q_k(\mathbf{x}) \geq 1 \end{cases} \tag{3.12}$$

In addition to the iteration number, this penalty function has two other parameters (α and β), which are changed based on the value of constraint violation. Thus, the total penalty parameter is dependent on the degree of violation in each constraint. Therefore, the handling of infeasible solutions will be more flexible than other penalty functions by tuning the dynamic parameters.

3.4   Comparison of optimization algorithms

3.4.1 A simple LNG process

Process analysis based on sub-optimal solutions can cause inappropriate understanding of the system. Especially when comparing different processes, the local optima will result in incorrect technical decisions. Therefore, selecting a proper optimization algorithm for process systems is vital to find its potential performance and rigorous comparison basis. Thus, in this chapter, two different types of optimization algorithms mentioned in Chapter 3.2 are compared for a simple LNG process having one mixed hydrocarbon refrigerant.

This process is called the single mixed refrigerant (SMR) process. As seen in Figure 3.1, the feed gas is pre-cooled, liquefied, and sub-cooled through heat exchanger HE-1 in the SMR system. In order to supply the cold duty of the heat exchanger, a high-pressure mixed refrigerant (M02) is throttled to low pressure and sent to HE-1. Next, the warm and low-pressure MR stream is pressurized through two-stage compression with intercooling. The sub-cooled natural gas is depressurized to ambient pressure and phase separated through flash drum V-1, producing end-flash gas and LNG.
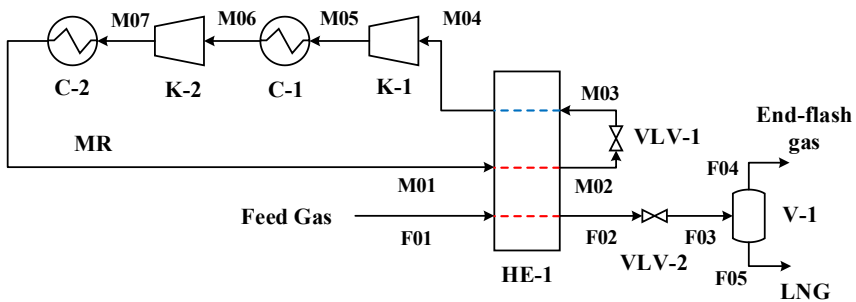
Figure 3.1 Process flow diagram of the SMR process.

Table 3.1 Conditions of the feed gas

Property	Unit	Value
Temperature	°C	22.0
Pressure	bar	60.0
Flow rate	kmol/s	1.0
Methane	mol %	91.60
Ethane	mol %	4.93
Propane	mol %	1.71
n-Butane	mol %	0.35
i -Butane	mol %	0.40
i-Pentane	mol %	0.01
Nitrogen	mol %	1.00

Table 3.2 Simulation conditions for the SMR process

Design parameters	Unit	Value
LNG pressure	bar	1.5
Condenser / intercooler outlet	°C	22.0
Compressor	Polytropic %	78.0

The SMR process is modeled in a commercial sequential modular simulation tool, Aspen HYSYS [132]. For the calculation of thermodynamic properties, the Peng-Robinson equation of state is applied. Feed gas conditions and other design parameter required for the simulation model are shown in Table 3.1 and Table 3.2.

The optimization formulation used in this study is given by Eq. (3.13). Optimization is performed to minimize the specific power consumption of the SMR process. The molar flow rates of components in the mixed refrigerant are selected as decision variables for this optimization. All pressure levels of the MR are also set to be variables. In addition, the outlet temperature of LNG from heat exchanger HE-1 is defined as a variable as seen in Table 3.3.

$$\min_{\mathbf{x}} f(\mathbf{x}) = P_{\text{specific}}(\mathbf{x}) = \frac{\dot{W}_{\text{comp}}(\mathbf{x})}{\dot{m}_{\text{LNG}}(\mathbf{x})}$$

$$\text{subject to} \quad g_1(\mathbf{x}) = 3 - \Delta T_{\text{min,HE-1}}(\mathbf{x}) \leq 0$$

$$g_2(\mathbf{x}) = -\Delta T_{\text{sup},m}(\mathbf{x}) \leq 0 \qquad\qquad m = \{\text{M04}, \text{M06}\} \qquad (3.13)$$

$$g_3(\mathbf{x}) = 1 - Pr_n(\mathbf{x}) \leq 0 \qquad\qquad n = \{\text{K-1}, \text{K-2}\}$$

$$g_4(\mathbf{x}) = Pr_n(\mathbf{x}) - 4 \leq 0$$

$$\mathbf{x}_{LB} \leq \mathbf{x} \leq \mathbf{x}_{UB}$$

In this optimization study, four types of inequality constraints are applied. First, the minimum temperature approach for heat exchanger HE-1 is constrained to 3 °C to avoid temperature crossover, considering some margin. In addition, the inlet streams of compressors are constrained to have positive superheating values to prevent liquid formation in the turbo-machinery. The pressure ratio of the units is also restricted between 1 and 4, considering practical issues.

Table 3.3 Decision variables and the starting point of the SMR process.

Variable	Unit	LB	UB	Starting point
$\dot{m}_{\text{N}_2}$	kmol/s	0.00	1.00	0.50
$\dot{m}_{\text{C}_1}$	kmol/s	1.00	2.00	1.50
$\dot{m}_{\text{C}_2}$	kmol/s	1.00	2.00	1.50
$\dot{m}_{\text{C}_3}$	kmol/s	0.00	0.40	0.20
$\dot{m}_{\text{iC}_4}$	kmol/s	0.50	1.50	1.00
$\dot{m}_{\text{nC}_4}$	kmol/s	0.00	0.40	0.20
$\dot{m}_{\text{iC}_5}$	kmol/s	0.00	0.02	0.01
$\dot{m}_{\text{nC}_5}$	kmol/s	0.00	0.40	0.20
p_{M03}	bar	1.30	6.00	3.65
p_{M05}	bar	4.00	10.00	9.13
p_{M07}	bar	10.00	20.00	14.00
T_{F02}	°C	-165.00	-145.00	-155.00

For a fair comparison of the different optimization solvers, the same starting point is used as seen in Table 3.3. Besides, the starting point is located in an infeasible region in order to see the global search ability of the tested algorithms. Multi-starting points are not considered in this work although they can increase the chance to find better solutions for the SQP algorithms.

Table 3.4 and Table 3.5 show the optimization results from the SQP, PSO, and DIRECT algorithms. The best solutions from the PSO algorithm indicate that this metaheuristic method can have similar performance as the SQP algorithm. The PSO with the annealing penalty function even gives a slightly lower objective function value than the SQP algorithm. The static2 penalty function with the PSO also gives a low specific power consumption, which is just 1.5 % higher than the results from the SQP.

However, the penalty functions static1 and static3 result in solutions that are violating constraints. The penalty values from the two static functions are proportional to the amount of constraint violation. Thus, if possible solutions violate constraints very little, the amount of penalty imposed to the objective function can also be negligible. Therefore, the PSO algorithm with the static1 and static3 penalties can fail to reject infeasible solutions that are close to the feasible region. However, the other static penalty function (static2) can avoid this problem by using an added penalty value based on the number of constraints violated. Thus, infeasible solutions close to the feasible region can be recognized as sub-optimal solutions and rejected during optimization with the static2 penalty.

Although the death and dynamic penalties fulfill the constraints, they give the highest objective function values, which are at least 8 % larger than the result of the SQP algorithm. As mentioned in Chapter 3.3, the death penalty function has less global search ability than other penalty functions since it does not search for areas near infeasible solutions where possible global optima may exist. For the dynamic penalty, a reduction in penalty parameters may be required to increase the global search ability.

Table 3.4 Best solutions for SQP and PSO with different penalty functions for the SMR process.

Property	Unit	SQP	PSO							
			Static1_{25}	Static1_{50}	Static2	Static3	Death	Dynamic	Annealing
$P_{specific}$	kWh/ton	234.45	235.50	251.27	237.92	240.43	253.82	256.74	233.98
$LMTD$	°C	3.99	3.94	5.05	4.12	3.87	4.08	4.32	3.92
UA	MW/°C	24.30	26.50	17.17	22.48	26.84	27.39	23.04	23.05
$\Delta T_{min,HE-1}$	°C	3.00	2.98	2.99	3.00	3.00	3.00	3.00	3.00
$\Delta T_{sup,M04}$	°C	7.42	7.33	11.99	7.16	5.01	9.00	11.93	6.41
$\Delta T_{sup,M06}$	°C	0.00	0.05	0.02	0.01	-0.01	0.01	0.02	0.00
Pr_{K-1}	-	1.51	1.48	1.73	1.46	1.35	1.57	1.73	1.43
Pr_{K-2}	-	2.00	1.90	1.99	2.08	2.03	1.83	1.90	2.21
$\dot{m}_{N_2}$	kmol/s	0.24	0.25	0.35	0.33	0.35	0.43	0.49	0.26
$\dot{m}_{C_1}$	kmol/s	1.00	1.05	1.04	1.07	1.22	1.33	1.20	1.00
$\dot{m}_{C_2}$	kmol/s	1.52	1.67	1.51	1.63	1.74	1.69	1.59	1.47
$\dot{m}_{C_3}$	kmol/s	0.00	0.10	0.00	0.00	0.00	0.00	0.00	0.08
$\dot{m}_{iC_4}$	kmol/s	0.81	0.50	0.79	0.50	0.84	0.81	0.58	0.50
$\dot{m}_{nC_4}$	kmol/s	0.07	0.34	0.06	0.32	0.04	0.26	0.39	0.22
$\dot{m}_{iC_5}$	kmol/s	0.02	0.01	0.02	0.01	0.00	0.00	0.02	0.01
$\dot{m}_{nC_5}$	kmol/s	0.27	0.30	0.07	0.14	0.25	0.19	0.06	0.23
p_{M03}	bar	3.66	3.64	5.79	5.26	5.03	4.66	5.47	4.28
p_{M05}	bar	5.52	5.38	10.00	7.68	6.81	7.31	9.45	6.12
p_{M07}	bar	11.05	10.23	19.96	15.98	13.80	13.39	17.94	13.49
T_{F02}	°C	-145.00	-145.00	-145.00	-145.03	-145.01	-152.40	-155.25	-145.27

Table 3.5 Best solutions for SQP and DIRECT with different penalty functions for the SMR process.

Property	Unit	SQP	DIRECT						
			Static1_{25}	Static1_{50}	Static2	Static3	Death	Dynamic	Annealing
$P_{specific}$	kWh/ton	234.45	262.60	255.29	257.84	257.79	254.66	254.70	254.66
$LMTD$	°C	3.99	4.53	4.00	4.10	4.12	4.08	4.08	4.08
UA	MW/°C	24.30	26.66	24.23	28.84	23.06	22.69	22.67	22.69
$\Delta T_{min,HE-1}$	°C	3.00	3.00	3.00	3.00	3.00	3.00	3.00	3.00
$\Delta T_{sup,M04}$	°C	7.42	8.05	6.80	6.61	1.46	8.70	8.76	8.70
$\Delta T_{sup,M06}$	°C	0.00	0.00	0.00	0.03	2.57	0.33	0.36	0.33
Pr_{K-1}	-	1.51	1.51	1.47	1.44	6.76	1.55	1.56	1.55
Pr_{K-2}	-	2.00	1.77	2.46	1.86	0.00	2.46	2.47	2.46
$\dot{m}_{N_2}$	kmol/s	0.24	0.48	0.38	0.48	0.39	0.37	0.37	0.37
$\dot{m}_{C_1}$	kmol/s	1.00	1.39	1.04	1.48	1.00	1.01	1.01	1.01
$\dot{m}_{C_2}$	kmol/s	1.52	1.89	1.48	1.79	1.48	1.38	1.38	1.38
$\dot{m}_{C_3}$	kmol/s	0.00	0.13	0.09	0.18	0.09	0.02	0.02	0.02
$\dot{m}_{iC_4}$	kmol/s	0.81	0.99	0.55	0.61	0.56	0.67	0.67	0.67
$\dot{m}_{nC_4}$	kmol/s	0.07	0.05	0.06	0.33	0.02	0.04	0.05	0.04
$\dot{m}_{iC_5}$	kmol/s	0.02	0.01	0.01	0.00	0.01	0.01	0.01	0.01
$\dot{m}_{nC_5}$	kmol/s	0.27	0.20	0.33	0.22	0.33	0.27	0.27	0.27
p_{M03}	bar	3.66	5.22	3.71	5.22	3.73	3.65	3.65	3.65
p_{M05}	bar	5.52	7.89	5.44	7.50	5.45	5.68	5.68	5.68
p_{M07}	bar	11.05	13.99	13.41	13.95	13.99	13.98	14.00	13.98
T_{F02}	°C	-145.00	-149.45	-159.65	-150.91	-160.48	-159.53	-159.57	-159.53
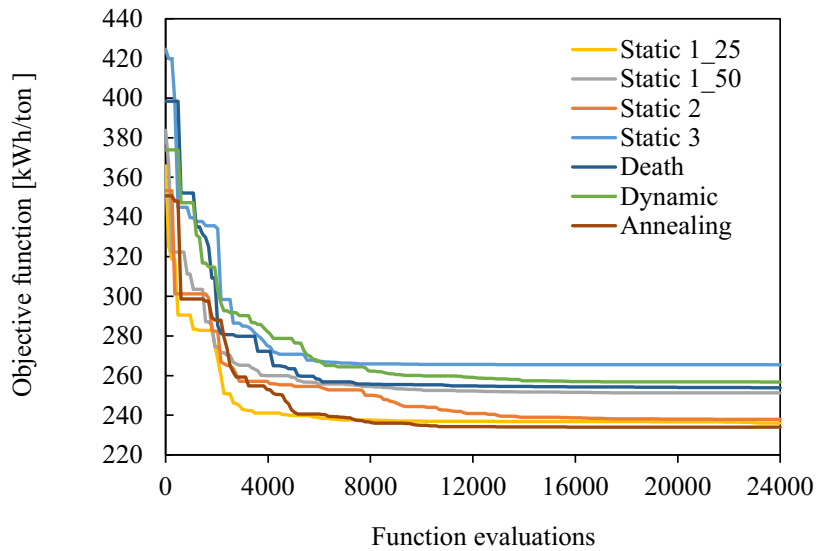
Figure 3.2 Convergence profiles using PSO for the SMR process.
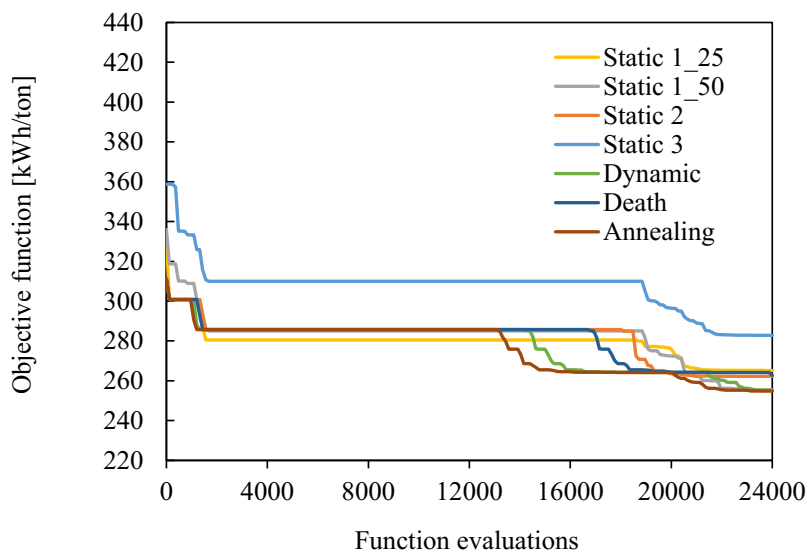
Figure 3.3 Convergence profiles using DIRECT for the SMR process

Unlike the PSO, the DIRECT algorithm satisfies constraints with any penalty functions. However, the objective values are at least 8.6 % larger than the SQP algorithm, showing poor performance of the DIRECT algorithm. Figure 3.2 and Figure 3.3 also indicate that the convergence speed of the DIRECT algorithm is slower than the PSO algorithm where most penalty functions have converged at around function evaluation number 10,000. The problem with this algorithm is well indicated in the optimal outlet temperature values for heat exchanger HE-1 (T_{F02}) in Table 3.5. As described in Chapter 3.2, the DIRECT algorithm evaluates only the mid value of the n-dimensional hyper cubes. Thus, if solutions are located near the boundary of the feasible region, it struggles to reach the optimum. Based on the results from the SQP and PSO algorithms, the optimal outlet temperature of HE-1 is assumed to be -145 °C, which is the lower bound of the variable. However, the deterministic global search algorithm (DIRECT) was not able to reach the lower bound as seen in Table 3.5.

The same problem can be found in the molar flow rate of propane ($\dot{m}_{C_3}$), which has its optimal value at the lower bound. These results mean that the extra partitioning of the hyper cubes applied in the DIRECT algorithm in this work was not helpful to prevent the problem. Instead, relaxation of variables may be required for the DIRECT algorithm to find optima, which will need extra computational time. Therefore, the SQP and PSO algorithm will be more suitable for optimization of LNG systems regardless of the location of optimal solutions. The quick convergence is also another merit of the PSO, compared to the DIRECT. Thus, in the following chapters, only the PSO algorithm is considered to be compared with the SQP solver in order to prove the global search ability of the meta-heuristic method.

3.4.2 Comparison with literature

The SQP and PSO algorithms are also compared with the results from literature where an external SQP solver is applied to optimize the SMR process built in Aspen HYSYS [133]. In this literature, the MR in the SMR system is pressurized by one stage compression and aftercooling as seen in Figure 3.4. In addition, the depressurization of the sub-cooled natural gas stream (F02) is not included. Other design parameters are given in Table 3.6.

Optimization is performed based on Eq. (3.14) and the decision variables are listed in Table 3.7.

$$\min_{\mathbf{x}} f(\mathbf{x}) = P_{\text{specific}}(\mathbf{x}) = \frac{\dot{W}_{\text{comp}}(\mathbf{x})}{\dot{m}_{\text{LNG}}(\mathbf{x})}$$

$$\text{subject to} \quad g_1(\mathbf{x}) = 2 - \Delta T_{\text{min,HE-1}}(\mathbf{x}) \leq 0 \tag{3.14}$$

$$g_2(\mathbf{x}) = -\Delta T_{\text{sup,M04}}(\mathbf{x}) \leq 0$$

$$\mathbf{x}_{LB} \leq \mathbf{x} \leq \mathbf{x}_{UB}$$

Unlike the SMR process in Chapter 3.4.1, the MR does not have pentane, and the outlet temperature of heat exchanger HE-1 is not selected as a variable. A minimum temperature difference is constrained to be 2 °C. A minimum superheating of the compressor inlet stream (M04) is set to be 0 °C. However, this literature does not restrict the pressure ratio of compressor K-1 during optimization. For a fair comparison, the same starting point as the literature is also applied to the SQP and PSO algorithms. The detailed information about the variables and starting point are shown in Table 3.7.
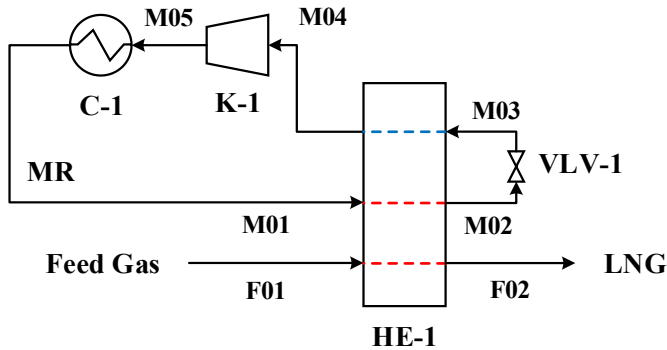
Figure 3.4 Process flow diagram of the SMR process from literature [133].

Table 3.6 Feed gas conditions and design parameters for the SMR process from the literature [133].

Property	Unit	Value
Feed gas composition		
Nitrogen	mol %	0.37
Methane	mol %	95.89
Ethane	mol %	2.96
Propane	mol %	0.72
n-Butane	mol %	0.06
Feed gas temperature	°C	20
Feed gas pressure	bar	60
Feed gas flow rate	kmol/s	1
LNG temperature (T_{F02})	°C	-164.2
Cooler outlet temperature	°C	20
Compressor	adiabatic %	80%

Table 3.7 Decision variables and feasible starting point for the SMR process from the literature [133].

Variable	Unit	LB	UB	Starting point
$\dot{m}_{N_2}$	kmol/s	0.00	2.00	0.40
$\dot{m}_{C_1}$	kmol/s	0.00	2.00	1.00
$\dot{m}_{C_2}$	kmol/s	0.00	2.50	1.20
$\dot{m}_{C_3}$	kmol/s	0.00	2.00	0.00
$\dot{m}_{iC_4}$	kmol/s	0.00	2.50	0.00
$\dot{m}_{nC_4}$	kmol/s	0.00	4.00	0.50
p_{M05}	bar	1.00	8.00	1.80
p_{M02}	bar	8.00	50.00	40.00

The optimization results shown in Table 3.8 indicate that the SQP solver built in Aspen HYSYS has almost the same performance as the SQP from the literature. Thus, the objective function value of the SQP solver in Aspen HYSYS is only 0.5 % larger than the results from the literature. The PSO algorithm with the static2 penalty function also results in almost the same objective function value as the SQP in HYSYS. Besides, the static2 penalty has a faster convergence than any other penalty functions as seen in Figure 3.5. Other penalty functions give sub-optimal solutions with slow convergence, resulting in objective function values to be at least 3 % larger than the results with the SQP from the literature. Especially the static1 penalty function with the penalty parameter of 25 gives an infeasible solution, allowing temperature cross in heat exchanger HE-1 due to the small penalty parameter.

Therefore, in this chapter, the SQP solver in Aspen HYSYS and the PSO algorithm are proven to be valuable tools for the optimization of LNG systems. However, for the PSO algorithm, a careful selection of penalty functions will be required to achieve proper performance.
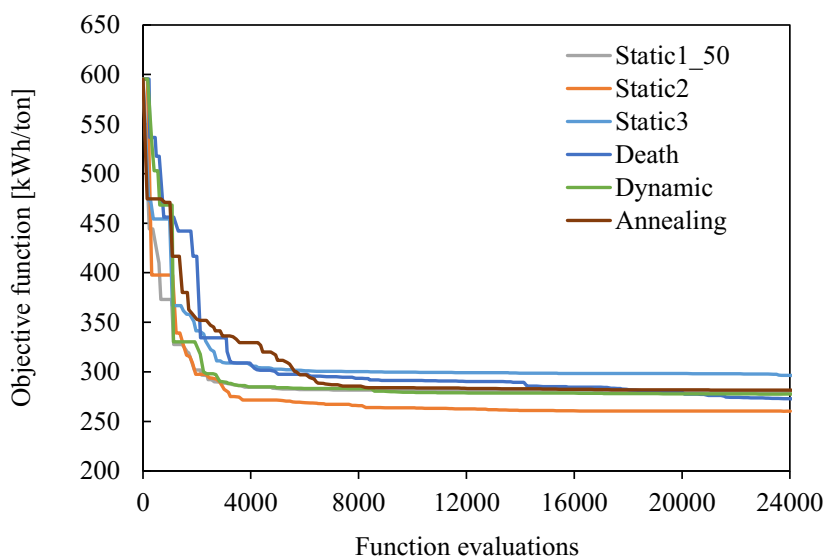
Figure 3.5 Convergence profiles using PSO for the SMR process from the literature.

Table 3.8 Best solutions of SQP and PSO with different penalty functions for the SMR process from the literature.

Property	Unit	SQP[a]	SQP[b]	PSO						
				Static1$_{25}$	Static1$_{50}$	Static2	Static3	Death	Dynamic	Annealing
$\dot{W}_{comp}$	MW	15.60	15.67	0.01	16.85	15.68	16.13	16.43	16.72	16.95
$P_{Specific}$	kWh/ton	259.10	260.26	0.62	279.82	260.36	267.86	272.84	277.65	281.47
$LMTD$	°C	2.96	3.03	-	2.94	3.06	2.97	3.56	2.98	3.38
UA	MW/°C	31.54	29.31	-	50.36	30.52	44.05	25.12	47.80	34.36
$\Delta T_{min,HE-1}$	°C	2.00	2.00	-6.59	2.00	2.00	1.87	2.00	2.00	2.00
$\Delta T_{sup,M04}$	°C	18.29	20.08	0.00	11.30	16.80	7.23	15.23	11.07	12.06
Pr_{K-1}	-	3.65	3.96	1.00	2.34	3.61	2.60	4.01	2.41	2.87
$\dot{m}_{N_2}$	kmol/s	0.00	0.33	2.00	0.93	0.40	0.68	0.44	0.87	0.83
$\dot{m}_{C_1}$	kmol/s	0.96	0.95	2.00	1.80	1.05	1.51	0.97	1.72	1.36
$\dot{m}_{C_2}$	kmol/s	0.03	1.31	2.50	2.39	1.46	2.08	1.46	2.30	2.05
$\dot{m}_{C_3}$	kmol/s	0.01	0.00	2.00	0.00	0.00	0.00	0.00	0.00	0.00
$\dot{m}_{iC_4}$	kmol/s	0.00	0.01	2.50	0.00	0.00	0.00	0.31	0.00	0.00
$\dot{m}_{nC_4}$	kmol/s	0.00	0.98	1.40	1.40	0.97	1.34	0.62	1.36	1.00
p_{M03}	bar	3.87	3.44	7.99	6.24	4.25	5.41	4.64	6.08	6.75
p_{M05}	bar	14.10	13.63	8.00	14.60	15.32	14.07	18.60	14.65	19.36

[a]Results from literature
[b]Results from the SQP used in this work.

3.4.3 A complex LNG process

The SQP and PSO algorithms are further tested by using a complex LNG process to find whether the two solvers can properly optimize systems having a search space with considerably more degrees of freedom. Figure 3.6 shows an LNG process with two mixed hydrocarbon refrigerants. This process is called the dual mixed refrigerant (DMR) process. Due to the multiple refrigeration cycles with mixed refrigerants and the multi-stage compression for each refrigerant, the search space during optimization is extensively increased. Therefore, global search algorithms such as the PSO will struggle to find optimal solutions, while requiring significant computational time.

In this process, the warm mixed refrigerant (WMR) is responsible for the pre-cooling and liquefaction of the feed gas. Then, the cold mixed refrigerant (CMR) sub-cools the liquefied LNG before it is throttled to ambient pressure. The WMR is pressurized by a combination of compressors and a pump, while the pressure level of the CMR is boosted by three-stage compression with intercooling. The simulations of the DMR process are performed by Aspen HYSYS. The information required to build the simulation model such as the feed gas composition and compressor efficiencies are given in Chapter 3.4.1. The optimization formulation for the DMR system is given by Eq. (3.15).
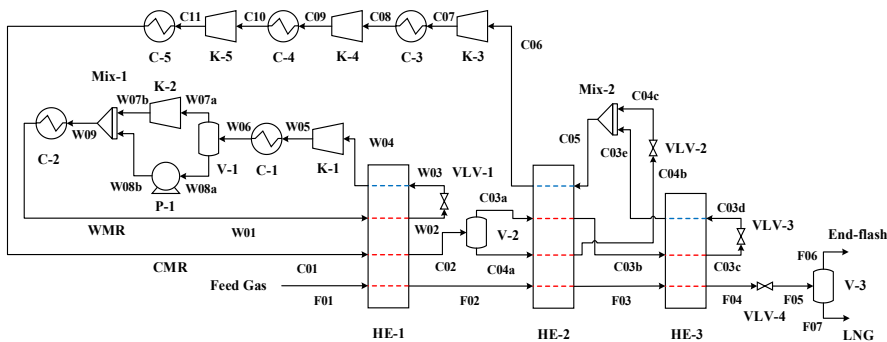
Figure 3.6 Process flow diagram of the DMR process.

$$\min_{\mathbf{x}} f(\mathbf{x}) = P_{\text{specific}}(\mathbf{x}) = \frac{\dot{W}_{\text{comp}}^{\text{total}}(\mathbf{x})}{\dot{m}_{\text{LNG}}(\mathbf{x})}$$

$$\text{subject to} \quad g_1(\mathbf{x}) = 3 - \Delta T_{\min,i}(\mathbf{x}) \le 0 \qquad i = \{\text{HE-}1, 2, 3\}$$

$$g_2(\mathbf{x}) = 5 - \Delta T_{\text{sup},j}(\mathbf{x}) \le 0 \qquad j = \{\text{W04}, \text{C06}\} \qquad (3.15)$$

$$g_3(\mathbf{x}) = Pr_k(\mathbf{x}) - 4 \le 0 \qquad k = \{\text{K-}1, 2, 3, 4, 5\}$$

$$g_4(\mathbf{x}) = 1 - Pr_k(\mathbf{x}) \le 0$$

$$\mathbf{x}_{LB} \le \mathbf{x} \le \mathbf{x}_{UB}$$

The molar flow rates of components in the two mixed refrigerants are selected as optimization variables. In addition, all pressure levels of the WMR and CMR are defined as decision variables. The outlet temperature levels of the first and second heat exchangers (HE-1 and HE-2) are also chosen as variables, considering the interaction between the WMR and CMR cycles. The detailed information about the variables and their starting point is listed in Table 3.9.

Table 3.9 Decision variables and a starting point for the DMR process.

Variable	Unit	LB	UB	Starting point
$\dot{m}_{\text{C}_2,\text{WMR}}$	kmol/s	0.00	1.00	0.58
$\dot{m}_{\text{C}_3,\text{WMR}}$	kmol/s	0.00	1.00	0.42
$\dot{m}_{\text{nC}_4,\text{WMR}}$	kmol/s	0.00	0.50	0.22
$\dot{m}_{\text{N}_2,\text{CMR}}$	kmol/s	0.00	0.25	0.09
$\dot{m}_{\text{C}_1,\text{CMR}}$	kmol/s	0.00	1.00	0.56
$\dot{m}_{\text{C}_2,\text{CMR}}$	kmol/s	0.00	1.00	0.44
$\dot{m}_{\text{C}_3,\text{CMR}}$	kmol/s	0.00	0.50	0.24
p_{W03}	bar	1.30	4.00	3.90
p_{W05}	bar	4.00	10.00	8.50
p_{W07}	bar	10.00	20.00	18.00
p_{C03d}	bar	1.30	4.00	3.60
p_{C07}	bar	4.00	10.00	8.50
p_{C09}	bar	10.00	25.00	20.30
p_{C11}	bar	25.00	60.00	48.60
T_{F02}	°C	-50.00	-25.00	-33.50
T_{F03}	°C	-130.00	-100.00	-116.50

During optimization, a minimum temperature approach for heat exchangers is set to be 3 °C, the same as for the SMR process in Chapter 3.4.1. A minimum superheating of compressor inlet streams is also constrained to be 5 °C. In addition, pressure ratios for compressors and the pump are also limited to be less than four.

The best solutions of the SQP and PSO algorithms and their performance parameters are given in Table 3.10 and Table 3.11. The results indicate that the PSO algorithm with penalty functions did not achieve the same objective function value as the SQP solver. The objective function values from the PSO algorithm are 1.6 % to 6.5 % higher than the solution from the local solver. The extensive search space also requires the global search algorithm to have a large number of function evaluations to find optimal solutions. Thus, as seen in Figure 3.7, the meta-heuristic algorithm is converged at a function evaluation number of around 60,000, which is five times larger than for the SMR process.

Therefore, the PSO algorithm will not be suitable for complex LNG systems since the solver struggles even to find local optima, while consuming significant computational time due to the large number of function evaluations required. Thus, for the following chapters, the PSO algorithm is applied for simple processes and the SQP algorithm is used for complex LNG systems.

Table 3.10 Best solutions of SQP and PSO with different penalty functions for the DMR process.

Property	Unit	SQP	PSO						
			Static1$_{25}$	Static1$_{50}$	Static2	Static3	Death	Dynamic	Annealing
$\dot{m}_{C_2,WMR}$	kmol/s	0.29	0.41	0.40	0.34	0.42	0.43	0.36	0.42
$\dot{m}_{C_3,WMR}$	kmol/s	0.27	0.18	0.21	0.24	0.22	0.36	0.27	0.20
$\dot{m}_{nC_4,WMR}$	kmol/s	0.34	0.35	0.33	0.31	0.34	0.21	0.32	0.34
$\dot{m}_{N_2,CMR}$	kmol/s	0.03	0.03	0.04	0.04	0.04	0.05	0.05	0.04
$\dot{m}_{C_1,CMR}$	kmol/s	0.49	0.51	0.52	0.52	0.52	0.53	0.54	0.52
$\dot{m}_{C_2,CMR}$	kmol/s	0.48	0.46	0.50	0.50	0.52	0.52	0.54	0.50
$\dot{m}_{C_3,CMR}$	kmol/s	0.24	0.21	0.21	0.23	0.20	0.19	0.22	0.22
p_{W03}	bar	3.37	3.76	3.98	4.00	3.76	4.00	3.78	4.00
p_{W05}	bar	7.59	9.99	8.84	8.43	8.91	10.00	9.06	9.35
p_{W07}	bar	13.89	16.98	16.76	15.52	16.85	18.12	15.61	17.17
p_{C03d}	bar	3.20	3.40	3.67	3.67	3.70	3.99	3.91	3.64
p_{C07}	bar	6.50	9.99	5.13	5.81	4.80	9.78	8.24	9.24
p_{C09}	bar	17.70	19.88	20.42	20.10	19.11	20.88	19.55	21.08
p_{C11}	bar	36.67	40.01	40.47	41.55	36.76	40.49	37.74	39.40
T_{F02}	°C	-30.03	-34.38	-31.93	-28.71	-33.93	-33.62	-30.63	-32.71
T_{F03}	°C	-119.31	-123.05	-120.69	-120.17	-118.10	-119.31	-117.34	-120.32

Table 3.11 Performance parameters and constraints of the DMR process with different penalty functions.

Property	Unit	SQP	PSO							
			$Static1_{25}$	$Static1_{50}$	Static2	Static3	Death	Dynamic	Annealing
$P_{specific}$	kWh/ton	205.65	211.42	210.13	210.56	208.97	218.67	209.54	210.13
$Duty_{HE-1}$	MW	19.34	19.95	19.57	18.84	20.48	20.26	19.84	20.09
$Duty_{HE-2}$	MW	18.77	17.97	18.59	19.31	18.22	18.29	19.32	18.46
$Duty_{HE-3}$	MW	2.29	1.90	2.17	2.24	2.46	2.32	2.62	2.20
UA_{HE-1}	MW/°C	5.03	4.97	5.05	5.15	5.19	2.51	5.37	5.11
UA_{HE-2}	MW/°C	4.68	4.12	4.48	4.57	4.48	4.51	4.74	4.45
UA_{HE-3}	MW/°C	0.45	0.41	0.45	0.48	0.49	0.50	0.51	0.47
$LMTD_{HE-1}$	°C	3.85	4.01	3.88	3.66	3.95	8.08	3.69	3.93
$LMTD_{HE-2}$	°C	4.01	4.36	4.15	4.23	4.07	4.06	4.08	4.15
$LMTD_{HE-3}$	°C	5.13	4.64	4.81	4.66	5.05	4.63	5.12	4.70
$\Delta T_{min,HE-1}$	°C	3.00	3.00	3.00	3.00	3.00	3.00	3.00	3.00
$\Delta T_{min,HE-2}$	°C	3.00	3.00	3.00	3.00	3.00	3.00	3.00	3.01
$\Delta T_{min,HE-3}$	°C	3.00	3.00	3.18	3.00	3.00	3.01	3.00	3.01
$\Delta T_{sup,W04}$	°C	7.94	6.83	6.24	5.34	6.93	15.30	6.98	5.97
$\Delta T_{sup,C06}$	°C	15.40	11.56	13.26	14.90	11.24	11.34	12.59	9.29
Pr_{K-1}	-		2.25	2.65	2.22	2.11	2.37	2.50	2.39	2.34
Pr_{K-2}	-		1.83	1.70	1.89	1.84	1.89	1.81	1.72	1.84
Pr_{K-3}	-		2.03	2.94	1.40	1.58	1.30	2.45	2.11	2.54
Pr_{K-4}	-		2.72	1.99	3.98	3.46	3.98	2.13	2.37	2.28
Pr_{K-5}	-		2.07	2.01	1.98	2.07	1.92	1.94	1.93	1.87
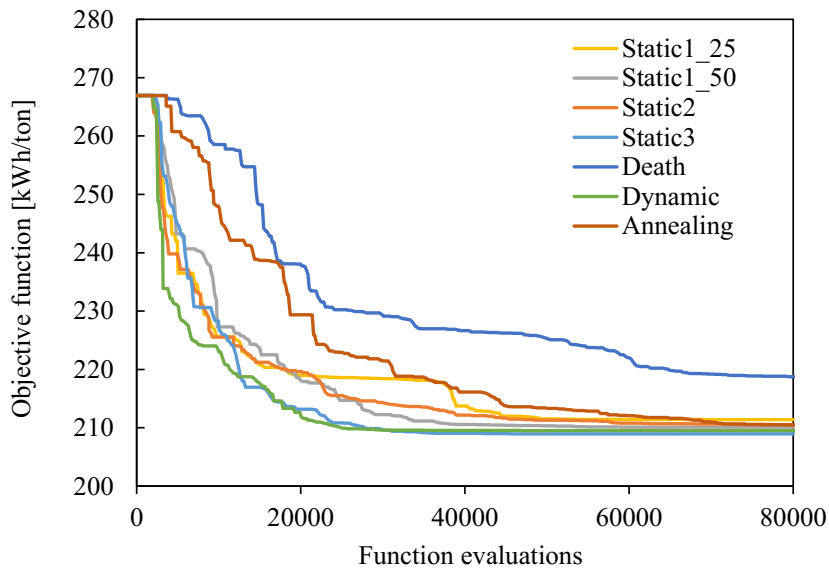
Figure 3.7 Convergence profiles using PSO for the DMR process

Chapter summary

o Apart from energy performance indicators, exergy analysis also has to be considered for a proper thermodynamic analysis and comparison of LNG systems, since exergy can evaluate the thermodynamic quality of input and output energies.

o For the optimization of simple LNG processes, both the SQP and PSO algorithms will be proper solvers. However, the PSO algorithm is not recommended for complex LNG systems due to its poor performance compared to the SQP.

Chapter 4   Energy analysis for LNG processes

In this chapter, base-load LNG processes are optimized using the SQP algorithm, which shows more robust performance for complex systems compared to some stochastic algorithms as seen in Chapter 2. The optimization is performed using energy consumption as the objective function to answer the following questions:

o   What is the most energy efficient DMR process?
o   Which LNG process is most suitable for FLNG?
o   What is the proper optimization formulation for complex LNG processes to improve their energy efficiency?

This chapter is based on the following publications:

–   Kim D, Gundersen T. Comparison of Liquefaction Processes for FLNG. The 28th International Ocean and Polar Engineering Conference (ISOPE 2018). Sapporo, Japan: International Society of Offshore and Polar Engineers (ISOPE); 2018.

–   Kim D, Gundersen T. Constraint Formulations for Optimisation of Dual Mixed Refrigerant LNG Processes. Chemical Engineering Transactions. 2017;61:643-8.

4.1   LNG processes for large scale LNG

Demand for natural gas has increased constantly to mitigate the greenhouse effect as a cleaner fuel. In particular, liquefied natural gas (LNG) produced for long-distance transport has been a major source of natural gas supply, accounting for over 30 % of world trade [8]. To meet such growing demand for LNG, there have been various types of LNG processes suggested for energy efficient production. For a large-scale production of LNG, in excess of 2-4 million ton per annum (MTPA), dual mixed refrigerant (DMR) processes have been considered as favorable technical solutions [9, 50, 51]. This is due to its low specific power, large train capacity and the less flammable refrigerant for its pre-cooling circuit compared to the C_3-MR process, which is the current market dominator for base-load LNG plants [8]. The mixed refrigerant (MR) for the pre-cooling circuit also gives better operational flexibility as it can handle the variation of feed gas conditions and ambient temperature [47, 55]. However, DMR processes are not a mature technology since it has been deployed only to a limited number of sites, and with only one of the several suggested configurations realized [8, 52-54]. Especially, the complex structure of DMR processes and the interaction between the two mixed refrigerants have been the challenges to developing the system.

Thus, Nogal et al. [55] optimized a DMR system, showing a better performance than a single mixed refrigerant (SMR) process, and the study suggested using multistage compression with intercooling to reduce both capital and operating costs for the two MR systems. A DMR process was also compared with various base-load liquefaction systems such as C_3-MR and multi fluid cascade (MFC) systems, indicating a high efficiency of the configuration with two MRs [93, 109]. For further improvement of DMR processes, different objective functions and constraint formulations were tested during optimization, resulting in a better thermodynamic efficiency with the objective function of total UA value and relaxed superheating constraints for the two MRs [134, 135]. Yang et al. [117] also conducted stochastic optimization studies for a DMR process with varying seawater temperature.

Besides, profit optimization was performed based on cost analysis, verifying that a DMR process is economically favorable for the production range between 2 to 4 MTPA compared to SMR and C_3-MR processes [51]. In addition, You et al. [136] performed risk analysis for two different DMR configurations for floating LNG facilities, ensuring the safety of the systems. Recently, Vikse et al. [137] even applied a nonsmooth multistream heat exchanger model to build a DMR process model, giving rigorous simulation results compared to commercialized tools such as Aspen Plus.

Nevertheless, detailed thermodynamic analysis on the effect of the different configurations for DMR processes has not yet been conducted. Instead, comparisons of DMR processes were performed with a lack of analysis about the structural differences [121, 138]. Therefore, in this chapter, DMR processes with different configurations are analyzed and compared in order to find the most energy efficient process structure. Mathematical optimization is also performed for the various DMR processes to have a fair performance comparison.

4.1.1 DMR processes

Natural gas is a mixture of hydrocarbons and other gases. Thus, when it is cooled down, it has a gliding temperature. To produce LNG, typically natural gas has to be cooled down to around -158 °C. During this process, natural gas is pre-cooled, liquefied and sub-cooled. These steps can be done using one, two, or even three cycles. The DMR system is a process having two refrigeration cycles. The first cycle decreases the temperature of the feed gas and the refrigerant for the second cycle down to around -50 °C. Then the second cycle liquefies and sub-cools the pre-cooled natural gas to around -158 °C.

Each cycle has its own hydrocarbon mixed refrigerant. Thus, in total, there are two mixed refrigerants in a DMR process. The one used for the pre-cooling cycle is called a warm mixed refrigerant (WMR). The other utilized for the liquefaction and sub-cooling part is referred to as a cold mixed refrigerant (CMR). As natural gas has a gliding cooling temperature, using mixed refrigerants has the advantage of having small gaps between hot streams and cold

streams in the heat exchangers. This small gap leads to a lower entropy generation through the heat exchanger, thus reducing irreversibility [43].

DMR processes can be categorized by the number of evaporation pressure levels on the WMR and CMR cycles. Besides, the phase separation of the pre-cooled CMR also affects the structure of the liquefaction and sub-cooling part in DMR processes. Based on this criterion, there are mainly four commercialized DMR processes as shown in Table 4.1.

Table 4.1 Categorization of DMR processes.

Process	WMR cycle	CMR cycle	
	Number of evaporating pressures	Number of evaporating pressures	Phase separation of pre-cooled CMR
AP-DMR (APCI) [28, 29]	1	1	1
Shell DMR (Shell) [30]	2	1	1
Liquefin (Air Liquide) [31]	3	1	0
Tealarc (Technip) [32]	3	1	1

4.1.1.1   AP-DMR process

Air Products and Chemicals Inc. (APCI), who is the market dominator with the C_3-MR system, has also suggested a DMR process, called AP-DMR [28, 29]. This process utilizes only one evaporating pressure level of the WMR and CMR, which makes the configuration simple. The schematic of this technology is illustrated in Figure 4.1.

The WMR is used for the pre-cooling of the feed stream and the CMR. First, the high pressure WMR is throttled by a Joule-Thomson valve to deliver the cold duty required in the pre-cooling step. Afterwards, the pressure level of the WMR is boosted by using not only compressors but also a pump, which reduces the power consumption for the pressure increase of the refrigerant. Then, the pre-cooled CMR is used for the liquefaction and sub-cooling of the pre-cooled feed stream.
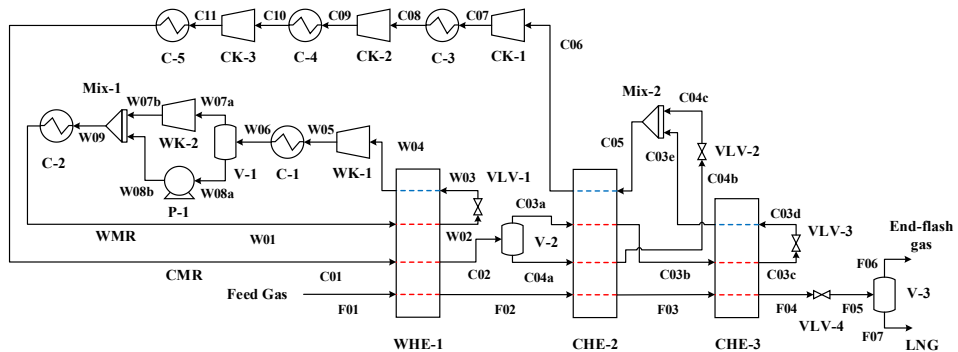
Figure 4.1 Process flow diagram of the AP-DMR process [28, 29].

In this second refrigeration cycle, the pre-cooled CMR (C02) from the WMR cycle is separated to the vapor and liquid streams, which are responsible for the liquefaction and sub-cooling of the feed gas respectively. Finally, the sub-cooled natural gas is expanded to ambient pressure to produce LNG (F07). Since this process is composed of two mixed refrigerants, one can manipulate the composition of the working fluids to adapt the variation of the feed gas, giving an operational flexibility. This process, however, has not been applied in the field.

4.1.1.2 Shell DMR process

Royal Dutch Shell also has offered a DMR process (named Shell DMR in this paper), which has a similar structure to the AP-DMR [30]. Compared to the AP-DMR, the Shell DMR has one more evaporating pressure level on the WMR as seen in Figure 4.2. The increase in the number of evaporating pressure levels results in extra decision variables such as the additional pressure level and the split ratio of stream W02. Thus, this system has a higher complexity than the DMR process from APCI, but a higher efficiency is expected.

However, the Shell DMR does not utilize pumps to boost the pressure of the WMR, which will bring a penalty on the process efficiency compared to the AP-DMR. In addition, the absence of pumps in the WMR cycle means the refrigerant is leaner than the one in the AP-DMR

Figure 4.2 Process flow diagram of the Shell DMR process [30].

process so that it is not condensed in intercoolers during compression. This lean WMR will also affect the process performance. Thus, the Shell DMR will be a proper process option for the comparison with the AP-DMR in order to evaluate the effect of the structural difference. It should be remarked that the Shell DMR is already proven technology as this system has been applied to an onshore base-load LNG plant and a floating LNG facility, showing the reliability of the system [8, 52-54].

4.1.1.3   Liquefin process

Air Liquide even proposes a process having three evaporating pressure levels for the WMR cycle, named Liquefin [31]. Thus, this system is more complex than the Shell DMR as depicted in Figure 4.3, having a larger number of decision variables. However, other design features of this technology compensate for the added complexity. First, the outlet temperature of the pre-cooling cycle in the Liquefin process is lower than the AP-DMR and Shell DMR processes. The low temperature leads to an identical power consumption for the WMR and CMR cycles, which is an advantageous condition when operating gas turbines [139]. Second, unlike other DMR processes, the CMR is not phase separated before entering the liquefaction and sub-cooling steps, making this system simpler. Therefore, the CMR cycle requires only one main heat exchanger (CHE-1).

Figure 4.3 Process flow diagram of the Liquefin process [31].

4.1.1.4 **Tealarc process**

Technip also provides a system, having a distinct process structure compared to other DMR processes [32]. The schematic of the technology is shown in Figure 4.4. Like the Liquefin process, this system (named Tealarc), has three evaporating pressure levels for the WMR. However, this WMR only cools down the CMR to around -50 °C. Then, the chilled CMR pre-cools, liquefies and sub-cools the feed gas. Thus, the CMR cycle needs an extra heat exchanger for the pre-cooling part, compared to other DMR processes.

This cold mixed refrigerant is also phase separated like the AP-DMR and Shell DMR processes before supplying the cold duty of the heat exchangers in the cycle. Therefore, this process has the most complex configuration compared to other DMR processes, resulting in the largest number of decision variables for optimization.

This system is sometimes categorized as a single mixed refrigerant process as the feed gas is liquefied by only one mixed refrigerant, which is the CMR. However, the Tealarc process is regarded as a DMR process in this chapter as this system have two-mixed refrigerants like other DMR processes.
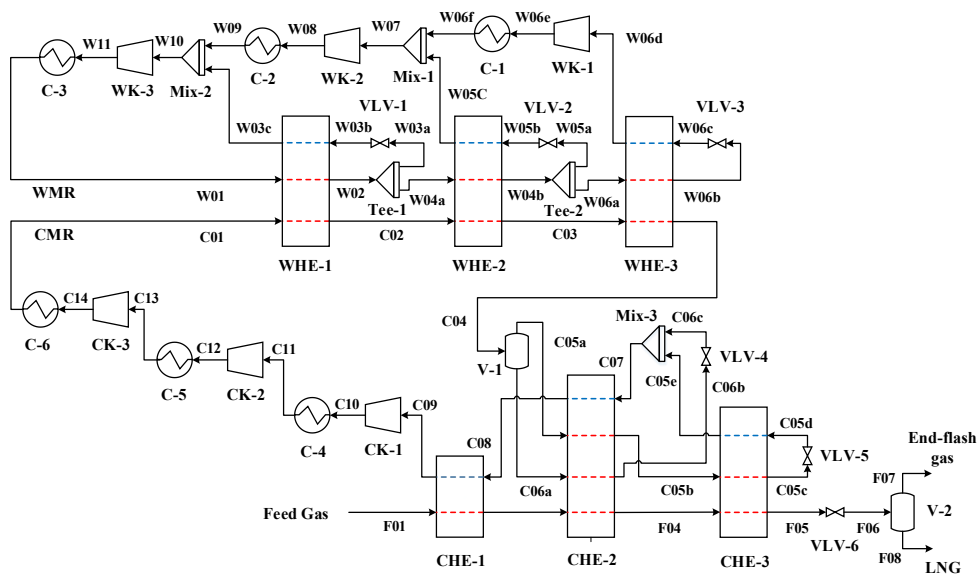
Figure 4.4 Process flow diagram of the Tealarc process [32].

4.1.2 Design basis and optimization

In this chapter, the simulation work was limited to the liquefaction processes only, disregarding various sub-systems in LNG plants such as acid gas removal, dehydration, mercury removal, NGL extraction and nitrogen removal. Aspen HYSYS [132] was used for the simulation, and the Peng-Robinson equation of state was selected for the calculation of thermodynamic properties in the simulation tool.

As seen in Table 4.2, the feed gas is regarded as pre-treated natural gas, thus not requiring further removal of heavier hydrocarbon in the DMR processes. In this chapter, natural gas was assumed to be cooled to -148 °C before being throttled to around ambient pressure. The detailed simulation conditions of the feed gas, LNG and rotating machinery are shown in Table 4.3.

Table 4.2 Feed gas conditions of the DMR processes.

Property	Unit	Value
Temperature	°C	22.00
Pressure	bar	60.00
Flow rate	kmol/s	1.00
Methane	mol %	91.60
Ethane	mol %	4.93
Propane	mol %	1.71
n-Butane	mol %	0.35
i -Butane	mol %	0.40
i-Pentane	mol %	0.01
Nitrogen	mol %	1.00

Table 4.3 Simulation conditions of the DMR processes.

Design parameters	Unit	Value
LNG temperature before expansion	°C	-148.0
LNG pressure	bar	1.5
Condenser / intercooler outlet	°C	22.0
Compressor	Polytropic %	78.0
Pump / Liquid turbine	Adiabatic %	75.0

For a fair comparison, all the DMR processes were optimized by the sequential quadratic programming (SQP) algorithm. The optimization formulation is given in Eq. (4.1). In this optimization, the WMR was assumed to be composed of ethane, propane, and butane. Nitrogen, methane, and ethane were also chosen to make the CMR. However, for the Tealarc process, butane was added to the CMR to cover the pre-cooling of the feed gas. Thus, all the molar flow rates of each component in the two MR were defined as decision variables. In addition, all the outlet temperature of heat exchangers were set to be the variables except for the last heat exchanger in the CMR cycle, which is fixed at -148 °C. All the pressure levels of MRs were also controlled as decision variables. Besides, the stream splitters in the Shell DMR, Liquefin,

and Tealarc processes were selected as variables during the optimization. The entire decision variables for each process are given in Table 4.4.

$$\min_{\mathbf{x}} f(\mathbf{x}) = P_{\text{specific}}(\mathbf{x}) = \frac{\dot{W}_{\text{comp}}^{\text{total}}(\mathbf{x})}{\dot{m}_{\text{LNG}}(\mathbf{x})}$$

$$\text{subject to} \quad \Delta T_{\min,i}(\mathbf{x}) \geq 3 \qquad i = \{\text{WHE, CHE}\}$$

$$\Delta T_{\text{sup},j,\text{inlet}}(\mathbf{x}) \geq 5 \qquad j = \{\text{WK, CK}\} \qquad (4.1)$$

$$1 \leq Pr_j(\mathbf{x}) \leq 4$$

$$\mathbf{x}_{LB} \leq \mathbf{x} \leq \mathbf{x}_{UB}$$

Optimization was performed to minimize the specific power consumption of the DMR processes, which is the total compression work divided by the mass flow rate of the LNG product. A minimum temperature difference for heat exchangers was constrained to be 3 °C in order to have a balance between the thermal efficiency and the area of the heat exchangers [86, 140]. The degree of superheating in the compressor inlet streams was also set to be larger than 5 °C to prevent liquid formation in the compressor [134]. The pressure ratio of the compressors was limited to be lower than 4, considering practical issues of the turbo-machinery [141].

4.1.3 Results

In this section, four different DMR processes were compared based on the optimization results in Table 4.5. During optimization, all the constraints were fulfilled as seen in Table 4.6. The results indicate that the Liquefin process has the largest specific power consumption compared to the other DMR processes. Although the Liquefin system has three evaporation pressure levels of the WMR, the process gives the largest averaged $LMTD$ value for the heat exchangers in the pre-cooling cycle. The large temperature gap between the hot and cold composite curves will result in significant entropy generation in the heat exchangers, while decreasing process efficiency.

Table 4.4 Decision variables and the best solutions of the DMR processes.

Variable	Unit	LB	UB	Best solution			
				AP-DMR	Shell DMR	Liquefin	Tealarc
$\dot{m}_{C_2,WMR}$	kmol/s	0.00	1.00	0.29	0.21	0.93	0.32
$\dot{m}_{C_3,WMR}$	kmol/s	0.00	1.00	0.27	0.70	0.94	0.68
$\dot{m}_{nC_4,WMR}$	kmol/s	0.00	0.50	0.34	0.20	0.01	0.03
$\dot{m}_{N_2,CMR}$	kmol/s	0.00	0.25	0.03	0.01	0.03	0.03
$\dot{m}_{C_1,CMR}$	kmol/s	0.00	1.00	0.49	0.44	0.33	0.51
$\dot{m}_{C_2,CMR}$	kmol/s	0.00	1.00	0.48	0.42	0.45	0.53
$\dot{m}_{C_3,CMR}$	kmol/s	0.00	0.50	0.24	0.21	0.06	0.10
$\dot{m}_{nC_4,CMR}$	kmol/s	0.00	0.25	-	-	-	0.02
$p_{LLP,WMR}$	bar	1.30	4.00	3.37	1.84	2.03	2.12
$p_{LP,WMR}$	bar	4.00	10.00	7.59	5.36	5.66	5.08
$p_{MP,WMR}$	bar	10.00	20.00	13.89	11.26	13.56	9.68
$p_{HP,WMR}$	bar	20.00	40.00	-	-	20.77	16.08
$p_{LLP,CMR}$	bar	1.30	4.00	3.2	2.57	2.19	3.71
$p_{LP,CMR}$	bar	4.00	10.00	6.5	4.10	7.14	8.86
$p_{MP,CMR}$	bar	10.00	25.00	17.7	16.39	15.01	17.23
$p_{HP,CMR}$	bar	25.00	60.00	36.67	33.19	25.80	32.96
	°C	-10.00	5.00	-	-6.42	-0.23	4.17
$T_{WHE,out}$	°C	-40.00	-20.00	-30.03	-39.15	-29.66	-20.25
	°C	-50.00	-20.00	-	-	-59.87	-46.44
	°C	-50.00	-20.00	-	-	-	-44.68
$T_{CHE,out}$	°C	-130.00	-100.00	-119.31	-126.33	-	-121.58
Tee-1	-	0.20	0.80	-	0.60	0.45	0.28
Tee-2	-	0.20	0.80	-	-	0.55	0.58

Since the Liquefin process is designed to have a colder outlet temperature of the pre-cooling cycle, a wider temperature range was covered by the WMR, compared to the other systems (see Table 4.4). Although mixed refrigerants are able to be adapted to the variations in the operating temperature by changing their compositions, it is harder to find the composition keeping the temperature gap between the hot and cold composite curves low through an increased temperature range, while fulfilling minimum temperature difference constraints. Eventually, on average, the *LMTD* values for the heat exchangers in the pre-cooling cycle were larger than other DMR processes.

This multiple mixing of substreams in the WMR due to the various evaporation pressure levels also causes an increase in entropy generation in the pre-cooling cycle. After delivering the cold duty in the heat exchanger, the three WMR streams with different pressure levels are mixed with the streams from the compressor outlets. The mixing of these streams having different temperature levels contribute to larger irreversibilities.

The Liquefin process also has the largest *LMTD* value for the heat exchanger in the CMR cycle compared to other processes, which causes an increase in power consumption. Unlike the Liquefin process, the pre-cooled CMR in other systems is phase separated and supplied to the heat exchangers for the liquefaction and sub-cooling of the feed gas. The phase separation gives extra flexibility of the MR to reduce *LMTD* values by throttling the vapor and liquid CMR at different temperature levels to supply the cold duty of the heat exchangers. However, the Liquefin process uses the CMR without phase separation, thus giving the largest temperature gap in heat exchanger CHE-1. The phase separation of the CMR also helps to prevent solid formation of the heavier components in the refrigerant.

Through the flash drum, the liquid CMR is supplied to the warmer heat exchanger in the cycle, while the vapor stream is sent to the coldest heat exchanger in the system. Thus, the heavier components in the liquid will have less chance to be solidified in the system, increasing process reliability. Nevertheless, as seen in Table 4.5, the Liquefin process delivered compression work equally distributed to the WMR and CMR cycle, which results in the easy operation of the gas turbines connected to the compressors.

Table 4.5 Performance parameters of the DMR processes.

Property		AP-DMR	Shell DMR	Liquefin	Tealarc
$P_{specific}$ [kWh/ton]		205.65	202.23	206.63	201.72
$\dot{W}_{comp}$ [MW]	WMR	2.20	1.36	1.28	0.73
		0.86	2.39	2.65	1.36
		0.03[a]	-	2.13	1.50
		3.09	3.75	6.06	3.59
	CMR	2.35	1.26	2.59	3.41
		3.96	4.58	2.02	2.32
		2.68	2.28	1.46	2.52
		8.99	8.12	6.07	8.25
	Total	12.07	11.87	12.13	11.84
$Duty_{HE}$ [MW]	WMR	19.34	12.33	12.61	4.29
			9.06	9.44	7.38
				8.31	5.76
		19.34	21.39	30.36	17.43
	CMR	18.77	16.75	13.99	3.67
		2.29	1.56		15.88
					2.06
		21.06	18.31	13.99	21.61
	Total	40.40	39.71	44.35	39.05
UA_{HE} [MW/°C]	WMR	5.03	2.85	2.43	1.01
			1.94	2.16	1.84
				2.00	1.39
		5.03	4.79	6.59	4.24
	CMR	4.68	4.11	2.62	0.90
		0.45	0.29		3.69
					0.41
		5.13	4.4	2.62	5.00
	Total	10.16	9.20	9.21	9.25
$LMTD_{HE}$ [°C]	WMR	3.85	4.32	5.19	4.26
			4.67	4.37	4.00
				4.15	4.13
		3.84	4.47	4.61	4.11
	CMR	4.01	4.07	5.34	4.09
		5.13	5.36		4.30
					5.01
		4.11	4.16	5.34	4.32
	Average	3.98	4.32	4.82	4.22

[a]Power consumption of pump P-1.

Table 4.6 Constraint values for the DMR processes.

Constraint	Unit	AP-DMR	Shell DMR	Liquefin	Tealarc
$\Delta T_{min,WHE}$	°C		3.00	3.00	3.00
	°C	3.00		3.00	3.00
	°C		3.00	3.00	3.00
$\Delta T_{min,CHE}$	°C	3.00	3.00		3.00
	°C	3.00	3.00	3.00	3.00
	°C				3.00
$\Delta T_{sup,WK,inlet}$	°C		5.82	5.71	5.02
	°C	7.94		17.59	12.30
	°C		5.00	5.13	16.69
$\Delta T_{sup,CK,inlet}$	°C	15.4	10.53	5.90	61.29
Pr_{WK}	-	2.25	2.91	2.79	2.39
	-	1.83	2.10	2.41	1.91
	-			1.53	1.66
Pr_{CK}	-	2.03	1.59	3.26	2.39
	-	2.72	4.00	2.10	1.94
	-	2.07	2.03	1.73	1.91

The AP-DMR process also consumes a substantial amount of compression power, close to the Liquefin system. It is noticeable that the AP-DMR process has such large power consumption although this system has the lowest average *LMTD* values for both the WMR and CMR cycles. The AP-DMR process was optimized to utilize the pump in the WMR cycle. Thus, the WMR became richer so that the working fluid can be condensed through cooler C-1 in Figure 4.1, which is different from the other processes.

A richer MR is not effective to reduce the *LMTD* value in a heat exchanger in the a colder temperature range due to the higher boiling temperature of the working fluid. Therefore, the outlet temperature of the pre-cooling cycle was increased in the AP-DMR process to reduce the temperature range for the colder part (see Table 4.4). As a result, the AP-DMR process has

a smaller heat exchanger duty in the WMR cycle and a larger duty in the CMR cycle compared to the Shell DMR process.

This heat duty distribution is not thermodynamically favorable since irreversibilities per unit duty are inversely proportional to temperature [42]. Even though the AP-DMR process can minimize entropy generation in the WMR cycle with a smaller average $LMTD$ and heat duty, the increased heat duty in the CMR cycle will bring a larger entropy generation in total. Thus, the AP-DMR shows that the increment of the compression work in the CMR cycle is greater than the reduction in the one in the WMR cycle, compared to the Shell DMR process. Therefore, the total compressor work of the AP-DMR process is larger than the Shell DMR process due to the distribution profile of the heat duty.

The Tealarc process, however, shows an even smaller power consumption for LNG production than the Shell DMR. The three evaporation pressure levels of the WMR and the use of a phase separator for the CMR give the largest flexibility to the process to reduce the temperature gap between hot and cold composite curves in the heat exchangers, resulting in the second smallest $LMTD$ value on average. Although the duty of the CMR cycle is the largest compared to other DMR systems due to the pre-cooling of the feed gas, the actual duty used for the liquefaction and sub-cooling of the natural gas is less than that of the Shell DMR process. Besides, the duty of the WMR cycle with the pre-cooling part of the CMR cycle is also smaller than the Shell DMR. Therefore, the low values in the average $LMTD$ and heat duty achieved by the complex structure result in the highest process efficiency compared to other DMR processes.

4.1.4 Conclusions

Different configurations of DMR technologies have been optimized to compare their process efficiency and analyze the effect of the structural differences. First, the use of the pump in the WMR cycle is not encouraged since it results in a larger cold duty for the CMR cycle where irreversibilities per unit duty are larger than in the pre-cooling cycle. However, the WMR cycle with pumps will be helpful to reduce the total compression work in the cycle, compensating the penalty on the CMR cycle. Although multiple evaporation pressures can be applied, a wider

operating temperature range of the WMR cycle is also unfavorable, resulting in a larger average *LMTD* value and entropy generation. However, the individual use of the phase separated CMR streams is advantageous to reduce the power consumption while increasing the complexity of the system. Thus, the Shell DMR with two evaporating pressure levels for the WMR and the CMR phase separator will be a well-balanced process with a high process efficiency and intermediate level of system complexity.

4.2 Alternative LNG processes for FLNG

The concept of floating LNG (FLNG) has attracted the attention of the gas industry as natural gas demand is expected to grow [8]. Deploying an FLNG vessel, however, has required the technical development of natural gas liquefaction processes to be suitable for the offshore environment. This has led many process suppliers and oil & gas operators to propose new liquefaction processes to be able to handle the harsh conditions.

Single mixed refrigerant (SMR) processes are one of the main suggestions for mid-scale FLNG, which is the range from 1.5 to 2 million ton per annum (MTPA) of LNG [45, 142]. The small number of units and simple operation make the SMR processes attractive to offshore applications in spite of a relatively low thermodynamic efficiency [46, 47]. For a large production of LNG, in excess of 2-4 (MTPA), dual mixed refrigerant (DMR) processes have been recommended. The DMR has a low specific power consumption and a large train capacity compared to other LNG processes [9, 50]. The mixed refrigerant (MR) for the pre-cooling cycle also gives better operational flexibility with the variation of feed gas conditions by changing the composition [47].

However, the large liquid inventory of hydrocarbons in the SMR and DMR processes will increase the risk of fire and explosion on an FLNG vessel. Thus, gas expander based systems have been considered as an alternative process option for small-scale FLNG due to the inherent safety, simplicity, and ease of operation [45, 143]. Nevertheless, the low thermodynamic efficiency and the small single train capacity make gas expander processes less favorable for

floating LNG ships. To improve such low efficiency, a dual nitrogen expander cycle has been used [23, 35]. The efficiency was further increased by introducing an additional pre-cooling cycle to a dual nitrogen expander process [34].

Therefore, the three types of liquefaction processes all have limitations when applied to FLNG. The SMR and DMR processes have a large amount of liquid inventory of hydrocarbon refrigerants. The various gas expander processes show a poor thermodynamic efficiency even with the extra pre-cooling cycle, which offsets the simplicity of gas expander processes [144].

4.2.1 FLNG Process options

4.2.1.1 Non-hydrocarbon cascade process

One of the process options for FLNG is a cascade process using non-hydrocarbon (non-HC) refrigerants [27]. By using such refrigerants, liquid hydrocarbon inventory is entirely removed in the liquefiers, achieving a high level of safety on the vessel. The schematic of the process is shown in Figure 4.5. Compared to the conventional cascade process [145], the propane cycle for pre-cooling of natural gas is replaced with a hydrofluorocarbon (HFC) refrigerant (R-410A), which has a similar normal boiling point (NBP = -52 °C) as C_3H_8 (NBP = -42 °C).

R-410A is a mixture of R-31 and R-125 (50/50 wt. %), and it behaves like a single component refrigerant since the blend is zeotropic but a near-azeotropic mixture [146]. Liquefaction of natural gas is conducted by a xenon refrigerant as a substitute for ethylene. Xenon is a non-flammable and non-toxic noble gas, having an NBP of -108 °C, which is close to the NBP of ethylene (NBP = -104 °C).

The last cycle of the conventional cascade process for sub-cooling of natural gas uses methane as a refrigerant. However, the methane cycle is replaced by a nitrogen removal unit (NRU) and multi-stage Joule-Thomson (J-T) expansion in the non-HC cascade process. Through the NRU, the liquefied feed is slightly cooled, and a gas stream is extracted as fuel to control the nitrogen content in the bottom product of the column. The liquefied feed is then sent to multi-stage
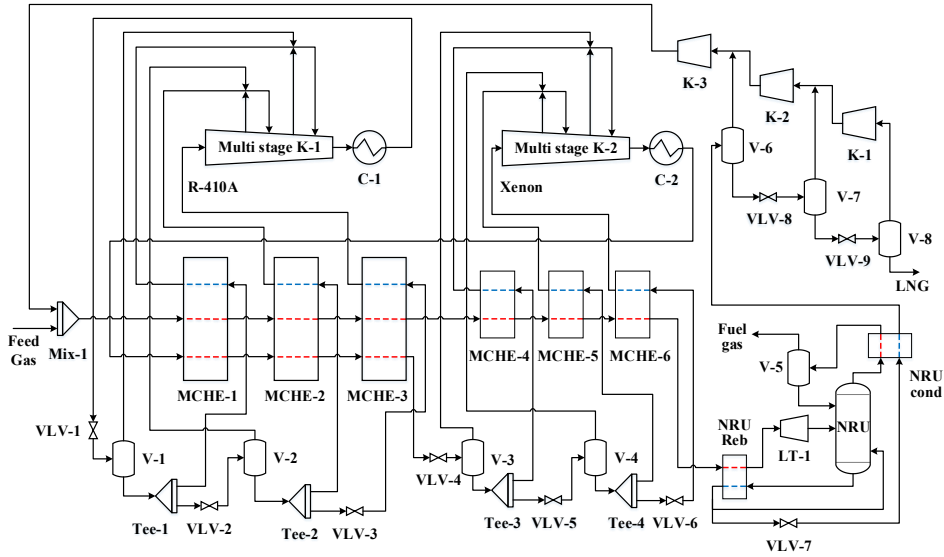
Figure 4.5 Process flow diagram of the non-hydrocarbon cascade process [27].

throttling steps to produce sub-cooled LNG. All the end-flash gases generated after J-T throttling is recycled and merged with the feed gas. Therefore, liquid hydrocarbon refrigerant inventory does not exist in the sub-cooling stage.

4.2.1.2 Triple gas expander process

To overcome the low efficiency of gas expander technologies, Technip developed a triple gas expander process [40]. This process consists of three gas expander cycles, and the refrigerants responsible for each cycle are the mixtures of methane, ethane, and nitrogen. The three refrigerants are always in gas phase in the process, and their initial compositions used in this chapter was adopted from the patent, listed in Table 4.7.

The schematic of the technology is shown in Figure 4.6. The triple gas expander process integrates the first cycle with the second cycle and the second cycle with the last one. This integration is achieved by sending a portion of the expanded refrigerant in the first cycle to the
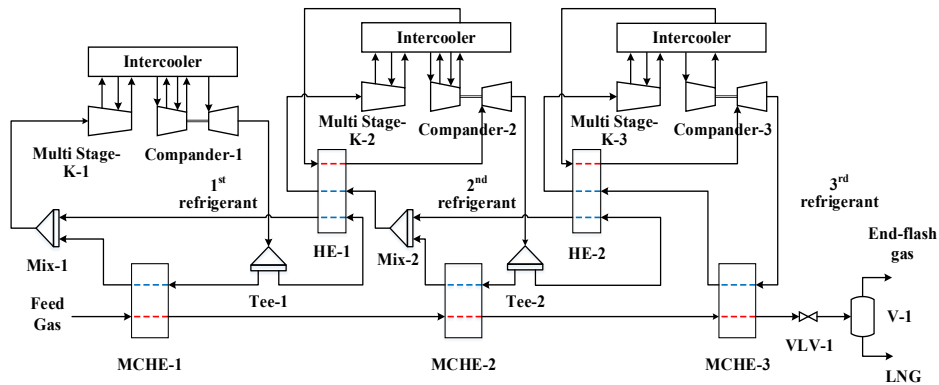
Figure 4.6 Process flow diagram of the triple gas expander process [40].

second cycle to reduce the degree of superheating of the second refrigerant before being compressed. The second cycle is also connected with the third cycle in the same way. This integration improves system efficiency by a good distribution of the refrigeration duty from one cycle to another [147].

Table 4.7 Initial refrigerant compositions of the triple gas expander process.

Refrigerant	Component	Unit	Value
1st Refrigerant	CH_4	mol %	87.50
	C_2H_6	mol %	8.50
	N_2	mol %	4.00
2nd Refrigerant	CH_4	mol %	93.00
	C_2H_6	mol %	0.50
	N_2	mol %	6.50
3rd Refrigerant	N_2	mol %	100.00
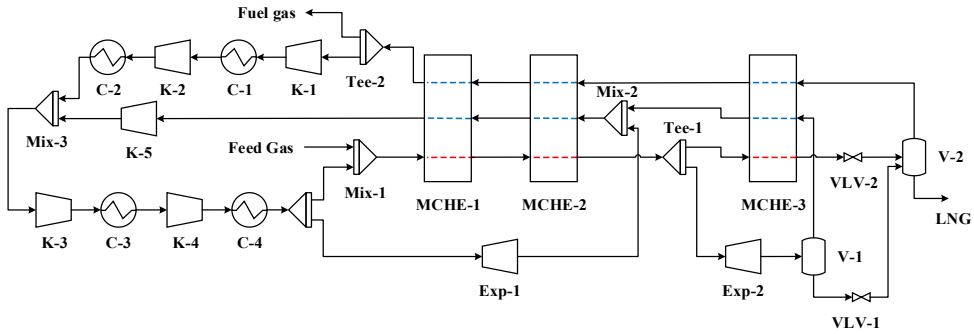
Figure 4.7 Process flow diagram of the self-liquefaction process [25].

4.2.1.3   **Self-liquefaction process**

For simplicity, an open cycle gas expander process was also suggested [25]. This self-liquefaction process utilizes the feed gas as a refrigerant, which is always in gas phase in the system. In addition, refrigerant make-up facilities like refrigerant storage tanks and make-up injection lines used in conventional LNG processes are not required [148, 149].

Pre-cooling and liquefaction of natural gas is conducted by an expander, and sub-cooling of the liquefied feed is performed by cold energy recovery of the end-flash gases produced by the J-T valves. The end-flash gases are recycled and merged with the feed gas. A part of the recycled end-flash gas is extracted as fuel gas after delivering cold duty to the main cryogenic heat exchangers in the open cycle gas expander system. The process flow diagram is shown in Figure 4.7.

4.2.2 **Design basis and optimization**

The SMR and AP-DMR processes introduced in Chapter 3.4 and Chapter 4.1.1 were selected as references for the comparison of the alternative liquefaction processes. The simulations were performed by Aspen HYSYS V 9.0 [132]. The feed gas is assumed to be sweetened, dehydrated natural gas, containing a small amount of heavier hydrocarbons. Thus, extraction of natural gas liquid (NGL) from the gas is not considered during liquefaction. The detailed conditions of the

feed gas are shown in Table 4.8. The conditions of the LNG and the end-flash gas are listed in Table 4.9. Due to the recycling of the end-flash gas in the non-flammable cascade and the self-liquefaction processes, an additional gas stream was extracted as a fuel gas from the systems. Besides, the amount of the fuel gas was controlled to be equal to the chemical energy value contained in the end-flash gas from the reference processes.

Table 4.8 Conditions of the feed gas.

Property	Unit	Value
Temperature	°C	22.00
Pressure	bar	60.00
Flow rate	kmol/s	6.50
Methane	mol %	91.60
Ethane	mol %	4.93
Propane	mol %	1.71
n-Butane	mol %	0.35
i -Butane	mol %	0.40
i-Pentane	mol %	0.01
Nitrogen	mol %	1.00

Table 4.9 Specifications of the LNG and the end-flash gas.

Property	Unit	Value
LNG production	MTPA	3.00
LNG temperature	°C	-157.70
LNG pressure	bar	1.40
End-flash production	kmol/s	0.55
End-flash temperature	°C	-157.70
End-flash pressure	bar	1.40
End-flash LHV	MJ/kmol	736.00
End-flash chemical energy	MW	405.00

The temperature and pressure levels of the fuel gas were not considered as restrictions since the cold energy recovery system of the end-flash or the fuel gases are not considered in this work. In addition, the cold energy recovery system will have a marginal effect on total process efficiency.

Optimization using SQP algorithms was performed to evaluate the different LNG processes. Except for the self-liquefaction system, the molar flow rates of components in their refrigerants were selected as decision variables. The pressure levels of the working fluids were also defined as optimization variables. The outlet temperature of all heat exchangers were set to be variables to manipulate the heat duty. Besides, the split ratio of stream splitters in the non-hydrocarbon cascade and the triple gas expander processes were also defined as decision variables. Minimum temperature approach in cryogenic heat exchangers was assumed to be 3 °C for all the processes. The minimum superheating value of the refrigerants at compressor inlets was also set to be 5 °C to protect compressors from liquid droplets. Pressure drops and heat leakage in equipment were disregarded. Other simulation conditions are summarized in Table 4.10.

Table 4.10 Simulation conditions of the alternative LNG processes.

Design parameters	Unit	Value
Equation of state	-	Peng-Robinson
Condenser / intercooler outlet	°C	22
Compressor	Polytropic %	78
Gas expander	Polytropic %	85
Pump / Liquid turbine	Adiabatic %	75
Compressor in a Compander	Polytropic %	73
Expander in a Compander	Polytropic %	83

4.2.3 Results

4.2.3.1   **Comparison of process options**

The process efficiency of the non-flammable liquefaction processes for FLNG was assessed and compared to the SMR and AP-DMR processes. Process performance was measured by specific power consumption, which is the power required per unit mass of LNG produced. Based on 3 MTPA production of LNG with plant availability of 330 days per year [44], specific power consumption for the alternative LNG processes was calculated. The results in Figure 4.8 indicate that the AP-DMR technology is the most efficient process compared to other LNG processes studied. However, the non-HC cascade system has a marginal penalty in specific power consumption of about 2 % compared to the SMR process. In addition, the SMR system has a significantly smaller number of units compared to the non-HC cascade process, making the MR scheme more favorable for offshore applications.

The triple gas expansion system gives a larger specific power consumption than the processes applying refrigerant boiling (i.e. the SMR, AP-DMR, and non-HC cascade). This is a typical feature of reversed Brayton processes since the heat transfer coefficient and the heat capacity of gaseous refrigerants are substantially lower than the boiling ones [150]. The poor thermodynamic properties will result in a larger flow rate of the refrigerants and thus power consumption for the same amount of LNG production. The self-liquefaction process, which is also based on gas phase refrigerants, consumes the largest amount of power for the LNG production. The fact that the composition of the refrigerant is fixed by the feed gas is one of the possible reasons for the low efficiency.

Table 4.11 indicates that the processes using refrigerant boiling have larger cold duties and *UA* values than the two gas expander based processes. Although the non-HC cascade process has a smaller duty and a *UA* value compared to the SMR and AP-DMR processes, the reduced heat exchanger area may be counter acted by the area required for the NRU and the multi-stage phase separators in the LNG sub-cooling stage.
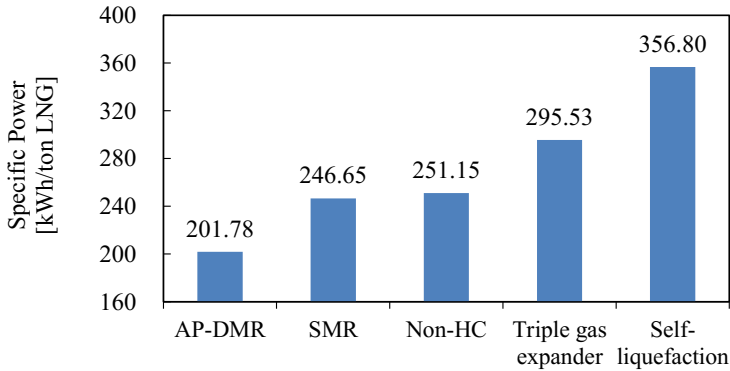
Figure 4.8 Specific power consumption of the alternative LNG processes.

The triple gas expander and the self-liquefaction processes may also require a large heat exchanger area since the heat transfer coefficients of refrigerants used in the MR based and cascade processes are regarded to be 5 to 15 times higher than the gaseous refrigerants [150]. Thus, a detailed heat exchanger design will be required to evaluate the size of heat exchangers for a comparison of the different type of LNG process.

The SMR and AP-DMR processes have a low level of process safety when applied to offshore installations. The mixed refrigerants (MRs) consist of hydrocarbon components, which are highly flammable. Especially, the propane component in the MRs can easily be accumulated on a deck floor in the event of leakage due to the dense vapor. The MR based processes also carry hydrocarbon inventory in liquid phase. Liquid form of hydrocarbons has a higher energy density, so the fire from the leakage is more intense than in gas phase. Blow-down of liquid refrigerants in the processes also needs a longer time than gaseous refrigerants in emergencies.

Table 4.11 Properties of cryogenic heat exchangers in the alternative LNG processes.

property	Unit	AP-DMR	SMR	Non-HC cascade	Triple gas expander	Self-liquefaction
Duty	MW	306.7	633.5	181.0	150.6	150.0
UA	MW/°C	68.1	148.6	34.6	11.9	31.7

Table 4.12 Refrigerant flow rates of the alternative LNG processes.

	Unit	AP-DMR	SMR	Non-HC cascade	Triple gas expander	Self-liquefaction
1st Cycle	kmol/h	38 936	92 374	31 451	45 159	127 986
2nd Cycle	kmol/h	33 761	-	24 815	73 777	-
3rd Cycle	kmol/h	-	-	16 102[a]	38 724	-
Total	kmol/h	72 697	92 374	72 368	157 660	127 986

[a]The end-flash gas from the multi-stage J-T expansion.

Therefore, the SMR and AP-DMR systems are relatively less safe options for FNLG although the flow rates of the refrigerants are smaller than the gas expander based processes as shown in Table 4.12.

In contrast to the SMR and DMR systems, the alternative LNG processes have a higher safety. The non-HC cascade process utilizes HFCs and a noble gas, which are almost non-flammable. R-410A used for the first cycle of the cascade process is a mixture of R-32 and R-125. R-32 is slightly flammable, but it has a very low flame propagation speed. R-125 is a non-flammable component. Therefore, R-410A is relatively safe to be used on a ship. Xenon applied to the second cycle is also non-flammable and even non-toxic. The third cycle using the end-flash gas obviously contains hydrocarbons but it is in gas phase throughout the system, and the flow rate is relatively small as seen in Table 4.12. Thus, no liquid hydrocarbon inventory is needed in the process, assuring a high level of safety.

The triple gas expander and the self-liquefaction processes show high inherent safety as well. Although the refrigerants used in this process consist of hydrocarbons, they are always in gas phase, avoiding liquid hydrocarbon inventory. Thus, the large flow rate of the refrigerants will only have a minor effect on the safety. When blow down of refrigerants are required in emergencies, the self-liquefaction process will be more favorable due to the smaller flow rate of the refrigerant compared to the triple gas expander process.

4.2.3.2   Sensitivity analysis

The composition of the feed gas was varied from lean to rich gas in order to identify the effect on the process efficiency of the LNG processes with non-flammable refrigerants. The variation of the composition in the feed gas is listed in Table 4.13.

The mole fraction of nitrogen in the feed gas was fixed to maintain the operating conditions of the NRU in the non-HC cascade process. The chemical energy of the end-flash gas varies with the feed gas composition. Thus, the flow rate of the fuel gas in the non-HC cascade and the self-liquefaction systems was manipulated to have the same amount of chemical energy as the end-flash gas in the MR processes.

Figure 4.9 indicates that when the feed gas is richer, the non-flammable processes are able to decrease the specific power consumptions. Notably, the non-HC cascade and the triple gas expander processes had the same reduction in specific power consumption as the MR based systems, showing proper operational flexibility with different feed gas. However, the self-liquefaction process has the smallest decrease in the specific power consumptions for the rich feed gas compared to other LNG systems. In this process, the composition of the refrigerant is fixed since the feed gas acts as the working fluid. Thus, the operational flexibility of this system is restricted, resulting in the small improvement of the specific power consumption with the rich feed gas.

Table 4.13 Variation of feed gas composition.

Component	Unit	Rich Gas	Base case	Lean Gas
Nitrogen	mol %	1.00	1.00	1.00
Methane	mol %	85.50	91.60	97.50
Ethane	mol %	9.00	4.93	1.00
Propane	mol %	3.00	1.71	0.30
n-Butane	mol %	0.70	0.35	0.09
i -Butane	mol %	0.78	0.40	0.10
i-Pentane	mol %	0.02	0.01	0.01
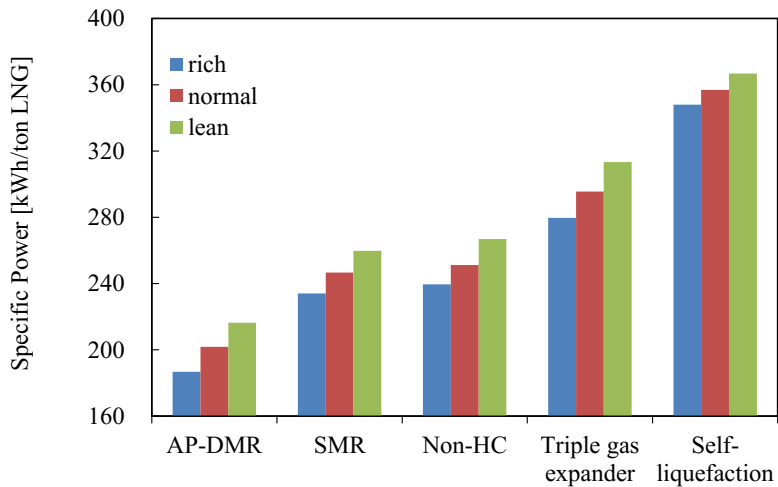
Figure 4.9 Variation of specific power consumption for the alternative LNG processes with different feed gas conditions.

Nevertheless, the self-liquefaction process with the lean feed gas has the minimum penalty in specific power consumption compared to other systems. Since the refrigerant also became rich in methane with the lean feed gas, the effect of the changes in feed gas composition on the power consumption was minimized in the self-liquefaction process.

4.2.4 Conclusions

This chapter evaluates process options for floating LNG and compares them with the SMR and AP-DMR as reference systems. When it comes to thermodynamic efficiency, only the non-HC cascade technology achieved a system efficiency close to the MR based system (SMR). Inherently, the gas expander based processes displayed a poor process efficiency. Especially, the self-liquefaction process showed the lowest efficiency compared to other LNG processes due to its simple structure. Although the alternative LNG processes consume considerable amount of power, they are much safer than the reference processes since they do not carry any liquid hydrocarbons in their systems. The non-HC cascade process applies hydrofluorocarbons and a noble gas as refrigerants, and the refrigerants in the expander based systems are always

in gas phase. The non-flammable LNG process options also have smaller UA values than the SMR and DMR systems, giving a smaller heat exchanger area. However, the complex configuration of the non-HC cascade process results in a large number of units. The number of rotating machines in the two gas expander based processes are even larger than other processes, increasing the capital cost of the process. Thus, a detailed cost analysis will be required to select the most suitable LNG process for floating facilities.

4.3   Problem formulation for complex LNG processes

As introduced in Chapter 4.1, there have been various studies to make the DMR process more energy efficient. The challenge is given by the fact that this system has a complex structure due to multiple cycles with mixed refrigerants. This grants flexibility in its configuration and operating conditions, but makes the system difficult to analyze and optimize due to the large size of the optimization problem. Thus, several papers have focused on the formulation of the optimization problem. Nevertheless, there has been less interest in the formulation of constraints that may result in energy savings such as refrigerant superheating and maximum heat exchanger conductance. Therefore, this chapter studies constraint formulations of refrigerant superheating in the DMR process, while considering both minimum temperature difference ($\Delta T_{\min}$) and maximum heat exchanger conductance ($UA_{\max}$) constraints in the cryogenic heat exchangers. This work also provides insight on the interaction between the two refrigerant cycles in the DMR process, which is affected by the implemented constraints.

4.3.1 Superheating in refrigeration cycles

For the typical refrigeration cycle based on vapor compression, some degree of refrigerant superheating at the condenser outlet is used for a practical purpose, which is to prevent liquid formation at the compressor inlet. However, various experimental works indicate that superheating will decrease the system efficiency [151]. Even though superheating allows the refrigerant to take a larger amount of heat in the evaporator, the higher temperature and larger

volume of the compressor inlet stream will increase compression power, which may exceed the increased refrigeration effect. Nevertheless, the effect of superheating on the refrigeration cycle has not been extensively examined as an optimization problem. Thus, Jensen and Skogestad (2007) optimized the refrigeration system with a single component refrigerant and proposed that superheating is not encouraged to achieve minimum compressor work [152]. However, they also suggested that refrigeration systems with internal heat exchange between the condenser and the evaporator, such as natural gas liquefaction processes, may need some degree of superheating.

The characteristics of refrigeration systems with superheating will vary depending on the type of refrigerant and the structure of the process. For refrigeration systems with a mixed refrigerant, the PRICO process was selected and optimized to verify the effect of superheating [153]. Unlike the typical refrigeration cycle, the PRICO process had higher energy efficiency when there is a certain degree of superheating. Processes operated by multiple refrigeration cycles with pure component refrigerants also had a distinctive characteristic with refrigerant superheating [140]. In the case of pure refrigerant cascade LNG processes, maximum refrigerant superheating was required to decrease the power consumption.

Despite the previous studies on superheating, optimization results of LNG processes are still misinterpreted such that superheating will reduce the energy efficiency, which is a common thought for vapor compression refrigeration [154]. In addition, fixed or limited bounds of superheating are still used in the optimization of the DMR processes even though the effect of superheating is determined by the structure of the refrigeration system. Thus, this chapter examines refrigerant superheating constraints on an LNG process having multiple cycles with mixed refrigerants. Since the above-mentioned optimization studies are performed with minimum temperature difference constraints for heat exchangers, maximum heat exchanger conductance constraints are also tested to see the change in the effect of superheating.

4.3.2 Design basis and optimization

The AP-DMR process introduced in Chapter 4.1.1 was studied as a representative of refrigeration systems with multiple cycles of two mixed refrigerants [28]. The process flow diagram is shown in Figure 4.10. Pre-treated natural gas was assumed as the feed gas and liquefied through the AP-DMR process. The end-flash step for the subcooled LNG was not included in this simulation. Table 4.14 shows other design conditions used in this work.

As seen in Eq. (4.2), the simulation model was optimized to minimize power consumption per unit mass of LNG produced.
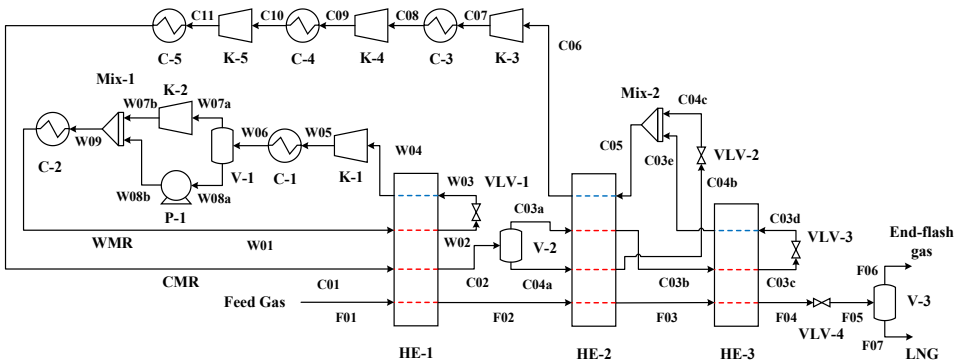
Figure 4.10 Process flow diagram of the AP-DMR process [28, 29].

Table 4.14 Simulation conditions and assumptions.

Design parameter	Unit	Value
Feed gas flow rate	kmol/s	1
Feed gas pressure	bar	60
Feed gas temperature	°C	22
LNG temperature	°C	-148
Compressor efficiency	Polytropic	78 %

$$\min_{\mathbf{x}} f(\mathbf{x}) = P_{\text{specific}}(\mathbf{x}) = \frac{\dot{W}_{\text{comp}}^{\text{total}}(\mathbf{x})}{\dot{m}_{\text{LNG}}(\mathbf{x})}$$

subject to $\quad \Delta T_{\min,i}(\mathbf{x}) \geq 3 \qquad\qquad i = \{\text{HE-}1,2,3\}$

$\qquad\qquad\qquad \Delta T_{\text{sup},j}(\mathbf{x}) \geq \Delta T_{\text{sup,min}} \qquad j = \{\text{W04}, \text{C06}\}$

$\qquad\qquad\qquad 1 \leq Pr_k(\mathbf{x}) \leq 4 \qquad\qquad k = \{\text{K-}1,2,3,4,5\}$

$\qquad\qquad\qquad \mathbf{x}_{LB} \leq \mathbf{x} \leq \mathbf{x}_{UB}$

(4.2)

The molar flow rates of components in both the warm mixed refrigerant (WMR) and the cold mixed refrigerant (CMR) were set as variables. The warm mixed refrigerant (WMR) consists of ethane, propane and n-butane, while the cold mixed refrigerant (CMR) contains nitrogen, methane, ethane and propane. In addition, all pressure levels of the WMR and the CMR and the outlet temperature of heat exchangers HE-1 and HE-2 were defined as variables so that the duty of the heat exchangers can be manipulated during optimization. The optimization problem applied minimum temperature difference constraints of 3 °C for all the heat exchangers. Minimum superheating was also constrained for the inlet streams of compressors K-1 and K-3, and various degrees of minimum superheating were tested as case studies.

4.3.3 Results

4.3.3.1   Effect of superheating with minimum temperature difference constraints

The AP-DMR process was optimized with different values of minimum superheating on the compressor inlet streams from 0 K to 25 K. As illustrated in Figure 4.11 (left), the lowest specific power consumption was achieved with the minimum superheating of 0 K and 5 K. The power consumption gradually increased with the larger constraint values. This means that specific superheating values are needed to achieve higher energy efficiency. This is a similar conclusion made in the previous study by Jensen and Skogestad (2009) for the PRICO single mixed refrigeration LNG process [153].
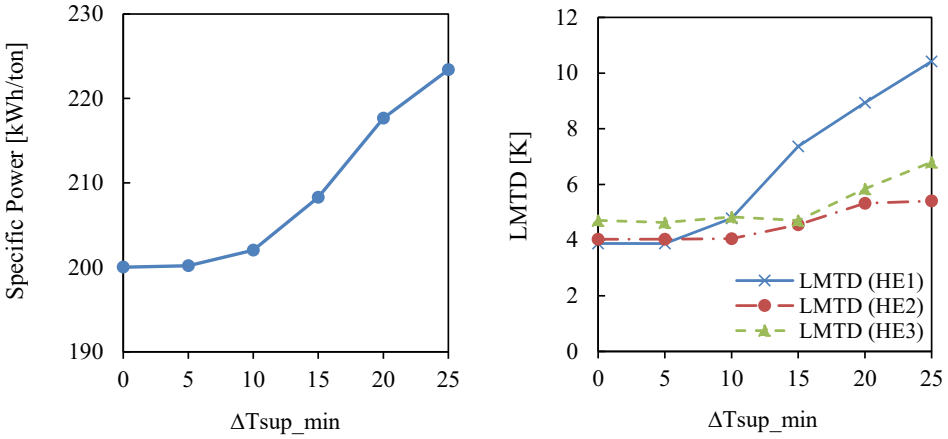
Figure 4.11 The variation of specific power consumption (left) and *LMTD* values of the heat exchangers (right) with minimum superheating requirement in the optimized cases with $\Delta T_{\min}$ constraints.
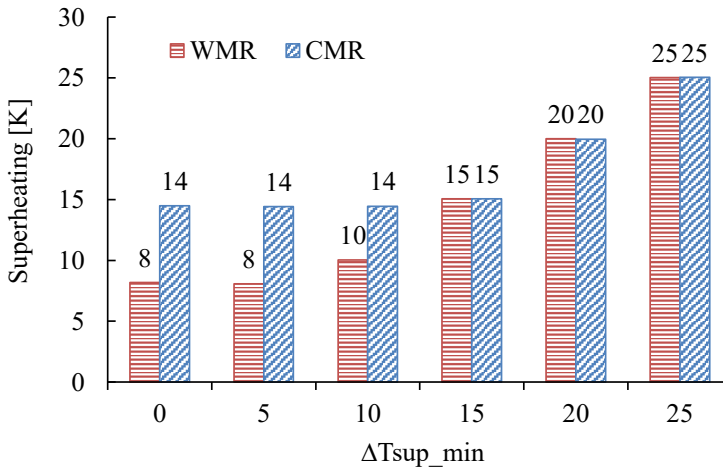
Figure 4.12 The variation of superheating values for the WMR and CMR with minimum superheating requirement in the optimized cases with $\Delta T_{\min}$ constraints.

As seen in Figure 4.12, the superheating values at the best-known solutions required around 8 K and 14 K for the WMR and the CMR respectively. After 10 K of minimum superheating, the WMR and/or the CMR did not reach the optimal superheating values due to the constraints, and rather settled at the minimum values of the constraints. Thus, constraint values that are higher than the optimal superheating values will lead to sub-optimal solutions, which means larger power consumption of the process.

This can also be observed by the *LMTD* values of the heat exchangers in Figure 4.11 (right). After 5 K of minimum superheating, the *LMTD* value of heat exchanger HE-1 increased significantly. The other heat exchangers also experienced a rise in the *LMTD* values after 10 K of minimum superheating. An increase in the *LMTD* values means larger temperature difference between hot and cold composite curves in the heat exchangers, which results in larger entropy generation due to increased irreversibilities.

4.3.3.2   Effect of superheating with maximum heat exchanger conductance constraints

Minimum temperature difference constraints are widely applied in modeling and optimization of processes with heat exchangers. By specifying the value of minimum temperature difference, one can manipulate the trade-off between process power consumption and heat exchanger area. Nevertheless, the minimum temperature difference does not optimally utilize the heat exchanger area since it results in a sub-optimal distribution of temperature driving forces particularly for systems operating below ambient temperature such as LNG processes [43, 153]. The temperature driving forces should be distributed proportional to the temperature level to achieve the optimal use of heat transfer area.

Thus, in this work, maximum heat exchanger conductance constraints were tested with the *UA* value from the best solution obtained by using minimum temperature difference constraints in the previous section. Eq. (4.3) is the optimization formulation with the *UA* value.

$$\min_{\mathbf{x}} f(\mathbf{x}) = P_{\text{specific}}(\mathbf{x}) = \frac{\dot{W}_{\text{comp}}^{\text{total}}(\mathbf{x})}{\dot{m}_{\text{LNG}}(\mathbf{x})}$$

subject to $UA_{\max}(\mathbf{x}) \geq \sum_i UA_{i, \Delta T_{\min}}$ $i = \{\text{HE-} 1, 2, 3\}$

$\Delta T_{\min, i}(\mathbf{x}) \geq 0.5$ (4.3)

$\Delta T_{\text{sup}, j}(\mathbf{x}) \geq \Delta T_{\text{sup,min}}$ $j = \{\text{W04}, \text{C06}\}$

$1 \leq Pr_k(\mathbf{x}) \leq 4$ $k = \{\text{K-} 1, 2, 3, 4, 5\}$

$\mathbf{x}_{LB} \leq \mathbf{x} \leq \mathbf{x}_{UB}$

Figure 4.13 (left) demonstrates that the use of the maximum heat exchanger conductance constraint also leads to a similar trend in specific power consumption as the use of minimum temperature difference constraints. However, the difference in the specific power consumption between the best and the worst cases was reduced to less than a half, compared to the one with $\Delta T_{\min}$ constraints. As expected, the best solution was improved from 200.1 to 196.6 kWh/ton LNG when using the $UA_{\max}$ constraint.
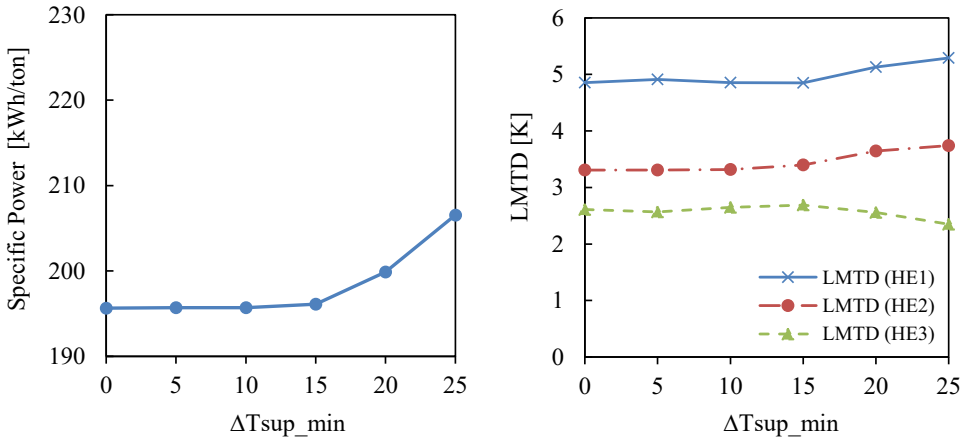
Figure 4.13 The variation of specific power consumption (left) and *LMTD* values of the heat exchangers (right) with minimum superheating requirement in the optimized cases with $UA_{\max}$ constraints.

Figure 4.14 The variation of superheating values for the WMR and CMR with minimum superheating requirement in the optimized cases with UA_{max} constraints.
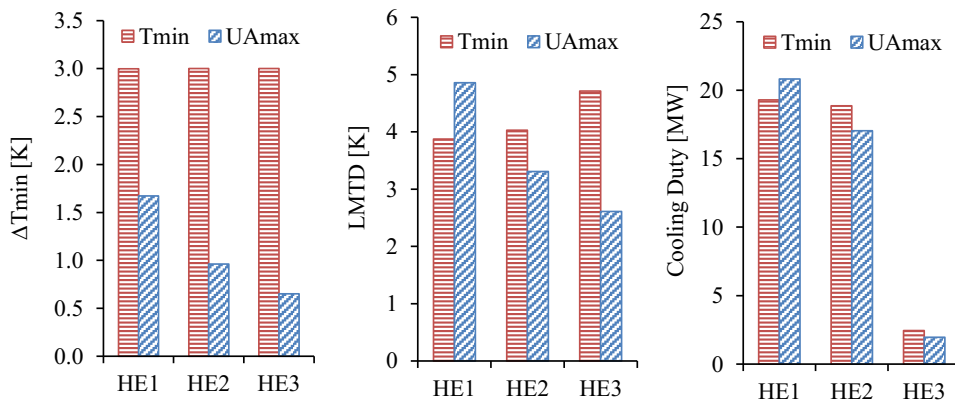
Figure 4.15 Comparison of ΔT_{min} (left), $LMTD$ (middle) and cooling duty (right) in the heat exchangers between the best solution with ΔT_{min} and UA_{max} constraints.

As illustrated in Figure 4.14, the optimal superheating values for the WMR and the CMR were 10 K and 12 K correspondingly. Thus, the superheating constraint values less than 15 K had no influence on the specific power consumption. From 15 K and higher superheating constraints, the specific power consumption increased almost proportionally to the difference between the optimal superheating values and the minimum superheating constraints.

As seen in Figure 4.13 (right), the effect of the minimum superheating constraints became less sensitive with the $UA_{\max}$ constraints due to the optimal distribution of temperature driving forces in the heat exchangers. At superheating constraint values larger than the optimal degree of superheating, the $LMTD$ of heat exchanger HE-3 operating at the lowest temperature is reduced, while the others have larger $LMTD$. The use of $UA_{\max}$ constraints results in smaller driving forces for the heat exchangers operating at lower temperatures and larger driving forces for heat exchangers operating at higher temperatures, which reduces total irreversibilities. This agrees with the results of the previous studies about the optimal use of heat exchanger area [42, 155].

Returning to the optimization case using $\Delta T_{\min}$ constraints, one should notice that the $LMTD$ for HE-3 increased more than the $LMTD$ for HE-2 for increasing values of the superheating constraint, thus increasing total irreversibilities. The superiority of the maximum heat exchanger conductance constraint over the minimum temperature difference constraint can be explained by comparing their best and worst cases. With the same UA value, the $UA_{\max}$ constraint reduced power consumption with 2 % points compared to the $\Delta T_{\min}$ constraint for the best case, and 8 % points for the worst case.

Figure 4.15 (left) and Figure 4.15 (middle) also illustrate that the maximum heat exchanger conductance constraint results in reduced $\Delta T_{\min}$ and $LMTD$ values for lower operating temperatures for the heat exchangers. Thus, the $UA_{\max}$ constraint guides the temperature driving forces to be proportional to temperature as explained before. In contrast, the constraint of minimum temperature difference results in larger $LMTD$ values for colder heat exchangers and smaller $LMTD$ values for warmer heat exchangers as illustrated in Figure 4.15 (middle). The maximum heat exchanger conductance constraint also redistributes the cooling duties of

the heat exchangers to be proportional to temperature as shown in Figure 4.15 (right). This means to place less duty on the heat exchangers having larger irreversibilities per unit duty, and irreversibilities are inversely proportional to temperature.

4.3.4 Conclusions

In this chapter, the effect of superheating constraints was examined for a dual mixed refrigerant LNG process. Unlike refrigeration processes with pure component refrigerants, the case studies indicate that a certain degree of superheating of the two mixed refrigerants is encouraged to improve the system efficiency for the DMR process. In order to find optimal superheating values, relaxation of the minimum superheating constraint is required since a high value of the minimum superheating constraint may lead to sub-optimal solutions, missing optimal superheating values.

In addition, the use of maximum heat exchanger conductance is recommended as constraints for the heat exchangers in the DMR process, since it gives higher energy efficiencies than the minimum temperature difference constraint. $UA_{\max}$ is superior to the $\Delta T_{\min}$ constraint due to an optimal distribution of temperature driving forces in the heat exchangers. The penalty of the sub-optimal superheating values was also reduced with the $UA_{\max}$ constraint, compared to the minimum temperature difference constraint.

Chapter summary

- o A large number of evaporation pressure levels for the WMR cycle with a proper operating temperature range and the phase separation of the pre-cooled CMR are the main contributors to an efficient DMR process.

- o Due to the low process efficiency, non-flammable LNG processes will not be favorable options for mid-scale LNG production, compared to systems using hydrocarbon mixtures as refrigerants.

- o The use of relaxed superheating constraints for the two MRs and the use of total UA value constraints with relaxed $\Delta T_{\min}$ constraints improve the efficiency of DMR processes.

Chapter 5   Cost analysis for LNG transport

In Chapter 4, various base-load LNG processes were optimized and evaluated using energy efficiency. Due to the high level of energy consumption in LNG processes, it is reasonable to use energy efficiency as an objective function especially to optimize the system in the conceptual design phase. However, economic evaluation will be more critical than energy analysis in some cases like small-scale LNG systems on LNG carriers. Therefore, such LNG processes are designed and optimized based on economic analysis in this chapter to answer the following questions:

- o Regarding economics, what are the design criteria for LNG systems on LNG carriers?
- o What is the advantage of cost analysis for LNG liquefaction processes?

This chapter is based on the following publications.

- – Kim D, Hwang C, Gundersen T, Lim Y. Process design and economic optimization of boil-off-gas re-liquefaction systems for LNG carriers. Energy (in review).

5.1   Introduction

Following the event when liquefied natural gas (LNG) was produced by external refrigerants and Joule-Thomson throttling for commercial purposes in 1941, the first long-haul transport of LNG was made from Louisiana in the US to Canvey Island in the UK in 1959 [57, 156]. This successful shipment resulted in LNG becoming an attractive option to supply energy over long distances, where it is not economical to use pipeline transmission of natural gas [6, 7]. Thus, LNG has been an important solution for energy security in many countries such as Japan and Korea, accounting for 10 % of global gas supply [8].

For the transportation of LNG, specially designed vessels with highly insulated storage tanks are used to avoid evaporation of the valuable cargo during a voyage [56, 57]. Nevertheless, it is inevitable to have heat leaks to the tanks, and a portion of LNG will vaporize on the liquid surface of the cargo, producing boil-off gas (BOG) [157]. The sloshing of LNG in the storage tanks due to ship motions also accelerates BOG generation [158]. Since the BOG increases the pressure level of the storage tanks and thus the mechanical stress of the structure, it has to be removed from the containment system [159].

In order to remove or utilize the BOG from the tank, steam turbine (ST) propulsion systems have been widely used since the 1960s [4, 64, 65]. The unnecessary BOG is burned in boilers to produce steam, which is fed to STs and turbo generators to supply propulsion and electric power [58, 65]. However, the ST system has a lower thermal efficiency compared to heavy fuel oil (HFO) driven two-stroke low speed diesel engines, which is the main propulsion principle for commercial ships [4, 59, 63-65]. This low efficiency of STs may require extra fuel supplied by the LNG cargo for modern LNG carriers, which minimize BOG production due to improved insulation technology. The larger amount of carbon dioxide in the exhaust gas compared to the internal combustion engines also made the ST propulsion system less favorable for LNG vessels.

In addition to low efficiency, STs have two additional disadvantages: First, improved insulation technologies [65] reduce the amount of BOG available. Second, the larger amount of carbon

dioxide in the exhaust gas from the boiler will causes problems for LNG vessels, where the International Maritime Organization (IMO) recently extended their restriction about CO_2 emission [4].

Thus, a dual fuel diesel electric (DFDE) propulsion system was developed in the early 2000s to use both HFO and BOG as fuel for diesel engines, which delivers a higher efficiency with less pollution compared to STs [59, 64, 65]. The DFDE system supplies a mixture of the pre-treated BOG and air into four-stroke diesel generator engines in order to produce electric power for motor-driven propellers and other electricity needs on the LNG vessel [58]. This system is also equipped with gas combustion units (GCU) to burn the surplus of BOG after being consumed as fuel. The DFDE quickly dominated the market share, and 30 % of the current LNG fleet is operated by this propulsion system [8].

However, the DFDE propulsion system does not fully utilize the power output of diesel engines due to the extra units required to deliver the combustion energy from the engines to the propellers such as electrical generators and propulsion motors [64, 65]. This electric system also requires additional parts, which demand more maintenance efforts [59]. As a consequence, ship engine manufacturers modified the conventional HFO fueled two-stroke slow speed diesel engines to adapt BOG as fuel and directly drive the impellers, which is more efficient than the four-stroke machinery applied to the DFDE [4, 69]. The injection of compressed BOG fuel into the engine cylinders enables the newly developed diesel engines to achieve the same efficiency as the conventional HFO driven diesel engines [69].

There are two main manufacturers providing such engines on the market: Man Diesel & Turbo with the M-type electronically controlled gas injection (ME-GI) engine and Win GD with the extra-long stroke dual fuel (X-DF) engine [160, 161]. The ME-GI system feeds high pressure BOG to the cylinders after the compression stroke, which is close to the Diesel cycle [69]. In contrast, the X-DF engine allows supplying relatively low pressure BOG to the combustion chamber by injecting it in the middle of the compression stroke, thus working as an Otto cycle [161]. As of 2018, there were 18 LNG vessels operated by the ME-GI based system and around

42 % of LNG carriers in the order books will be built with the high pressure gas injection engine [8].

With the improved efficiency of the propulsion system, less BOG is consumed as fuel on voyages, and the rest is burned in a GCU. The amount of BOG treated in the GCU is a significant economic loss of the cargo, and this increases during low load operations. Thus, there have been various suggestions for the ME-GI based propulsion system to re-liquefy the valuable product and return it to the LNG tanks.

The EcoRel system from Cryostar liquefies BOG through a nitrogen gas expander refrigeration cycle [160, 162]. A part of the liquefied BOG is then sent to the storage tank, and the rest is pressurized by LNG pumps and vaporized to be fed to the engine. Wärtsilä (Hamworthy) also supplies a re-liquefaction system (the Mark III type), having similar principles as the EcoRel [160, 163]. The drawback of these two processes is that the entire BOG is always liquefied although some part of the liquid product has to be re-vaporized as fuel for the engines, wasting the cold energy.

Instead, Wärtsilä (Hamworthy) modified the Mark III system so that BOG is pressurized in gas phase by the Laby-GI compressors (reciprocating type) to supply fuel for the propulsion system [160]. Thus, the BOG from the cargo tank does not need to be liquefied all the time, and this can save energy consumed in the liquefaction cycle when liquefaction of BOG is not required during voyages. However, some of the energy savings will be offset by the larger power consumption in the compressor, compared to liquid compression in the pumps. TGE Marine Gas Engineering also offers a cascade liquefaction system with the Laby-GI compressors in order to overcome the inherent low efficiency of the N2 expander refrigeration cycle [164].

Although the above mentioned liquefaction technologies minimize the amount of LNG wasted in the form of BOG and bring a larger amount of the cargo to LNG import terminals, they need extra equipment and increased capital cost. One of the alternatives is to employ a less efficient but simpler liquefaction system such as the Joule-Thomson (JT) cycle. This process, also known as the Linde-Hampson process, compresses a feed gas above the critical pressure and

depressurizes it through a JT valve in order to liquefy the gas by temperature drop without an external working fluid [165].

The use of the self-reliquefaction process in the propulsion system with the high pressure gas injection engine will only require a heat exchanger and a phase separator in addition to the Laby-GI compressor where the pressurization of BOG is achieved. The simple structure of the JT cycle will reduce the number of units and thus capital cost for a BOG liquefaction facility, while accepting a reasonable increase in power consumption due to the low efficiency of the process.

Therefore, this chapter suggests self-reliquefaction processes using the JT cycle for the propulsion system with high pressure gas injection engines on LNG carriers. The costs of the reliquefaction systems are estimated and compared with the propulsion scheme without BOG reliquefaction in order to ensure the economic feasibility of the additional JT cycle based processes. The capital and operating costs of the systems are calculated based on equipment size, wasted BOG, and utility consumption. For a fair comparison, all the propulsion systems are optimized using a stochastic algorithm to minimize the capital and operating cost by finding proper operating conditions for the total system. Various improved process schemes are also suggested to reduce the total cost while keeping the equipment count low. A sensitivity analysis is also performed with respect to LNG price, since this is one of the most important parameters affecting the economics of the liquefaction system.

5.2   Process design

5.2.1 Fuel supply system without BOG liquefaction

The propulsion system considered in this chapter has two types of engines; generating electricity (DFDE engines) and driving the propeller of the vessel (high pressure gas injection engines). Thus, as seen in Figure 5.1, the fuel supply system requires two fuel gas streams with different pressure specifications. First, the BOG produced in the storage tank is sent to the first
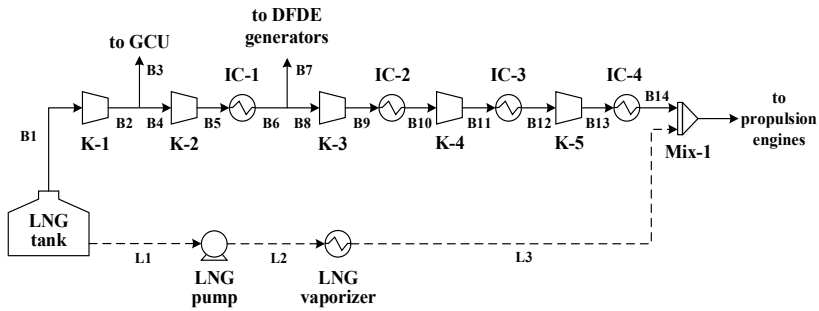
Figure 5.1 Process flow diagram for the fuel supply system without BOG liquefaction.

compressor (K-1). Due to the cryogenic temperature of stream B1 at the inlet of K-1, the outlet stream of the compressor (B2) has a low enough temperature to avoid any intercooling for the next compression stage. Then, the unnecessary part of stream B2 is fed to the GCU to be burned. The rest of the BOG is further pressurized through the second compressor (K-2) and cooled by the intercooler (IC-1). The intermediate pressure BOG (B6) is then split into streams B7 and B8, which will be supplied to the DFDE generators and the high pressure compressors, respectively. Stream B8 is passed through a three-stage compression (K-3 – K-5) and intercooling (IC-2 – IC-4) to meet the fuel requirement and then delivered to the propulsion engines.

If there is a lack of BOG to run the two engines, LNG from the storage tank is extracted to supply additional fuel for the gas injection engines. This LNG is boosted by the high pressure pump (LNG pump) and evaporated in a heat exchanger (LNG vaporizer). In this chapter, the LNG supply scheme is not considered, assuming that BOG produced in the tanks is sufficient to operate the propulsion system. The system described in Figure 5.1 is referred to as the reference fuel supply system in this chapter.

5.2.2 Fuel supply system with BOG liquefaction

The reference fuel supply system is modified to include the BOG self-reliquefaction system. The re-liquefaction is performed by extracting a relatively high pressure BOG during multi-
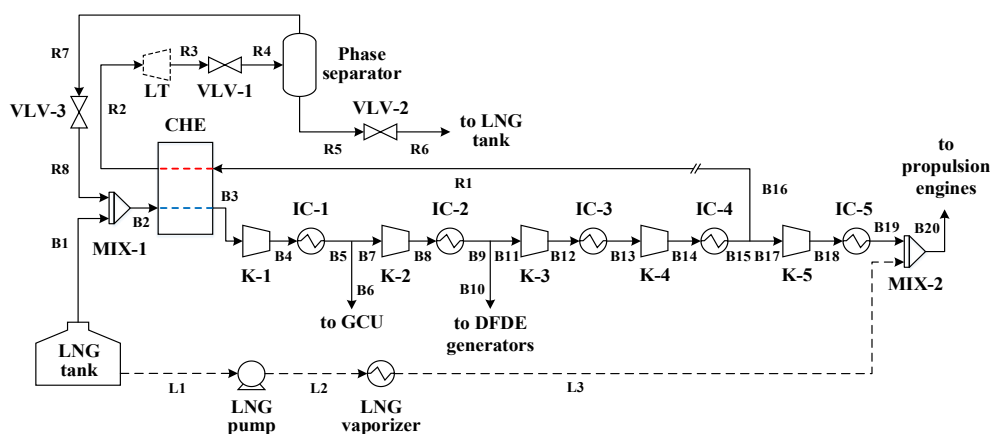
Figure 5.2 Process flow diagram for the fuel supply system with the LT process (the LT-JT process is indicated by the dotted equipment LT).

stage compression in order to use it as a refrigerant in the JT cycle for BOG liquefaction. Thus, a part of the pressurized BOG (B16) from compressor K-4 is recycled to the cryogenic heat exchanger (CHE) after being cooled by the intercooler (IC-4) as seen in Figure 5.2.

Due to friction in the long return pipeline, the pressure level of the recycled stream (R1) is reduced and supplied to the cold box where it is liquefied. The pre-cooled and liquefied BOG stream from the CHE (R2) is then depressurized through JT valve VLV-1. The throttled stream R4 is separated to liquid (R5) and vapor (R7) products in the phase separator. Stream R5 is returned to the LNG storage tank after adjusting the pressure level by another JT valve (VLV-2) to be suitable for injection into the tank. Stream R7 is further depressurized by JT valve VLV-3 to have the same pressure level as the BOG from the tank (B1). The two gas streams are mixed and sent to heat exchanger CHE to supply the cold duty. This process is referred to as the JT process.

Unlike the reference system, the inlet stream of the compressor K-1 does not have a cryogenic temperature since the mixed stream (B2) is heated in heat exchanger CHE. Thus, the fuel supply system with BOG liquefaction will require an extra intercooler (IC-1) to cool the superheated outlet stream of the first compressor. If, however, the outlet temperature of

compressor K-1 is equal to or lower than that of the intercoolers, the intercooler IC-1 will be disregarded during simulation and economic evaluation of the system.

One of the possible modifications of the system is the use of a cryogenic liquid turbine (LT) together with the JT valve (VLV-1) for the depressurization process of the high pressure liquefied BOG (R2). Since LTs can be used in a limited range of pressure drop to avoid vapor production at the outlet, a JT valve is also installed downstream to take the rest of the pressure change required in the system.

The LT in the liquefaction process allows stream R2 to have an isentropic expansion, resulting in a larger temperature reduction and smaller vapor fraction in the outlet stream with a given pressure drop compared to isenthalpic expansion in JT valves [166]. Thus, through the phase separator, the combination of an LT and a JT valve will produce a larger amount of liquid product (LNG) and a colder vapor stream, which is used as part of the refrigerant in the system.

Besides, the LT converts the pressure energy into work, decreasing the total power consumption of the fuel supply system although the turbo-machinery requires extra capital cost. Thus, in this chapter, the use of the LT in the fuel supply system with BOG liquefaction is considered as an option to improve the economics of the total system and compared with the case without the LT. This process configuration is referred to as the LT-JT system.

5.2.3 Utilization of the recycled cold BOG

The top product from the phase separator tends to have a much lower temperature than the BOG from the LNG tanks. However, the previous schemes do not utilize the cold energy of stream R8, instead it is mixed with the BOG (B1), thus increasing entropy generation due to the temperature difference. Instead, as seen in Figure 5.3, the two cold streams can be sent to heat exchanger CHE separately to deliver their cold energy and then mixed at the outlet of the exchanger. Although the low temperature of stream R8 increases log mean temperature difference (*LMTD*) of the CHE and thus entropy generation, such large temperature difference results in smaller heat exchanger area, reducing the cost of the exchanger.
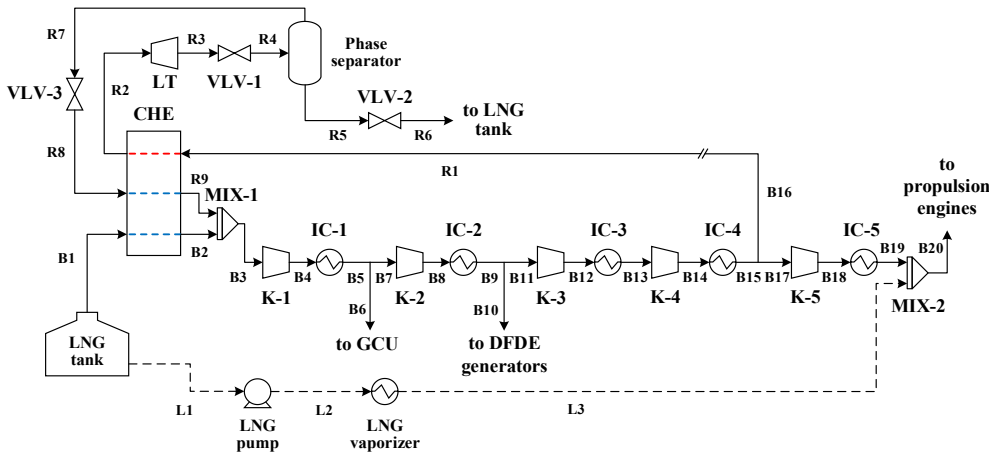
Figure 5.3 Process flow diagram for the fuel supply system with the LP mix LT-JT process.

In addition, the two cold streams at the CHE outlet have almost the same temperature, resulting in smaller entropy generation through the mixer (MIX-1). Stream R8 will also make it possible to manipulate design parameters of the CHE, such as *LMTD* and heat exchanger area by controlling the two JT valves (VLV-1 and VLV-3), and thus the temperature and pressure of stream R8. This modification is referred to as the LP mix LT-JT process.

Due to the mixing process in the LP mix LT-JT system, the vapor product from the phase separator (R7) has to be throttled by JT valve VLV-3 to the pressure level of stream B1, which is just above atmospheric pressure. As an alternative, the CHE outlet stream of the recycled BOG (R9) can be mixed with the slightly pressurized BOG stream (B6) (see Figure 5.4). This configuration is referred to as the IP mix LT-JT process. Since stream R9 bypasses compressor K-1 and intercooler IC-1, the duties of the turbo-machinery and the heat exchanger are reduced, saving both capital and operating costs.
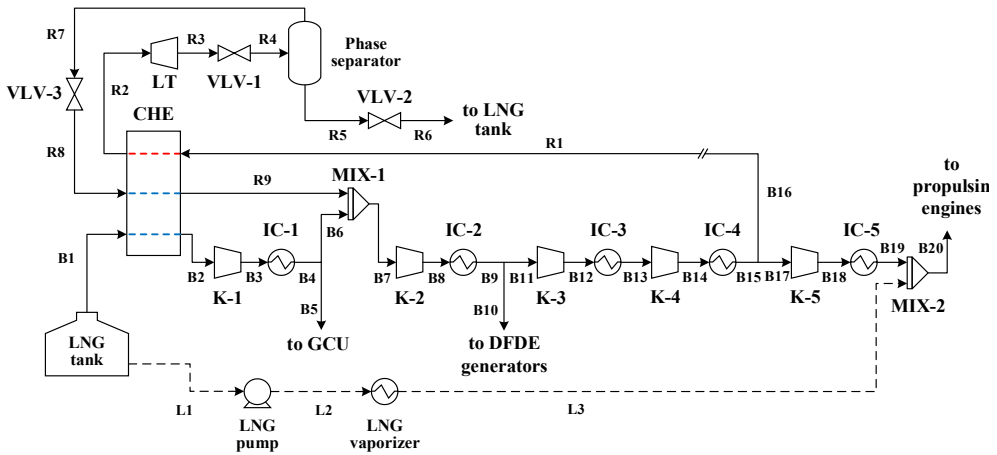
Figure 5.4 Process flow diagram for the fuel supply system with the IP mix LT-JT process.

Using the same principle as the IP mix LT-JT system, the recycled BOG stream (R9) heated in the CHE can be mixed with the high pressure BOG stream (B10), thus bypassing two stages of compression and intercooling. Figure 5.5 shows the configuration with the high pressure mixing, which is referred to as the HP mix LT-JT process. If stream R9 is mixed with the BOG streams from the third or fourth compressors (K-3 and 4), the throttling pressure at VLV-1 will be limited to the discharge pressure of the compressors, which is more than 40 bar. Due to the high throttling pressure, vapor will not form in the JT valve and the structure of the process will be identical to the LT-JT process, except there is no flow in the phase separator top product (stream R7 and R8). Therefore, further mixing of the recycled BOG with other compressor outlet streams is not considered in this chapter.

The three configurations utilizing the recycled BOG are also tested without the liquid turbine in consideration of the downtime for the turbo-machinery. They are referred to as the LP, IP and HP mix JT processes. This test will indicate the effect of the modified process schemes on the liquefaction systems using only Joule Thomson valves.

5.3   Design basis

5.3.1 Simulation conditions

In this work, the scope of simulation models was limited to the fuel supply systems and the liquefaction processes on LNG carriers. Thus, other sub-systems related to LNG tanks, gas combustion units, propulsion engines, cooling water systems were not considered. In addition, the auxiliary fuel supply system using LNG is also out of scope as mentioned Section 2.1.

The fuel supply systems were modeled and simulated by using Aspen HYSYS V9 with the Peng-Robinson equation of state (EOS) [132]. Heat leaks are neglected for all process units in the systems, assuming that these are highly insulated. However, it should be noticed that the imperfect insulation in real cases will allow some heat losses, despite the fact that a high level of insulation is applied to cryogenic systems on-site. This will result in minor deviations for the simulation results. Other specifications for the equipment are listed in Table 5.1.
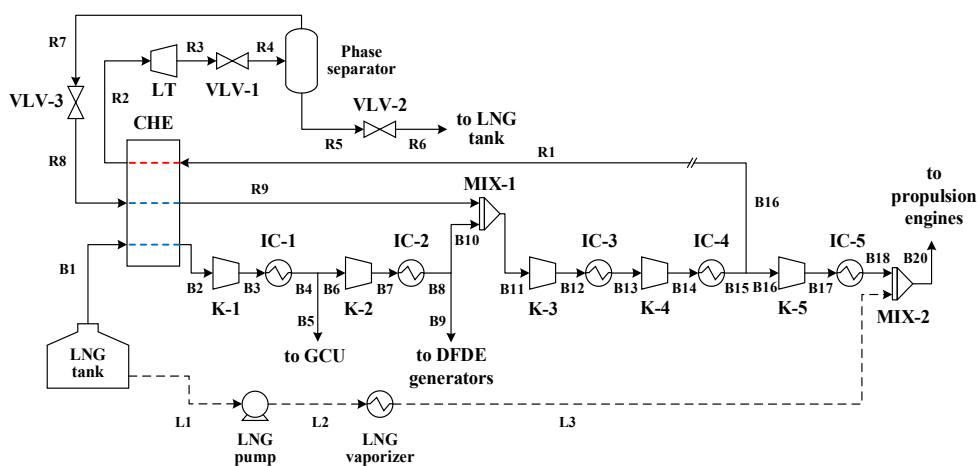
Figure 5.5 Process flow diagram for the fuel supply system with the HP mix LT-JT process.

Table 5.1 Design parameters for the fuel supply system.

Parameters	Unit	Value
Compressor isentropic efficiency	%	75
Liquid expander isentropic efficiency	%	75
Intercooler outlet temperature	°C	45
Intercooler Δp	bar	0.5
Heat exchanger ΔT_{min}	°C	3
Heat exchanger Δp	bar	0.03 - 1

5.3.2 BOG feed

The LNG stored in the cargo tanks is assumed to have a composition that gives a gross heating value within the acceptable range for the EU market [167]. This composition and other LNG conditions are shown in Table 5.2. The BOG supplied to the fuel supply system is expected to have higher temperature and lower pressure values than the stored LNG due to heat leaks and pressure drop through the cargo tanks and pipelines [158, 168] (see Table 5.3).

Regarding the amount of BOG, the calculation of the boil-off rate (BOR) of the LNG in the cargo tanks will require comprehensive CFD models since it is a complex function of the ambient temperatures (air and sea water), characteristics of the tanks (dimensions and thickness), and vessel movement [159]. Besides, the vaporization of the lighter components in the LNG will continue during voyages, making the LNG rich in heavier hydrocarbon components. The composition change in the stored LNG with time is known as the weathering (aging) process, and this also affects the vaporization mechanism and thus the amount and the composition of the BOG in the tank [157]. In industry, 0.1 to 0.15 vol % of stored LNG per day is known as a typical BOR for LNG vessels [56, 157, 158].

Table 5.2 The conditions of the stored LNG.

Parameters	Unit	Value
LNG composition		
Nitrogen	mol %	0.37
Methane	mol %	95.89
Ethane	mol %	2.96
Propane	mol %	0.72
n-Butane	mol %	0.06
LNG temperature	°C	-161.80
LNG pressure	bar	1.06
LNG density	kg/m^3	437.89
BOR	vol % / d	0.1

Table 5.3 The conditions of BOG from the storage tank.

Parameters	Unit	Value
BOG composition		
Nitrogen	mol %	0.48
Methane	mol %	99.49
Ethane	mol %	0.03
BOG temperature	°C	-120.00
BOG pressure	bar	1.03

Thus, a constant value of BOR is applied in this work to estimate the amount of BOG as seen in Table 5.2. With the given BOR, the amount of BOG can be calculated by

$$\dot{m}_{\text{BOG}} = r_{\text{BOR}} \cdot V_{\text{tank}} \cdot Lv_{\text{tank}} \cdot \rho_{\text{LNG}} \tag{5.1}$$

where r_{BOR} is the rate of boil-off, V_{Tank} is the total volume of the storage tanks, Lv_{Tank} is the average liquid level of the tanks in percentage, and ρ_{LNG} is the density of the LNG [169]. In

this work, a typical large size LNG carrier with membrane type storage tanks (a volume of 170,000 m3) is considered, and 95 vol % of the tanks are assumed to be filled with cargo. Thus, based on Eq. (5.1) , 2946.5 kg/h of BOG is thought to be generated during voyages. In the simulation model, a uniform heat input to the storage tanks was assumed to produce the given amount of BOG, and the corresponding composition is shown in

.Products

Two DFDE generators are assumed to be operated at 50 % load to produce 4000 kW to supply the electricity needed on the LNG vessel. The specific fuel oil consumption (SFOC) with gas fuel operation is 7671 kJ/kWh for the generators from the reference model by assuming an intermediate engine load with power production [170]. For the engines, the MAN Diesel & Turbo 5G70 model is considered to deliver the power output of 9938 kW for an intermediate speed voyage, and the SFOC is assumed to be 6280 kJ/kWh [160]. The required mass flow rates of fuel to the engines for electricity production and propulsion power are then obtained from Eq. (5.2).

$$\dot{m}_{fuel} = \frac{P_{engine} \cdot SFOC_{engine}}{LHV_{fuel}} \qquad (5.2)$$

where P_{engine} and $SFOC_{engine}$ are the power requirement and the SFOC of the engines, and LHV_{fuel} is the lower heating value (LHV) of the two fuels. Except for the reference fuel supply system, the mass flow rates of the two fuels will vary since the LHV depends on the composition, which is changing due to the recycled BOG and its liquefaction ratio.

The re-liquefied BOG is throttled to 2.5 bar, and the two-phase stream is sent to the LNG cargo tanks. Thus, the vapor product is mixed with the BOG produced in the storage tanks and recycled to the fuel supply system. The pressure level of the BOG extracted for the GCU is specified to 3.5 bar in order to overcome pressure drops in pipelines and auxiliary equipment [60, 160]. Table 5.4 indicates other conditions for the fuels and re-liquefied BOG applied in this chapter.

Table 5.4 Specifications of the products.

Parameters	Unit	Value
DFDE fuel temperature	°C	45
DFDE fuel pressure	bar	11.5
DFDE fuel mass flow rate[a]	kg/h	621
Propulsion fuel temperature	°C	45
Propulsion fuel pressure	bar	300
Propulsion fuel mass flow rate[a]	kg/h	1262
Re-liquefied BOG pressure	bar	2.5
BOG pressure for GCU	bar	3.5

[a]Only for the reference fuel supply system.

5.4 Economic analysis and optimization

5.4.1 LNG price and BOG loss

Initially, the LNG price is set to 5 USD/MMBtu (1MMBtu = 1055 MJ) by assuming that the LNG carrier sails from the US to Spain [171]. This price is used to estimate the economic loss of the BOG burned in the GCU. The amount of BOG wasted will differ based on the voyage status of the LNG carrier. During voyages, the BOG will be used for the engines, and the rest is sent to the GCU. During the unloading of the cargo at an import terminal, it is assumed that only the DFDE is operated and the surplus of the BOG is burned. Thus, for the estimation of the amount of BOG burned in a year, the voyage schedule is considered as seen in Table 5.5. In this chapter, an annual vessel operation with 12 cycles is considered.

5.4.2 Cost evaluation

The total annual cost (TAC) is estimated [112] for the reference fuel supply system and the other configurations with BOG liquefaction in order to evaluate the economic advantage of the

Table 5.5. The voyage schedule of the LNG vessel.

Parameters	Unit	Value
Voyage speed	kts	15.5
Voyage	d/cycle	12
Unloading	d/cycle	0.5
Number of cycles	cycles/yr	12

additional liquefaction facilities. The TAC consists of the annual total capital investment (ATCI), the annual total operating cost (ATOC), and the cost related to the annual BOG losses as seen in Eq. (5.3).

$$TAC = ATCI + ATOC + C_{\text{BOG loss}} \tag{5.3}$$

Regarding the ATCI, an LNG vessel is assumed to operate for 20 years [172], and an annual interest rate of 10 % is applied to estimate the annual investment cost for the equipment.

$$ATCI = TCI \cdot \left(\frac{i(1+i)^n}{(1+i)^n - 1} \right) \tag{5.4}$$

where i is the annual interest rate and n is the service life of the vessel. The total capital investment (TCI) is defined by Eq. (5) where Q is the set of units in the system.

$$TCI = F_{\text{Ext}} \cdot \sum_j C_P^j \cdot F_{BM}^j, \qquad j \in Q \tag{5.5}$$

C_P^j represents the purchased cost of equipment j, and F_{BM}^j is the factor for bare module costs related to operating pressure, material and installation of equipment j. The factor for bare module cost is listed in Table 5.6. Extra cost is also considered in estimation of TCIs by applying a factor (F_{Ext}), which is assumed to be 1.18 [31].

Table 5.6. Coefficients for capital cost calculation [112].

Equipment	F_{BM}	K_1	K_2	K_3
Compressor	7	2.29	1.36	-0.10
Liquid Turbine	6.2	2.25	1.50	-0.16
Heat exchanger	4.3	4.67	-0.16	0.15
Intercooler	3.3-8.8	2.77	0.73	0.08
Phase separator	10.3-36.9	3.50	0.45	0.11

The purchased cost is a function of the capacity of units (A) as shown in Eq. (5.6) [112]. The coefficients (K_1, K_2, K_3) for the cost function are shown in Table 5.6 for various process equipment.

$$\log_{10} C_P^j = K_1 + K_2 \log_{10} A + K_3 (\log_{10} A)^2 \tag{5.6}$$

As indicated in Eq. (5.7), the fixed cost, the maintenance cost and the cost for supplies are estimated as a fraction of the ATCI (F_{CTO}), while the utility cost is calculated from the electricity price (v_e) for total power consumption in compressors and the cooling water price (v_{CW}) for the cooler duties. In this work, f_{CTO} is assumed to be 0.066 [112].

$$ATOC = F_{CTO} \cdot ATCI + \left(v_e \sum P_{comp} + v_{CW} \sum D_{CW} \right) \tag{5.7}$$

The annual cost for BOG loss is represented by Eq. (5.8) where the sum of the annual BOG loss during voyages and unloading is considered based on the voyage schedule.

$$C_{\text{BOG loss}} = v_{LNG} \cdot N_{\text{cycle}} \cdot \left(L_{\text{BOG}}^{\text{voyage}} \cdot t_{\text{voyage}} + L_{\text{BOG}}^{\text{unloading}} \cdot t_{\text{unloading}} \right) \tag{5.8}$$

5.4.3 Optimization

The reference fuel supply system and its modifications with BOG liquefaction were optimized applying the same optimization formulation for a fair comparison. The optimization studies were performed to minimize the TAC with the decision variables **x** as seen in Eq. (5.9).

$$\min_{\mathbf{x}} f(\mathbf{x}) = TAC$$

$$\text{subject to} \quad \Delta T_{\text{min,CHE}} \geq 3$$

$$\Delta p_{\text{VLV-1}} \geq 0$$

$$x_{\text{LT,out}}^{\text{vap}} = 0 \qquad\qquad (5.9)$$

$$1.5 \leq Pr_{\text{K-5}} \leq 4$$

$$\mathbf{x}_{LB} \leq \mathbf{x} \leq \mathbf{x}_{UB}$$

The outlet pressure of the first compressor was fixed to meet the pressure requirement for the BOG stream sent to the GCU. The discharge pressures of the second and fifth compressors were specified to meet the fuel pressure requirements for the DFDE and the propulsion engines. The system was optimized by varying the pressure ratio of only the third and fourth compressors from 1.5 to 4, considering practical issues [141]. To avoid a high pressure ratio of compressor K-5 due to low discharge pressure of the fourth compressor (K-4), the ratio was constrained to be below 4.

The precooling temperature of the recycled BOG and the outlet pressure of valve VLV-1 were also manipulated as decision variables. Besides, the mass flow rate of the BOG sent to the GCU was selected as a key variable, which will affect the capacity of the liquefaction facility and its cost. The upper bound of the variable was set to the BOG flow rate supplied to the GCU in the reference system.

If the system contains an LT, the outlet pressure of the turbo-machinery was also included as a variable in the optimization formulation. The vapor fraction of the outlet stream from the LT

was constrained to zero to avoid efficiency drop due to vapor production in the turbo-machinery [173, 174]. Since there is an overlap in the ranges for the variables of the outlet pressures between the LT and the JT device (VLV-1), the pressure drop through the valve was restricted to be larger than zero. A minimum temperature difference of 3 K in the cryogenic heat exchanger was also applied to constrain the processes, which is the value that reflects a balanced trade-off between capital and operating cost of the system [86, 140].

The optimization was performed by the particle swarm optimization (PSO) algorithm. PSO is a derivative-free stochastic algorithm based on candidate solutions (particles), thus it is suitable for black box functions where derivative information is either not available or noisy and costly if finite differences are considered [175, 176]. The optimization results for the fuel supply systems are shown in Table 5.7.

Table 5.7. Bounds for the decision variables and the best solutions obtained.

Variable	Unit	LB	UB	Optimal value					
				Reference	JT	LT-JT	LP mix LT-JT	IP mix LT-JT	HP mix LT-JT
$\dot{m}_{GCU}$	kg/h	0.0	1070.4	1070.4	0.0	0.0	0.0	0.0	0.0
$Pr_{K\text{-}3}$	-	1.5	4.0	3.8	3.9	3.8	3.9	3.9	3.9
$Pr_{K\text{-}4}$	-	1.5	4.0	3.1	3.1	3.1	3.2	3.1	3.3
p_{R3}	bar	5.0	60.0	-	-	7.9	7.7	8.7	12.0
p_{R4}	bar	2.5^a	20.0	-	2.5	2.5	2.5	4.0	12.0
T_{R2}	°C	-122.0	-60.0	-	-119.6	-120	-120.2	-117.4	-117.2

^{a}4.0 for the LP mix LT-JT process and 12.0 for the HP mix LT-JT process.

5.5   Results

5.5.1   Comparison of process options

In this section, the simulation and optimization results for the liquefaction processes using the JT cycle and its variations are addressed and compared with the reference system. Table 5.8

indicates that the fuel supply systems with BOG liquefaction have a smaller total annual cost than the reference process. Although the TCI is increased by at least 2.34 million USD when the BOG liquefaction is included in the fuel supply system, the TAC is reduced by at least 9.4 % compared to the reference scheme. Therefore, with an LNG price of 5 USD/MMBtu, an additional BOG self re-liquefaction facility in the fuel supply system will provide a larger profit than the reference system.

Due to the additional equipment and the increase in compression power, the ATCI and the ATOC of the fuel supply systems with BOG liquefaction are more than the double compared to the reference configuration. The main contributor to the cost increment is the extra compression power and the additional heat exchanger for the liquefaction of BOG. However, the liquefaction systems managed to recover almost all the BOG wasted in the GCU in the reference process during voyages as seen in Table 5.8. Thus, the BOG losses in the fuel supply systems with BOG liquefaction only occur during unloading when all the BOG except for the fuel demand of the DFDE engine is burned in the GCU. Therefore, the loss of the cargo in the form of BOG through the GCU is decreased by 91.7 % compared to the reference system, thus compensating for the increased values of the ATCI and the ATOC in the liquefaction systems.

It is important to mention that the liquefaction ratios of the BOG condensation systems are less than one as seen in Table 5.8. This relatively low liquefaction ratio means that the BOG sent to the liquefiers do not need to be fully liquefied in order to prevent the BOG from being burned in the GCU. The result is liquefaction systems with smaller duty and TAC.

Regarding the configurations with BOG liquefaction, the systems with an LT require less TAC than the JT processes except for the HP mix LT-JT process. The addition of the turbo-machinery to the JT system (the LT-JT process) results in 2.4 % savings in the TAC. The reduction in TAC comes mostly from reduced compression power and reduced heat exchanger cold duty. As seen in Table 5.8, the liquefaction systems with an LT have a higher liquefaction ratio than the systems using JT valves only. This high liquefaction ratio leads to a smaller flow rate of the vapor product in the phase separator, which is mixed with the BOG from the storage tank. The reduction in flow rate of the process feed stream results in smaller duties for all the

Table 5.8. Optimization results with process performance parameters (LNG price = 5 USD/MMBtu).

		Unit	Reference	JT	LT-JT	LP mix LT-JT	IP mix LT-JT	HP mix LT-JT
Liquefaction ratio[a]		-	-	0.75	0.80	0.80	0.83	0.97
$\dot{m}_{LNG}$		kg/h	-	1063.34	1063.67	1063.70	1063.31	1062.92
$\dot{m}_{GCU}$		kg/h	1070.42	0.00	0.00	0.00	0.00	0.00
$\dot{W}_{comp}$		kW	511.09	1097.41	1071.33	1069.25	1055.61	1098.98
$\dot{W}_{LT}$		kW	-	0.00	8.59	8.57	8.61	9.10
$P_{specific}{}^{b}$		kWh/kg	-	0.46	0.44	0.44	0.44	0.46
MCH	$Duty$	kW	-	268.47	251.95	251.17	253.86	261.74
	UA	MW/°C	-	26.55	21.47	21.23	20.47	19.17
	$LMTD$	°C	-	10.11	11.74	11.83	12.40	13.65
	ΔT_{min}	°C	-	3.52	3.24	3.43	4.80	8.36
TCI		k$	2032.69	4509.45	4421.16	4413.08	4370.17	4467.56
ATCI	Compressor	k$/yr	234.16	421.75	414.34	413.74	409.84	422.19
	LT	k$/yr	-	-	3.98	3.97	3.99	4.26
	CHE	k$/yr	-	75.31	68.77	68.45	67.45	65.69
	Intercooler	k$/yr	4.60	16.93	16.53	16.50	16.35	16.92
	Separator	k$/yr	-	15.69	15.69	15.69	15.69	15.69
	Total	k$/yr	238.76	529.68	519.31	518.36	513.32	524.76
ATOC	Other[c]	k$/yr	134.16	297.63	289.56	289.03	289.19	311.57
	Net power	k$/yr	226.06	485.39	470.05	469.14	463.09	482.05
	Intercooler	k$/yr	2.10	6.86	6.65	6.64	6.56	6.85
	Total	k$/yr	362.31	789.87	766.27	764.81	758.84	800.47
BOG loss		k$/yr	948.69	78.83	78.83	78.83	78.83	78.83
TAC		k$/yr	1549.76	1398.38	1364.41	1362.00	1350.99	1404.06

[a]Liquid fraction of the phase separator inlet stream.

[b]The fraction of the total compression work related to recycled BOG mass flow rate divided by the final liquid product entering the storage tank.

[c]The fixed cost, the maintenance cost and the cost for supplies.

equipment in the systems, thus decreasing the ATCI and the ATOC. The small power production from the LT also helps to decrease the operating cost.

It is noticeable that the processes with an LT have increased $LMTD$ values in the CHE compared to the JT system. Although the increase in the $LMTD$ value causes larger entropy generation and lower thermodynamic efficiency of the system, it decreases the UA value and the capital cost of the exchanger.

In summary, the LT based liquefaction facilities have lower or equal specific power consumption of BOG reliquefaction compared to the JT process, indicating that they are able to improve the process thermodynamic efficiency, even with an increased $LMTD$ value. Therefore, the liquefaction systems with an LT result in better trade-off points where the benefit from decreasing the UA value is larger than the penalty of the increased $LMTD$ value.

Regarding the variations of the LT based systems, the LP mix LT-JT configuration shows a marginal decrease in TAC compared to the LT-JT process. The mixing of the BOG from the tank and the vapor product from the phase separator increases entropy generation in the mixer (MIX-1) due to the large temperature difference of the streams. In contrast, the LP mix LT-JT system mixes the two cold streams after they pass through the CHE. The mixing at the CHE outlet decreases the entropy generation in the mixer as the streams have almost the same temperature. Although the economic improvement is minor, the smaller entropy generation reduces the compressor work.

The IP mix LT-JT system also shows some savings in the TAC compared to the LT-JT process. As mentioned in Section 2.3, the vapor stream from the phase separator by-passes the first stage compressor and intercooler and is supplied to the second compressor. This simple modification leads to a reduction in the duty of the compressor and the intercooler. Thus, these units have the smallest capital cost compared to other system options.

In contrast to other LT based processes, the HP mix LT-JT system has a larger TAC than the LT-JT system. As seen in Table 5.7, the optimization results of the high pressure mixing configuration indicate that it has a throttling pressure of 12 bar. This high depressurization

pressure results in a phase separator with marginal vapor product, as it can be observed by the liquefaction ratio of 0.97 for the HP mix LT-JT system in Table 5.8. As a result, this system eventually has almost the same characteristics as the LT-JT process without the vapor stream from the phase separator. Thus, the optimization work performed for the HP mix LT-JT system is similar to the work done for the LT-JT process, however with a reduced lower bound for the throttling pressure, which is constrained to the discharge pressure of the second compressor. The limited bound of the outlet pressure of the JT valve (VLV-1) leads to sub-optimal solutions for the configuration, resulting in larger TACs with higher specific power consumption for LNG production in the HP mix LT-JT system (see Table 5.8).

The configurations used in the LP and IP mix LT-JT systems are also advantageous even when the liquid turbine is unavailable as seen in Table 5.9. Without the LT, the LP and IP mix configurations can achieve noticeable savings in TAC compared to the basic JT system. In addition, the IP mix JT process even has a TAC close to the cost for the LT-JT system. Therefore, the IP mix JT configuration is a promising alternative to BOG liquefaction systems with an LT if the reliability of the turbo-machinery is not sufficiently high.

Table 5.9. The optimization result of the LP, IP and HP mix JT processes.

Parameter	Unit	JT	LT-JT	LP mix JT	IP mix JT	HP mix JT
TAC	k$/yr	1398.38	1364.41	1395.72	1366.65	1428.21

5.5.2 Sensitivity analysis

LNG price is an important parameter when evaluating the economics of the fuel supply systems for LNG vessels. The price is directly linked to the BOG burned in the GCU as a loss of the cargo. To measure the effect on the process, sensitivity analysis is performed with varying LNG price from 2 to 8 (USD/MMBtu). Not surprisingly, Figure 5.6 indicates that the TAC of the reference system increases with the LNG price. The configuration and operating conditions of the reference process are not affected by the price during optimization, and the TAC is changed only due to the economic loss of the BOG wasted in the GCU. Detailed cost evaluation

based on the LNG price is listed in Table 5.10. Thus, the economics of the reference fuel supply system is sensitive to the LNG price as the process always burns a significant amount of BOG all the time. If the LNG price increases from 2 to 8 USD/MMBtu, the TAC of the reference system is more than doubled.

In contrast, the fuel supply systems with BOG liquefaction are less sensitive to the LNG price as illustrated in Figure 5.6. All the liquefaction schemes show some increase in their TAC from 2 to 4 USD/MMBtu. However, they only have marginal increase in the TAC from 4 to 8 USD/MMBtu. As indicated in Table 5.11, the optimization results for LNG prices equal to or greater than 4 USD/MMBtu show that the liquefaction facilities have been optimized to have almost no BOG burned in the GCU. Thus, BOG losses only occur during unloading, which is the reason for the minor increase in the TAC from 4 to 8 USD/MMBtu.
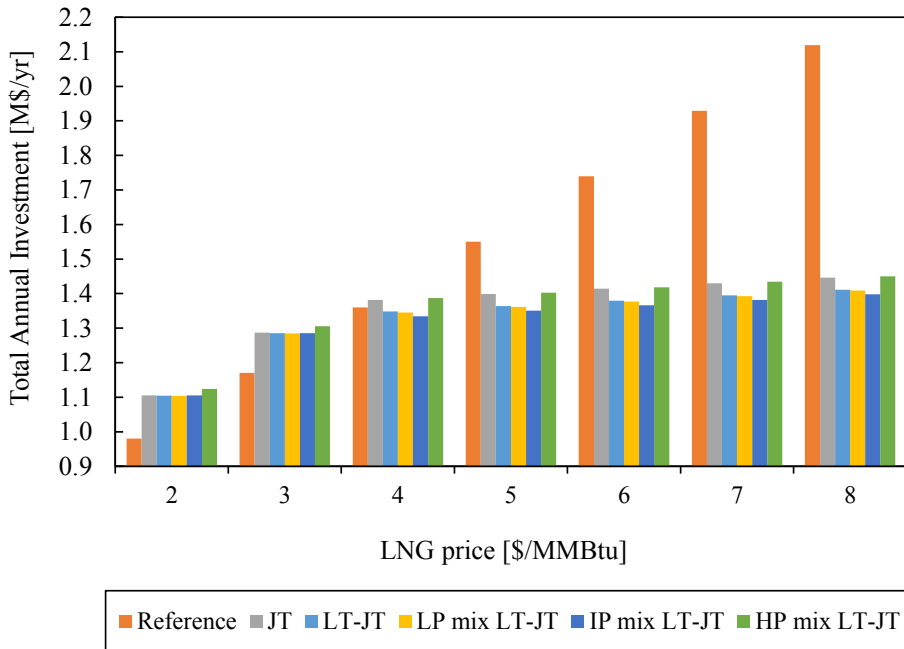
Figure 5.6 Total annual cost as function of LNG price.

Table 5.10 Cost breakdown of fuel supply systems as function of LNG price

System	2 $/MMBtu					3 $/MMBtu					4 $/MMBtu				
	TCI	ATCI	ATOC	BOG	TAC	TCI	ATCI	ATOC	BOG	TAC	TCI	ATCI	ATOC	BOG	TAC
Reference	2033	239	362	379	981	2033	239	362	569	1170	2033	239	362	759	1360
JT	2678	315	425	366	1105	2698	317	432	538	1287	4404	517	768	97	1382
LT-JT	2679	315	425	365	1105	2708	318	434	533	1285	4418	519	766	63	1348
LP mix LT-JT	2676	314	425	365	1104	2707	318	434	532	1284	4411	518	765	63	1346
IP mix LT-JT	2674	314	426	365	1105	2714	319	438	528	1285	4369	513	759	63	1336
HP mix LT-JT	2679	315	444	365	1124	2704	318	452	535	1305	4470	525	800	63	1388

System	5 $/MMBtu					6 $/MMBtu					7 $/MMBtu				
	TCI	ATCI	ATOC	BOG	TAC	TCI	ATCI	ATOC	BOG	TAC	TCI	ATCI	ATOC	BOG	TAC
Reference	2033	239	362	949	1550	2033	239	362	1138	1739	2033	239	362	1328	1929
JT	4509	530	790	79	1398	4509	530	790	95	1414	4509	530	790	110	1430
LT-JT	4418	519	766	79	1364	4418	519	766	95	1379	4418	519	766	110	1395
LP mix LT-JT	4411	518	765	79	1362	4411	518	765	95	1378	4411	518	765	110	1393
IP mix LT-JT	4369	513	759	79	1351	4369	513	759	95	1367	4369	513	759	110	1383
HP mix LT-JT	4470	525	800	79	1404	4470	525	800	95	1420	4470	525	800	110	1435

System	8 $/MMBtu				
	TCI	ATCI	ATOC	BOG	TAC
Reference	2033	239	362	1518	2119
JT	4509	530	790	126	1446
LT-JT	4418	519	766	126	1411
LP mix LT-JT	4411	518	765	126	1409
IP mix LT-JT	4369	513	759	126	1399
HP mix LT-JT	4470	525	800	126	1451

Table 5.11. Mass flow rates of the LNG product and the BOG sent to the GCU for different LNG prices.

LNG price [$/MMBtu]	Reference		JT		LT-JT		LP mix LT-JT		IP mix LT-JT		HP mix LT-JT	
	$\dot{m}_{LNG}$	$\dot{m}_{GCU}$	$\dot{m}_{LNG}$	$\dot{m}_{GCU}$	$\dot{m}_{LNG}$	$\dot{m}_{GCU}$	$\dot{m}_{LNG}$	$\dot{m}_{GCU}$	$\dot{m}_{LNG}$	$\dot{m}_{GCU}$	$\dot{m}_{LNG}$	$\dot{m}_{GCU}$
2	0	1070	40	1030	45	1025	45	1025	45	1025	43	1027
3	0	1070	63	1007	73	997	75	995	83	987	69	1001
4	0	1070	1015	55	1064	0	1064	0	1063	0	1063	0
5	0	1070	1063	0	1064	0	1064	0	1063	0	1063	0
6	0	1070	1063	0	1064	0	1064	0	1063	0	1063	0
7	0	1070	1063	0	1064	0	1064	0	1063	0	1063	0
8	0	1070	1063	0	1064	0	1064	0	1063	0	1063	0

For LNG prices below 4 USD/MMBtu, all the liquefaction processes increase the amount of BOG wasted in the GCU with decreasing LNG price, as seen in Table 5.11. The increase in the burned BOG results in reduced liquefaction requirements in the systems (i.e. smaller LNG production from BOG).

Thus, when the LNG price is below 4 USD/MMBtu, the configurations with BOG liquefaction are optimized to considerably reduce LNG production, since the economic benefit from smaller equipment sizes related to reduced liquefaction demand overcomes the cost of larger BOG losses. Therefore, if the LNG price is below 4 USD/MMBtu, liquefaction of BOG is less attractive than simply burning it, at least from an economic point of view.

It should also be noticed that although the optimization of all configurations with BOG liquefaction systems try to decrease the TAC by minimizing the LNG production for LNG prices below 4 USD/MMBtu, they all have higher annual cost compared to the reference system. The larger number of units is the main reason for the higher TAC. Even though the capacity of the units is minimized, the fixed charge term of the purchased cost (coefficient K1 in Eq. (6)) adds considerably to the total investment cost. Other equipment related costs such as maintenance and supplies will also contribute to the larger TAC.

For LNG prices above 4 USD/MMBtu, the fuel supply systems with BOG liquefaction will have lower total annual cost than the reference process. The LT based systems, except for the HP mix configuration, will be more economical than the reference process from slightly below 4 USD/MMBtu. Other liquefaction schemes are profitable compared to the reference system when the LNG price is above 4 USD/MMBtu. The higher TAC of the reference process than the configurations with BOG liquefaction are mainly caused by the increase in BOG losses, which are proportional to the LNG price. Therefore, there are economic benefits from liquefaction facilities on LNG carriers when the LNG price is higher than 4 USD/MMBtu.

Among the fuel supply systems with BOG liquefaction, the IP mix LT-JT configuration is the most economic to be used on LNG ships when the LNG price is higher than 4 USD/MMBtu, and it is followed by the LP mix LT-JT and the LT-JT configurations. The JT and the HP mix LT-JT systems have similar TACs, which are larger than the other LT based processes. This is the same trend as observed with a fixed LNG price of 5 USD/MMBtu in Section 5.1. However, if the LNG price drops to 2 or 3 USD/MMBtu, all configurations with liquefaction facilities have almost identical TACs except for the HP mix LT-JT system. The minimized LNG production and reduced equipment sizes in the processes weaken the characteristics of each configuration. In the case of the HP mix LT-JT process, the restricted throttling pressure causes sub-optimal operating conditions, giving a larger TAC than for other liquefaction systems.

5.6 Conclusions

For an LNG vessel propelled by the high pressure gas injection engines, a reference fuel supply system and its variations with BOG liquefaction based on the Joule-Thomson (JT) cycle were optimized and compared. Total annual cost was selected as the objective function for the optimization in order to evaluate the economic benefit of the additional liquefaction facilities compared to the reference system.

With an LNG price of 5 USD/MMBtu, the optimization results indicate that the reliquefaction systems employed on the vessel improve the economics of the LNG carrier with lower TAC

values than the reference configuration, saving at least 9.4 % of the TAC. The relatively simple structure of the liquefaction processes results in a marginal increase in capital cost while minimizing cargo loss, making the additional facilities economically profitable on LNG carriers. The use of a liquid turbine (LT) and the simple structure modifications lead an even smaller TAC value of the liquefaction systems.

The sensitivity analysis with different LNG prices indicates that the installation of the liquefaction systems on LNG carriers is profitable compared to the reference process when the LNG price is above 4 USD/MMBtu. Compared to the liquefaction processes, the reference fuel supply system with an LNG price of 8 USD/MMBtu even results in at least 46 % point increase in the TAC value due to the high cost of the BOG loss in the GCU. However, if the LNG price is below 4 USD/MMBtu, the reference fuel supply system will be superior to the configurations with BOG liquefaction since the BOG losses have a small impact on the economics of the LNG vessel compared to the additional capital investment, which is the major concern of the liquefaction systems. In conclusion, the optimal design of the fuel supply system for LNG carriers will be dependent on the LNG price.

Chapter summary

o The small-scale LNG processes have important design criteria such as the liquefaction capacity (equipment size) and the loss of product, which cannot be evaluated by energy efficiency.

o Therefore, cost analysis is essential for the design of the small capacity systems to evaluate not only the liquefaction performance but also the economic feasibility of the sub-system in the total process.

Chapter 6　　Exergy analysis for LNG value chain: LNG processes

In previous chapters, LNG systems were only evaluated by energy or cost analysis. Exergy efficiency is also a widely used post design tool to measure the thermodynamic performance of cryogenic processes. Unfortunately, a number of exergy efficiencies have been proposed in literature with different definitions. In addition, most existing exergy efficiencies have not been developed to handle sub-ambient processes. Thus, in this chapter, different exergy efficiencies are tested to answer the following questions:

- o What is the most suitable type of exergy efficiency to be used as the basis of objective performance comparison?
- o What is the requirement for the exergy efficiency to measure the performance improvement of complex LNG processes, having changes in temperature, pressure and composition?
- o How to extend the previously developed *ETE* from our group to systems with changes in composition?

This chapter is based on the following publications.

– Kim D, Gundersen T. Development and use of exergy efficiency for complex cryogenic processes. Energy Conversion and Management. 2018;171:890-902.

6.1   Introduction

With the current focus on global warming and the use of fossil fuels, energy efficiency is an important performance measure in industrial plants. As a post-design tool, energy efficiency has been applied to various energy systems in order to evaluate and compare them, thus finding opportunities to improve the processes. Such definitions of energy efficiency are case-dependent based on the characteristics of a process, which means a general mathematical expression for energy efficiency does not exist [177]. This may bring misinterpretations into the definitions of energy efficiency and produce inconsistent results even for the same system. Thus, there is a need for an objective performance parameter for energy conversion efficiency. Another limitation of using energy efficiency is that it does not take energy quality into account when measuring process performance. Different energy forms have different qualities, for example, the value of heat cannot be directly compared with the value of power because the energy quality of the heat will vary, depending on the temperature level. In the case of refrigeration processes where work is transformed into a cooling duty, there is no proper definition for energy efficiency [95]. Instead, a coefficient of performance is used, which unfortunately gives equal values to heat and power.

Unlike energy analysis, exergy accounts for both quantity and quality of various energy forms, which is why exergy has been recommended as a measure of system performance [178]. Due to the characteristics of entropy generation below ambient temperature, exergy efficiency is a good performance indicator, especially for low temperature processes in a post-design phase. Regarding liquefied natural gas (LNG), specific power consumption per produced amount of LNG is widely used to evaluate the performance of liquefiers, since there is no proper energy efficiency definition for such processes. However, this value does not consider the cold energy of the produced LNG. The LNG generally contains a significant amount of cold exergy (around 1000 kJ/kg), and this exergy is utilized in many LNG terminals [179]. Thus, the cold energy of the produced LNG has to be included when measuring the performance of the liquefaction process. In addition, the specific power consumption will depend on local environmental conditions (i.e. climate). An LNG plant located in a warm climate region will always show a

larger power consumption than one in cold climate, even when they have exactly the same processing system. In contrast, exergy can represent various energy forms in one standard (i.e. heat, work and power), while considering the effect of the environment conditions, particularly temperature and pressure. Therefore, exergy efficiency would be a good candidate to measure the performance of processes in order to have an objective and consistent analysis.

Such an exergy efficiency can be formulated in various ways, but tends to fall into two main categories [177]. One is the input-output efficiency, which is the ratio between the exergy leaving and entering the system. The input-output efficiency is defined by a simple formulation and applicable to any types of processes, thus widely used [180]. Yet, this efficiency definition may not be ideal for process evaluation and comparison [94, 180-183]. The input-output efficiency may show only a marginal difference with changes in process performance, since it is not focusing on the task of a process. Thus, there have been various suggestions for exergy efficiency, considering the purpose of a system [183-188]. These are called the consumed-produced or task efficiencies, which is the second category of exergy efficiency. The consumed-produced efficiency describes what is consumed to deliver a specific or targeted product from a process.

Nevertheless, it is difficult to determine which efficiency definition is the right one to use due to their inconsistent results for a typical process. Several definitions of the consumed-produced efficiency suggested in the literature do not contain general mathematical expressions, thus causing room for different interpretations [96]. This has resulted in different definitions of exergy efficiency for the same system, from small units to large systems such as Joule Thomson valves, gas expanders, air separation units (ASUs), LNG processes and processes for offshore platforms [67, 89, 91, 95, 180, 189-193]. Thus, there have been attempts to develop more generalized task efficiencies by removing so-called transit exergy from consideration, which is defined as the amount of exergy that is preserved across a system [187]. However, this definition requires a high calculation effort. Zanchini also formulated an exergy efficiency that can generalize some of the task efficiencies, while being applicable for both flowing and non-flowing systems [191]. Nguyen et al. suggested an efficiency for offshore platforms, which can

cover various processes with decomposition of exergy to the chemical component level [94]. None of the efficiencies mentioned above have explicit definitions for cases where processes operate across or below ambient temperature.

Thus, a new general exergy efficiency, the Exergetic Transfer Effectiveness (ETE) was developed to handle all operating conditions with less computational effort by defining exergy sources and sinks as consumed and produced exergy [194]. The ETE also allows encapsulating the actual transfer of exergy in a process, indicating the purpose of the system. Such careful definition is achieved by focusing on the effect of temperature and pressure changes, and by decomposing exergy into different forms.

However, the use of the ETE has so far been limited to processes without chemical reactions or compositional changes, simply because the decomposition of exergy forms to identify sources and sinks had not been developed to include chemical exergy. Thus, this chapter extends the ETE by including chemical exergy to cover all types of processes at all operating conditions with a general mathematical expression. The extended ETE and other consumed-produced efficiencies are then thoroughly classified and compared, indicating the characteristics of the efficiency definitions. This chapter also compares the ETE with the input-output efficiency and selected task efficiencies, where generalized formulas have been suggested.

The comparison is conducted by applying them to a natural gas liquefaction process referred to as the dual mixed refrigerant (DMR) process. The DMR process is a good candidate to study the capability of exergy efficiencies to manage changes in temperature, pressure and chemical composition. This comparison of exergy efficiencies will provide guidance about a proper choice of exergy efficiency based on their characteristics (classification). The mathematical optimization of the DMR process is also performed to evaluate exergy efficiencies for the optimal operating conditions. Although exergy efficiency is a post design tool to measure the improvement of systems, the comparison of the efficiency values for the initial and the optimal operating conditions have not been made in previous literature. Thus, this chapter conducts the

comparison in order to evaluate the performance of exergy efficiencies whether they properly reflect the improvement of the process after optimization.

6.2 Exergy

Exergy is the maximum available work obtained by bringing a system to equilibrium with its environment [195]. Thus, it is a function of both the state of the system and its environment. However, there are various exergy classifications suggested with different exergy forms [194]. Thus, in this work, the classification suggested by Marmolejo Correa and Gundersen is used with further decomposition of exergy [96].

Based on the classification, exergy of a material stream flowing through a system can be expressed by two components, thermo-mechanical exergy ($\dot{E}^{TM}$) and chemical exergy ($\dot{E}^{Ch}$) as seen in Eq. (6.1) [187]. This will be referred to as the *first level* of exergy decomposition. Due to the nature of the processes studied, kinetic, potential, electrical and nuclear exergies are not considered.

$$\dot{E}^{Total} = \dot{E}^{TM} + \dot{E}^{Ch} \tag{6.1}$$

Thermo-mechanical exergy represents the available work obtained from the material stream by bringing it from its original state to its environment temperature (T_0) and pressure (p_0) through reversible processes and is given by:

$$\dot{E}^{TM} = \dot{H}(T, p) - \dot{H}(T_0, p_0) - T_0[\dot{S}(T, p) - \dot{S}(T_0, p_0)] \tag{6.2}$$

Thermo-mechanical exergy, also referred to as physical exergy in various literature [182, 183, 195], can be further decomposed to temperature based exergy ($\dot{E}^{T}$) and pressure based exergy ($\dot{E}^{p}$) as seen in Eq. (6.3). These terms indicate the temperature and pressure portions of the available work ($\dot{E}^{TM}$), respectively. Similar to thermo-mechanical exergy, temperature based

exergy and pressure based exergy can be defined by Eq. (6.4) and Eq. (6.5). This decomposition is not unique, thus it does not have a specific physical meaning. Nevertheless, it has proven advantageous when analyzing processes.

$$\dot{E}^{\text{TM}} = \dot{E}^{\text{T}} + \dot{E}^{\text{p}} \tag{6.3}$$

$$\dot{E}^{\text{T}} = \dot{H}(T,p) - \dot{H}(T_0,p) - T_0[\dot{S}(T,p) - \dot{S}(T_0,p)] \tag{6.4}$$

$$\dot{E}^{\text{p}} = \dot{H}(T_0,p) - \dot{H}(T_0,p_0) - T_0[\dot{S}(T_0,p) - \dot{S}(T_0,p_0)] \tag{6.5}$$

Chemical exergy is the reversible work obtained by bringing the material stream with environment temperature and pressure to equilibrium with the chemical composition of the environment. Thus, chemical exergy is independent of the temperature and pressure level of the material stream. Similar to thermo-mechanical exergy, chemical exergy has two parts, referred to as compositional exergy ($\dot{E}^{\text{Comp}}$) and reactional exergy ($\dot{E}^{\text{Reac}}$) as introduced in Eq. (6.6).

$$\dot{E}^{\text{Ch}} = \dot{E}^{\text{Comp}} + \dot{E}^{\text{Reac}} \tag{6.6}$$

Compositional exergy indicates the work required to separate a mixture into pure chemical components(i) as seen in Eq. (6.7). The value of compositional exergy for mixtures is negative due to the interactions between chemical components in real gases and the work needed to increase the partial pressure of each component separated from the mixture to environment pressure. For ideal gases and ideal mixtures, only the latter will remain in the expression for compositional exergy. Compositional exergy is also referred to as mixing exergy since it represents the reduction in exergy due to mixing pure components [181, 196].

$$
\begin{aligned}
\dot{E}^{\text{Comp}} &= \dot{H}(T_0,p_0) - \sum_i x_i \dot{H}_i^{\text{pure}}(T_0,p_0) - T_0\big[\dot{S}(T_0,p_0) - \sum_i x_i \dot{S}_i^{\text{pure}}(T_0,p_0)\big] \\
&= RT_0 \sum_i \dot{n}_i \ln x_i \ \text{ for ideal gas and ideal mixture}
\end{aligned}
\tag{6.7}
$$

For reference species in the environment, reactional exergy is the reversible work obtained from a pure component stream at T_0 and p_0 by bringing it to the partial pressure of the component in the environment (Eq. (6.8)). Thus, the value of reactional exergy for reference species depends on the concentration of the species in the environment. In Eq. (6.8), $\bar{e}_{i,0}^{\text{Chem}}$ stands for the standard chemical exergy of component i at ambient conditions. In this work, the reference species and concentrations were implemented from Szargut to calculate molar reactional exergy of a pure component, which is also referred to as the standard chemical exergy [197]. The standard chemical exergy for species not present in the environment will be calculated by an extra step, which is a reversible reaction to convert the non-reference components to reference components.

$$\dot{E}^{\text{Reac}} = \Sigma x_i \dot{n}_i \bar{e}_{i,0}^{\text{Chem}} \tag{6.8}$$

Then, the four components of exergy ($\dot{E}^{\text{T}}, \dot{E}^{\text{p}}, \dot{E}^{\text{Comp}}, \dot{E}^{\text{Reac}}$) are regarded as the *second level* of exergy decomposition. Finally, these exergy components can be further decomposed to the chemical component level in a mixture by performing numerical calculations, and this will be referred to as the *third level* of exergy decomposition in this chapter. The partial molar exergy can be determined by Eq. (6.9) where EX is the set of exergy components in the *second level* decomposition. Figure 6.1 shows an overview of exergy decompositions defined and used in this work. Based on this decomposition of exergy, various definitions of exergy efficiency can be categorized in the next section.

$$\bar{e}_i^m = \left(\frac{\partial \dot{E}_{\text{mixture}}^m}{\partial \dot{n}_i} \right)_{T,p,\dot{n}_{l \neq i}}, \quad m \in \text{EX} \tag{6.9}$$

Apart from the exergy carried by a process stream, heat can also flow into a system, having an exergy value as seen in Eq. (6.10).

$$\dot{E}^{\text{Q}} = \dot{Q} \times \left(1 - \frac{T_0}{T} \right) \tag{6.10}$$
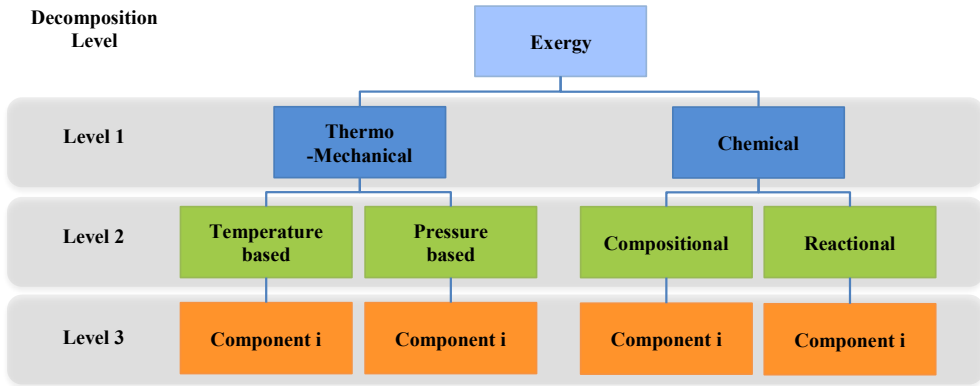
Figure 6.1 Decomposition of exergy for a material stream.

In this chapter, the exergy of heat ($\dot{E}^Q$) is also included in the definitions of exergy efficiency in the next section in order to handle systems with heat input and output although it is not the case for the process candidate evaluated by the exergy efficiencies in this chapter.

Use of an efficiency parameter helps to evaluate and compare processes with different operating conditions and configurations. For an objective comparison, applying an efficiency definition containing an explicit expression is essential to achieve consistent results as a performance parameter. Efficiencies having ambiguous definitions will leave room for different interpretations when applied to the same process.

Thus, for exergy efficiency, several definitions have been suggested with general mathematical expressions for the sake of consistency [94, 187, 194]. Such generalized equations for the definitions allow handling all types of processes that are experiencing changes in both thermo-mechanical and chemical exergies. Therefore, the following generalized exergy efficiencies were selected and compared as performance indicators in this chapter in order to evaluate their accuracy and consistency for a complex process.

6.3   Generalized exergy efficiencies

6.3.1 Input-output exergy efficiency

One of the generalized exergy efficiencies can be classified as the input-output efficiency. This efficiency is expressed as the ratio between all the exergy leaving and entering the system as seen in Eq. (6.11).

$$\eta_{\text{in}-\text{out}} = \frac{\sum \text{Exergy out}}{\sum \text{Exergy in}} \tag{6.11}$$

The input-output efficiency is regarded as a reasonable performance parameter for systems having most of the output streams as valuable products [177]. The input-output efficiency can also be an alternative to the consumed-produced efficiency. The task efficiency, which is another name for the consumed-produced efficiency, requires a definition of the necessary exergy inputs and the desired exergy products of a system. In addition, describing the consumption and production for dissipative units or complex processes will be even more challenging. The input-output efficiency, however, can be applied to any type of process due to the simple definition of the numerator and the denominator. On the other hand, the simplicity reduces the ability of the input-output efficiency to properly address the task or purpose of a system.

6.3.2 Consumed-produced exergy efficiency

There are also a number of exergy efficiencies classified as the consumed-produced type of efficiency. These efficiencies address the task of a process and are expressed by the ratio between the produced and the consumed amount of exergy:

$$\eta_{\text{consumed}-\text{produced}} = \frac{\text{Produced Exergy}}{\text{Consumed Exergy}} \tag{6.12}$$

Depending on the definition of the consumed and produced exergies, the value of the efficiency can vary. Kotas [183] defined them as desired outputs and necessary inputs. Tsatsaronis [182] used exergy of products and exergy of fuel for the definition of the task efficiency. The aforementioned definitions, however, do not have general mathematical expressions. Thus, they may result in different interpretations. Therefore, the following task efficiencies suggesting generalized formulas are in this chapter considered candidates for evaluation of complex processes having changes in temperature, pressure and chemical composition.

6.3.2.1   Coefficient of exergy efficiency

Brodyansky et al. [187] defined an exergy efficiency, offering general mathematical expressions for changes in both thermo-mechanical and chemical exergy. It is called the Coefficient of Exergy Efficiency (CEE) and expressed by subtracting the transit exergy from the inlet and outlet streams:

$$CEE = \frac{\sum \text{Exergy out} - \text{Transit Exergy}}{\sum \text{Exergy in} - \text{Transit Exergy}} \qquad (6.13)$$

The transit exergy is the amount of exergy that does not undergo any change across a process. Thus, by subtracting the transit exergy from the total exergy entering and leaving the system, the CEE only focuses on the amount of exergy that is changed through the process, which is directly related to the task of the system. Table 6.1 shows the formulas of transit exergy for thermo-mechanical, chemical, work and heat exergies. Here, work exergy will be pure electricity or shaft work supplied or produced by turbo-machinery in a process. $T_{\min}$ and $T_{\max}$ are the lowest and highest temperatures among the inlet and outlet streams of a system. Due to the detailed definition of the thermo-mechanical transit exergy in the CEE, the ambient conditions are partly accounted for.

However, the CEE does not decompose thermo-mechanical exergy to the second or third level (see Figure 6.1), and chemical exergy is decomposed to the chemical component level without splitting it into compositional and reactional exergy. This may give an inaccurate estimation of

consumed and produced exergies. In addition, Table 6.1 indicates that the calculation procedure for the transit part of thermo-mechanical exergy requires extra streams, which have different conditions than the original inlet and outlet streams. This will increase the computing effort for the CEE [189]. Due to the definition of transit work exergy, the CEE considers only net work as consumed or produced exergy.

Table 6.1 Transit part of exergy components [187].

Transit exergy
Thermo-mechanical exergy

a. Systems operating above T_0:
$\dot{E}^{tr} = \min \begin{bmatrix} \dot{E}_{in}^{TM}(T_{min}, p_{in}) & \dot{E}_{in}^{TM}(T_{min}, p_{out}) \\ \dot{E}_{out}^{TM}(T_{min}, p_{in}) & \dot{E}_{out}^{TM}(T_{min}, p_{out}) \end{bmatrix}$
  b. Systems operating below T_0:
$\dot{E}^{tr} = \min \begin{bmatrix} \dot{E}_{in}^{TM}(T_{max}, p_{in}) & \dot{E}_{in}^{TM}(T_{max}, p_{out}) \\ \dot{E}_{out}^{TM}(T_{max}, p_{in}) & \dot{E}_{out}^{TM}(T_{max}, p_{out}) \end{bmatrix}$
  c. Systems operating across T_0:
$\dot{E}^{tr} = \min \begin{bmatrix} \dot{E}_{in}^{TM}(T_0, p_{in}) & \dot{E}_{in}^{TM}(T_0, p_{out}) \\ \dot{E}_{out}^{TM}(T_0, p_{in}) & \dot{E}_{out}^{TM}(T_0, p_{out}) \end{bmatrix}$

Chemical exergy $\dot{E}^{tr} = \sum_i \dot{n}_i \min \begin{bmatrix} \bar{e}_{in,i}^{Ch} & \bar{e}_{out,i}^{Ch} \end{bmatrix}$
Work exergy $\dot{E}^{tr} = \min [\dot{E}_{in}^{W} \quad \dot{E}_{out}^{W}]$
Exergy of heat $\dot{E}^{tr} = \min [\dot{E}_{in}^{Q} \quad \dot{E}_{out}^{Q}]$

6.3.2.2   Component-by-component exergy efficiency

As part of an effort to develop a performance parameter for offshore oil and gas processing, Nguyen et al. [94] developed an exergy efficiency with explicit formulas, which is referred to as the Component-by-Component exergy efficiency (called CBC in this chapter). Eq. (6.14) represents the CBC where Z is the set of chemical components, I is the set of inlet streams, and

O is the set of outlet streams. The CBC pays attention to the changes in partial molar thermo-mechanical exergy of each chemical component between inlet and outlet streams across a process ($\Delta \dot{E}_{j,k}^{TM}$) (Eqs. (6.15)-(6.17)). If the partial molar exergy value of an inlet stream is larger than the one of an outlet stream, the reduction will be considered as consumed exergy and vice versa. For Eq. (6.17), only multiple inlet streams with one outlet stream or one inlet stream with multiple outlet streams are considered for a unit or a process.

$$CBC = \frac{\sum_j \sum_k \left(\Delta \dot{E}_{j,k}^{TM}\right)^+ + \Delta \dot{E}^{Ch}}{\sum_j \sum_k \left(\Delta \dot{E}_{j,k}^{TM}\right)^- + \dot{E}^{W_{net}} + \dot{E}^Q}, \qquad i \in Z, j \in I, k \in O \tag{6.14}$$

where

$$\left(\Delta \dot{E}_{j,k}^{TM}\right)^+ = \begin{cases} \sum_i \dot{n}_{i,j,k}(\bar{e}_{i,k}^{TM} - \bar{e}_{i,j}^{TM}) \text{ if } \bar{e}_{i,k}^{TM} > \bar{e}_{i,j}^{TM} \\ 0 \qquad\qquad \text{ if } \bar{e}_{i,k}^{TM} < \bar{e}_{i,j}^{TM} \end{cases} \tag{6.15}$$

$$\left(\Delta \dot{E}_{j,k}^{TM}\right)^- = \begin{cases} 0 \qquad\qquad \text{ if } \bar{e}_{i,k}^{TM} > \bar{e}_{i,j}^{TM} \\ \sum_i \dot{n}_{i,j,k}(\bar{e}_{i,j}^{TM} - \bar{e}_{i,k}^{TM}) \text{ if } \bar{e}_{i,k}^{TM} < \bar{e}_{i,j}^{TM} \end{cases} \tag{6.16}$$

$$\dot{n}_{i,j,k} = \begin{cases} \dot{n}_{i,k} \qquad\quad \text{ if } \dot{n}_{i,j} > \dot{n}_{i,k} \\ \dot{n}_{i,j} \qquad\quad \text{ if } \dot{n}_{i,j} < \dot{n}_{i,k} \end{cases} \tag{6.17}$$

$\dot{n}_{i,j,k}$ represents the molar flow rate of component i flowing from the inlet stream j to the outlet stream k. The CBC is mainly intended for petroleum separation processes. Thus, the formula for exergy efficiency assumes that chemical exergy is always increasing and there is no heat produced in the separation process. The increment in chemical exergy ($\Delta \dot{E}^{Ch}$) is regarded as produced exergy, while the heat used in the separation is regarded as consumed exergy. This explains the numerator and denominator in Eq. (6.14). However, in the case of mixers, the total chemical exergy of the inlet streams will decrease due to reduction in compositional exergy. Further, in the case of exothermic reactions, heat will be produced. Thus, in our work, the CBC exergy efficiency was modified to properly cover both positive and negative changes in chemical exergy and heat of reaction (Eqs. (6.18)-(6.20)). In addition, net work was regarded as consumed exergy since the original CBC does not consider the case where work is produced

from a process. The CBC applies decomposition of thermo-mechanical exergy only to the component level (i.e. the *third level*). Without the *second level* decomposition of thermo-mechanical exergy, the effect of variation in temperature and pressure will not be correctly represented by the CBC. In addition, the efficiency does not consider further decomposition of chemical exergy, and this will result in inaccurate consumed and produced exergies.

$$CBC = \frac{\sum_j \sum_k \left(\Delta \dot{E}_{j,k}^{\text{TM}}\right)^+ + \left(\Delta \dot{E}^{\text{Ch}}\right)^+ + \dot{E}^{Q_{\text{prod}}}}{\sum_j \sum_k \left(\Delta \dot{E}_{j,k}^{\text{TM}}\right)^- + \left(\Delta \dot{E}^{\text{Ch}}\right)^- + \dot{E}^{W_{\text{net}}} + \dot{E}^{Q_{\text{cons}}}}, \tag{6.18}$$

where

$$\left(\Delta \dot{E}^{\text{Ch}}\right)^+ = \begin{cases} \sum_k \dot{E}_k^{\text{Ch}} - \sum_j \dot{E}_j^{\text{Ch}} & \text{if } \sum_k \dot{E}_k^{\text{Ch}} > \sum_j \dot{E}_j^{\text{Ch}} \\ 0 & \text{if } \sum_k \dot{E}_k^{\text{Ch}} < \sum_j \dot{E}_j^{Ch} \end{cases} \tag{6.19}$$

$$\left(\Delta \dot{E}^{\text{Ch}}\right)^- = \begin{cases} 0 & \text{if } \sum_k \dot{E}_k^{\text{Ch}} > \sum_j \dot{E}_j^{\text{Ch}} \\ \sum_j \dot{E}_j^{\text{Ch}} - \sum_k \dot{E}_k^{\text{Ch}} & \text{if } \sum_k \dot{E}_k^{\text{Ch}} < \sum_j \dot{E}_j^{\text{Ch}} \end{cases} \tag{6.20}$$

6.3.2.3   Exergy Transfer Effectiveness

Marmolejo Correa and Gundersen also suggested a generalized exergy efficiency that is particularly applicable to low temperature processes, called the Exergy Transfer Effectiveness (ETE) [194]. The efficiency defines the consumed and produced exergies as exergy sources and exergy sinks respectively:

$$ETE = \frac{\sum \text{Exergy Sinks}}{\sum \text{Exergy Sources}} \tag{6.21}$$

An exergy sink is an exergy component that increases across a unit or system, whereas an exergy source has a decrease in its exergy value. Thus, ETE can easily be formulated by knowing the changes of exergy components across a unit. ETE also considers the ambient temperature and pressure when decomposing thermo-mechanical exergy to the *second level*. This gives accurate efficiency estimation for a process operating across or below ambient temperature. Based on the definition of ETE, work and heat supplied to a system will be

considered consumed exergy, while work and heat delivered from a system will be considered produced exergy. However, the original *ETE* only considered thermo-mechanical exergy, so it cannot be utilized for a process undergoing chemical reactions and compositional changes. Therefore, the *ETE* has been extended to handle such systems in this work. Due to the simple concept of exergy sinks and sources, the efficiency can vary with different combinations of exergy decomposition levels. Thus, in this work, the extended *ETE* includes decomposition of exergy to the *first*, *second*, and *third level*, called *ETE 1*, *ETE 2* and *ETE 3* respectively. *ETE 3* with exergy decomposition to the *third level* for both thermo-mechanical and chemical exergies can be expressed by Eqs. (6.22)-(6.26). For the *ETE*, we define a set for streams that operate across ambient:

$$\mathbb{S} = \left\{ (j \in I, k \in O) : T_j > T_0 > T_k \ \lor \ T_k > T_0 > T_j \right\} \tag{6.22}$$

Then for m ∈ EX and i ∈ Z we have:

$$ETE = \frac{\sum_m \sum_j \sum_k \left(\Delta \dot{E}_{j,k}^m \right)^+ + \ \dot{E}^{W_{\text{prod}}} + \ \dot{E}^{Q_{\text{prod}}}}{\sum_m \sum_j \sum_k \left(\Delta \dot{E}_{j,k}^m \right)^- + \ \dot{E}^{W_{\text{cons}}} + \ \dot{E}^{Q_{\text{cons}}}}, \tag{6.23}$$

where

$$\left(\Delta \dot{E}_{j,k}^m \right)^+ = \begin{cases} \sum_i \dot{n}_{i,j,k} (\bar{e}_{i,k}^m - \bar{e}_{i,j}^m) \ if \ \bar{e}_{i,k}^m > \bar{e}_{i,j}^m \\ 0 \qquad\qquad if \ \bar{e}_{i,k}^m < \bar{e}_{i,j}^m \end{cases}, \tag{6.24}$$

$$\left(\Delta \dot{E}_{j,k}^m \right)^- = \begin{cases} 0 \qquad\qquad if \ \bar{e}_{i,k}^m > \bar{e}_{i,j}^m \\ \sum_i \dot{n}_{i,j,k} (\bar{e}_{i,j}^m - \bar{e}_{i,k}^m) \ if \ \bar{e}_{i,k}^m < \bar{e}_{i,j}^m \end{cases}, \tag{6.25}$$

However, for $(j, k) \in \mathbb{S}$

$$\left(\Delta \dot{E}_{j,k}^T \right)^+ = \sum_i \dot{n}_{i,j,k} \ \bar{e}_{i,k}^T, \tag{6.26}$$

$$\left(\Delta \dot{E}_{j,k}^T \right)^- = \sum_i \dot{n}_{i,j,k} \ \bar{e}_{i,j}^T. \tag{6.27}$$

For *ETE 1* and *ETE 2*, Eqs. (6.23)-(6.27) do not contain subscript i and EX will be $\{\dot{E}^{TM}, \dot{E}^{Ch}\}$ and $\{\dot{E}^T, \dot{E}^p, \dot{E}^{Conc}, \dot{E}^{Reac}\}$ respectively. The set $\mathbb{S}$ indicates the cases where units or systems

are operated across the ambient temperature. With Eqs. (6.23)-(6.27), *ETE* can accurately evaluate the performance of processes operating across T_0. For equipment or processes with multiple inlets and outlets, exergy can still be decomposed to the third (component) level, but then a summation of the inlet streams on one hand and the outlet streams on the other hand will replace the exergy sources and sinks in the exergy efficiency calculations.

All exergy efficiencies discussed in this chapter can then be classified based on the level of exergy decomposition and whether ambient temperature is considered, as shown in Table 6.2. The classification will help to indicate the characteristics of the efficiency definitions, and thereby identifying the reasons for their possibly poor accuracy as performance indicators.

Table 6.2 Classification of exergy efficiencies.

	Exergy Decomposition Level		T_0
	Thermo-Mechanical	Chemical	consideration
Input-output	X	X	X
CEE	1	3 [a]	✔
CBC	3[a]	1	X
ETE 1	1	1	X
ETE 2	2	2	✔
ETE 3	3	3	✔

[a]Level 2 decomposition not included

6.4   Design basis and optimization

For the evaluation of the selected exergy efficiencies, the dual mixed refrigerant (DMR) process for liquefaction of natural gas was studied as a representative of cryogenic systems, having multiple cycles with two mixed hydrocarbon refrigerants [28]. The process flow diagram is shown in Figure 6.2, and the simulations were performed with Aspen HYSYS V9 using Peng-Robinson equations of state [132].
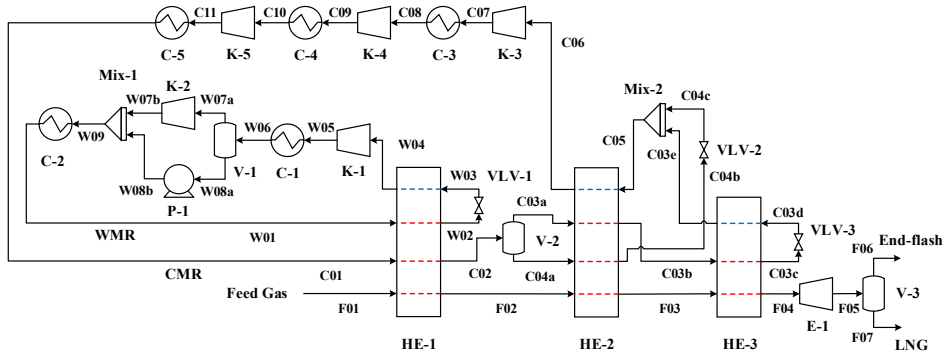
Figure 6.2 The AP-DMR process flow diagram [28, 29].

A pre-treated natural gas having small amounts of heavier hydrocarbons (F01) is fed to heat exchanger HE-1 and pre-cooled together with the cold mixed refrigerant (CMR) and the warm mixed refrigerant (WMR). The pre-cooled WMR (W02) is then subject to Joule Thomson throttling in valve VLV-1 to reduce its temperature and returned to HE-1. The heated WMR from the heat exchanger (W04) is pressurized through multi-stage compression and intercooling so that the WMR after further cooling in C-2 and HE-1 can produce sufficient cold duty for HE-1 by throttling. If liquid forms in intercooler C-1, it is sent to pump P-1 to boost the pressure level.

The feed stream from the first heat exchanger (F02) is passed through HE-2 and HE-3 to be liquefied and sub-cooled before it is depressurized by liquid expander E-1, discharging the two-phase stream (F05). The mixture is separated into vapor (F06) and liquid (F07) products by phase separator V-3. The pre-cooled CMR (C02) is responsible for the liquefaction and the sub-cooling of the feed gas. The liquid part of the stream (C04a) is further cooled by heat exchanger HE-2 and depressurized by valve VLV-2 in order to liquefy the feed stream in the second heat exchanger. The vapor part of the CMR (C03a) is cooled in the second and third heat exchanger and throttled to sub-cool the feed gas in HE-3, and the rest of the cold energy is delivered to HE-2. Table 6.3 and Table 6.4 show simulation conditions and design parameters used in this work.

Table 6.3 Simulation conditions for the DMR process.

Description	Unit	Value
Feed gas flow rate	kmol/s	1.00
Feed gas temperature	°C	22.00
Feed gas pressure	bar	60.00
LNG temperature	°C	-157.90
LNG pressure	bar	1.40
Feed gas composition		
Nitrogen	mol %	1.01
Methane	mol %	91.59
Ethane	mol %	4.93
Propane	mol %	1.71
i-Butane	mol %	0.35
n-Butane	mol %	0.40
i-Pentane	mol %	0.01

Table 6.4 Design parameters for the DMR process.

Process parameters	Unit	Value
Compressor polytropic efficiency	%	78
Expander adiabatic efficiency	%	87
Cooler outlet temperature	°C	22
Total Δp in heat exchangers	bar	0.6
Δp in vessels (liquid/vapor outlet)	bar	0.1/0.2
Pressure drop in coolers	bar	0.1

The DMR process was optimized to minimize the net power consumption. As key decision variables, the compositions of the WMR (ethane, propane and n-butane) and the CMR (nitrogen, methane, ethane and propane were varied during optimization. Besides, the discharge pressures of the turbo-machinery in the system were selected as variables. The outlet temperatures of heat exchangers HE-1 and HE-2 were also manipulated so that the heat exchanger cold duties can be varied. The three cryogenic heat exchangers were constrained to a minimum temperature difference of 3 K, considering the trade-off between the capital and operating costs of the process [86, 140].

A minimum superheating of 5 K was also applied to compressor inlet streams to prevent liquid formation at the inlet of the equipment, which is a proper value for the optimization of the DMR process [134]. The liquid expander E-1 and the phase separator V-3 are not affected by the optimization since the operating conditions of these units are not selected as optimization variables in this work. The optimization is performed by SQP (sequential quadratic programming), which is a local solver. The detailed process stream data for the initial case and the final case (optimal solution) are listed in Table 6.5 and Table 6.6.

Table 6.5 Stream conditions for the initial case of the DMR process.

Stream	Vapor Fraction	T	p	$\dot{n}$	$\dot{E}^{\mathrm{T}}$	$\dot{E}^{\mathrm{P}}$	$\dot{E}^{\mathrm{Conc}}$	$\dot{E}^{\mathrm{Reac}}$
	[-]	[°C]	[bar]	[kmol/s]	[kW]	[kW]	[kW]	[kW]
F01	1.00	22.0	60.0	1.00	0.7	9 749.7	-960.1	892 561.4
F02	1.00	-33.5	59.7	1.00	355.3	9 739.1	-960.1	892 561.4
F03	0.00	-115.7	59.4	1.00	4 568.2	9 729.1	-960.1	892 561.4
F04	0.00	-148.0	59.4	1.00	6 697.2	9 728.3	-960.1	892 561.4
F05	0.06	-157.0	1.5	1.00	15 187.5	969.3	-960.1	892 561.4
F06	1.00	-158.1	1.3	0.06	209.9	38.5	-50.2	46 785.4
F07	0.00	-157.9	1.4	0.94	15 099.4	749.0	-871.7	845 776.0
W01	0.17	22.0	17.9	1.22	9.1	7 459.1	-3 108.5	2 382 943.2
W02	0.00	-33.5	17.6	1.22	876.0	7 445.4	-3 108.5	2 382 943.2
W03	0.02	-36.5	4.4	1.22	3 894.9	4 285.6	-3 108.5	2 382 943.2
W04	1.00	10.8	4.1	1.22	29.6	4 083.9	-3 108.5	2 382 943.2
W05	1.00	47.5	8.6	1.22	74.4	6 131.6	-3 108.5	2 382 943.2
W06	0.97	22.0	8.5	1.22	6.9	6 100.6	-3 108.5	2 382 943.2
W07a	1.00	21.5	8.3	1.18	1.8	5 841.3	-2 969.7	2 285 541.2
W07b	1.00	63.3	18.0	1.18	616.5	7 281.4	-2 969.7	2 285 541.2
W08a	0.00	21.6	8.4	0.04	0.3	162.7	-98.5	97 402.0
W08b	0.00	22.5	18.0	0.04	0.1	166.4	-98.5	97 402.0
W09	1.00	55.7	18.0	1.22	613.0	7 463.4	-3 108.5	2 382 943.2
C01	1.00	22.0	48.5	1.34	1.5	11 901.1	-4 057.6	1 644 174.9
C02	0.30	-33.5	48.2	1.34	1 257.2	11 886.6	-4 057.6	1 644 174.9
C03a	1.00	-33.6	48.0	0.40	134.0	3 699.1	- 964.2	334 107.9
C03b	0.00	-115.7	47.7	0.40	1 980.9	3 694.0	-964.2	334 107.9
C03c	0.00	-148.0	47.7	0.40	2 845.3	3 693.6	-964.2	334 107.9
C03d	0.14	-158.4	3.9	0.40	4 997.6	1 316.7	-964.2	334 107.9
C03e	0.79	-118.7	3.8	0.40	1 595.0	1 311.6	-964.2	334 107.9
C04a	0.00	-33.5	48.1	0.94	853.5	8 094.0	-2 734.0	1 310 067.0
C04b	0.00	-115.7	47.8	0.94	3 767.4	8 086.7	-2 734.0	1 310 067.0
C04c	0.11	-124.7	3.8	0.94	8 306.2	3 045.9	-2 734.0	1 310 067.0
C05	0.32	-123.4	3.8	1.34	10 235.0	4 359.5	-4 057.6	1 644 174.9
C06	1.00	-41.2	3.6	1.34	525.6	4 113.6	-4 057.6	1 644 174.9
C07	1.00	28.4	10.6	1.34	1.3	7 594.9	-4 057.6	1 644 174.9
C08	1.00	22.0	10.5	1.34	1.0	7 565.3	-4 057.6	1 644 174.9
C09	1.00	68.8	20.3	1.34	215.4	9 573.7	-4 057.6	1 644 174.9
C10	1.00	22.0	20.2	1.34	1.1	9 559.3	-4 057.6	1 644 174.9
C11	1.00	86.9	48.6	1.34	482.4	11 905.9	-4 057.6	1 644 174.9

Table 6.6 Stream conditions for the final case of the DMR process.

Stream	Vapor Fraction	T	p	$\dot{n}$	$\dot{E}^{\mathrm{T}}$	$\dot{E}^{\mathrm{p}}$	$\dot{E}^{\mathrm{Conc}}$	$\dot{E}^{\mathrm{Reac}}$
	[-]	[°C]	[bar]	[kmol/s]	[kW]	[kW]	[kW]	[kW]
F01	1.00	22.0	60.0	1.00	0.7	9 749.7	-960.1	892 561.4
F02	1.00	-30.6	59.7	1.00	313.7	9 739.1	-960.1	892 561.4
F03	0.00	-118.1	59.4	1.00	4 705.2	9 729.1	-960.1	892 561.4
F04	0.00	-148.0	59.4	1.00	6 697.2	9 728.3	-960.1	892 561.4
F05	0.06	-157.0	1.5	1.00	15 187.5	969.3	-960.1	892 561.4
F06	1.00	-158.1	1.3	0.06	209.9	38.5	-50.2	46 785.4
F07	0.00	-157.9	1.4	0.94	15 099.4	749.0	-871.7	845 776.0
W01	0.00	22.0	15.1	0.90	5.4	4 696.0	-2 412.9	1 940 490.6
W02	0.00	-30.6	14.8	0.90	574.8	4 690.7	-2 412.9	1 940 490.6
W03	0.02	-33.6	3.7	0.90	2 397.8	2 774.7	-2 412.9	1 940 490.6
W04	1.00	18.2	3.4	0.90	5.4	2 596.4	-2 412.9	1 940 490.6
W05	1.00	59.1	8.3	0.90	295.0	4 251.8	-2 412.9	1 940 490.6
W06	0.55	22.0	8.2	0.90	6.0	4 237.0	-2 412.9	1 940 490.6
W07a	1.00	21.5	8.0	0.50	0.7	2 437.3	-1 236.3	959 704.2
W07b	1.00	55.6	15.2	0.50	146.0	3 011.0	-1 236.3	959 704.2
W08a	0.00	21.6	8.1	0.40	2.6	1 526.0	- 927.5	980 786.4
W08b	0.00	22.3	15.2	0.40	0.7	1 553.2	-927.5	980 786.4
W09	0.49	44.0	15.2	0.90	205.1	4 697.5	-2 412.9	1 940 490.6
C01	1.00	22.0	41.4	1.31	1.4	11 260.5	-3 752.4	1 678 086.8
C02	0.30	-30.6	41.1	1.31	1 266.4	11 243.3	-3 752.4	1 678 086.8
C03a	1.00	-30.7	40.9	0.40	119.4	3 510.1	-897.0	367 764.7
C03b	0.00	-118.1	40.7	0.40	2 109.3	3 504.2	-897.0	367 764.7
C03c	0.00	-148.0	40.6	0.40	2 906.3	3 503.7	-897.0	367 764.7
C03d	0.07	-152.9	4.1	0.40	4 907.7	1 353.6	-897.0	367 764.7
C03e	0.70	-121.1	4.0	0.40	1 928.9	1 348.8	-897.0	367 764.7
C04a	0.00	-30.7	41.0	0.92	861.6	7 673.2	-2 514.4	1 310 322.1
C04b	0.00	-118.1	40.8	0.92	3 908.8	7 663.9	-2 514.4	1 310 322.1
C04c	0.06	-121.9	4.0	0.92	8 140.4	3 091.7	-2 514.4	1 310 322.1
C05	0.25	-121.1	4.0	1.31	10 388.0	4 442.4	-3 752.4	1 678 086.8
C06	1.00	-33.7	3.8	1.31	406.7	4 214.1	-3 752.4	1 678 086.8
C07	1.00	32.3	10.6	1.31	6.0	7 445.9	-3 752.4	1 678 086.8
C08	1.00	22.0	10.5	1.31	1.0	7 417.0	-3 752.4	1 678 086.8
C09	1.00	74.4	22.1	1.31	273.8	9 613.6	-3 752.4	1 678 086.8
C10	1.00	22.0	22.0	1.31	1.1	9 600.9	-3 752.4	1 678 086.8
C11	1.00	68.3	41.5	1.31	238.8	11 266.3	-3 752.4	1 678 086.8

6.5 Results

This chapter shows the values of the selected exergy efficiencies for both the initial and the final cases of the DMR process in order to illustrate the improvement of the process and the accuracy of the efficiencies. Regarding the coolers, the exergy efficiencies were not measured since the heat from the compressor discharge streams is absorbed by cooling water, and its exergy is wasted to the environment. Thus, the coolers do not have any produced exergy.

6.5.1 Compressors

Table 6.7 indicates that all consumed-produced type of efficiency definitions give reasonable (similar) values for the compressors, whereas the input-output efficiency shows values close to 100 %. As seen in Table 6.8, the chemical exergy of hydrocarbons is significantly larger than other exergy components, thus diluting the effect of other exergy components in the input-output efficiency. This also results in a negligible change in the value of the input-output efficiency between the initial and final cases. The changes in compressor performance as measured by other efficiency definitions are also relatively small except for compressor K-2 and exergy efficiency *ETE 3*.

In conclusion, the input-output efficiency will give inaccurate optimization results for equipment handling hydrocarbons. In Table 6.8, the final case for compressor K-1 produces less thermo-mechanical exergy, while also consuming less compression power, compared to

Table 6.7 Exergy efficiencies of compressors for the initial and final cases [%].

Unit	K-1		K-2		K-3		K-4		K-5	
Operating condition	Across T_0		Across T_0		Across T_0		Across T_0		Across T_0	
Case	Initial	Final	Initial	Final	Initial	Final	Initial	Final	Initial	Final
Input-output	99.98	99.97	99.98	99.98	99.95	99.95	99.97	99.96	99.96	99.97
CEE	78.51	78.96	79.14	78.92	78.31	78.27	79.40	79.57	79.96	79.38
CBC	78.27	78.91	79.12	78.90	75.37	75.90	79.40	79.57	79.95	79.37
ETE 1	78.27	78.91	79.12	78.90	75.37	75.90	79.40	79.57	79.95	79.37
ETE 2	78.51	78.96	79.14	78.92	78.30	78.27	79.40	79.57	79.96	79.38
ETE 3	78.51	78.96	83.84	83.08	78.30	78.27	79.40	79.57	79.96	79.38

the initial case. The decrease in compression power (consumed) is larger than the decrease in thermo-mechanical exergy (produced), thus the performance of the compressor is improved. However, the input-output efficiency has a small decrease after optimization, whereas all consumed-produced type of efficiencies show an increase. During compression, the equipment consumes less cold temperature based exergy due to the warmer inlet temperature below ambient and produces more hot temperature based exergy as a result of the warmer outlet temperature above ambient. However, the input-output efficiency may not catch this effect of thermo-mechanical exergy since it is based on total exergy, while the portion of thermo-mechanical exergy in total exergy is negligible, compared to chemical exergy.

When a compressor operates across ambient temperature, some of the consumed-produced efficiencies may also give inaccurate efficiency values if they do not decompose thermo-mechanical exergy into temperature and pressure based exergies. Table 6.7 shows that CBC and $ETE\ 1$, which only use total thermo-mechanical exergy without decomposition, have slightly lower efficiency values, compared to CEE, $ETE\ 2$ and $ETE\ 3$, handling both temperature and pressure based exergies. Although CEE does not split thermo-mechanical exergy into temperature and pressure based terms, the use of transit exergy in CEE can have a similar effect as the decomposition into two terms.

Table 6.8 Exergy decomposition for compressor K-1 in the initial and final cases.

Case	Unit	Initial			Final		
		In	Out	Δ	In	Out	Δ
T	[°C]	10.8	47.5	-	18.2	59.1	-
p	[bar]	4.1	8.6	-	3.4	8.3	-
Compression power	[kW]	2 673.5	-	-	2 464.7	-	-
$\dot{E}^{TM}$	[kW]	4 113.5	6 206.0	2 092.5	2 601.8	4 546.8	1 945.0
$\dot{E}^{T}$	[kW]	29.6	74.4	44.8	5.4	295.0	289.6
$\dot{E}^{P}$	[kW]	4 083.9	6 131.6	2 047.7	2 596.4	4 251.8	1 655.4
$\dot{E}^{Ch}$	[kW]	2 379 834.7	2 379 834.7	0.0	1 938 078.1	1 938 078.1	0.0
$\dot{E}^{Conc}$	[kW]	-3 108.5	-3 108.5	0.0	-2 412.9	-2 412.9	0.0
$\dot{E}^{Reac}$	[kW]	2 382 943.2	2 382 943.2	0.0	1 940 491.0	1 940 491.0	0.0
$\dot{E}^{Total}$	[kW]	2 383 948.2	2 386 040.7	2 092.5	1 940 679.9	1 942 624.9	1 945.0

The underestimated values of CBC and $ETE\ 1$ are due to the nature of temperature based exergy across ambient temperature. As indicated in Table 6.9, compressor K-1 increases the stream temperature from 10.7 °C at the inlet to 47.5 °C at the outlet. Thus, the compressor operates across the ambient temperature of 25 °C. Figure 6.3 shows that the temperature based exergy of the WMR that is compressed in K-1 is first reduced from the inlet temperature to the ambient temperature and then increased from T_0 to the outlet temperature. As a result, the WMR in K-1 is first a source (consumed exergy) and then becomes a sink (produced exergy) for the temperature based exergy. However, the thermo-mechanical exergy of the WMR increases monotonically across the compressor as seen in Table 6.9. This will give incorrect values for consumed and produced exergies in CBC and $ETE\ 1$ due to the incomplete information about changes in temperature based exergy.

However, CEE, $ETE\ 2$ and $ETE\ 3$ only show marginal differences compared to CBC and $ETE\ 1$, while demanding larger computational efforts due to the decomposition of thermo-mechanical exergy [186]. Yet, the minor improvement of accuracy in the exergy efficiency may have a noticeable impact when analyzing optimization results. As seen in Table 6.7, CEE, $ETE\ 2$ and $ETE\ 3$ for K-3 show a slight reduction in their efficiency values after optimization, while CBC and $ETE\ 1$ have the opposite trend, thus giving incorrect indications for the effect of optimization.
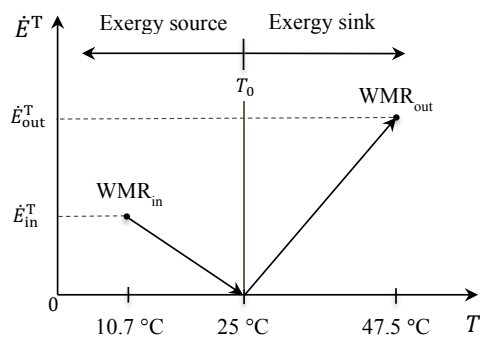
Figure 6.3 Changes in temperature based exergy of compressor K-1 operating across T_0.

Table 6.9 Exergy decomposition for the inlet and outlet streams of compressor K-1.

	Unit	Inlet	Ambient T_0	Outlet	Δ (Outlet-Inlet)
Temperature	[°C]	10.7	25	47.5	-
Pressure	[bar]	4.1	5.5	8.6	-
$\dot{E}^{TM}$	[kW]	4 113.5	4 911.9	6 206.0	2 092.5
$\dot{E}^{T}$	[kW]	29.6	0	74.4	44.8
$\dot{E}^{P}$	[kW]	4 083.9	4 911.9	6 131.6	2 047.7
$\dot{E}^{Ch}$	[kW]	2 379 834.5	2 379 834.5	2 379 834.5	0.0
$\dot{E}^{Comp}$	[kW]	-3 108.5	-3 108.5	-3 108.5	0.0
$\dot{E}^{Reac}$	[kW]	2 382 943.0	2 382 943.0	2 382 943.0	0.0
$\dot{E}^{Total}$	[kW]	2 383 948.0	2 384 746.4	2 386 040.5	2 092.5

One noticeable result is the larger efficiency value of *ETE 3* for compressor K-2. Generally, all the exergy components that include partial molar exergies increase through a compressor operating across ambient temperature. However, in the case of K-2, partial molar temperature based exergy shows a different behavior, and this affects the exergy sinks and sources in such a way that *ETE 3* is larger than other consumed-produced efficiencies. Even though *CBC* decomposes thermo-mechanical exergy to the component level, it has a different behavior than *ETE 3*. Since *CBC* does not decompose partial molar thermo-mechanical exergy into temperature and pressure based terms, it will not account for the effect of temperature based exergy.

6.5.2 Throttling valves and the liquid expander

For throttling valves in Table 6.10, the input-output efficiency does not give meaningful efficiency values due to the large chemical exergy of the streams. *ETE 1* also fails to measure the performance of the valves, delivering a 0 % efficiency value. Below ambient temperature, the purpose of a throttling valve is to reduce the temperature of a stream by reducing the pressure through the valve. Thus, pressure based exergy is converted to temperature based exergy across the valve, while having some exergy losses.

Table 6.10 Exergy efficiencies of valves and one expander for the initial and final cases [%].

Unit	VLV-1		VLV-2		VLV-3		E-1	
Operating condition	Below T_0	Below T_0	Below T_0	Below T_0	Below T_0	Below T_0	Below T_0	Below T_0
Case	Initial	Final	Initial	Final	Initial	Final	Initial	Final
Input-output	99.99	99.99	99.96	99.97	99.93	99.96	99.99	99.99
CEE	80.34	74.69	67.04	54.76	81.87	71.17	99.29	99.29
CBC	94.74	93.47	72.56	73.00	72.48	70.93	93.56	93.56
ETE 1	0.00	0.00	0.00	0.00	0.00	0.00	71.90	71.90
ETE 2	95.54	95.15	90.04	92.55	90.55	93.08	99.14	99.14
ETE 3	96.01	95.60	90.63	92.88	91.90	93.92	99.23	99.23

However, *ETE 1* only accounts for the changes in thermo-mechanical and chemical exergy. The former is always reduced due to the irreversibilities of the equipment (that are large for valves), thus it acts as consumed exergy, while the latter is not changed since there is no chemical reaction or compositional changes. As a result, there will be no produced exergy in this unit, resulting in a zero efficiency using the definition of *ETE 1*. The *CEE* and *CBC* efficiencies tend to underestimate the performance of the valves, compared to *ETE 2* and *ETE 3*. Similar to *ETE 1*, the *CEE* and *CBC* efficiency definitions only use thermo-mechanical exergy without decomposition, which means that information about the conversion between temperature and pressure based exergies is lost. However, *CEE* and *CBC* avoid zero efficiency values for valves since the transit exergy and the partial molar thermo-mechanical exergy in their definitions are able to partly account for these effects.

In conclusion, the *CEE* and *CBC* may not properly measure the improvement in the performance of the valves after optimization. In the final case, all the valves except VLV-1 have higher exergy efficiencies for *ETE 2* and *ETE 3*. As seen in Table 6.11, the ratio by which pressure based exergy is converted to temperature based exergy is increased from 0.91 to 0.93 for VLV-3 with smaller exergy loss ($\Delta \dot{E}^{\text{Total}}$) in the final case, fulfilling the purpose of a throttling valve operating below ambient temperature. In contrast, the values of *CEE* and *CBC* are significantly decreased after optimization for this valve. Therefore, decomposition of thermo-mechanical exergy into temperature and pressure based exergies is essential to calculate accurate exergy efficiencies for equipment operating below ambient temperature.

Table 6.11 Exergy decomposition for valve VLV-3 in the initial and final cases.

Case	Unit	Initial			Final		
		In	Out	Δ (Out-In)	In	Out	Δ (Out-In)
$\dot{E}^{TM}$	[kW]	6 538.9	6 314.2	-224.7	6 410.1	6 261.3	-148.8
$\dot{E}^{T}$	[kW]	2 845.3	4 997.6	2 152.3	2 906.3	4 907.7	2 001.3
$\dot{E}^{p}$	[kW]	3 693.6	1 316.7	-2 376.9	3 503.7	1 353.6	-2 150.1
$\dot{E}^{Ch}$	[kW]	333 143.7	333 143.7	0.0	366 867.7	366 867.7	0.0
$\dot{E}^{Comp}$	[kW]	-964.2	-964.2	0.0	-897.0	-897.0	0.0
$\dot{E}^{Reac}$	[kW]	334 107.9	334 107.9	0.0	367 764.7	367 764.7	0.0
$\dot{E}^{Total}$	[kW]	339 682.7	339 458.0	-224.7	373 277.8	373 129.0	-148.8

Liquid expanders operating below ambient temperature have two tasks. The primary task is to provide cooling (temperature based exergy) and the secondary task is to produce power. The source is pressure based exergy. Thus, the input-output efficiency, CBC and $ETE\ 1$ are not appropriate efficiency definitions for such units because they have incomplete information about the conversion between pressure and temperature based exergies. The high values of CEE, $ETE\ 2$ and $ETE\ 3$ mean good conversion of pressure based exergy into temperature based exergy and work, explaining why liquid turbines are considered a good alternative to throttling valves for the end-flash step in LNG processes [166]. As mentioned earlier, the operating conditions of expander E-1 and the end-flash are not selected as optimization variables in this work. This is why the columns for initial and final efficiencies are identical in Table 6.10. Again, $ETE\ 1$ is not able to properly measure the efficiency of turbines below ambient temperature.

6.5.3　Heat exchangers and mixers

In Table 6.12, all consumed-produced efficiencies have similar values for heat exchangers, and they are all improved after optimization, especially for HE-1. This is mainly due to the reduced values of $LMTD$ for all the heat exchangers in the final case as seen in Table 6.13. The input-output efficiency again fails to produce meaningful values, approaching 100 % due to the large reactional exergy of hydrocarbons. Regarding CEE and CBC, they give slightly different values compared to $ETE\ 1$, 2 and 3.

Table 6.12 Exergy efficiencies of heat exchangers and mixers for the initial and final cases [%].

Unit	HE-1		HE-2		HE-3		MIX-1		MIX-2	
Operating condition	Below T_0		Below T_0		Below T_0		Across T_0		Below T_0	
Case	Initial	Final	Initial	Final	Initial	Final	Initial	Final	Initial	Final
Input-output	99.98	99.99	99.98	99.98	99.97	99.99	99.99	99.99	99.99	99.99
CEE	60.33	82.47	89.94	92.12	87.81	93.44	84.54	94.25	98.76	98.77
CBC	59.95	82.28	90.01	92.48	87.92	93.76	77.74	91.19	98.36	98.72
ETE 1	59.95	82.24	89.91	92.10	87.81	93.44	99.85	99.95	99.98	99.98
ETE 2	59.95	82.24	89.91	92.10	87.81	93.44	99.85	99.95	99.99	99.98
ETE 3	59.95	82.24	89.92	92.37	87.81	93.44	87.19	92.72	98.73	98.99

The two efficiency definitions CEE and CBC consider the effect of pressure drop as exergy sources only (consumed exergy) on both the hot and cold stream sides. However, below ambient temperature, the pressure drop for hot streams reduces the increment of thermo-mechanical exergy through a heat exchanger. In addition, cold streams have a larger decrease in thermo-mechanical exergy through a heat exchanger due to the pressure drop.

Table 6.13 $LMTD$ values of the heat exchangers [°C].

Unit	HE-1		HE-2		HE-3	
Case	Initial	Final	Initial	Final	Initial	Final
$LMTD$	12.31	3.88	5.19	4.04	8.87	4.63

As a result, $ETE\ 2$ and $ETE\ 3$ have a smaller exergy sink and a larger exergy source compared to CEE and CBC, thus decreasing the exergy efficiency of the heat exchangers. Nevertheless, this effect is marginal in this work since pressure drops in the heat exchangers are small. However, with large pressure drops, the effect can be significant [194].

Unlike units having no changes in chemical exergy, mixers have significant differences between efficiency definitions as shown in Table 6.12. The input-output efficiency gives almost 100 % efficiency, thus not properly showing the performance of the equipment. As mentioned in Section 2.3.3, $ETE\ 1$ and $ETE\ 2$ are defined in order to handle changes in both thermo-mechanical and chemical exergies by decomposing them to the *first* ($\dot{E}^{TM}$, $\dot{E}^{Ch}$) and *second level* ($\dot{E}^{T}$, $\dot{E}^{p}$, $\dot{E}^{Comp}$, $\dot{E}^{Reac}$). However, they also give similar efficiency values as the

input-output efficiency. Values for MIX-1 in Table 6.14 indicate that due to mixing, stream Inlet1 experiences an increase in reactional exergy (18,167.0 kW), which then becomes an exergy sink. At the same time, reactional exergy of stream Inlet2 decreases by the same amount and becomes an exergy source. Since the changes in reactional exergy of stream Inlet1 and Inlet2 are substantially larger than the variations in other exergy components, they dominate both the exergy sink and source terms in the definition of *ETE 1* and *ETE 2*. Thus, they give efficiency values close to 100 %, since the sink and source sides of the reactional exergy are similar.

In contrast, *CEE*, *CBC* and *ETE 3* successfully give distinctive efficiency values for the units having chemical exergy changes. Due to the decomposition of chemical exergy to the chemical component level, *CEE* and *ETE 3* can prevent reactional exergy from dominating both exergy sink and source terms. After this decomposition, the efficiency definitions are able to account for the difference in partial molar reactional exergy between the inlet streams and the outlet stream for the mixer. The molar reactional exergy of each component, however, does not change because all the streams include the same components. However, the streams have different compositions, thus different molar compositional exergy values for the components. In the case of chemical exergy in *CBC*, only the difference in chemical exergy between the sum of the two inlet streams and the outlet stream is considered. Since there is no chemical reaction happening in the unit, reactional exergy is cancelled, and only the changes in compositional exergy are left in the difference between inlet and outlet.

Table 6.14 Exergy decomposition for mixer MIX-1 in the initial case.

Stream		Inlet1	Inlet2	Outlet	Outlet1[a] - Inlet1		Outlet2[a] - Inlet2	
Flow [kmol/s]		1.1798	0.0406	1.2204	1.1798		0.0406	
Unit		[kJ/kmol]	[kJ/kmol]	[kJ/kmol]	[kJ/kmol]	[kW]	[kJ/kmol]	[kW]
$\bar{e}^{TM}$	$\bar{e}^{T}$	522.6	1.3	502.3	-20.3	-23.9	501.0	20.3
	$\bar{e}^{P}$	6 171.6	4 100.3	6 115.5	-56.1	-66.2	2015.2	81.8
$\bar{e}^{Ch}$	$\bar{e}^{Comp}$	-2 517.1	-2 426.9	-2 547.1	-30.0	-35.4	-120.2	-4.9
	$\bar{e}^{Reac}$	1 937 187.0	2 400 280.0	1 952 585.0	15 398.0	18 167.0	-447 695.0	-18 167.0
$\bar{e}^{Total}$		1 941 364.1	2 401 954.7	1 956 655.7	15 291.6	18 041.5	-445 299.0	-18 069.8

[a]Outlet1 = (m_{Inlet1}/m_{Outlet}) ×Outlet, Outlet2 = (m_{Inlet2}/m_{Outlet}) ×Outlet

Therefore, *CEE*, *CBC* and *ETE 3* can disregard the reactional exergy in efficiency calculations, resulting in meaningful performance values. However, the *CEE* and *CBC* efficiencies will not contain accurate information about the changes in partial molar temperature and pressure based exergies. In addition, for *CEE*, calculating the transit part of thermo-mechanical exergy across the units is required, and this demands a large computational effort, compared to *CBC* and *ETE 3* [189]. Hence, *ETE 3* has a clear advantage in measuring the performance of mixers compared to other efficiency definitions.

In an analysis of LNG processes, mixers appear to have no important thermodynamic purpose since the equipment is just mixing streams that are separated upstream. Thus, exergy analysis of mixers has either been omitted or just performed for an illustrative purpose [93, 185]. However, in the final cases in Table 6.12, all the consumed-produced efficiencies clearly indicate a performance improvement of the mixers. Table 6.15 shows that the optimizer reduces the temperature difference between the two inlet streams. This results in a smaller amount of entropy generation in the mixer and thus higher exergy efficiency. Therefore, exergy analysis of mixers may be necessary to measure the performance improvement of the process.

Table 6.15 Operating temperatures of MIX-1.

Case	Initial			Final		
	Inlet-1	Inlet-2	Outlet	Inlet-1	Inlet-2	Outlet
Temperature [°C]	63.3	22.5	55.7	55.6	22.3	44.0

6.5.4 Phase separators and total process

Phase separators used in the LNG process have a similar trend in the efficiency values as mixers. Table 6.16 indicates that efficiency definitions without the decomposition of chemical exergy to the *third level*, such as the input-output efficiency, *ETE 1* and *ETE 2*, give approximately 100 % efficiency values for the phase separators. During phase separation, the total amount of exergy remains the same if there is no pressure drop or heat exchange as

illustrated in Figure 6.4. However, the total compositional exergy of the vapor and liquid streams increases since this exergy form is a measure of the degree of mixing.

This increment is compensated by decreasing thermo-mechanical exergy, while keeping total exergy across the unit unchanged. Thus, the performance of phase separators depends on the conversion ratio from thermo-mechanical exergy to compositional exergy.

In addition, the amount of exergy destruction (indicated by $\dot{E}^D$ in Fig. 4) due to pressure drop affects temperature based, pressure based and compositional exergies. This means that decomposition of exergy at least to the *second level* ($\dot{E}^T$, $\dot{E}^p$, $\dot{E}^{Comp}$, $\dot{E}^{Reac}$) is required to properly measure the performance of phase separators. Thus, *ETE 1* is not suitable for this type of equipment. In addition, a phase separator will split a stream into two outlet streams, one with higher and one with lower molar reactional exergy compared with the inlet stream. This makes reactional exergy dominating both the exergy sink and source terms in *ETE 2*, giving close to 100 % efficiency.

Table 6.16 Exergy efficiency of phase separators and the total process for the initial and final cases [%].

Unit	V-1		V-2		V-3		Process	
Operating condition	below T_0		below T_0		below T_0		below T_0	
Case	Initial	Final	Initial	Final	Initial	Final	Initial	Final
Input-output	99.99	99.99	99.99	99.99	99.99	99.99	99.02	99.34
CEE	60.93	95.95	99.52	99.42	98.98	98.98	63.13	71.66
CBC	51.30	95.14	99.64	97.01	83.22	83.22	42.98	52.68
ETE 1	99.67	99.98	99.99	99.99	99.76	99.76	64.02	72.44
ETE 2	99.67	99.98	99.99	99.99	99.78	99.78	73.26	80.18
ETE 3	71.00	96.85	99.75	97.89	84.61	84.61	63.43	71.92
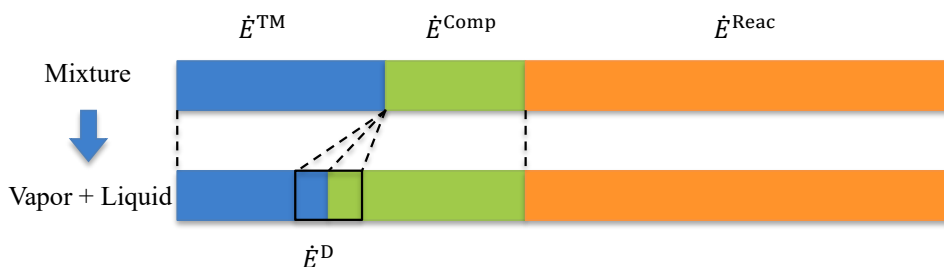
Figure 6.4 Relationship between exergy components across a phase separator.

In contrast, CEE, CBC and $ETE\ 3$ give reasonable efficiency values for the phase separators since they can disregard the large values of reactional exergy in both the consumed and produced exergy terms in the same way as for mixers. However, CEE and CBC tend to underestimate the efficiency values due to lack of detailed information about changes in temperature and pressure based exergies, showing the superiority of $ETE\ 3$.

Similar to the case with mixers, CEE, CBC and $ETE\ 3$ also in general indicate performance improvement of phase separators after optimization. The task of phase separators is to divide an inlet stream into a vapor and a liquid stream. Table 6.17 indicates that the optimizer manipulates the LNG process to have more even molar flow rates in the vapor and liquid outlet streams, while having constant pressure drop as indicated in Section 3, Table 4. This means a larger degree of separation is achieved for the same pressure drop in the final case. As mentioned in Section 3, the operating conditions of the end-flash (V-3) are not selected as optimization variables in this work, resulting in identical efficiency values for the initial and final case.

Table 6.17 Vapor fraction in phase separators.

Unit	V-1		V-2	
Case	Initial	Final	Initial	Final
Vapor fraction	0.966	0.553	0.298	0.301

In the DMR process studied in this chapter, the feed gas undergoes changes in both thermo-mechanical and chemical exergies, producing LNG and off-gas from the end-flash as products. The feed and product streams are all below ambient temperature. Like other equipment having changes in chemical exergy, the significant quantity of chemical exergy dominates the inlet and outlet total exergy, making the input-output efficiency of the total process close to 100 % as seen in Table 6.16.

In contrast, all the consumed-produced efficiencies give more reasonable values for the performance of the LNG process. The CBC underestimates the efficiency value compared to other efficiency definitions. In the LNG process, the feed gas is cooled and liquefied below ambient temperature. This increases the temperature based exergy of the feed and such increment becomes an exergy sink. The pressure based exergy of the feed gas is reduced due to the end-flash step and this reduction is regarded as an exergy source. However, the CBC just considers the changes in total thermo-mechanical exergy so it does not include the precise information about the variation in temperature and pressure based exergies. This makes the CBC inaccurate for evaluation of LNG processes. $ETE\ 1$ and $ETE\ 2$ overestimate the performance of the total process compared to other consumed-produced efficiencies. Similar to the case with phase separators, $ETE\ 1$ and $ETE\ 2$ will not handle this process properly since the two products experience considerable changes in molar reactional exergy compared to the feed gas. This will dilute the effect of variations in other exergy components.

However, CEE and $ETE\ 3$ give appropriate efficiency values for the LNG process by considering temperature and pressure based exergies and the *third level* decomposition of chemical exergy. The difference between the two efficiencies occurs since $ETE\ 3$ counts the power consumed in the compressors as an exergy source and the power produced in the liquid turbine as an exergy sink whereas CEE only considers the net work required/produced by the turbo-machinery as an exergy source/sink. The compressors consume electricity, which is pure exergy, and the liquid turbine produces power at the cost of pressure based exergy. Thus, exergy efficiencies using net work will not recognize such transfer between pressure based exergy and power, and thus being thermodynamically inaccurate. Therefore, $ETE\ 3$ provides

the most accurate value of exergy efficiency for LNG processes, especially for processes with multiple products.

6.6   Recommendations

A case study with an advanced LNG process was performed to compare the selected exergy efficiencies, including the input-output efficiency. The results demonstrate that the input-output efficiency shows values close to 100 % and only marginal changes after the process optimization due to the large chemical exergy of the streams (typical for hydrocarbon processes). Thus, the input-output efficiency does not provide meaningful efficiency values for units and systems handling hydrocarbons, and thus poorly reflecting the changes in process performance.

In contrast, all the consumed-produced types of efficiency definitions gave reasonable values for all units and the total process containing hydrocarbon streams. However, exergy efficiencies using thermo-mechanical exergy without decomposition (only *first level* of exergy decomposition) such as *CEE*, *CBC* and *ETE 1* did not give accurate efficiency values for equipment producing refrigeration duty (throttling valves and the liquid expander) and units operating across ambient temperature. The inaccuracy of these efficiencies is caused by the inability to account for the conversion between temperature and pressure based exergies, which is the main principle of refrigeration and liquefaction processes such as natural gas liquefaction and natural gas liquid (NGL) extraction processes. Thus, when the DMR process was optimized, the efficiencies using only the *first level* of exergy decomposition give inaccurate changes in their values since they do not properly address the task of the system.

Although it can reflect the conversion between temperature and pressure based exergies, decomposing exergy to the *second level* (*ETE 2*) also gave less accurate efficiency values for units and the total process having compositional changes compared to the *third level* (*ETE 3*). Nevertheless, *ETE 2* is recommended for systems having temperature, pressure, and

compositional changes due to the simple calculation method and the ability to handle all operating temperatures above, across and below ambient.

To properly account for the performance of equipment and processes having compositional changes, decomposing exergy into the chemical component level (the *third level* of exergy decomposition, such as $ETE\ 3$) was required. In the case of CEE and CBC, decomposing to the *third level* is only done for chemical exergy, not thermo-mechanical exergy (temperature and pressure based exergy components). This is required for units or systems operating across ambient temperature. In contrast, $ETE\ 3$ delivered reasonable exergy efficiency values for all types of equipment and systems at all operating conditions without information loss about exergy transfer, while demanding minor calculation efforts compared to CEE. Therefore, $ETE\ 3$ has a clear advantage in measuring the performance of processes with changes in chemical exergy, giving consistent and reliable efficiency values even for the evaluation of the improvement in optimized systems.

6.7   Conclusion

In this chapter, consumed-produced type exergy efficiencies were classified according to the level of exergy decomposition, in order to indicate the characteristics of the efficiency definitions. Due to the inaccuracy of the task exergy efficiencies for different types of system with various operating conditions, this chapter extends the Exergy Transfer Effectiveness (ETE), by including chemical exergy. This modification is to offer general formulas for processes having changes in temperature, pressure and chemical composition. The result is an exergy efficiency containing accurate information about exergy transfer in processes. The ETE also properly reflects the changes in process performance after optimization, which is the main task of an efficiency index as a post-design tool for diagnosing industrial processes with respect to potential improvements. Thus, the use of the ETE is recommended for cryogenic processes, while considering the appropriate selection of the exergy decomposition level. The generalized

formula also makes the *ETE* applicable for other unit operations such as chemical reaction, combustion and membrane separation. Such applications are possible future works.

Chapter summary

- o Various exergy efficiencies are case dependent and their definitions lack a mathematical expression, thus resulting in different interpretations.
- o With generalized formulations, consumed-produced exergy efficiencies are recommended to measure the performance of systems.
- o To evaluate accurate performance variation due to both thermo-mechanical and chemical changes, a detailed decomposition of exergy in the efficiency formulation is required. This is the key property of the extended *ETE* developed in this chapter.

Chapter 7 Exergy analysis for LNG value chain: LNG regasification

In the previous chapter, an exergy efficiency with a general mathematical expression (extended ETE) was suggested for cryogenic systems having changes in temperature, pressure, and composition. Then, in this chapter, exergy efficiency is applied to complex cryogenic distillation systems to evaluate ETE as a post design tool. The result are also compared with the energy efficiency of the systems to answer the following questions:

- o Does energy/exergy efficiency properly reflect the performance of cryogenic processes?
- o Is exergy efficiency a better performance indicator than energy efficiency?

This chapter is based on the following publication.

- – Kim D, Giametta REH, Gundersen T. Optimal Use of Liquefied Natural Gas (LNG) Cold Energy in Air Separation Units. Industrial & Engineering Chemistry Research. 2018;57(17):5914-23.

7.1   Introduction

To bring natural gas into distribution networks, transport in liquefied form can be the most economical and convenient solution for remote places. Thus, natural gas is liquefied and transported at -162 °C and slightly above atmospheric pressure by liquefied natural gas (LNG) carriers. Most often, the tail end of the distribution networks and the end-users require the LNG to be in gas phase. Such regasification is achieved at LNG import terminals. In the terminals, the transported LNG is unloaded from the carriers at a typical flow rate of 12,000 cubic meters per hour and filled in storage tanks. The stored LNG is then pumped to a vaporization system at a pressure between 80 and 120 bar depending on the gas export requirements [198]. After being pressurized, the LNG is converted to gas phase by heat exchange in vaporizers. There are two main types of vaporizers on the market: open rack vaporizers (ORV), which represent around 70 % of the installations, and submerged combustion vaporizers (SCV), representing a 20 % share [14]. Other options are ambient air vaporizers (AAV), shell and tube exchange vaporizers (STV) and intermediate fluid vaporizers (IFV) [70]. Several vaporizers are required to achieve the total regasification capacity of a typical import terminal. The best combination of vaporizer types depends on site ambient conditions [199].

Due to the increasing demand for LNG, the total world regasification capacity also expanded to 851 million tons per annum (MTPA) in 2018 with 121 regasification terminals [8]. Consequently, a significant amount of LNG cold energy has been wasted to seawater or air in typical regasification processes although it could have been utilized in various processes to improve their efficiency. However, there are several aspects to be considered when recovering the LNG cold energy in other systems. First, the duty and temperatures available for heat integration during LNG regasification depend on the gas distribution pressure [71]. Another common constraint is the long distance between the cold energy (exergy) available at the regasification terminal and the potential users.

To overcome the distance limitation, carbon dioxide can be liquefied at the LNG terminal and transported in pipelines to for example food processing facilities or buildings requiring air

conditioning [76]. Nevertheless, the operating temperature of the refrigeration application is limited to -60 °C due to the freezing point of the intermediate working fluid (CO_2). Therefore, this example cannot recover LNG cold energy in the whole temperature range available during regasification, which will result in sub-optimal use of LNG cold energy.

Low-temperature power generation is another option to utilize the LNG cold energy. However, power production using Rankine cycles does not go below -90 °C when ethane is used as a working fluid [73]. In the case of Brayton cycles, one could go down to -140 °C using nitrogen as a working fluid, but this has not yet been implemented in real applications.

Freezing or evaporation-condensation desalination are also possible options to be integrated with LNG regasification. However, the use of a glycol-water solution as an intermediate working fluid will limit the operating temperature to -15 °C [74]. By using LNG cold energy, heavy hydrocarbons can be extracted from the stored LNG having a heating value above the distribution requirements. This integration covers temperatures from -160 °C but only to -105 °C [75]. Therefore, this option does not fully replace conventional vaporization processes since there is still a considerable amount of cold energy left to be recovered from the LNG.

Unlike the integration options mentioned above, an air separation unit (ASU) is a system that can fit in the temperature range of LNG vaporization. Due to the low operating temperature of air separation units (from -170 °C to -190 °C), which is closer to the LNG temperature than any other options, supplying parts of the cold duty in an ASU is regarded as a promising alternative for utilizing the cold energy of LNG. Hence, this integration has already been applied in several LNG import terminals since the 1970s [77].

However, air separation has complex process configurations with a single column, double column, or even triple column distillation, including sophisticated internal heat integration [200, 201]. Thus, there have been several suggestions for integration of LNG regasification processes with different ASU designs, showing distinctive characteristics [77, 90, 202, 203]. Most suggestions integrate LNG regasification with conventional two-column or novel single-column ASU processes. Besides, the structure and performance of the ASU processes

combined with LNG regasification vary depending on the way LNG cold energy is utilized. Therefore, these integration solutions were simulated and assessed to understand their strengths and weaknesses in depth under fair conditions.

In this work, ASU processes integrated with LNG regasification are categorized based on the method for utilization of LNG cold energy. A single-column ASU configuration is applied as a reference process to be combined with an LNG stream [204]. A comparison between the two systems is conducted by considering both energy and exergy as performance measures. A discussion is also made on the optimal use of LNG cold energy, depending on the integration method.

7.2   Process design

7.2.1 Single column ASU

ASU processes differ mainly by the number of distillation columns in the cold box and the operating pressure levels. These differences affect the products (purity, phase and pressure) as well as the power consumption and the capital cost of the ASU. Nitrogen (78.12 mol % and normal boiling point (NBP) of -195.9 °C) and oxygen (20.95 mol % and NBP of -182.9 °C) are the two components normally recovered from the air through the ASU. Noble gases present in the atmosphere can also be extracted by multi-column processes and further purification of the product streams.

In this work, a single-column ASU process using a recuperative vapor recompression heat pump [204] is selected as a design basis to be integrated with LNG regasification. This novel configuration produces pure nitrogen and intermediate purity oxygen (95 mol %) at atmospheric pressure, which matches the requirements for oxy-combustion applications in coal-based power plants. The advantages of this process, compared to traditional double column ASU processes, are the reduced number of columns and the reduced power consumption (less air compression).

An adjusted version of the novel single column ASU [204] was modeled in HYSYS V9.0 [132] and is shown in Figure 7.1. Mainly, this model is based on the configuration referred to as Cycle 6, which is more practical with respect to deployment. In this process, the air feed (A01) is slightly compressed (i.e. using a fan) to compensate for pressure losses through the system, and then split into streams A04a and A05a. Stream A04a is pressurized and delivered to the main heat exchanger (MHE) to be cooled before being sent to an expander (E-A). This depressurization of cold stream A04f will reduce the cold duty of the MHE, and stream A04g is further cooled in the MHE to be slightly condensed. Stream A05a is also cooled in the MHE and mixed with the partially liquefied air stream A04h. The mixed stream A06 is supplied to the distillation column (Dist-Col) at an intermediate level to be separated into a bottom liquid X01 and an overhead vapor N01. The pure nitrogen gas stream (N01) is returned to the MHE to supply refrigeration duty and being warmed to ambient temperature, producing a nitrogen vent stream N03.

A part of the nitrogen product (N04a) is compressed and cooled to a cryogenic temperature in the MHE. The pre-cooled nitrogen stream N04d enters the MHE again via the integrated heat exchanger (Cond-Reb), boiling the liquid oxygen (LO2) product (X01). Then the nitrogen
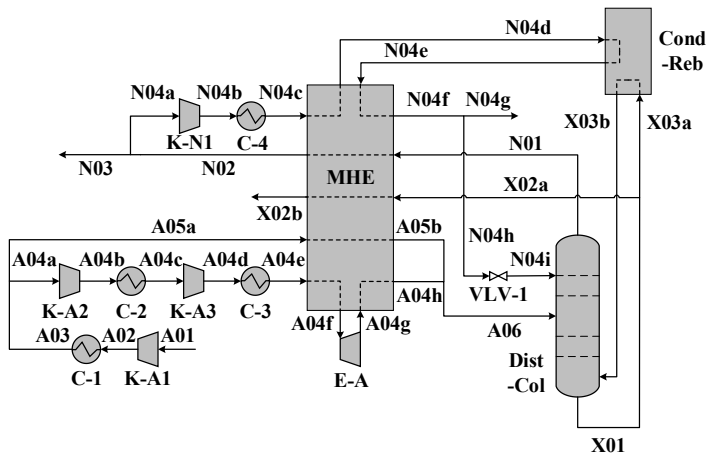
Figure 7.1 Process flow diagram for the single column ASU (modified from Cycle 6 in ref [204]).

stream that is sub-cooled through the MHE (N04f) is split to provide a liquid nitrogen (LN2) product (N04g) and reflux to the column (N04h) after throttling (N04i). The liquid oxygen stream X01 from the bottom of the column is split into two branches. One branch (X03a) is vaporized in the heat exchanger Cond-Reb, and the other branch (X02a) is sent to the MHE to provide cooling duty and be vaporized to the final oxygen product.

7.2.2 Single column ASU with an LN2 production cycle (Option 1)

The novel single column ASU process produces very little liquid nitrogen and oxygen since it was primarily aimed at oxy-combustion coal-based power generation. Thus, one of the options to utilize LNG cold energy is to supply additional refrigeration to the ASU to enable it to deliver liquid products, which can be transported long-distance. One way to achieve this integration is connecting a sub-process for liquid nitrogen production to ASU systems[90, 202]. Thus, the single column ASU process was modified to include the LN2 production cycle having the LNG stream as a refrigeration source (Figure 7.2). This integration is referred to as Option 1 in this chapter.

This integration scheme has an almost identical structure as the single column ASU except that a part of the nitrogen vent stream (N05) is sent to a liquid nitrogen production system. This recycled nitrogen stream goes through multi-stage compression and intercooling via the nitrogen heat exchanger (NHE), while gasifying the compressed LNG stream L02. The fully condensed nitrogen stream (N15) leaves the NHE and enters a throttling valve to be depressurized before feeding a vessel. The gas stream from the phase separator (N17a) provides a cold duty to the NHE and goes back to the second recycled nitrogen compressor while the liquid stream (N18) is divided into three parts. One (N21a) is used for the cooling demand of the nitrogen reflux (N04d) in the Cond-Reb and the MHE. The second part (N19a) is compressed by a pump (P-N) with a relatively small power consumption and evaporated via the NHE before being depressurized in turbo-expanders. The expansion will produce power and supply cold duty to the NHE in order to liquefy the recycled nitrogen stream N08. The last part (N20) is then provided as a liquid nitrogen product.
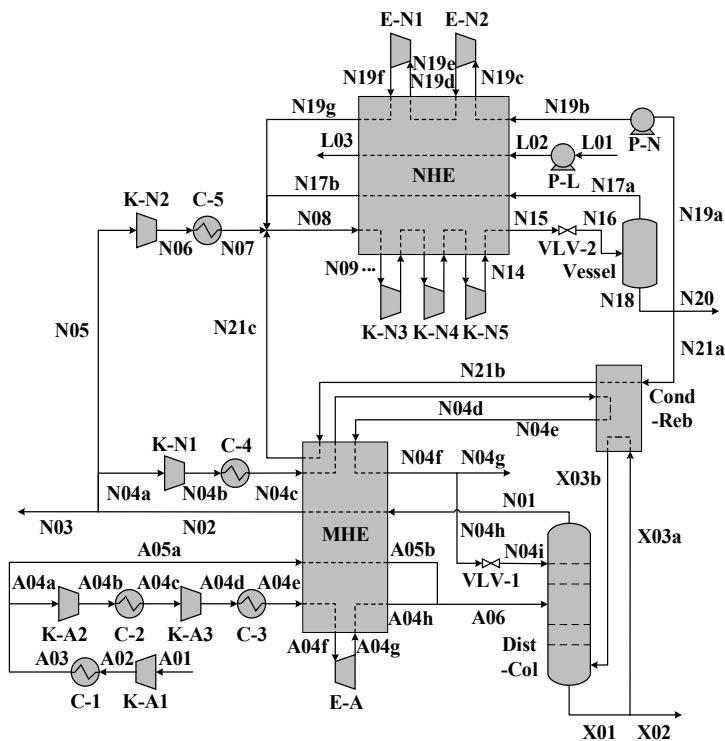
Figure 7.2 Process flow diagram for the single column ASU with an LN2 production cycle.

Finally, it should be emphasized that, unlike the single column ASU process, a part of the liquid oxygen product from the ASU (X01) does not need to be supplied to the MHE, rather it is directly extracted as a liquid product (X02).

7.2.3 Single column ASU with pre-cooling (Option 2)

In Option 1, LNG cold energy is supplied to the NHE where the recycled nitrogen stream is cooled. However, the LNG stream does not exactly match the cold duty of the NHE, increasing the temperature difference in the heat exchanger. Instead, the LNG stream can be used for pre-cooling of air, reflux nitrogen, and the recycled nitrogen stream [203]. By adjusting the pre-cooling temperature, LNG cold energy can be well fit to the cold duty of the pre-cooling heat

exchanger, reducing driving forces. The single column ASU with the pre-cooling scheme is referred to as Option 2 in this chapter. For the pre-cooling of air, reflux nitrogen, and recycled nitrogen, the LN2 production system in Option 1 is integrated into the main heat exchanger (MHE) and LNG cold energy is supplied to the MHE. Besides, the cold part of the MHE is separated as an independent heat exchanger (Sub-HE) to sub-cool the air, the reflux nitrogen and the recycled nitrogen as seen in Figure 7.3.

By splitting the MHE, the intermediate temperature of the air, reflux nitrogen, and the recycled nitrogen stream can be manipulated depending on the state of the LNG stream, resulting in a better temperature match between the streams in the MHE and thus an improved use of the cold LNG. Thus, the LNG stream pumped from a storage tank (L02) provides refrigeration only to the MHE. The typical intermediate temperature will be close to the supplied LNG temperature.
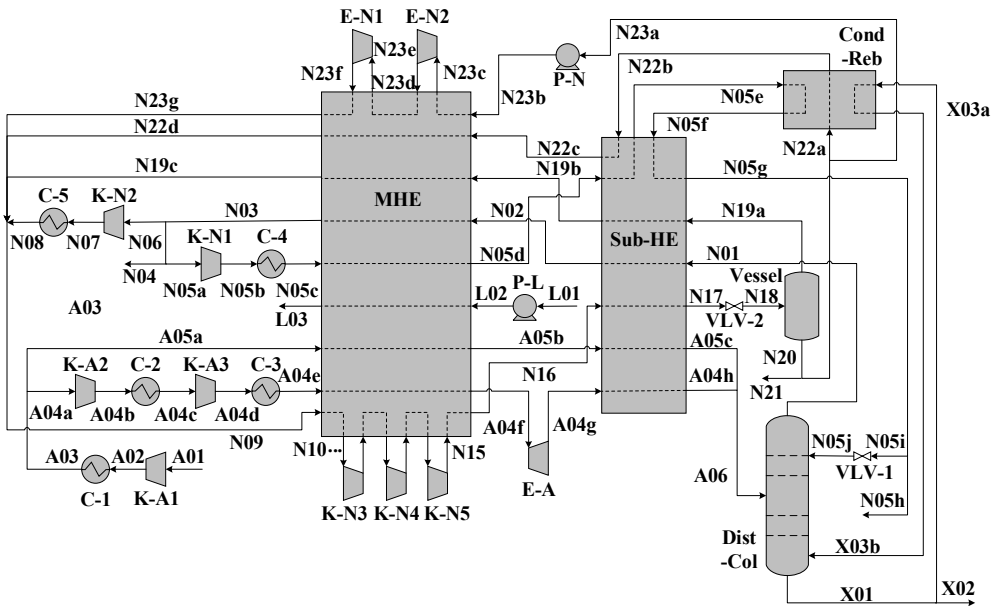
Figure 7.3 Process flow diagram for the single column ASU with pre-cooling.

7.3 Design basis

7.3.1 Scope of the models

Cryogenic air separation is performed after air compression and purification where water and other impurities are removed by adsorption on molecular sieves. Then, the purified air is cooled to the dew point temperature and separated by cryogenic distillation in a cold box, which is heavily insulated to limit heat losses [205]. Since the air purification step is not of primary concern in this work, it is disregarded in all the models of ASU processes integrated with LNG vaporization. However, the LNG pumping system is included in the integration schemes.

In the case of the reference single column ASU system, a simplified LNG vaporization system was included to evaluate the total performance of the ASU and the regasification process stand-alone so that it can be compared with the two integration options. The LNG vaporization system is composed of a pump to pressurize the LNG feed and a heater to evaporate the compressed LNG. The stand-alone reference ASU system, which does not include the LNG regasification was also simulated to measure the original performance of the ASU. Other design specifications for thermodynamic properties and equipment in the processes are indicated in Table 7.1.

Table 7.1 Design parameters for the ASU systems.

Process parameters	Value
Equation of state	Peng-Robinson
Compressor polytropic efficiency [%]	78
Expander polytropic efficiency [%]	78
Pump adiabatic efficiency [%]	75
Cooler outlet temperature [°C]	26
$\Delta T_{\min}$ in heat exchangers [°C]	1

7.3.2 LNG feed

The required natural gas pressure at the outlet of the LNG regasification terminal depends on the end-users, ranging from 6 to 25 bar for power stations, 30 bar for local distribution and over 60 bar for long-distance distribution [73]. This parameter has a noticeable influence on the performance of the integration solutions because the compression to the selected distribution pressure consumes pumping power and the pressure level affects the available cold energy of the LNG [71]. This work will focus on long-distance gas distribution, selecting a gas outlet pressure of 60 bar for the models. Due to the importance of the LNG pumping pressure, it was varied from 20 bar to 100 bar in order to measure the effect on the process performance in Section 6.2. In the review of existing ASU systems integrated with LNG regasification, the flow rates of the LNG feed range from 8 tons per hour for small-scale to 68 tons per hour for large-scale integration processes, and the larger scale has been the latest trend [77]. Thus, a flow rate of 3300 kmol per hour (equivalent to around 58 tons per hour) was selected for large-scale ASU systems integrated with LNG vaporization. Other design conditions related to LNG are shown in Table 7.2.

Table 7.2 Conditions of LNG feed.

Conditions	Unit	Value
LNG feed temperature	°C	-162.0
LNG feed pressure	bar	1.3
LNG export pressure	bar	60.0
LNG feed flow rate	kmol/h	3300.0
LNG feed composition		
Nitrogen	mol %	1.01
Methane	mol %	91.59
Ethane	mol %	4.93
Propane	mol %	1.71
i-Butane	mol %	0.35
n-Butane	mol %	0.40
i-Pentane	mol %	0.01

7.3.3 Air feed

For simplification, the air feed is assumed to consist of N_2 and O_2 only. Since noble gas production is not studied in this work, the presence of argon, helium, etc. is neglected. Further, it is assumed that the air pre-treatment (not included in the simulation models) completely removes water and carbon dioxide. Conditions of the air feed are provided in Table 7.3.

Table 7.3 Conditions of air feed.

Conditions	Unit	Value
Air feed temperature	°C	25.00
Air feed pressure	bar	1.01
Air feed flow rate	kmol/h	2426.00
Air feed composition		
Nitrogen	mol %	79.06
Oxygen	mol %	20.94

7.3.4 Product specification

The classic indicator to evaluate ASU designs is the power consumption per amount of liquid nitrogen or oxygen produced. However, the compression work required is varying depending on the quantity of liquid products from the ASU systems. The desired product purities are other factors influencing the performance of the ASU schemes. Thus, the product flow rates and purities were set to be equal for all the ASU processes integrated with LNG regasification.

During the simulation work, the maximum flow rate that could be reached for liquid nitrogen produced from the recycled nitrogen was around 415 kmol per hour with a purity of 99.5 mol % in the single column ASU with an LN2 production cycle. These values were used as specifications for the alternative integration option (ASU with pre-cooling).

Pure liquid oxygen is also produced in all the models. The flow rate of liquid oxygen is varying based on the configuration of the integration systems since it is constrained by the reflux needed

in the distillation column and the heat balance of the integrated condenser-reboiler. Thus, the amount of liquid oxygen product was fixed at the quantity of the vapor oxygen produced in the reference single ASU system, which is one of the design targets for the integration schemes. None of the processes provided gaseous oxygen, however, they do produce a gaseous nitrogen stream, which is vented to the atmosphere.

The reference single column ASU was manipulated to produce liquid nitrogen from the nitrogen reflux in order to be compared with the integration schemes delivering liquid products. Due to the lack of cold duty without LNG cold energy utilization, the maximum achievable amount of liquid nitrogen was 158 kmol per hour based on the one-column ASU. Thus, this value is set for the liquid nitrogen product from the nitrogen reflux in the stand-alone single column ASU and the two integration options. However, sufficient amounts of pure gaseous oxygen and nitrogen with a purity above 99.5 mol % are produced in the stand-alone single column ASU.

Apart from product flow rate and purity, other conditions such as temperature and pressure will vary among the ASU processes, thus having different exergy values. Besides, there will always be a minor difference between the specifications and the actual products. Thus, evaluation and comparison based on energy may not be adequate. Exergy efficiency, however, can account for varying compositions, flow rates, temperatures and pressures of the product streams, as will be explained in Section 5. Thus, the temperature and pressure levels of the products will vary depending on the ASU processes, accepting a marginal difference in their purity and flow rate.

The LNG stream supplying a cold duty to existing ASU systems integrated with LNG regasification is generally warmed to ambient temperature either in cryogenic heat exchangers or intercoolers for air and nitrogen compressors [77, 90, 203]. This leads to large temperature gaps in the cryogenic exchangers and the intercoolers, causing significant amounts of entropy generation. Thus, the outlet temperature of the LNG product was not restricted to ambient temperature in order to find optimal use of the LNG cold energy in the integration schemes. The detailed specifications for ASU products are summarized in Table 7.4.

Table 7.4 Product specifications for the ASU systems.

Condition	Unit	LN2[a]	LN2[b]	LO2	LNG
Temperature	°C	vary	vary	vary	vary
Pressure	bar	4.5	vary	vary	60
Purity	mol %	> 99.5	> 99.5	> 99.9	-
Flow rate	kmol/h	158	415	499	3300

[a]LN2 extracted from the nitrogen reflux

[b]LN2 extracted from the recycled nitrogen

7.4 Optimization and exergy analysis

7.4.1 Optimization

To perform a fair comparison between the two integration options, they were both subject to some kind of optimization. Since optimizing a distillation column is complex, the design conditions related to the column were disregarded. The variables related to the air compressors, and the high pressure as well as the molar flow rate of the nitrogen reflux were not adjusted, in order to conform with the reference ASU design. This will allow focusing on the heat integration part of the ASU systems, indicating the actual potential of utilizing the LNG cold energy. Thus, all the inlet temperatures and outlet pressures of the multi-stage compressors for the recycled nitrogen were set as variables. The final temperature of the recycled nitrogen to be throttled before producing liquid nitrogen is also considered a variable. In addition, all the inlet temperatures and outlet pressures of the multi-stage expanders for the recycled nitrogen were also defined as variables in addition to the pressure level of the booster pump for the recycled nitrogen. Besides, the molar flow rate of the by-passed air, the recycled nitrogen and the liquefied nitrogen sent to the integrated heat exchanger (Cond-Reb) were selected as variables. For integration Option 2, the intermediate temperatures of the streams flowing between the MHE and the Sub-HE were set as extra variables. The values of the ranges for the variables are listed in Table 7.5 for Option 1 and Table 7.6for Option 2.

With the decision variables $\mathbf{x}$, the two integration schemes were optimized for the objective function and constraints in Eq (7.1), where $a \in H$ and $b \in K$. H represents the set of cryogenic heat exchangers and K is the set of compressors.

$$
\begin{aligned}
&\min_{\mathbf{x}} && f(\mathbf{x}) = \frac{\dot{W}_{\text{net}}}{\dot{m}_{\text{LN2}} + \dot{m}_{\text{LO2}}} \\
&\text{subject to} && \Delta T_{\text{min,a}} \geq 1 && (7.1) \\
& && Pr_{\text{b}} \leq 3 \\
& && \mathbf{x}_{LB} \leq \mathbf{x} \leq \mathbf{x}_{UB}
\end{aligned}
$$

The objective is to minimize power consumption per amount of total liquid products. A minimum temperature difference of 1 K is applied for all heat exchangers as a constraint, which is a common practice in cryogenic processes[206]. The maximum pressure ratio of compressors is set to 3. The optimization is performed by sequential quadratic programming (SQP) due to the nonlinearity of the system. The optimization results are shown in Table 7.5 and Table 7.6 in the Supporting Information for Option 1 and Option 2 respectively.

7.4.2 Exergy analysis

Exergy is the maximum available work obtained by bringing a system to equilibrium with its environment. Thus, exergy analysis, which is a combination of the first and second laws of thermodynamics, is based not only on the condition of a system but also the environment. Different energy sources having different qualities such as temperature, pressure and composition can be measured by exergy. These features make exergy efficiency more reliable than energy efficiency, showing the real performance of processes. Exergy analysis also allows identifying where exergy is destroyed in a process, in other words, the location of entropy generation. This gives guidelines to improve efficiency by highlighting units having the largest exergy destruction. Thus, in this work, exergy analysis is regarded as a valuable post design tool together with specific power consumption.

Table 7.5 Bounds of the decision variables for optimization of Option 1 and the best solution (the LNG pumping pressure = 60 bar).

Variable	Unit	Lower bound	Upper bound	Optimum value
T_{N09}	°C	-120.0	-60.0	-120.0
T_{N11}	°C	-175.0	-160.0	-167.3
T_{N13}	°C	-135.0	-105.0	-108.2
T_{N15}	°C	-175.0	-160.0	-175.0
T_{N17b}	°C	-145.0	-115.0	-137.8
T_{N19c}	°C	-110.0	-75.0	-88.2
T_{N19e}	°C	-155.0	-115.0	-132.8
T_{N19g}	°C	-80.0	-50.0	-65.1
p_{N10}	bar	8.5	11.5	11.4
p_{N12}	bar	28.0	32.5	28.0
p_{N14}	bar	50.0	80.0	50.0
p_{N19b}	bar	30.0	120.0	34.0
p_{N19d}	bar	11.0	25.0	25.0
P_{N19f}	bar	3.8	8.5	3.8
$\dot{n}_{A05a}$	kmol/h	0.0	450.0	240.0
$\dot{n}_{N05}$	kmol/h	400.0	700.0	415.5
$\dot{n}_{N21a}$	kmol/h	400.0	700.0	700.0

Table 7.6 Bounds of the decision variables for optimization of Option 2 and the best solution (the LNG pumping pressure = 60 bar).

Variable	Unit	Lower bound	Upper bound	Optimum value
T_{A05b}	°C	-165.0	-145.0	-162.7
T_{N02}	°C	-180.0	-150.0	-167.8
T_{N10}	°C	-100.0	-40.0	-96.0
T_{N12}	°C	-178.0	-175.2	-165.0
T_{N14}	°C	-155.0	-110.0	-132.3
T_{N16}	°C	-168.0	-155.0	-167.4
T_{N17}	°C	-175.0	-155.0	-173.2
T_{N19b}	°C	-175.0	-150.0	-172.4
T_{N22c}	°C	-180.0	-160.0	-176.0
T_{N23c}	°C	-125.0	-85.0	-125.0
T_{N23e}	°C	-130.0	-110.0	-130.0
T_{N23g}	°C	-80.0	-50.0	-60.0
p_{N11}	bar	5.5	20.0	6.7
p_{N13}	bar	20.0	40.0	20.0
p_{N15}	bar	40.0	85.0	41.8
p_{N23b}	bar	40.0	80.0	40.0
p_{N23d}	bar	8.0	15.0	11.3
p_{N23f}	bar	3.8	8.5	3.8
$\dot{n}_{A05a}$	kmol/h	0.0	450.0	450.0
$\dot{n}_{N06}$	kmol/h	400.0	700.0	410.2
$\dot{n}_{N22a}$	kmol/h	400.0	700.0	700.0

Exergy analysis requires decomposition of exergy, which can vary depending on the type of process. Thus, various exergy decompositions have been suggested, showing different definitions of exergy efficiency [96, 185, 187, 188, 197] as discussed in Chapter 0. In this work, one of the approaches to exergy decomposition ($\dot{E}^{\mathrm{T}}, \dot{E}^{\mathrm{p}}, \dot{E}^{\mathrm{Comp}}, \dot{E}^{\mathrm{Reac}}$) was used to perform an objective and consistent exergy analysis [96]. Kinetic, potential, electrical and nuclear exergies were not considered in the exergy decomposition. The detailed information about the decomposition is given in Chapter 6.2.

This work applies the Exergy Transfer Effectiveness (ETE) to evaluate the exergy efficiency of the ASU systems integrated with LNG regasification [194]. This exergy efficiency was developed for low-temperature processes, offering a general mathematical expression. Still, the use of the ETE is limited to changes in temperature and pressure of a system (i.e. only thermo-mechanical exergy). Thus, an extended version of ETE recently developed in our group has been used to analyze the integration schemes by including the compositional and reactional exergy terms as introduced in Chapter 6.3.2 [118]. Consequently, the extended definition can handle all changes in flow rate, concentration, pressure, and temperature in the ASU systems integrated with LNG regasification. Besides, this indicator can evaluate and compare the performance of the integration processes, even in cases with different products, due to the definition of the extended ETE.

The ETE is defined as the ratio between exergy sinks and exergy sources as shown by Eq. (7.2).

$$ETE = \frac{\sum \mathrm{Exergy\ Sinks}}{\sum \mathrm{Exergy\ Sources}} \tag{7.2}$$

An exergy increase of a process or unit is considered an exergy sink, while an exergy decrease indicates an exergy source. Likewise, compression work is an exergy source, while expansion work is an exergy sink.

The extended ETE with the four exergy components ($\dot{E}^{\mathrm{T}}, \dot{E}^{\mathrm{p}}, \dot{E}^{\mathrm{Comp}}, \dot{E}^{\mathrm{Reac}}$) can then be defined by Eqs. (7.3)-(7.5), where $j \in C, k \in I, m \in O$.

$$ETE = \frac{\sum_j\left(\Delta\dot{E}^j\right)^+ + \dot{W}_{\text{exp}}}{\sum_j\left(\Delta\dot{E}^j\right)^- + \dot{W}_{\text{comp}}} \tag{7.3}$$

where

$$\left(\Delta\dot{E}^j\right)^+ = \begin{cases} \displaystyle\sum_m \dot{E}_m^j - \sum_k \dot{E}_k^j & \text{if } \displaystyle\sum_k \dot{E}_k^j < \sum_m \dot{E}_m^j \\ 0 & \text{if } \displaystyle\sum_k \dot{E}_k^j > \sum_m \dot{E}_m^j \end{cases} \tag{7.4}$$

$$\left(\Delta\dot{E}^j\right)^- = \begin{cases} 0 & \text{if } \displaystyle\sum_k \dot{E}_k^j < \sum_m \dot{E}_m^j \\ \displaystyle\sum_k \dot{E}_k^j - \sum_m \dot{E}_m^j & \text{if } \displaystyle\sum_k \dot{E}_k^j > \sum_m \dot{E}_m^j \end{cases} \tag{7.5}$$

Eqs. (7.3)-(7.5) represent the ETE where C is the set of four exergy components, I is the set of inlet streams, and O is the set of outlet streams.

7.5   Results

7.5.1   Comparison of alternatives

In this section, the simulation results of the two different ASU systems integrated with LNG vaporization are assessed and compared with the reference single column ASU process. Specific power consumption per unit mass of liquid products is measured as a process performance index, and Table 7.7 indicates that integration Option 2 has smaller specific power consumption than Option 1 with almost the same amount of liquid products. The specific power for the reference ASU system was significantly larger since the process was originally developed for gas products. Thus, the ETE that can handle differences in products was calculated for all the ASU processes. The exergy efficiency values show that integration Option 2 is again the most efficient process followed by Option 1 and the reference ASU system.

Table 7.7 Simulation results for the reference single column ASU and its integration schemes with LNG regasification.

Process	Recycled N₂	LN2	LO2	Power consumption	Exergy destruction	*ETE*
	[kmol/h]	[kg/h]	[kg/h]	[kWh/kg]	[kW]	[%]
ASU	3639	4429	-	1.346	9979	47.93
Option 1	3730	16067	15975	0.310	7337	57.34
Option 2	3749	16076	15975	0.281	6158	61.05

The results in Table 7.7 clearly indicate that integration of an ASU with LNG regasification reduces power consumption and improves exergy efficiency for the entire system. The entries in Table 7.7 for ASU (1st row) is for stand-alone ASU and LNG regasification (i.e. not integrated). Both Option 1 and Option 2 show that the total system efficiency is significantly improved compared to the reference single column ASU, since considerably less LNG cold exergy is wasted in the regasification process. Nevertheless, the two integration options will have a lower exergy efficiency than the ideal case where the stand-alone ASU is assumed to receive the maximum work that can be produced from the cold energy utilized in integration Option 1 and 2. In that case, the *ETE* of the stand-alone ASU reaches 79.25 % and 78.93 % respectively.

Option 2 required the largest flow rate of recycled nitrogen, followed by Option 1 and the reference ASU system as seen in Table 7.7. Table 7.8 shows that Option 2 also demands the largest heat exchange area (*UA*) among the three cases due to lower values for log mean temperature difference (*LMTD*). This will result in a higher capital cost for Option 2 than the other alternatives. However, the low *LMTD* values indicate a close to optimal temperature match in the heat exchangers with the cold LNG stream, thus improving the process efficiency. In the case of Option 1, an optimal heat integration in the MHE and the NHE was not possible, resulting in large *LMTD*s. This also explains the higher exergy efficiency of Option 2 than Option 1.

Table 7.8 Heat exchangers in the reference single column ASU process and its integration schemes with LNG regasification.

		ASU		Option 1			Option 2		
	Unit	MHE	Cond -Reb	MH E	NHE	Cond -Reb	MH E	Sub -HE	Cond -Reb
$\Delta T_{\min}$	[K]	1.00	1.00	1.00	1.00	1.00	1.00	1.00	1.00
LMTD	[K]	3.10	1.13	7.82	2.42	1.26	2.09	3.87	1.26
UA	[MW/K]	2.62	1.25	0.91	5.83	1.90	8.77	0.22	1.90

7.5.2 Sensitivity analysis

The pressure level of the LNG product is usually dependent on the conditions of gas distribution networks. Thus, the pumping pressure of the stored LNG was varied from 20 bar to 100 bar in order to measure the effect of the different properties of LNG cold energy on the two integration schemes. The two integration options were also optimized under the different LNG pressure levels to find optimal operating conditions. The results illustrated in Figure 7.4 indicate that the specific power consumption increases with LNG pressure for both Option 1 and Option 2. The power consumption was increased by 10.6 % in Option 1 and 13.4 % in Option 2 when the pressure level was increased from 20 bar to 100 bar. This shows that Option 2 has a larger penalty for achieving an optimal heat integration with increased pressure than Option 1.

Regarding exergy efficiency, the *ETE* value for Option 1 increases with the LNG pressure, showing only a marginal increase after 80 bar as illustrated in Figure 7.4. The exergy efficiency for Option 2 even experiences a small decrease at 100 bar, explaining the sharper increase in specific power consumption with the LNG pressure than Option 1. Nevertheless, integration Option 2 has a smaller specific power consumption and a higher exergy efficiency at any given LNG pressure levels.
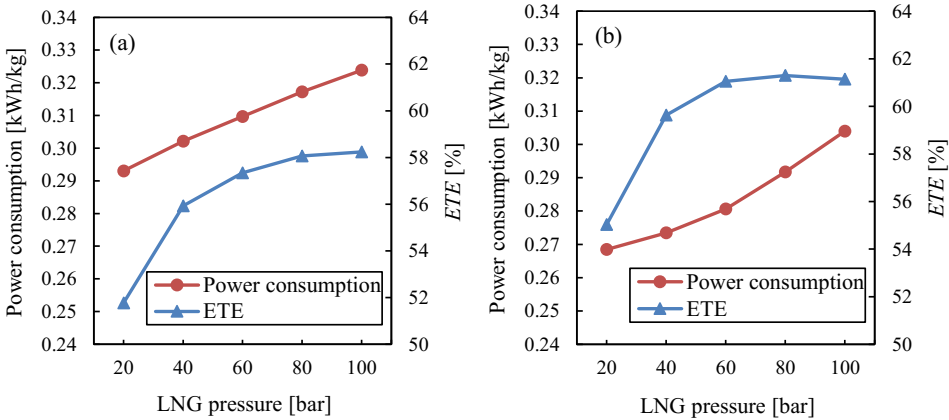
Figure 7.4 Variation of specific power consumption and exergy efficiency in integration Option 1 (a) and Option 2 (b) for different values of LNG pressure.

When it comes to exergy destruction, Figure 7.5 demonstrates that the main sources of thermodynamic losses for both Option 1 and Option 2 are turbo-machinery, followed by heat exchangers and valves, while mixers represents small losses. The amount of exergy destruction in Option 2 is smaller than Option 1, especially in the sum of turbo-machinery and heat exchangers, thus resulting in an efficient work and heat exchange network with the cold LNG stream.

The changes in exergy destruction for heat exchangers as function of LNG pressure is similar for Option 1 and Option 2. The amount of destruction decreases up to 60 bar and then increases for higher pressures, indicating that the optimal temperature match in the heat exchangers will be achieved at the LNG pressure of 60 bar. This trend in the exergy destruction with LNG pressure explains the considerable improvement of the *ETE* until 60 bar in Figure 4. Besides, the increase in exergy destruction after 60 bar is one of the reasons for the marginal increase in the exergy efficiency over 60 bar.

Unlike heat exchangers, the exergy destruction in turbo-machinery was proportional to the LNG pressure level for both integration options. The main contributor to this increment is the
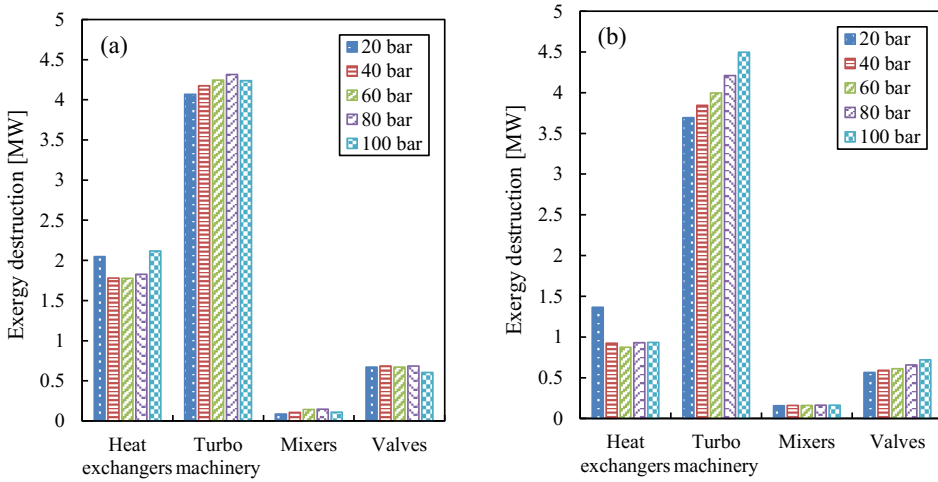
Figure 7.5 Variation of exergy destruction for main equipment in integration Option 1 (a) and Option 2 (b) for different values of LNG pressure.

LNG pump, having a larger loss with a higher outlet pressure. However, for Option 1 at 100 bar, the exergy destruction in the turbo-machinery was slightly reduced. This decrease is a consequence of the inadequate temperature match in the heat exchangers, requiring less pressure ratio in the recycled nitrogen expanders. The poor heat integration also results in smaller pressure drops in some throttling valves, which is the reason for the sudden decrease in exergy destruction for integration Option 1 at 100 bar. Nevertheless, the total exergy destruction of Option 1 at 100 bar is still the largest compared to other LNG pressure levels.

The units that are accounting for the largest share of the exergy destruction in heat exchangers are the NHE in Option 1 and the MHE in Option 2, which are the exchangers integrated with the LNG cold stream. Thus, the temperature difference between hot and cold composite curves in the two heat exchangers is plotted in Figure 7.6 to investigate their performance for different LNG pressures.

When the LNG pressure is 20 bar, the NHE has a significant temperature difference at around - 80 °C for the hot composite, increasing irreversibilities. This considerable gap contributed to

large exergy destructions in heat exchangers as depicted in Figure 7.5. At the LNG pressure of 100 bar, the NHE also shows a large temperature difference at around -100 °C.

The exergy destruction of the NHE at 100 bar shows a lower temperature difference in the hot end of the exchanger compared to other pressure levels. However, the penalty of the large temperature difference at colder temperatures exceeds the benefit of reduced temperature difference in the hot-end, resulting in the largest exergy destruction for the heat exchangers as seen in Figure 7.5. This is due to the characteristics of entropy generation caused by the temperature difference in a heat exchanger, which increases exponentially at lower temperatures. Thus, smaller driving forces at lower temperatures in a heat exchanger minimize total irreversibilities, while allowing an optimal use of heat exchanger area [42].

This indicates that the temperature difference profiles at 40 bar and 60 bar are close to the optimal distribution of driving forces, resulting in the lowest exergy destruction, as illustrated in Figure 7.5. The situation at 80 bar is similar to 100 bar in the sense that larger temperature differences in the middle of the NHE cannot be compensated by smaller temperature differences in the hot end, thus exergy losses are increased compared to the 60 bar case.

Similar to the NHE in Option 1, the temperature difference in the MHE in Option 2 at the LNG pressure of 20 bar is considerably larger at around -80 °C compared to other LNG pressure levels, resulting in the largest exergy destruction in heat exchangers, as seen in Figure 7.5. At LNG pressures higher than 20 bar, the distributions of the driving forces are almost identical, providing similar exergy destruction values as shown in Figure 7.5. One noticeable feature is that integration Option 2 managed to keep the temperature difference below 5 K in the cold end of the MHE for all LNG pressure levels. Therefore, the exergy destruction values of heat exchangers in Option 2 at any LNG pressure levels are lower than Option 1. This means that integration Option 2 provides an excellent flexibility to manipulate the system to achieve optimal distribution of the driving forces in the heat exchangers, leading to a higher process efficiency.
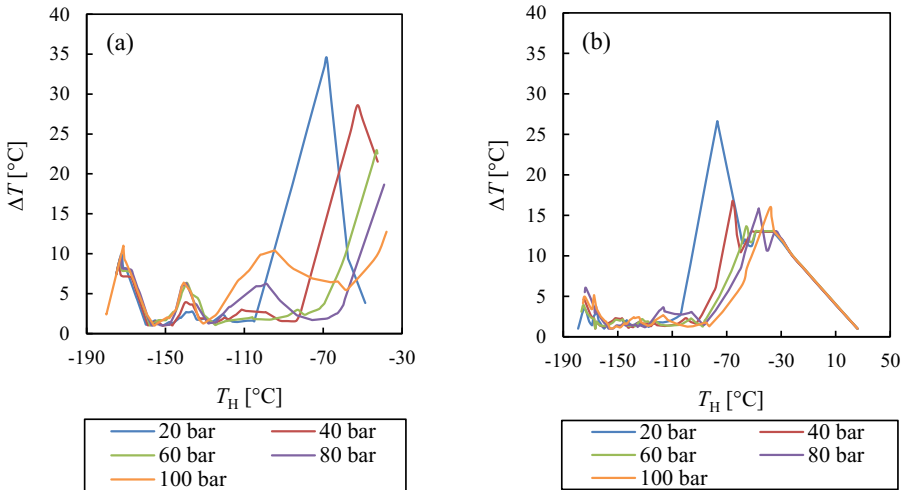
Figure 7.6 Temperature difference in the NHE for integration Option 1 (a) and in the MHE for integration Option 2 (b) for different values of LNG pressure.

Exergy destruction will not be a sufficient explanation to the changes in exergy efficiency with various LNG pressure levels since it is also related to the products of the integration schemes. In this work, the LNG stream leaving the integration processes is the product that has the largest effect on the changes in exergy efficiency, since the conditions of the final LNG product vary depending on the LNG pumping pressure levels. Other products such as LN2 and LO2 do not experience a substantial change in exergy values after optimizing the two integration options with different LNG pressure levels.

Figure 7.7 illustrates the temperature and pressure based exergy values of the final LNG product and the total exergy destruction for the two integration processes. Regarding the LNG product, it is obvious that the pressure based exergy increases with LNG pumping pressure. However, the temperature based exergy decreases with increasing LNG pressure. This is related to the special behavior of temperature based exergy below ambient temperature, i.e. it decreases with higher temperatures, which is opposite of the behavior above ambient.
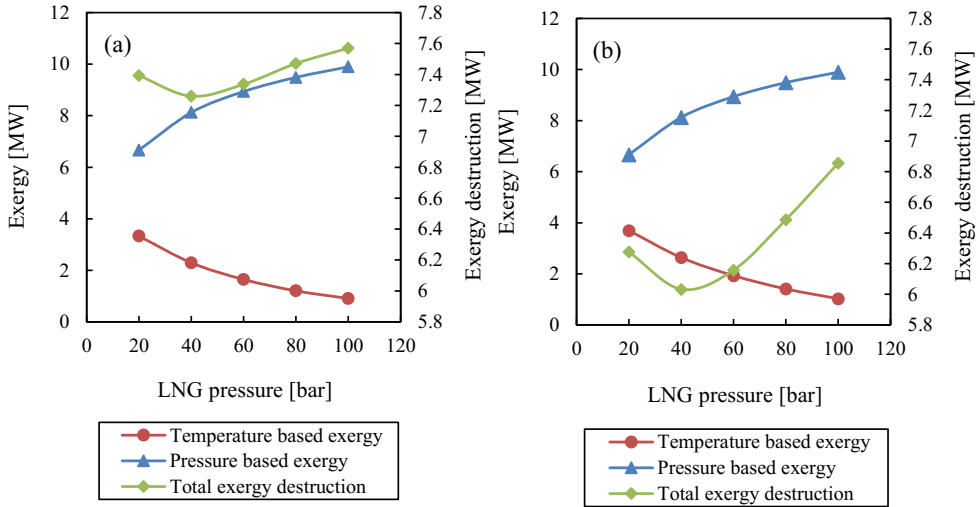
Figure 7.7 Variation of temperature and pressure based exergy of the LNG product and total exergy destruction in Option 1 (a) and Option 2 (b) for different values of LNG pressure.

Thus, the thermo-mechanical exergy of the final LNG will increase less at larger LNG pumping pressures. Such slow increase in exergy of the LNG product is compensated by the larger total exergy destruction with higher LNG pressures as seen in Figure 7.7. Therefore, the improvement in exergy efficiency starts diminishing after 40 bar where the lowest exergy destruction occurs in both integration options. In the case of Option 2, the exergy efficiency even indicates a decrease after 80 bar (see Figure 7.4) due to the sharp increase in total exergy destruction after 40 bar.

7.6   Conclusions

A single column air separation unit (ASU) has been integrated with an LNG stream in two different ways to try to achieve the best possible utilization of the cold energy available from LNG regasification. The cold energy of the LNG stream has been used as an extra refrigeration source either in a liquid nitrogen production cycle (Option 1) or for pre-cooling of air and

nitrogen streams (Option 2). After optimization, energy and exergy analyses have been applied to measure the performance of the two different integration schemes.

The energy analysis indicates that the single column ASU process with pre-cooling from LNG regasification has a lower specific power consumption (0.281 kWh/kg) than the integration option with a liquid nitrogen production cycle (0.310 kWh/kg). Integration Option 2 also shows a higher exergy efficiency than Option 1 due to an improved heat integration with the cold LNG stream, resulting in smaller temperature differences in the heat exchangers. However, Option 2 will require the largest capital cost due to a larger recycled nitrogen flow rate and larger heat exchanger area.

A sensitivity analysis with different LNG pumping pressure levels shows that the specific power consumption is increased with higher LNG pressure for both integration options. This indicates that the improved heat integration (smaller driving forces) resulting in reduced compression power does not compensate for the power consumption required to increase LNG pressure. On the other hand, the exergy efficiency increased with the LNG pumping pressure since the exergy values of the products also increased. This is not considered in energy analysis, which is an inaccurate performance index for such processes. With different LNG pressures, Option 2 consistently has a higher exergy efficiency than Option 1, since this integration scheme is able to keep the driving forces in the heat exchangers low independent of the pressure level. Particularly, Option 1 shows a large temperature difference in the nitrogen heat exchanger at the lowest and highest LNG pressure levels, causing a significant increase in exergy destruction.

Unlike existing integration solutions between ASU processes and LNG regasification, the integration schemes studied in this work result in a final LNG product that still has a low temperature. This could be utilized in other low temperature applications and represents an additional benefit from the solutions proposed in this chapter. Hence, a proper selection of an additional process utilizing the cold LNG product should be considered in the case of ASU processes integrated with LNG regasification in order to further improve the utilization of the LNG cold exergy.

Chapter summary

o For cryogenic processes, an energy performance indicator does not reflect the thermodynamic value of the products (pressure and especially temperature) and gives an inaccurate evaluation of the systems.

o In contrast, an exergy efficiency measures the quality changes in the pressure and temperature of the products, allowing the performance index to be an objective comparison index.

Chapter 8　Exergy analysis for LNG value chain: LNG processes with NGL extraction

In the last two chapters, exergy has been used as a post-design tool for an evaluation purpose. The results indicate that exergy efficiency can provide a representative measure for the thermodynamic performance and thus be used in comparative evaluation of cryogenic systems. Further, in this chapter, exergy efficiency is tested as an objective function for the optimization of complex cryogenic processes to answer the following questions:

- o　In design phase, can exergy efficiency be used as an objective function for the optimization of complex processes?
- o　What are the advantages using exergy efficiency as an objective function for cryogenic systems compared to energy efficiency?

8.1   Introduction

For global energy security, natural gas is one of the important energy sources with high mobility in the form of liquid [8]. During the liquefaction of natural gas, heavier hydrocarbons (HHC) like natural gas liquid (NGL) are often extracted from the feed gas. The extraction is performed to prevent the freeze-out of the HHCs in the liquefier and control the heating value of the liquefied natural gas (LNG) to meet the export specifications. The recovered HHCs are treated and sold as an additional product (NGL), helping project profitability due to the high economic value of these components. In addition, the hydrocarbons from the extraction schemes are further fractionated and used to make-up the refrigerants in the LNG processes.

NGL recovery from natural gas can be conducted upstream or as an integral part of a liquefaction system. The former scheme is achieved by a Joule-Thomson valve, a gas expander, and a scrub column. The latter requires an integration of the NGL extraction process with the LNG process, which may increase the complexity of design and operation. Traditionally, upstream NGL extraction systems were proposed for pipeline gas production as one of the treatment steps. Some of the typical systems are industry standard single stage (ISS) process, gas sub-cooled process (GSP), and recycle split vapor (RSV) process [207-209]. Since the upstream NGL systems are not designed for LNG processes, various configurations for the integration of the NGL recovery schemes in LNG processes have also been suggested [46, 88, 210-213].

Nevertheless, there have been few studies providing a comparative analysis between the two types of NGL extraction systems, and they are mainly for the comparison of the upstream NGL recovery configurations [99, 108, 214]. Thus, an optimization work was also conducted based on cost analysis in order to compare the upstream and the integration schemes [110]. However, this study does not indicate the maximum achievable thermodynamic performance of the two different schemes, which can be the basis for process improvement. Therefore, this chapter provides a comparative thermodynamic analysis for the two types of NGL extraction systems (upstream and integration) by performing optimization studies.

The NGL recovery processes tend to be analyzed and optimized using an energy performance indicator (power consumption) to improve the systems [88, 210, 212-216]. However, the energy efficiency for such cryogenic systems does not reflect the accurate thermodynamic performance of the processes since the indicator is not able to include the quality of the products such as temperature, pressure, and composition [118, 119]. The direct comparison of heat at different temperature levels with electric power is another undesirable property of the energy performance indicator for NGL extraction systems where both heat and power are consumed.

Thus, an exergy efficiency is selected as objective function for the optimization of the NGL and LNG production systems. This key performance indicator (KPI) considers temperature, pressure, and compositional changes in energy and product streams [118]. An optimization based on exergy analysis will indicate the thermodynamic optimal operating conditions of the configurations making it possible to conduct a fair comparison of the processes. Energy performance indicators such as specific energy consumption is also tested as an objective function for the optimization in order to compare the results with the best solutions achieved by optimizing exergy efficiency. For the natural gas liquefaction part, a dual mixed refrigerant (DMR) LNG process is selected and optimized with the NGL recovery systems.

8.2 Process design

8.2.1 DMR process with upstream NGL extraction

The upstream HHC extraction is typically performed by gas expander based systems. Through turbo-machinery equipment, the temperature of the feed gas is reduced due to the expansion, supplying the cold duty of the NGL extraction system. Thus, there have been various extraction schemes using gas expanders [207-209, 217]. In this work, we choose a simple upstream NGL extraction system called industry standard single stage (ISS) process in order to focus on the fundamental difference between upstream and integrated configurations [208, 209].
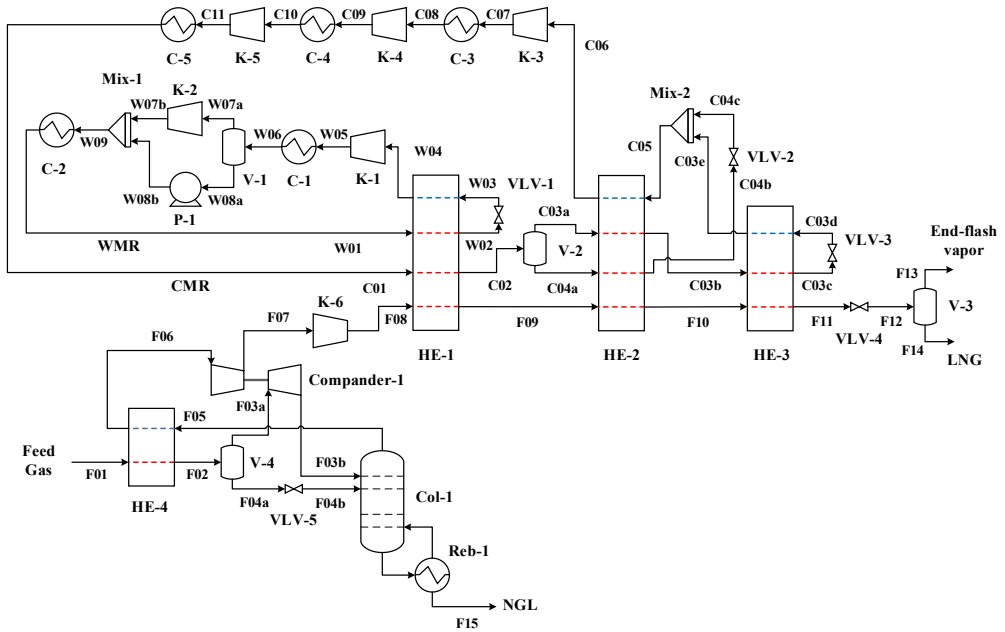
Figure 8.1 Process flow diagram of the DMR process with upstream NGL extraction (ISS-LNG system) [208, 209].

A DMR process is selected and integrated with the ISS scheme in order to represent the liquefaction system in this work [28]. This liquefaction process contains two refrigeration cycles having mixed hydrocarbon refrigerants.

Figure 8.1 shows the entire system for upstream NGL extraction and LNG production, which is referred to as the ISS-LNG system. The feed gas is sent to heat exchanger HE-4 and cooled to be partially condensed. The two-phase mixture stream is then separated to vapor (F03a) and liquid (F04a) streams in phase separator V-4. The liquid stream is throttled by Joule-Thomson (JT) valve VLV-5 and sent to distillation column Col-1 as one of the feed streams. Stream F03a is also expanded through the expander part of a compander (Compander-1) and delivered to the distillation column. A compander is a kind of turbo-machinery where a compressor and expander are installed on the same shaft. The bottom product from the column is partially

vaporized in heat exchanger Reb-1 to remove lighter hydrocarbons in the NGL product (F15). The heat duty of the re-boiler is assumed to be supplied by steam.

The top vapor product from the column is returned to heat exchanger HE-4 to provide its cold duty. Due to the depressurization of the feed gas via the expander and JT valve, the lean vapor product from the column (F06) is recompressed through the compressor part of Compander-1. The compression power is supplied by the power generated during the expansion of stream F03a. Compressor K-6 further boosts the compressed stream (F07) and sends it to the liquefaction process. The high-pressure lean gas stream (F08) is sent to heat exchanger HE-1 to be pre-cooled and the cooling duty is produced by a refrigeration cycle operated by a warm mixed refrigerant (WMR).

The pre-cooled natural gas is then liquefied through heat exchanger HE-2 and sub-cooled by HE-3. The cold duty of HE-2 and HE-3 is supplied by a refrigeration cycle with a cold mixed refrigerant (CMR). The sub-cooled LNG is then depressurized to near ambient pressure for storage and transportation purposes. The throttled LNG stream F12 is separated in the flash drum (V-3) to a nitrogen rich vapor stream (End-flash vapor) and the LNG product.

8.2.2 DMR process integrated with NGL extraction

Unlike the ISS-LNG system, the extraction of HHCs can be performed in the middle of a liquefaction system as seen in Figure 8.2 [28]. This configuration is referred to as the NGL-LNG system. The feed gas is pre-cooled by heat exchanger HE-1 in the DMR process and throttled by a JT valve (VLV-5). In contrast to the ISS process, the depressurized stream (F03) is sent directly to distillation column Col-1 as a feed stream without any heat integration. The liquid product extracted from the bottom of the column is then heated in heat exchanger Reb-1 to vaporize lighter hydrocarbons and the remaining stream is the NGL product (stream F11). The top vapor stream of Col-1 is compressed in the boost compressor (K-6) to compensate the reduced pressure level of the feed gas. The pressurized gas stream is then liquefied and sub-cooled in heat exchanger HE-2 and HE-3 before being throttled to ambient pressure to produce end-flash vapor and LNG.
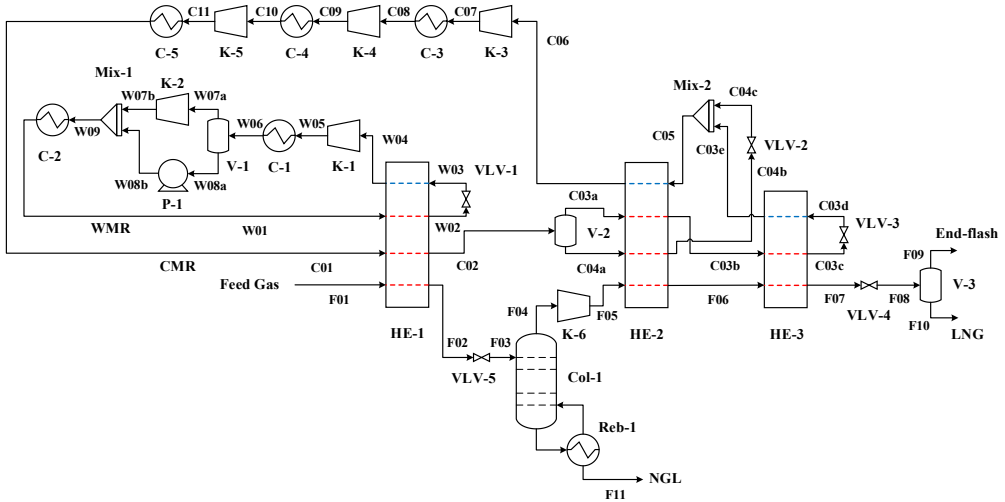
Figure 8.2 Process flow diagram of the DMR process integrated with NGL extraction (NGL-LNG system) [28].

In this configuration, the integration of NGL recovery and LNG production allows reducing the number of units for HHC extraction compared to the ISS system. However, the performance of the NGL extraction part in this integration scheme will directly affect the liquefaction process, giving extra difficulties in the optimization and operation of the total system.

8.2.3 DMR process integrated with refluxed NGL extraction

In order to improve the process efficiency, the NGL extraction part of the integrated scheme has the same level of complexity as the ISS-LNG process. Thus, a refluxed distillation system with a condenser was implemented in the DMR process to be compared with the ISS system with the same number of units. This configuration is referred to as the refluxed NGL-LNG system.

Similar to the ISS process, the feed gas is cooled by heat exchanger HE-4 as seen in Figure 8.3. A portion of the WMR is expanded by JT valve VLV-4 and supplied to HE-4 to cover the

cooling demand in the exchanger and then returned to the WMR refrigeration cycle for the DMR process. The cold feed gas is then depressurized through VLV-5 and fed to distillation
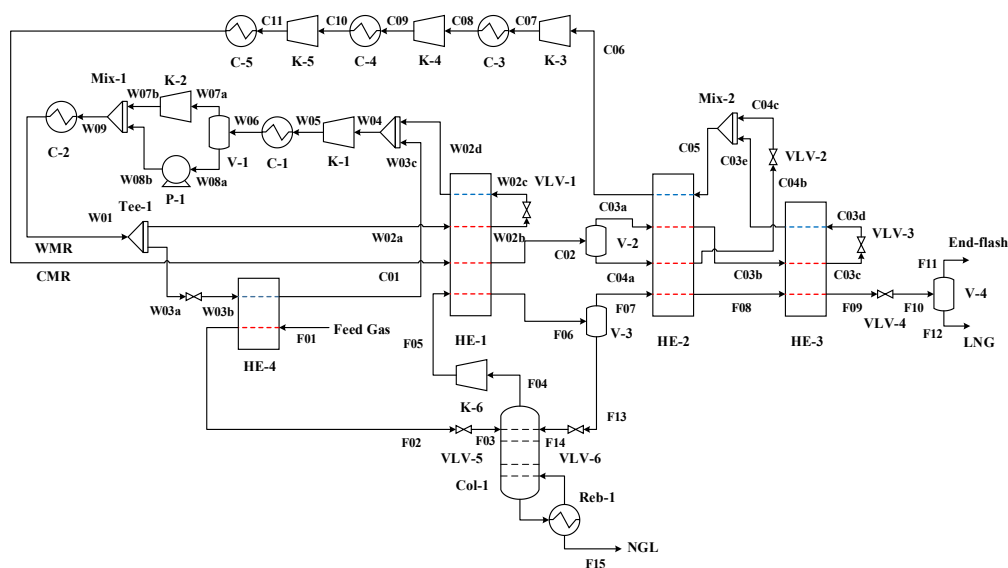
Figure 8.3 Process flow diagram of the DMR process integrated with refluxed NGL extraction (refluxed NGL-LNG system) [30].

column Col-1. The bottom product of Col-1 is reboiled in heat exchanger Reb-1 to reduce methane slip to the NGL product. The top vapor stream from the column is compressed and sent to heat exchanger HE-1 in the DMR process. The partially condensed feed gas from HE-1 is separated to vapor (F07) and liquid (F13) streams. The liquid stream F13 is returned to the distillation column after being throttled by JT valve VLV-6. This reflux stream (F14) is used to achieve deeper extraction of HHCs from the feed gas. The vapor stream F07 is then further cooled in heat exchangers HE-2 and HE-3 and depressurized to deliver end-flash vapor stream and the LNG product.

8.3   Design basis

8.3.1 Simulation conditions

Natural gas from reservoirs is treated in gas processing plants and delivered to an LNG plant through pipelines to produce LNG. The pipeline gas is sent to gas cleaning stages in the LNG plant where sour gases and water are removed. The pre-treated gas is then fed to the NGL and LNG production systems. Although the gas cleaning steps are essential for the total LNG system, the focus in this work is on the NGL and LNG process schemes for the simulation and optimization studies in this chapter. Other utility processes of the LNG plant such as end-flash gas handling, power generation, heat production, and cooling water systems were not included in the simulation model. The NGL and LNG production systems were simulated by Aspen HYSYS V9 with the Peng-Robinson equation of state (EOS) [132]. Pressure drops and heat losses of equipment are neglected in the simulation models. Other simulation conditions of process units are given in Table 8.1.

Table 8.1 Simulation conditions of the integration schemes.

Design parameters	Unit	Value
Condenser / intercooler outlet	°C	22
Compressor	Polytropic %	78
Pump	Adiabatic %	75
Compressor in a compander	Polytropic %	73
Expander in a compander	Polytropic %	83
Distillation column trays	stages	20

8.3.2 Feed gas and products

The removal of benzene, toluene, and xylene (BTX) is essential for NGL extraction systems, since these components easily freeze-out even with marginal fractions during the liquefaction process [218]. Thus, the vapor product from NGL recovery systems have to contain a low

level of BTX so that the stream can be liquefied in LNG production systems. However, the aromatic hydrocarbon components tend to be excluded in many studies about NGL systems [46, 83, 88, 99, 108, 110, 192, 211-213, 215, 216]. Thus, the previous research does not guarantee that the gas product from their NGL systems contains a sufficiently small amount of BTX when aromatic components are included in the feed gas. Therefore, in this work, hydrocarbons from methane (C_1) to decane (C_{10}) and the aromatic components (BTX) are included in the feed gas.

As mentioned in Chapter 8.3.1, pre-treated gas is sent to the NGL and LNG production systems. Due to the gas cleaning processes, sour components and water are not contained in the feed gas. Other feed gas conditions are seen in Table 8.2.

Table 8.2 Feed gas conditions.

Property	Unit	Value
Temperature	°C	22.00
Pressure	bar	60.00
Flow rate	kmol/hr	35000.00
Nitrogen	mol %	1.00
Methane	mol %	91.00
Ethane	mol %	4.90
Propane	mol %	1.70
i-Butane	mol %	0.35
n-Butane	mol %	0.40
i-Pentane	mol %	0.15
n-Pentane	mol %	0.15
n-Hexane	mol %	0.13
n-Heptane	mol %	0.10
n-Octane	mol %	0.04
n-Nonane	mol %	0.01
n-Decane	mol %	0.01
Benzene	mol %	0.03
Toluene	mol %	0.02
m-Xylene	mol %	0.01

To prevent the solidification of HHCs in the LNG process, the amount of BTX in the vapor product from the NGL extraction systems is limited to 10 ppm. The fraction of C5+ is also set to be smaller than 0.1 mol % in the vapor product in order to maximize the production of NGL, which is more valuable than LNG. The pressure level of LNG and end-flash products are set to be 1.5 bar for storage and transport purposes. The nitrogen content in the final LNG product is also controlled to be less than 1 mol % to meet sales gas specifications.

8.4   Performance indicator and optimization

The NGL and LNG production systems are operated by using electric power for compressors and hot steam for the reboiler of the distillation column. During the evaluation of the systems, however, the heat delivered by steam is typically disregarded for the calculation of energy performance indicators [88, 210, 215]. However, to be more accurate, we use specific energy consumption including heat as an energy performance indicator to evaluate the NGL extraction and LNG process [177].

$$En_{\text{specific}} = \frac{\dot{W}_{\text{comp}}^{\text{total}} + \dot{Q}_{\text{Col-1}}}{\dot{m}_{\text{NGL}} + \dot{m}_{\text{LNG}}} \tag{8.1}$$

Although heat is included in the specific energy consumption, the thermodynamic value of heat varies depending on the temperature. Thus, the direct inclusion of heat with work will result in an inaccurate thermodynamic evaluation of the system. In addition, the two products (NGL and LNG) will have changes in temperature, pressure, and composition during optimization. This variation will not be noticed by the energy performance indicator.

Thus, exergy will be an alternative to the energy performance indicator to consider all quality changes in the heat and products. Exergy is the maximum available work obtained by bringing a system to equilibrium with its environment based on temperature, pressure, and composition. Thus, all quality variations in process streams and different energy forms can be measured by exergy, resulting in a reliable measure for thermodynamic performance.

Nevertheless, exergy analysis has mostly been used as a post-design tool for NGL extraction systems to find the sources of irreversibilities and measure the improvement of the processes [99, 211, 212, 219, 220]. In contrast, there has been a study using the total exergy loss in NGL recovery processes as objective function to optimize such complex systems [99]. However, similar to the energy performance indicator, exergy loss does not consider the quality of the products, thus giving inaccurate optimization solutions.

Therefore, in this chapter an exergy efficiency (extended Exergy Transfer Effectiveness - ETE) is used as a performance indicator to optimize the NGL-LNG production systems [118]. This consumed-produced type of exergy efficiency properly reflects the changes in both thermo-mechanical (temperature and pressure) and chemical quality of the products. For the calculation of the ETE, exergy is composed of four elements, reflecting the work potential of temperature, pressure, composition, and reaction ($\dot{E}^{\mathrm{T}}$, $\dot{E}^{\mathrm{p}}$, $\dot{E}^{\mathrm{Comp}}$, $\dot{E}^{\mathrm{Reac}}$) in a stream. The general definition of each element is given in Chapter 6.2. In this chapter, however, the exergy of heat ($\dot{E}^{\mathrm{Q}}$) supplied to the reboiler is calculated by the exergy difference of the steam that passes a heat exchanger having the heat duty Q. The ETE is defined by the ratio between exergy sinks and exergy sources as indicated by Eq. (8.2).

$$ETE = \frac{\sum \text{Exergy Sinks}}{\sum \text{Exergy Sources}} \tag{8.2}$$

An exergy increase through a process is considered an exergy sink, while a decrease in exergy represents an exergy source. Thus, compression work will be an exergy source, while expansion work is an exergy sink. In addition, the heat consumed in the reboiler will be an exergy source.

The extended ETE with the four exergy components ($\dot{E}^{\mathrm{T}}$, $\dot{E}^{\mathrm{p}}$, $\dot{E}^{\mathrm{Comp}}$, $\dot{E}^{\mathrm{Reac}}$) and the exergy of heat is defined by Eqs. (8.3)-(8.5), where $j \in C, k \in I, m \in O$.

$$ETE = \frac{\sum_j \left(\Delta \dot{E}^j\right)^+ + \dot{W}_{\mathrm{exp}}}{\sum_j \left(\Delta \dot{E}^j\right)^- + \dot{E}^{\mathrm{Q}}_{\mathrm{reb}} + \dot{W}_{\mathrm{comp}}} \tag{8.3}$$

where

$$\left(\Delta\dot{E}^j\right)^+ = \begin{cases} \displaystyle\sum_m \dot{E}_m^j - \sum_k \dot{E}_k^j & if \ \displaystyle\sum_k \dot{E}_k^j < \sum_m \dot{E}_m^j \\ 0 & if \ \displaystyle\sum_k \dot{E}_k^j > \sum_m \dot{E}_m^j \end{cases} \tag{8.4}$$

$$\left(\Delta\dot{E}^j\right)^- = \begin{cases} 0 & if \ \displaystyle\sum_k \dot{E}_k^j < \sum_m \dot{E}_m^j \\ \displaystyle\sum_k \dot{E}_k^j - \sum_m \dot{E}_m^j & if \ \displaystyle\sum_k \dot{E}_k^j > \sum_m \dot{E}_m^j \end{cases} \tag{8.5}$$

Eqs. (8.3)-(8.5) represent the ETE where C is the set of four exergy components, I is the set of inlet streams, and O is the set of outlet streams.

Thus, with the two suggested performance parameters (En_{specific} and ETE), optimization studies using a local solver based on a sequential quadratic programming (SQP) algorithm, were conducted with the problem formulation provided by Eqs. (8.6)-(8.8).

$$\min_{\mathbf{x}} f(\mathbf{x}) = \text{Obj}_1(\mathbf{x}) \lor \text{Obj}_2(\mathbf{x})$$

$$\begin{aligned} \text{subject to} \ \ & \Delta T_{\text{min,a}}(\mathbf{x}) \geq 3 & a &= \{\text{HE-}1,2,3,4\} \\ & \Delta T_{\text{sup,}b}(\mathbf{x}) \geq 0 & b &= \{\text{W04, C06}\} \\ & 1 \leq Pr_c(\mathbf{x}) \leq 4 & c &= \{\text{K-}1,2,3,4,5,6\} \\ & x_{N_2}^{\text{LNG}}(\mathbf{x}) \leq 1 \text{ mol \%} \\ & \textstyle\sum_d x_d^{\text{Col-1 vap}}(\mathbf{x}) \leq 0.1 \text{ mol \%} & d &= \{\text{i-}C_5, \text{n-}C_5 \dots, \text{m-Xylene}\} \\ & \textstyle\sum_e x_e^{\text{Col-1 vap}}(\mathbf{x}) \leq 10 \text{ ppm} & e &= \{\text{Benzene, Toluene, m-Xylene}\} \\ & \mathbf{x}_{\text{LB}} \leq \mathbf{x} \leq \mathbf{x}_{\text{UB}} \end{aligned} \tag{8.6}$$

where

$$\text{Obj}_1 = En_{\text{specific}}(\mathbf{x}) \tag{8.7}$$

$$\text{Obj}_2 = ETE(\mathbf{x}) \tag{8.8}$$

During the optimization, all the product specifications mentioned in Chapter 8.3.2 are regarded as constraints. In order to fulfil the balance between thermodynamic performance and cost of heat exchangers, the minimum temperature difference is set to be larger than 3 K [86, 140]. The degree of superheating at the compressor inlet streams is also constrained to be larger than zero Kelvin to protect compressor blades from droplets. The maximum pressure ratio of compressors is limited to be less than 4 due to practical issues [141]. The decision variables and the optimization results for the NGL and LNG production systems are shown in Table 8.3 with corresponding constraint values in Table 8.4.

8.5   Results

In this chapter, the DMR process with upstream or integrated NGL extraction was optimized and compared based on two performance indicators (specific energy consumption and exergy efficiency). All processes also fulfilled the constraints such as C_{5+} and BTX contents in the vapor stream entering the liquefaction system.

The optimization results with the energy performance indicator (Obj_1 in Table 8.5) shows that the refluxed NGL-LNG process has the smallest specific energy consumption. The upstream NGL extraction system (ISS-LNG process) also indicates a low specific energy consumption, having a marginal difference compared to the refluxed NGL-LNG system. The simple integration scheme of NGL and LNG production (NGL-LNG system), however, has the largest specific energy consumption. This large energy consumption indicates that the integration may not be thermodynamically advantageous compared to the upstream HHC extraction when the NGL recovery system is not thoroughly heat integrated with the liquefaction system.

Table 8.3 Bounds of the decision variables and the best solutions for the integration schemes.

Variable	Unit	Bound		ISS-LNG		NGL-LNG		Refluxed NGL-LNG	
		LB	UB	Obj_1	Obj_2	Obj_1	Obj_2	Obj_1	Obj_2
$\dot{m}_{C_1,WMR}$	kmol/hr	1000	13000	6044	3772	7151	4677	3114	2487
$\dot{m}_{C_2,WMR}$	kmol/hr	20000	38000	30058	25597	32686	28173	29808	25935
$\dot{m}_{C_3,WMR}$	kmol/hr	2000	14000	9471	12563	13737	10875	8112	9472
$\dot{m}_{nC_4,WMR}$	kmol/hr	100	9000	5679	6556	6582	7531	8471	8131
$\dot{m}_{N_2,CMR}$	kmol/hr	2000	10000	2000	2000	2000	2000	2000	2021
$\dot{m}_{C_1,CMR}$	kmol/hr	10000	25000	17810	18457	19042	18677	19119	19043
$\dot{m}_{C_2,CMR}$	kmol/hr	10000	25000	19639	18842	18800	19526	20995	20659
$\dot{m}_{C_3,CMR}$	kmol/hr	500	12000	4908	6436	4946	5307	3251	3747
$p_{LP,WMR}$	bar	5.00	15.00	12.10	9.65	11.47	9.65	7.24	6.36
$p_{MP,WMR}$	bar	15.00	30.00	22.92	17.28	20.36	18.34	17.47	17.54
$p_{HP,WMR}$	bar	25.00	55.00	36.91	27.17	30.11	30.05	30.35	30.10
$p_{LLP,CMR}$	bar	2.00	8.00	4.41	4.05	4.91	4.31	4.96	4.58
$p_{LP,CMR}$	bar	8.00	20.00	17.36	16.34	14.73	15.92	19.66	18.31
$p_{MP,CMR}$	bar	20.00	35.00	27.22	27.85	23.95	25.90	27.78	27.92
$p_{HP,CMR}$	bar	35.00	60.00	41.07	41.02	41.21	39.90	38.14	37.53
$T_{HE-1,out}$	°C	-55.00	-35.00	-34.24	-31.53	-35.56	-35.00	-41.01	-41.05
$T_{HE-2,out}$	°C	-135.00	-110.00	-117.24	-118.86	-113.80	-117.85	-115.37	-116.89
$T_{HE-3,out}$	°C	-160.00	-145.00	-145.00	-149.23	-145.00	-148.28	-145.00	-147.50
$T_{HE-4,out}$	°C	-40.00	-10.00	-30.85	-30.84	-	-	-19.27	-19.92
$x_{C_1,NGL}$	mol %	0.00	5.00	5.00	0.83	5.00	2.71	5.00	2.99
p_{Col-1}	bar	30.00	55.00	43.75	43.88	43.59	43.09	55.00	55.00
p_{K-6}	bar	50.00	70.00	58.39	60.39	63.93	58.83	55.46	55.00
Tee-1	-	0.75	1.00	-	-	-	-	0.86	0.86

Table 8.4 Constraint values from the best solutions of the integration schemes with different objective functions.

Parameter	Unit	ISS-LNG		NGL-LNG		Refluxed NGL-LNG	
		Obj_1	Obj_2	Obj_1	Obj_2	Obj_1	Obj_2
$\Delta T_{min,HE-1}$	°C	3.00	3.00	3.00	3.00	3.00	3.00
$\Delta T_{min,HE-2}$	°C	3.00	3.00	3.00	3.00	3.00	3.00
$\Delta T_{min,HE-3}$	°C	3.00	3.00	3.00	3.00	3.00	3.00
$\Delta T_{min,HE-4}$	°C	3.00	3.01	-	-	3.00	3.00
$\Delta T_{sup,W04}$	°C	0.11	0.22	0.30	0.02	0.07	0.06
$\Delta T_{sup,C06}$	°C	13.10	14.29	26.24	23.33	9.10	9.44
Pr_{K-1}	-	1.89	1.79	1.78	1.90	2.41	2.76
Pr_{K-2}	-	1.61	1.57	1.47	1.64	1.74	1.72
Pr_{K-3}	-	3.94	4.00	3.00	3.69	3.96	4.00
Pr_{K-4}	-	1.57	1.70	1.63	1.63	1.41	1.52
Pr_{K-5}	-	1.51	1.47	1.72	1.54	1.37	1.34
Pr_{K-6}	-	1.19	1.22	1.47	1.37	1.01	1.00
x_{C5+}	mol %	0.04	0.04	0.04	0.04	0.08	0.07
x_{BTX}	ppm	9.80	10.00	10.00	10.00	10.00	9.80

In the case of the refluxed NGL-LNG system, the condenser part of the NGL extraction column (Col-1) is integrated with the DMR process, allowing the column to have a reflux stream from the top vapor product. This reflux increases the separation performance of the distillation column, which enables the process unit to operate at a higher pressure than the equipment in the NGL-LNG system as seen in Table 8.3. Therefore, the refluxed NGL-LNG system requires less compression power to compensate the reduced pressure level of the feed gas compared to the simple integration scheme. Thus, the boost compressor (K-6) in the refluxed process is not needed, since its pressure ratio has a value very close to one (Pr_{K-6} in Table 8.4). The operating pressure level of the column in the NGL-LNG system is even lower than the ISS-LNG process, which will require a larger duty of the boost compressor and thus the largest specific energy

consumption compared to the other systems. In the same way as for the energy performance indicator, the ISS-LNG and the refluxed NGL-LNG systems achieved the highest exergy efficiency values of 69.49 % and 69.23 % respectively, while the NGL-LNG process obtained an *ETE* value of 68.07 %.

Even though the two alternative objective functions are closely related, in particular below ambient temperature, the results clearly show that minimizing specific energy consumption (Obj$_1$) gives other solutions than the ones obtained by maximizing exergy efficiency (Obj$_2$). Minimizing specific energy consumption results in a penalty in exergy efficiency between 0.19 and 0.57 % points for the three process configurations, while maximizing exergy efficiency results in a penalty in specific energy consumption between 0.91 and 1.72 kWh/ton. However, the differences in specific energy consumption and exergy efficiency values between the optimization results from the two objective functions (Obj$_1$ and Obj$_2$) are marginal. The largest increase in specific energy consumption is 0.80 % for the refluxed NGL-LNG, while the largest decrease in exergy efficiency is 0.82 % for the ISS-LNG process.

Nevertheless, the changes in operating conditions of the systems from the results of energy and exergy based optimization are significant and meaningful. Especially, Table 8.5 indicates the noticeable increase in column reboiler duty and compression power for the three process configurations when switching objective function from energy to exergy.

Table 8.5 Performance parameters with different objective functions for the integration schemes.

Parameter	Unit	ISS-LNG		NGL-LNG		refluxed NGL-LNG	
		Obj$_1$	Obj$_2$	Obj$_1$	Obj$_2$	Obj$_1$	Obj$_2$
En_{specific}	kWh/ton	215.26	216.65	221.66	222.57	214.93	216.65
ETE	%	68.92	69.49	67.66	68.07	69.04	69.23
$W_{\text{comp}}^{\text{total}}$	MW	118.89	122.27	122.48	125.52	119.27	121.77
$\dot{Q}_{\text{Reb-1}}$	MW	5.03	5.80	4.97	5.31	4.47	5.01
$\dot{E}^{\dot{Q}_{\text{Reb-1}}}$	MW	1.16	1.60	1.15	1.36	1.54	1.84

This behavior can be explained by the best solutions of the decision variables from the minimization results with Obj_2. First, Table 8.3 indicates that the minimization of the *ETE* results in a lower methane fraction in the NGL product for all the systems compared to the results from Obj_1. Thus, the NGL product becomes richer in heavier hydrocarbons, while having leaner LNG product as seen in the low heating values (LHV) in Table 8.6. This means that the *ETE* objective function guides the process towards a higher HHC separation efficiency.

Although the sharper separation gives a larger reboiler duty and a smaller production of NGL due to the evaporation of methane, this is compensated by the higher heating value of the NGL and the larger production of LNG. Thus, as seen in Table 8.5, there is a minor difference in the lower heating value (LHV) of the NGL between the results from the two objective functions. Besides, the actual value of the additional heat input to the reboiler (exergy of heat) is half of the increment in heat duty, which will be an acceptable increase for the deeper separation.

Table 8.6 Products of the NGL and LNG production with the specific energy consumption per unit calorific value of the products.

Parameter	Unit	ISS-LNG		NGL-LNG		Refluxed NGL-LNG	
		Obj_1	Obj_2	Obj_1	Obj_2	Obj_1	Obj_2
NGL	kmol/s	0.23	0.22	0.23	0.22	0.14	0.13
LHV_{NGL}	MJ/kmol	2431.56	2507.94	2438.12	2486.48	2781.34	2816.62
LHV_{NGL}	MW	566.55	556.76	563.20	552.00	378.26	377.43
LNG	kmol/s	8.54	8.82	8.54	8.76	8.64	8.81
LHV_{LNG}	MJ/kmol	852.62	850.56	853.01	851.44	864.93	863.19
LHV_{LNG}	MW	7284.82	7500.22	7280.44	7459.50	7475.62	7600.40
End-flash gas	kmol/s	0.95	0.68	0.96	0.74	0.94	0.78
$LHV_{End\text{-}flash\,gas}$	MJ/kmol	743.93	730.64	744.42	733.91	743.62	736.01
$LHV_{End\text{-}flash\,gas}$	MW	703.02	499.02	712.41	542.36	701.24	576.29
$\dfrac{\dot{W}_{comp} + \dot{Q}_{Reb-1}}{LHV_{total}}{}^{a}$	-	0.0145	0.0150	0.0149	0.0153	0.0145	0.0148

$^{a}LHV_{total} = LHV_{NGL} + LHV_{LNG} + LHV_{End\text{-}flash\,gas}$

In contrast, Table 8.3 indicates that the objective function based on the energy performance parameter resulted in the methane fraction in the NGL product reaching its upper bound. Since the specific energy consumption is unable to measure the compositional quality change and thus the separation performance, the objective function leads the NGL and LNG production systems to have the reboiler duty as small as possible by allowing a larger methane fraction in the NGL. Although the optimization using the energy performance indicator succeeded in reducing the total energy consumption, Obj_1 allows the systems to have a larger amount of methane slip through the NGL product.

Table 8.3 also shows that all the systems optimized by the exergy efficiency have a lower outlet temperature of the last heat exchanger in the DMR system ($T_{HE-3,out}$) compared to the results from minimization of the specific energy consumption. This temperature reduction increases the cold duty of the liquefaction process and thus the power consumption as seen in Table 8.5.

However, the colder outlet temperature of HE-3 gives a larger degree of sub-cooling in the liquefied natural gas stream. This colder LNG stream results in a larger fraction of liquid product after being throttled to around ambient pressure. Thus, the *ETE* objective function increases the final LNG product by decreasing the outlet temperature of HE-3, while reducing the end-flash vapor, compared to the results from minimization with Obj_1.

The main reason for the larger production of the final LNG is that the exergy efficiency measures the quality of the products (NGL, LNG, and end-flash vapor). This is in contrast to the specific energy consumption that only consider total energy consumption and mass flow rates of NGL and LNG. As seen in Table 8.7, the molar temperature based exergy value of the final LNG product is significantly larger than the end-flash vapor since the vapor product does not have any latent heat to be utilized. Therefore, the optimization based on the *ETE* objective function leads the system to have a lower sub-cooling temperature for larger production of LNG, which increases the total exergy value of the two products. The reduction in the outlet temperature of HE-3 also increases the molar temperature based exergy of the final LNG and end-flash vapor, thus increasing the produced exergy.

Table 8.7 Molar temperature based exergy of the final LNG product from the optimization results using different objective functions.

Parameter	Unit	ISS-LNG		NGL-LNG		refluxed NGL-LNG	
		Obj_1	Obj_2	Obj_1	Obj_2	Obj_1	Obj_2
$T_{\text{cold products}}$[a]	°C	-145.0	-157.0	-145.0	-156.9	-145.0	-156.8
$\dot{e}_{\text{LNG}}^{\text{T}}$	kJ/kmol	15865.0	15890.9	15863.2	15883.6	15835.9	15852.2
$\dot{e}_{\text{End-flash vapor}}^{\text{T}}$	kJ/kmol	3310.4	3315.8	3309.9	3314.2	3303.9	3307.3

[a]LNG and end-flash vapor

In contrast, the optimization using Obj_1 forced the sub-cooling temperature to be as warm as possible, reaching the upper bound as seen in Table 8.3. As a result, the refrigeration duty and the compression work was decreased, while the production of the final LNG was reduced. Since the effect of decreasing work consumption was larger than the effect of product reduction in the specific energy consumption, the system was optimized to have a warm outlet temperature from the liquefaction process. Thus, the energy based objective function did not maximize the LNG product since the specific energy consumption ignores the thermodynamic quality of the liquid stream. Instead, the optimization with Obj_1 allowed the system to have a larger amount of end-flash gas although the gas stream was disregarded as a product in the formulation of the specific energy consumption. The higher economic value of the final LNG compared to the end-flash vapor also indicates that a smaller production of the liquid product is not a realistic solution for this system.

To include the quality of the NGL and LNG in the energy performance indicator, the calorific value of the two products can substitute the mass flow rates in the formulation of the specific energy consumption as seen in Table 8.6 [221]. This performance indicator shows that the operating conditions from Obj_2 give a larger energy consumption per calorific value than the one from Obj_1. This result does not mean the operating conditions from Obj_1 is thermodynamically better since the performance indicator with the heating values only reflects

the changes in chemical energy of the products, while the temperature, pressure, and compositional changes are not covered.

Therefore, the exergy efficiency will be the most suitable objective function to optimize the complex distillation and liquefaction system since this indicator can reflect both the separation performance and the thermodynamic quality of the products. Thus, this performance indicator resulted in the processes where the amount of NGL production is maintained with a lower methane content, and the amount of the LNG product is maximized while reducing the end-flash vapor, which has lower thermodynamic and economic values.

8.6　Discussion and conclusions

The DMR process with upstream or integrated NGL extraction has been optimized to be evaluated and compared. The NGL and LNG production systems consume both work and heat to deliver multiple products (NGL, LNG, end-flash gas). Thus, two different objective functions, specific energy consumption and exergy efficiency, have been applied in the optimization studies in order to evaluate the effectiveness of the two different performance indicators for the complex systems.

The optimization results using the specific energy consumption as objective function indicated that the LNG process integrated with the NGL extraction using a refluxed column has the smallest specific energy consumption and a high exergy efficiency. However, the operating conditions from the minimization studies using the energy performance indicator show that the systems were optimized to maximize the methane content in the NGL product. Although the reboiler duty of the distillation column was decreased due to the high methane fraction allowed in the NGL, the methane product (LNG) was also reduced, meaning a lower HHC separation performance of the system. Besides, the degree of sub-cooling in the natural gas stream was minimized to decrease the refrigeration duty and its compressor work. The low degree of sub-cooling resulted in a smaller production of the liquid stream (LNG) after the sub-cooled natural gas stream is throttled to ambient pressure. Although the specific energy consumption focuses

on the production of NGL and LNG, the performance indicator guided the system to produce a larger amount of end-flash gas, which is less valuable than the LNG product.

Unlike the energy performance indicator, the minimization of the *ETE* resulted in a smaller methane fraction in the NGL product by having a larger reboiler duty. Nevertheless, the additional reboiler duty is compensated by the increased heating value of the NGL product and the increase in LNG production since more methane ends up there. Therefore, the exergy efficiency was able to manipulate the operating conditions to have a higher HHC separation performance.

Besides, the objective function based on the *ETE* succeeded in maximizing the LNG by lowering the sub-cooling temperature of the natural gas, while reducing the end-flash vapor. A higher thermodynamic (exergy) value of the LNG product than the end-flash vapor was the main reason for the exergy based objective function to guide the system to have a larger degree of sub-cooling. Thus, the optimization using exergy efficiency resulted in more realistic operating conditions for the NGL and LNG production systems since it reflects the HHC separation performance and the thermodynamic value of the LNG cold energy.

Based on the optimization results using the *ETE*, none of the two configurations having the DMR process integrated with NGL extraction perform thermodynamically better than the liquefaction system with upstream HHC recovery. Thus, the integration of the NGL and LNG processes will not be beneficial unless further development is made for the integrated system. Although the difference in the exergy efficiency between the schemes with upstream and integrated HHC recovery is only marginal, more advanced upstream NGL extraction technologies such as the gas sub-cooled and the recycle split vapor processes will increase the performance difference, making the integration systems less attractive.

Chapter summary

- o Exergy efficiency is a better performance indicator than energy efficiency, since it can evaluate the changes in product quality such as temperature, pressure, and composition, while handling different forms of energy on a fairer basis according to their thermodynamic quality.

- o Thus, exergy efficiency is encouraged to be used as an objective function for the optimization of complex processes, which use both heat and power to produce multiple products.

Chapter 9   Conclusion and future work

9.1   Conclusion

This thesis aims to evaluate and improve the process efficiency of systems in the LNG value chain in order to reduce the environmental footprint and improve project profitability of the chain. This thesis mainly focuses on LNG related systems such as natural gas liquefaction, LNG reliquefaction during transportation, and LNG regasification at importing terminals.

For an objective evaluation and comparison of different technical solutions for LNG systems, mathematical optimization is essential. For the optimization of simple LNG systems, both local (SQP) and global search algorithms (PSO) were found to be proper solvers, returning almost the same objective value. However, a careful setting of penalty functions for constraint handling is required for the PSO algorithm to achieve equally good solutions as the local solver. In addition, the metaheuristic algorithm (PSO) is not recommended for complex LNG processes, since it requires a larger computational time with a poorer objective value compared to the SQP algorithm. Thus, the local solver will be a proper solver for LNG systems having a large number of variables and constraints.

Different configurations of the DMR system have been optimized and compared by using the SQP solver in order to analyze the effect of the structural differences. For the warm mixed refrigerant (WMR) cycle, using pumps are not recommended since this reduces the temperature range that the warm cycle can cover, resulting in poor performance for the cold mixed refrigerant (CMR) cycle. It was also found that phase separation of the pre-cooled CMR is beneficial to reduce the power consumption of the process. Besides, a large number of

evaporating pressure levels for both the WMR and CMR is also needed to improve energy efficiency. If only one cycle has a large number of evaporating pressures, it results in sub-optimal operating temperature ranges for the two cycles, reducing the system performance.

The DMR process is also optimized and compared with non-flammable LNG processes. Although the non-flammable LNG processes have very complex structures to increase their inherently low efficiency, they consume more power than the DMR process. However, the non-flammable liquefaction systems will be suitable for offshore applications due to their non-hydrocarbon refrigerants. Nevertheless, the DMR process will still be a valid option for floating LNG since the use of propane, which is the most hazardous component, can be minimized by changing the composition of the WMR.

For the optimization of the DMR process, the constraint formulations were found to be important to improve its energy efficiency. Especially, it is recommended to relax the minimum superheating constraint. In the best solutions of the DMR process, a certain degree of superheating was always observed in the two mixed refrigerants. Thus, if a high value of the minimum superheating constraint is given, it may lead to sub-optimal solutions, missing optimal superheating values. Using maximum heat exchanger conductance with relaxed minimum temperature difference constraint is also encouraged since this constraint formulation can result in an optimal distribution of temperature driving forces in cryogenic heat exchangers.

Although LNG processes are typically optimized to minimize power consumption, it is also important to consider cost optimization for small-scale liquefaction technologies, which tend to have a significant effect on the profitability of an entire system as a sub-process. Thus, a simple process based on self-liquefaction is recommended for LNG carriers to handle boil-off-gas (BOG). The conventional method, which is to burn the BOG, was found to be more expensive compared to the BOG handling system with the liquefaction process. The low break-even-point of around 4 USD of LNG price will make this self-liquefaction system a favorable option for LNG vessels to minimize the loss of cargo.

Another performance parameter to be considered for the optimization and evaluation of LNG systems is exergy efficiency. Unlike energy performance parameters, exergy can reflect the quality of products, thus giving an accurate thermodynamic efficiency of systems. Based on the categorization of various exergy efficiencies according to the level of exergy decomposition, consumed-produced exergy efficiencies are recommended to measure the performance of systems. However, the extension of the Exergy Transfer Effectiveness (ETE) by including chemical exergy is suggested due to the inaccuracy of the consumed-produced exergy efficiencies for different types of systems with various operating conditions. The extended ETE offers general formulas for processes having changes in temperature, pressure and chemical composition. Therefore, the use of the extended ETE is encouraged to evaluate complex cryogenic systems handling different forms of products such as heat, power, and chemical materials.

One good example for the validation of the extended ETE is the system in LNG import terminals. LNG cold energy is typically wasted to the environment during regasification at the terminal before it is distributed to end-users. For the utilization of the LNG cold energy, air separation units (ASUs) are recommended since their operating conditions fit well in the temperature range of LNG vaporization. The cold energy is recommended to be used for pre-cooling of air and nitrogen streams instead of using it to supply cooling to a liquid nitrogen production cycle in the ASU system. This system, however, has variations in the quality of the products (liquid O_2, liquid N_2, gasified LNG) with the LNG supply pressure, making energy performance indicators inappropriate to evaluate the ASU process. Thus, the extended ETE was found to be a proper performance indicator for the system, reflecting the effect of differences in the purification and temperature of the products.

The extended ETE is also recommended as a better objective function than energy performance indicators for LNG systems. In the optimization of the DMR process integrated with NGL extraction, the energy based objective function shows that the LNG process integrated with the NGL extraction using a refluxed column gives the smallest specific energy consumption. However, the objective function of the extended ETE indicates that upstream NGL extraction

is the most efficient process thermodynamically, having a higher quality of products (LNG and NGL) while maintaining product quantity. Moreover, the exergy based objective function was found to give different operating conditions compared to the energy based objective function, providing increased quality of products (LNG and NGL) with similar energy consumption. Therefore, for LNG systems using both heat and power to produce multiple products, exergy efficiency is encouraged to be used as an objective function to find the best operating conditions that correspond to thermodynamic optima of the processes.

9.2   Future work

Although the global search algorithms show a poor performance for complex LNG processes, they are still attractive options to optimize LNG systems built in commercial simulation tools where accurate derivative information is unavailable. Therefore, modification of existing global search algorithms is required to make these perform better. In addition, more advanced methods for constraint handling are required in the near-global solvers in order to increase the global search ability for complex LNG processes.

To analyze the effect of the structure in detail, more case studies are needed for DMR processes. In particular, all possible combinations of pumps, phase separators, stream splitters, and multi pressure evaporation in the systems have not been tested and analyzed.

One thing that has a significant effect on the economics of LNG carriers is the voyage profiles. Depending on the sailing schedule such as voyage speed and distance, the amount of BOG production and the fuel requirement of the propulsion system will also change. Thus, thorough cost optimization is recommended to find the most suitable BOG handling systems for different voyage profiles.

The integration of ASU processes and LNG regasification results in a final LNG product still having a very low temperature e.g. below -50 °C. The rest of the LNG cold energy is typically sent to the compressor intercoolers, resulting in excessive driving forces in the intercoolers and

significant amounts of entropy generation. Instead, a power production system using Rankine cycles can be applied between the LNG stream from the main heat exchanger and the air and nitrogen streams from the compressors as heat sink and heat sources respectively. The use of Rankine cycles will allow effective use of the LNG cold energy and the waste heat from the intercoolers.

The DMR processes integrated with NGL extraction turned out not to be proper examples to verify the advantages of using the extended *ETE* as objective function due to the marginal differences, compared to energy based objective functions. The significant amount of power consumption in the liquefaction part becomes dominant in the calculation of exergy efficiency, thus offsetting the effect of changes in temperature, pressure, and composition of products. Therefore, the extended *ETE* has to be tested for other processes such as BOG reliquefaction, air separation, nitrogen removal, and helium extraction systems, where compression work is not as large as in cryogenic liquefaction processes.

References

[1] BP p.l.c. BP Statistical Review of World Energy. 67th edition. London, UK: BP p.l.c.; 2018. Online accessed: 18.10.2018, https://www.bp.com/content/dam/bp/business-sites/en/global/ corporate/pdfs/energy-economics/statistical-review/bp-stats-review-2018-full-report.pdf.

[2] International Energy Agency (IEA). World Energy Outlook 2018. International Energy Agency (IEA); 2018. Online accessed: 18.10.2018, https://www.iea.org/weo2018.

[3] BP p.l.c. BP Energy Outlook. 2018 edition. London, UK: BP p.l.c.; 2018. Online accessed: https://www.bp.com/content/dam/bp/business-sites/en/global/corporate/pdfs/energy-economic s/energy-outlook/bp-energy-outlook-2018.pdf.

[4] Ekanem Attah E, Bucknall R. An analysis of the energy efficiency of LNG ships powering options using the EEDI. Ocean Engineering. 2015;110:62-74.

[5] Thomson H, Corbett JJ, Winebrake JJ. Natural gas as a marine fuel. Energy Policy. 2015;87:153-67.

[6] Paltsev S. Economics and geopolitics of natural gas: Pipelines versus LNG. Proceedings of the 12th International Conference on the European Energy Market (EEM). Lisbon, Portugal: Institute of Electrical and Electronics Engineers (IEEE); 2015.

[7] Ríos-Mercado RZ, Borraz-Sánchez C. Optimization problems in natural gas transportation systems: A state-of-the-art review. Applied Energy. 2015;147:536-55.

[8] International Gas Union (IGU). 2018 World LNG Report. 27th World Gas Conference ed. Fornebu, Norway: International Gas Union (IGU); 2018. Online accessed: 18.10.2018, https://www.igu.org/sites/default/files/node-document-field_file/IGU_LNG_2018_0.pdf.

[9] Bukowski J, Liu YN, Pillarella M, Boccella S, Kennington W. Natural Gas Liquefaction Technology for Floating LNG Facilities. Proceedings of the 17th International Conference & Exhibition on Liquefied Natural Gas (LNG17). Houston, USA: Gas Technology Institute (GTI); 2013.

[10] International Energy Agency (IEA). Offshore Energy Outlook. International Energy Agency (IEA); 2018. Online accessed: 18.10.2018, https://www.iea.org/weo/offshore.

[11] Cornot-Gandolphe S. LNG Cost Reductions and Flexibility In LNG Trade Add to Security of Gas Supply. Energy Prices & Taxes. 2005(1st Quarter).

[12] Chandra V. Fundamentals of Natural gas: an International Perspective. 2nd ed. Tulsa, USA: PennWell Corporation; 2006.

[13] Zakarian E, Morgan JEP. Managing Liquid Accumulation in Large Diameter Gas-Condensate Pipelines. Proceedings of Offshore Technology Conference. Houston, USA: Offshore Technology Conference; 2017.

[14] Mokhatab S, Mak JY, Valappil JV, Wood DA. Handbook of Liquefied Natural Gas. Boston, USA: Gulf Professional Publishing; 2014.

[15] Shukri T. LNG Technology Selection. Hydrocarbon Engineering. 2004(February).

[16] Kulitsa M, Wood DA. LNG rollover challenges and their mitigation on Floating Storage and Regasification Units: New perspectives in assessing rollover consequences. Journal of Loss Prevention in the Process Industries. 2018;54:352-72.

[17] Wilkinson D, Johnson G. Nitrogen Rejection Technology for Abu Dhabi. Proceedings of the GPA GCC 18th Annual Technical Conference. Oman: GPA GCC; 2010.

[18] Kim D, Gundersen T. Helium Extraction from LNG End-Flash. Chemical Engineering Transactions. 2015;45:595-600.

[19] Roberts MJ, Agrawal R, Daugherty TL. Single mixed refrigerant gas liquefaction process. U.S. Patent No. 6,347,531 B1; 2002.

[20] Swenson LK. Single mixed refrigerant, closed loop process for liquefying natural gas. US Patent No. 4,033,735; 1977.

[21] Stockmann R, Bölt M, Steinbauer M, Pfeiffer C, Paurola P, Förg W, et al. Process for liquefying a hydrocarbon-rich stream. US Patent 6,334,334 B1; 2002.

[22] Neeraas B, Sandvik T. Dual Nitrogen Expansion Process. WO Patent No. 2009/130466 A2; 2009.

[23] Dubar CA. Liquefaction Process. U.S. Patent No. 5,768,912 A; 1997.

[24] Nilsen ISL. Method and system for producing LNG. U.S. Patent No. 2010/0132405 A1; 2010.

[25] Maunder AD, Skinner GF. Process for Liquefaction of Natural Gas. WO Patent No. 2012/172281 A2; 2012.

[26] Fischer-Calderon E. Self-refrigerated LNG process. U.S. Patent No. 6,564,578; 2003.

[27] Oelfke RH, Miller MR. Liquefied Natural Gas Production. WO Patent No. 2014/116363 A1; 2014.

[28] Roberts MJ, Agrawal R. Dual Mixed Refrigerant Cycle for Gas Liquefaction. U.S. Patent No. 6,269,655 B1; 2001.

[29] Bukowski J, Liu YN, Boccella S, Kowalski L. Innovations in Natural Gas Liquefaction Technology for Future LNG Plants and Loating LNG Facilities. Proceedings of International Gas Union Research Conference 2011. Seoul, Korea: International Gas Union (IGU); 2011.

[30] Grootjans HF, Nagelvoort RK, Vink KJ. Liquefying a Stream Enriched in Methane. U.S. Patent No. 6,370,910 B1; 2002.

[31] Paradowski H, Rojey A. Multi-steps Cooling by Heat Exchanging with the Compressed Coolant. U.S. Patent No. 6,150,389; 2000.

[32] Paradowski H, DuFresne JP. Process analysis shows how to save energy. Hydrocarbon Process. 1983;62(7):103-8.

[33] Gaumer L, Newton C. Combined cascade and multicomponent refrigeration system and method. U.S. Patent No. 3,763,658; 1973.

[34] Fredheim A, Paurola P. Natural Gas Liquefaction Process. U.S. Patent No. 7,386,996 B2; 2008.

[35] Foglietta JH. LNG Production Using Dual Independent Expander Refrigeration Cycles. U.S. Patent No. 6,412,302 B1; 2002.

[36] ConocoPhillips. Brochure: ConocoPhillips Optimized Cascade Process. ConocoPhillips Company; 2018. Online accessed: 12.12.2018, http://static.conocophillips.com/files/resources /18-0269-lng-wgc-brochure-pages.pdf.

[37] Bauer H, Franke H, Sapper R, Schier M, Bolt M, Pettersen J, et al. Natural Gas Liquefaction Process. U.S. Patent No. 2008/0006053 A1; 2008.

[38] Roberts MJ, Agrawal R. Hybrid cycle for the production of liquefied natural gas. U.S. Patent No. 6,308,531; 2001.

[39] Yoon J-I, Choi W-J, Lee S, Choe K, Shim G-J. Efficiency of Cascade Refrigeration Cycle Using C3H8, N2O, and N2. Heat Transfer Engineering. 2013;34(11-12):959-65.

[40] Paradowski H, Vovard S. Process for the Production of a Subcooled Liquefied Natural Gas Stream from a Natural Gas Feed Stream, and associated Installation. U.S. Patent No. 2010/0126214 A1; 2010.

[41] Songhurst B. LNG plant cost escalation. Oxford Institute for Energy Studies; 2014.

[42] Austbø B, Gundersen T. Impact of problem formulation on LNG process optimization. AIChE Journal. 2016;62(10):3598-610.

[43] Austbø B, Gundersen T. Optimal distribution of temperature driving forces in low-temperature heat transfer. AIChE Journal. 2015;61(8):2447-55.

[44] Vink KJ, Nagelvoort RK. Comparison of Baseload Liquefaction Processes. Proceedings of the 12th International Conference & Exhibition on Liquefied Natural Gas (LNG12). Perth, Australia: Gas Technology Institute (GTI); 1998.

[45] Barclay M, Denton N. Selecting offshore LNG processes. LNG Journal. 2005:34-6.

[46] Lee S, Long NVD, Lee M. Design and optimization of natural gas liquefaction and recovery processes for offshore floating liquefied natural gas plants. Industrial and Engineering Chemistry Research. 2012;51(30):10021-30.

[47] Teles APF, Abreu AdSd, Saad AC, Mello DCd, Campos FB, Silva JP, et al. Evaluation of Floating Liquefied Natural Gas Units for Brazilian Scenarios. Proceedings of Offshore

Technology Conference (OTC) 2010. Houston, USA: Offshore Technology Conference (OTC); 2010.

[48] Zhu J, Li Y, Liu Y, Wang W. Selection and Simulation of Offshore LNG Liquefaction Process. Proceedings of the 20th International Offshore and Polar Engineering Conference (ISOPE 2010). Beijing, China: International Society of Offshore and Polar Engineers (ISOPE); 2010.

[49] Wood D, Mokhatab S, Economides MJ. Offshore Natural Gas Liquefaction Process Selection and Development Issues. Proceedings of 2007 SPE Annual Technical Conference and Exhibition. Anaheim, USA: Society of Petroleum Engineers (SPE);2007.

[50] Gilmour N, Deveney D. Floating LNG: Shell's Recent History and Current Approach. Proceedings of the 16th International Conference & Exhibition on Liquefied Natural Gas (LNG16). Oran, Algeria: Gas Technology Institute (GTI); 2010.

[51] Lee I, Moon I. Strategies for Process and Size Selection of Natural Gas Liquefaction Processes: Specific Profit Portfolio Approach by Economic Based Optimization. Industrial & Engineering Chemistry Research. 2018;57(17):5845-5857.

[52] Van Nispen DJ, Hodgson BS, Sims CE, Leong K, Willyams I. Prelude FLNG - Field Development Challenges. Proceedings of International Petroleum Technology Conference. Bangkok, Thailand: International Petroleum Technology Conference (IPTC); 2016.

[53] Boekhorst A, Steenson B, van der Velde H. FLNG: Applying Advanced Technology to Bring More Natural Gas to Market. Proceedings of Offshore Technology Conference (OTC) 2015. Houston, USA: Offshore Technology Conference (OTC); 2015.

[54] Verburg R, Kaart S, Benckhuijsen B, Collins P, Nagelvoort R. Sakhalin Energy's Initial Operating Experience, From Simulation to Reality: Making the DMR Process Work. Proceedings of the 16th International Conference & Exhibition on Liquefied Natural Gas (LNG16). Oran, Algeria: Gas Technology Institute (GTI); 2010.

[55] Nogal FD, Kim J-K, Perry S, Smith R. Optimal Design of Mixed Refrigerant Cycles. Industrial & Engineering Chemistry Research. 2008;47(22):8724-40.

[56] Gavory T, de Seze PE. Sloshing In Membrane LNG Carriers And Its Consequences From a Designer's Perspective. Proceedings of the 19th International Offshore and Polar Engineering Conference (ISOPE 2009). Osaka, Japan: International Society of Offshore and Polar Engineers (ISOPE); 2009.

[57] Timmerhaus KD, Reed RP. Cryogenic Engineering. International Cryogenics Monograph Series: Springer-Verlag New York; 2007.

[58] Fernández IA, Gómez MR, Gómez JR, Insua ÁB. Review of propulsion systems on LNG carriers. Renewable and Sustainable Energy Reviews. 2017;67:1395-411.

[59] Lee Y, Cho T, Lee J, Kwon O. Trends and Technologies in LNG Carriers and Offshore LNG Facilities. Proceedings of Offshore Technology Conference (OTC) 2008. Houston, USA: Offshore Technology Conference (OTC); 2008.

[60] Feger D. Gas Combustion Units: High Performance Technologies for Safe Disposal of Excess Boil Off Gas on the New Generation of LNG Carriers. Proceedings of the 15th international conference and exhibition on liquified natural gas (LNG 15). Barcelona, Spain: Gas Technology Institute (GTI); 2007.

[61] Anderson TN, Ehrhardt ME, Foglesong RE, Bolton T, Jones D, Richardson A. Shipboard Reliquefaction for Large LNG Carriers. Proceedings of the 1st Annual Gas Processing Symposium. Amsterdam, Netherlands: Elsevier; 2009.

[62] Chang D, Rhee T, Nam K, Lee S, Kwak B, Ha J. Economic Evaluation of Propulsion Systems for LNG Carriers. Proceedings of 23rd International Conference & Exhibition for the LNG, LPG and Natural Gas Industries. Bangkok, Thailand: Gastech; 2008.

[63] Gilmore R, Hatzigrigoris S, Mavrakis S, Spertos A, Vordonis A. LNG Carrier Alternative Propulsion Systems. Proceedings of the Greek Section of the Society of Naval Architects and Marine Engineers (SNAME). Athens, Greece: Society of Naval Architects and Marine Engineers (SNAME); 2005.

[64] Yeo D, Ahn B, Kim J, Kim I. Propulsion Alternatives for Modern LNG Carriers. Proceedings of the 15th international conference and exhibition on liquified natural gas (LNG15). Barcelona, Spain: Gas Technology Institute (GTI); 2007.

[65] Wayne WS, Hodgson M. The Options and Evaluation of Propulsion Systems for the Next Generation of LNG Carriers. Proceedings of the 23rd World Gas Conference. Amsterdam, Netherlands: International Gas Union (IGU); 2006.

[66] Kwak D-H, Heo J-H, Park S-H, Seo S-J, Kim J-K. Energy-efficient design and optimization of boil-off gas (BOG) re-liquefaction process for liquefied natural gas (LNG)-fuelled ship. Energy. 2018;148:915-29.

[67] Tan H, Zhao Q, Sun N, Li Y. Enhancement of energy performance in a boil-off gas re-liquefaction system of LNG carriers using ejectors. Energy Conversion and Management. 2016;126:875-88.

[68] Sayyaadi H, Babaelahi M. Multi-objective optimization of a joule cycle for re-liquefaction of the Liquefied Natural Gas. Applied Energy. 2011;88(9):3012-21.

[69] R Juliussen L, J Kryger M, Andreasen A. MAN B&W ME-GI Engines. Recent Research and Results. Proceedings of the International Symposium on Marine Engineering (ISME). Kobe, Japan: The Institute of Marine Engineering, Science and Technology (IMAREST); 2011.

[70] Egashira S. LNG Vaporizer for LNG Re-gasification Terminal. Kobelco Technology Review. 2013;32:64-9.

[71] Kanbur BB, Xiang L, Dubey S, Choo FH, Duan F. Cold utilization systems of LNG: A review. Renewable and Sustainable Energy Reviews. 2017;79(Supplement C):1171-88.

[72] Sung T, Kim KC. LNG Cold Energy Utilization Technology. Energy Solutions to Combat Global Warming: Springer International Publishing; 2017.

[73] Romero Gómez M, Ferreiro Garcia R, Romero Gómez J, Carbia Carril J. Review of thermal cycles exploiting the exergy of liquefied natural gas in the regasification process. Renewable and Sustainable Energy Reviews. 2014;38(Supplement C):781-95.

[74] Efrat T. Utilizing Available "Coldness" from Liquefied Natural Gas (LNG) Regasification Process for Seawater Desalination. Proceedings of International Desalination Association World Congress 2011. Perth, Australia: International Desalination Association (IDA); 2011.

[75] Uwitonze H, Han S, Jangryeok C, Hwang KS. Design process of LNG heavy hydrocarbons fractionation: Low LNG temperature recovery. Chemical Engineering and Processing: Process Intensification. 2014;85(Supplement C):187-95.

[76] La Rocca V. Cold recovery during regasification of LNG part two: Applications in an Agro Food Industry and a Hypermarket. Energy. 2011;36(8):4897-908.

[77] Xu W, Duan J, Mao W. Process study and exergy analysis of a novel air separation process cooled by LNG cold energy. Journal of Thermal Science. 2014;23(1):77-84.

[78] Jiang K. Economic Analysis of LNG Cold Energy Utilization. Energy Solutions to Combat Global Warming: Springer International Publishing; 2017.

[79] Qyyum MA, Minh LQ, Ali W, Hussain A, Bahadori A, Lee M. Feasibility study of environmental relative humidity through the thermodynamic effects on the performance of natural gas liquefaction process. Applied Thermal Engineering. 2018;128:51-63.

[80] Nguyen T-V, Rothuizen ED, Markussen WB, Elmegaard B. Thermodynamic comparison of three small-scale gas liquefaction systems. Applied Thermal Engineering. 2018;128:712-24.

[81] Na J, Lim Y, Han C. A modified DIRECT algorithm for hidden constraints in an LNG process optimization. Energy. 2017;126:488-500.

[82] Park K, Won W, Shin D. Effects of varying the ambient temperature on the performance of a single mixed refrigerant liquefaction process. Journal of Natural Gas Science and Engineering. 2016;34:958-68.

[83] Ghorbani B, Hamedi M-H, Amidpour M, Mehrpooya M. Cascade refrigeration systems in integrated cryogenic natural gas process (natural gas liquids (NGL), liquefied natural gas (LNG) and nitrogen rejection unit (NRU)). Energy. 2016;115:88-106.

[84] Park JH, Khan MS, Lee M. Modified coordinate descent methodology for solving process design optimization problems: Application to natural gas plant. Journal of Natural Gas Science and Engineering. 2015;27:32-41.

[85] Lee I, Tak K, Lee S, Ko D, Moon I. Decision Making on Liquefaction Ratio for Minimizing Specific Energy in a LNG Pilot Plant. Industrial & Engineering Chemistry Research. 2015;54(51):12920-7.

[86] Xu X, Liu J, Cao L. Optimization and analysis of mixed refrigerant composition for the PRICO natural gas liquefaction process. Cryogenics. 2014;59:60-9.

[87] Uwitonze H, Han S, Jangryeok C, Hwang KS. Design process of LNG heavy hydrocarbons fractionation: Low LNG temperature recovery. Chemical Engineering and Processing: Process Intensification. 2014;85:187-95.

[88] Khan MS, Chaniago YD, Getu M, Lee M. Energy saving opportunities in integrated NGL/LNG schemes exploiting: Thermal-coupling common-utilities and process knowledge. Chemical Engineering and Processing: Process Intensification. 2014;82(0):54-64.

[89] Nguyen T-V, de Oliveira Júnior S. System evaluation of offshore platforms with gas liquefaction processes. Energy. 2018;144:594-606.

[90] Tesch S, Morosuk T, Tsatsaronis G. Advanced exergy analysis applied to the process of regasification of LNG (liquefied natural gas) integrated into an air separation process. Energy. 2016;117, Part 2:550-61.

[91] Najibullah Khan NB, Barifcani A, Tade M, Pareek V. A case study: Application of energy and exergy analysis for enhancing the process efficiency of a three stage propane pre-cooling cycle of the cascade LNG process. Journal of Natural Gas Science and Engineering. 2016;29:125-33.

[92] Morosuk T, Tesch S, Hiemann A, Tsatsaronis G, Bin Omar N. Evaluation of the PRICO liquefaction process using exergy-based methods. Journal of Natural Gas Science and Engineering. 2015;27, Part 1:23-31.

[93] Vatani A, Mehrpooya M, Palizdar A. Advanced exergetic analysis of five natural gas liquefaction processes. Energy Conversion and Management. 2014;78:720-37.

[94] Nguyen T-V, Voldsund M, Elmegaard B, Ertesvåg IS, Kjelstrup S. On the definition of exergy efficiencies for petroleum systems: Application to offshore oil and gas processing. Energy. 2014;73:264-81.

[95] Rian AB, Ertesvåg IS. Exergy Evaluation of the Arctic Snøhvit Liquefied Natural Gas Processing Plant in Northern Norway—Significance of Ambient Temperature. Energy & Fuels. 2012;26(2):1259-67.

[96] Marmolejo-Correa D, Gundersen T. A comparison of exergy efficiency definitions with focus on low temperature processes. Energy. 2012;44(1):477-89.

[97] Morosuk T, Tsatsaronis G. Comparative evaluation of LNG – based cogeneration systems using advanced exergetic analysis. Energy. 2011;36(6):3771-8.

[98] Szargut J, Szczygiel I. Utilization of the cryogenic exergy of liquid natural gas (LNG) for the production of electricity. Energy. 2009;34(7):827-37.

[99] Shin J, Yoon S, Kim J-K. Application of exergy analysis for improving energy efficiency of natural gas liquids recovery processes. Applied Thermal Engineering. 2015;75:967-77.

[100] Watson HAJ, Vikse M, Gundersen T, Barton PI. Optimization of single mixed-refrigerant natural gas liquefaction processes described by nondifferentiable models. Energy. 2018;150:860-76.

[101] Wahl PE, Løvseth SW. Formulating the optimization problem when using sequential quadratic programming applied to a simple LNG process. Computers & Chemical Engineering. 2015;82:1-12.

[102] Qyyum MA, Long NVD, Minh LQ, Lee M. Design optimization of single mixed refrigerant LNG process using a hybrid modified coordinate descent algorithm. Cryogenics. 2018;89:131-40.

[103] Moein P, Sarmad M, Ebrahimi H, Zare M, Pakseresht S, Vakili SZ. APCI- LNG single mixed refrigerant process for natural gas liquefaction cycle: Analysis and optimization. Journal of Natural Gas Science and Engineering. 2015;26:470-9.

[104] Wahl PE, Løvseth SW, Mølnvik MJ. Optimization of a simple LNG process using sequential quadratic programming. Computers & Chemical Engineering. 2013;56:27-36.

[105] Jacobsen MG, Skogestad S. Active constraint regions for a natural gas liquefaction process. Journal of Natural Gas Science and Engineering. 2013;10:8-13.

[106] Dutta A, Karimi IA, Farooq S. Heating Value Reduction of LNG (Liquefied Natural Gas) by Recovering Heavy Hydrocarbons: Technoeconomic Analyses Using Simulation-Based Optimization. Industrial & Engineering Chemistry Research. 2018;57(17):5924-32.

[107] Lee I, Moon I. Economic Optimization of Dual Mixed Refrigerant Liquefied Natural Gas Plant Considering Natural Gas Extraction Rate. Industrial & Engineering Chemistry Research. 2017;56(10):2804-14.

[108] Park JH, Khan MS, Andika R, Getu M, Bahadori A, Lee M. Techno-economic evaluation of a novel NGL recovery scheme with nine patented schemes for offshore applications. Journal of Natural Gas Science and Engineering. 2015;27:2-17.

[109] Wang M, Khalilpour R, Abbas A. Thermodynamic and economic optimization of LNG mixed refrigerant processes. Energy Conversion and Management. 2014;88:947-61.

[110] Jin C, Lim Y. Economic evaluation of NGL recovery process schemes for lean feed compositions. Chemical Engineering Research and Design. 2018;129:297-305.

[111] Sayyaadi H, Babaelahi M. Thermoeconomic optimization of a cryogenic refrigeration cycle for re-liquefaction of the LNG boil-off gas. International Journal of Refrigeration. 2010;33(6):1197-207.

[112] Turton R. Analysis, synthesis, and design of chemical processes. 4th ed. Upper Saddle River, USA: Pearson Education; 2013.

[113] Nocedal J, Wright SJ. Numerical Optimization. 2nd ed. USA: Springer New York; 2006.

[114] Biegler L. Nonlinear Programming: Concepts, Algorithms, and Applications to Chemical Processes, USA: Society for Industrial and Applied Mathematics; 2010.

[115] Austbø B, Løvseth SW, Gundersen T. Annotated bibliography—Use of optimization in LNG process design and operation. Computers & Chemical Engineering. 2014;71:391-414.

[116] Biegler LT, Grossmann IE. Retrospective on optimization. Computers & Chemical Engineering. 2004;28(8):1169-92.

[117] Yang HJ, Hwang KS, Lee CJ. Stochastic Optimization of a Natural Gas Liquefaction Process Considering Seawater Temperature Variation Based on Particle Swarm Optimization. Industrial & Engineering Chemistry Research. 2018;57(6):2200–2207.

[118] Kim D, Gundersen T. Development and use of exergy efficiency for complex cryogenic processes. Energy Conversion and Management. 2018;171:890-902.

[119] Kim D, Giametta REH, Gundersen T. Optimal Use of Liquefied Natural Gas (LNG) Cold Energy in Air Separation Units. Industrial & Engineering Chemistry Research. 2018;57(17):5914-23.

[120] Won W, Lee KS. An energy-efficient operation system for a natural gas liquefaction process: Development and application to a 100 ton-per-day plant. Computers & Chemical Engineering. 2017;97:208-19.

[121] Gadhiraju V. Cryogenic Mixed Refrigerant Processes. USA: Springer New York; 2008.

[122] Floudas CA. Deterministic Global Optimization: Theory, Methods and Applications. USA: Springer US; 2010.

[123] Dowling AW, Biegler LT. A framework for efficient large scale equation-oriented flowsheet optimization. Computers & Chemical Engineering. 2015;72:3-20.

[124] Lee W, An J, Lee JM, Lim Y. Design of single mixed refrigerant natural gas liquefaction process considering load variation. Chemical Engineering Research and Design. 2018;139:89-103.

[125] Yu H, Kim D, Gundersen T. A study of working fluids for Organic Rankine Cycles (ORCs) operating across and below ambient temperature to utilize Liquefied Natural Gas (LNG) cold energy. Energy. 2019;167:730-9.

[126] He T, Ju Y. A novel conceptual design of parallel nitrogen expansion liquefaction process for small-scale LNG (liquefied natural gas) plant in skid-mount packages. Energy. 2014;75:349-59.

[127] Kennedy J, Eberhart R. Particle swarm optimization. Proceedings of the IEEE International Conference on Neural Networks: IEEE; 1995.

[128] Jones DR, Perttunen CD, Stuckman BE. Lipschitzian optimization without the Lipschitz constant. Journal of Optimization Theory and Applications. 1993;79(1):157-81.

[129] Jordehi AR. A review on constraint handling strategies in particle swarm optimisation. Neural Computing and Applications. 2015;26(6):1265-75.

[130] Parsopoulos KE, Vrahatis MN. Particle swarm optimization method for constrained optimization problems. 2002;76(1):214-20.

[131] Yeniay Ö. Penalty function methods for constrained optimization with genetic algorithms. Mathematical and computational Applications. 2005;10(1):45-56.

[132] Aspen Technology Inc. Aspen HYSYS V9. Cambridge, USA: Aspen Technology Inc.; 2016.

[133] Austbø B. Use of Optimization in Evaluation and Design of Liquefaction Processes for Natural Gas. Trondheim, Norway: NTNU; 2015.

[134] Kim D, Gundersen T. Constraint Formulations for Optimisation of Dual Mixed Refrigerant LNG Processes. Chemical Engineering Transactions. 2017;61:643-8.

[135] Khan MS, Karimi IA, Lee M. Evolution and optimization of the dual mixed refrigerant process of natural gas liquefaction. Applied Thermal Engineering. 2016;96:320-9.

[136] You W, Park J, Jung S, Lim Y. Risk and efficiency analysis of dual mixed refrigerant liquefaction process configurations for floating liquefied natural gas at conceptual design stage. Process Safety Progress. 2018 (In press).

[137] Vikse M, Watson H, Gundersen T, Barton PJP. Simulation of Dual Mixed Refrigerant Natural Gas Liquefaction Processes Using a Nonsmooth Framework. Processes. 2018;6(10):193.

[138] Hwang J-H, Ku N-K, Roh M-I, Lee K-Y. Optimal Design of Liquefaction Cycles of Liquefied Natural Gas Floating, Production, Storage, and Offloading Unit Considering Optimal Synthesis. Industrial & Engineering Chemistry Research. 2013;52(15):5341-56.

[139] Martin P-Y, Pigourier J, Boutelant P. An Innovative Process to Reduce LNG Costs. Proceedings of 22nd World Gas Conference. Tokyo, Japan: International Gas Union (IGU); 2003.

[140] Austbø B, Gundersen T. Using Thermodynamic Insight in the Optimization of LNG Processes. Computer Aided Chemical Engineering. 2014;33:1273-8.

[141] Finlayson BA. Introduction to Chemical Engineering Computing. Hoboken, USA: John Wiley & Sons, Inc.; 2012.

[142] Meek HJ, Cariou H, Schier M. SS: Offshore Floating LNG - LNG FPSO Development - bringing two industries together. Proceedings of Offshore Technology Conference (OTC) 2009. Houston, USA: Offshore Technology Conference (OTC); 2009.

[143] Foglietta JH. Production of LNG using Dual Independent Expander Refrigeration Cycles. Proceedings of AIChE Spring National Meeting. New Orleans, USA: American Institute of Chemical Engineers (AIChE); 2002.

[144] Maråk KA, Neeraas BO. Comparison of Expander Processes for Natural Gas Liquefaction. Proceedings of the 16th International Conference & Exhibition on Liquefied Natural Gas (LNG16). Oran, Algeria: Gas Technology Institute (GTI); 2010.

[145] Ransbarger W. A fresh look at LNG process efficiency. LNG Industry. 2007(Spring).

[146] Prah F. REFRIGERANT 410A. Illinois: Refrigeration Service Engineers Society; 2006.

[147] Gadelle D, Simonetti T, Vovard S. A New Liquefaction Process Suitable for Offshore. Proceedings of the 17th International Conference & Exhibition on Liquefied Natural Gas (LNG17). Houston, USA: Gas Technology Institute (GTI); 2013.

[148] Howe B, Skinner G, Maunder T. Dual Expander Methane Cycle Liquefaction Technology Applied to FLNG. Proceedings of Abu Dhabi International Petroleum Exhibition

& Conference (ADIPEC) 2013 Technical Conference. Abu Dhabi: Abu Dhabi International Petroleum Exhibition & Conference (ADIPEC); 2013.

[149] Howe B, Skinner G, Maunder T. Expanding Horizons. LNG Industry: Palladian Publications Ltd.; 2013.

[150] Schmidt WP, Ott CM, Liu YN, Kennington WA. How the Right Technical Choices Lead to Commercial Success. Proceedings of the 16th International Conference & Exhibition on Liquefied Natural Gas (LNG16). Oran, Algeria: Gas Technology Institute (GTI); 2010.

[151] Yang M-H, Yeh R-H. Performance and exergy destruction analyses of optimal subcooling for vapor-compression refrigeration systems. International Journal of Heat and Mass Transfer. 2015;87:1-10.

[152] Jensen JB, Skogestad S. Optimal operation of simple refrigeration cycles: Part I: Degrees of freedom and optimality of sub-cooling. Computers & Chemical Engineering. 2007;31(5–6):712-21.

[153] Jensen JB, Skogestad S. Single-cycle mixed-fluid LNG process Part I: Optimal design. Proceedings of the 1st Annual Gas Processing Symposium. Amsterdam, Netherlands: Elsevier; 2009.

[154] Mortazavi A, Alabdulkarem A, Hwang Y, Radermacher R. Development of a robust refrigerant mixture for liquefaction of highly uncertain natural gas compositions. Energy. 2016;113:1042-50.

[155] Chang H-M, Chung MJ, Lee S, Choe KH. An efficient multi-stage Brayton–JT cycle for liquefaction of natural gas. Cryogenics. 2011;51(6):278-86.

[156] Bosma P, Klein Nagelvoort R. Liquefaction Technology Developments through History. Proceedings of the 1st Annual Gas Processing Symposium. Amsterdam, Netherlands: Elsevier; 2009.

[157] Migliore C, Tubilleja C, Vesovic V. Weathering prediction model for stored liquefied natural gas (LNG). Journal of Natural Gas Science and Engineering. 2015;26:570-80.

[158] Romero Gómez J, Romero Gómez M, Lopez Bernal J, Baaliña Insua A. Analysis and efficiency enhancement of a boil-off gas reliquefaction system with cascade cycle on board LNG carriers. Energy Conversion and Management. 2015;94:261-74.

[159] Miana M, Legorburo R, Díez D, Hwang YH. Calculation of Boil-Off Rate of Liquefied Natural Gas in Mark III tanks of ship carriers by numerical analysis. Applied Thermal Engineering. 2016;93:279-96.

[160] Turbo MD. ME-GI Dual Fuel MAN B&W Engines A Technical, Operational and Cost-effective Solution for Ships Fuelled by Gas. MAN Diesel & Turbo; 2014.

[161] WinGD. Application of WinGD X-DF engines for LNG fuelled vessels. WinGD; 2017.

[162] Cryostar. The Cryostar Magazine. 2008.

[163] Melaaen E. Gas Supply System for Gas Engines. U.S. Patent No. 2011/0146341 A1; 2011.

[164] TGE Marine Gas Engineering. Efficient, Low Cost LNG BOG Handling by Integration of Cascade Liquefaction and Laby-GI Fuel Gas Compressor for Compressor for ME-GI Propulsion System. TGE Marine Gas Engineering. Online accessed: 12.12.2018, http://

www.tge-marine.com/files/bog_cascade_reliquefaction_tge_bca_internet.pdf.

[165] Maytal B-Z, Pfotenhauer JM. Miniature Joule-Thomson Cryocooling. USA: Springer New York; 2013.

[166] Barclay M, Yang CC. Offshore LNG: The Perfect Starting Point for the 2-Phase Expander? Proceedings of Offshore Technology Conference (OTC) 2006. Houston, Texas, USA: Offshore Technology Conference (OTC); 2006.

[167] Kavalov B, Petric H, Georgakaki A. Liquefied Natural Gas for Europe - Some Important Issues for Consideration. EUR – Scientific and Technical Research series. Luxembourg: Office for Official Publications of the European Communities; 2009.

[168] Shin Y, Lee YP. Design of a boil-off natural gas reliquefaction control system for LNG carriers. Applied Energy. 2009;86(1):37-44.

[169] Dobrota Ð, Lalić B, Komar I. Problem of boil-off in LNG supply chain. Transactions on maritime science. 2013;2(02):91-100.

[170] Wärtsilä. WÄRTSILÄ 34DF PRODUCT GUIDE. Wärtsilä; 2017. Online accessed: 12.12.2018, https://www.wartsila.com/products/marine-oil-gas/engines-generating-sets/dual-fuel-engines/wartsila-34df.

[171] U.S. Energy Information Administration (EIA). Natural Gas. U.S. Energy Information Administration (EIA); 2018. Online accessed: 12.12.2018, https://www.eia.gov/dnav/ng/

ng_move_expc_s1_a.htm.

[172] Shin Y, Kim JW, Lee H, Hwang C. Sloshing Impact of LNG Cargoes In Membrane Containment Systems In the Partially Filled Condition. Proceedings of the 13th International Offshore and Polar Engineering Conference (ISOPE 2003). Honolulu, USA: International Society of Offshore and Polar Engineers (ISOPE); 2003.

[173] Wang K, Sun J, Song P. Experimental study of cryogenic liquid turbine expander with closed-loop liquefied nitrogen system. Cryogenics. 2015;67:4-14.

[174] Kaupert K, Hays L, Gandhi S, Kaehler C. Flashing Liquid Expanders for LNG Liquefaction Trains. Proceedings of the 17th International Conference & Exhibition on Liquefied Natural Gas (LNG17). Houston, USA: Gas Technology Institute (GTI); 2013.

[175] Marini F, Walczak B. Particle swarm optimization (PSO). A tutorial. Chemometrics and Intelligent Laboratory Systems. 2015;149:153-65.

[176] Rios LM, Sahinidis NV. Derivative-free optimization: a review of algorithms and comparison of software implementations. Journal of Global Optimization. 2013;56(3):1247-93.

[177] Lior N, Zhang N. Energy, exergy, and Second Law performance criteria. Energy. 2007;32(4):281-96.

[178] Rosen MA, Dincer I, Kanoglu M. Role of exergy in increasing efficiency and sustainability and reducing environmental impact. Energy Policy. 2008;36(1):128-37.

[179] Romero Gómez M, Ferreiro Garcia R, Romero Gómez J, Carbia Carril J. Review of thermal cycles exploiting the exergy of liquefied natural gas in the regasification process. Renewable and Sustainable Energy Reviews. 2014;38:781-95.

[180] Kanoğlu M, Çengel YA, Dinçer İ. Efficiency evaluation of energy systems: Springer Science & Business Media; 2012.

[181] Ghannadzadeh A, Thery-Hetreux R, Baudouin O, Baudet P, Floquet P, Joulia X. General methodology for exergy balance in ProSimPlus® process simulator. Energy. 2012;44(1):38-59.

[182] Tsatsaronis G. Thermoeconomic analysis and optimization of energy systems. Progress in Energy and Combustion Science. 1993;19(3):227-57.

[183] Kotas TJ. The Exergy Method of Thermal Plant Analysis. 3rd ed. London, UK: Exergon Publishing Company with Paragon Publishing; 2012.

[184] Morris DR, Steward FR. Exergy analysis of a chemical metallurgical process. Metallurgical Transactions B. 1984;15(4):645-54.

[185] Bejan A, Tsatsaronis G, Moran M. Thermal Design and Optimization. New York, USA: John Wiley & Sons, Inc.; 1995.

[186] Lazzaretto A, Tsatsaronis G. SPECO: A systematic and general methodology for calculating efficiencies and costs in thermal systems. Energy. 2006;31(8–9):1257-89.

[187] Brodyansky VM, Sorin MV, Goff PL. The Efficiency of Industrial Processes: Exergy Analysis and Optimization. Amsterdam, Netherlands: Elsevier; 1994.

[188] Kotas TJ. The exergy method of thermal plant analysis. London: Butterworths, 1985.

[189] Cornelissen RL. Thermodynamics and sustainable development; the use of exergy analysis and the reduction of irreversibility. Enschede, Netherlands: Universiteit Twente; 1997.

[190] Voldsund M, Nguyen T-V, Elmegaard B, Ertesvåg IS, Kjelstrup S. Thermodynamic Performance Indicators for Offshore Oil and Gas Processing: Application to Four North Sea Facilities. Oil and Gas Facilities. 2014;3(06):51-63.

[191] Zanchini E. A more general exergy function and its application to the definition of exergy efficiency. Energy. 2015;87:352-60.

[192] Ghorbani B, Hamedi M-H, Amidpour M, Shirmohammadi R. Implementing absorption refrigeration cycle in lieu of DMR and C3MR cycles in the integrated NGL, LNG and NRU unit. International Journal of Refrigeration. 2017;77:20-38.

[193] Qyyum MA, Ali W, Long NVD, Khan MS, Lee M. Energy efficiency enhancement of a single mixed refrigerant LNG process using a novel hydraulic turbine. Energy. 2018;144:968-76.

[194] Marmolejo Correa D, Gundersen T. A new efficiency parameter for exergy analysis in low temperature processes. International Journal of Exergy. 2015;17(2):135-70.

[195] Szargut J. International progress in second law analysis. Energy. 1980;5(8):709-18.

[196] Sato N. Chemical Energy and Exergy. Amsterdam, Netherlands: Elsevier Science B.V.; 2004.

[197] Szargut J. Chemical exergies of the elements. Applied Energy. 1989;32(4):269-86.

[198] Wang M, Zhang J, Xu Q. A novel conceptual design by integrating NGL recovery and LNG regasification processes for maximum energy savings. AIChE Journal. 2013;59(12):4673-85.

[199] Patel D, Mak J, Rivera D, Angtuaco J. LNG vaporizer selection based on site ambient conditions. Proceedings of the 17th International Conference & Exhibition on Liquefied Natural Gas (LNG17). Houston, USA: Gas Technology Institute (GTI); 2013.

[200] van der Ham LV, Kjelstrup S. Exergy analysis of two cryogenic air separation processes. Energy. 2010;35(12):4731-9.

[201] Kerry FG. Industrial gas handbook: gas separation and purification: CRC Press; 2007.

[202] Jieyu Z, Yanzhong L, Guangpeng L, Biao S. Simulation of a Novel Single-column Cryogenic Air Separation Process Using LNG Cold Energy. Physics Procedia. 2015;67:116-22.

[203] Mehrpooya M, Moftakhari Sharifzadeh MM, Rosen MA. Optimum design and exergy analysis of a novel cryogenic air separation process with LNG (liquefied natural gas) cold energy utilization. Energy. 2015;90:2047-69.

[204] Fu C, Gundersen T. Recuperative vapor recompression heat pumps in cryogenic air separation processes. Energy. 2013;59:708-18.

[205] Agrawal R, Herron DM. Air Liquefaction: Distillation. Encyclopedia of Separation Science. Oxford, UK: Academic Press; 2000.

[206] Higginbotham P, White V, Fogash K, Guvelioglu G. Oxygen supply for oxyfuel CO_2 capture. International Journal of Greenhouse Gas Control. 2011;5(Supplement 1):S194-S203.

[207] Campbell RE, Wilkinson JD, Hudson HM. Hydrocarbon Gas Processing. U.S. Patent No. 5,568,737; 1994.

[208] Campbell RE, Wilkinson JD. Hydrocarbon Gas Processing. U.S. Patent No. 4,278,457; 1981.

[209] Bucklin RW. Method and Equipment for Treating Hydrocarbon Gases for Pressure Reduction and Condensate Recovery. U.S. Patent No. 3,292,380; 1966.

[210] Uwitonze H, Lee I, Hwang KS. Alternatives of integrated processes for coproduction of LNG and NGLs recovery. Chemical Engineering and Processing: Process Intensification. 2016;107:157-67.

[211] Mehrpooya M, Hossieni M, Vatani A. Novel LNG-Based Integrated Process Configuration Alternatives for Coproduction of LNG and NGL. Industrial & Engineering Chemistry Research. 2014;53(45):17705-21.

[212] He T, Ju Y. Design and optimization of a novel mixed refrigerant cycle integrated with NGL recovery process for small-scale LNG plant. Industrial and Engineering Chemistry Research. 2014;53(13):5545-53.

[213] Vatani A, Mehrpooya M, Tirandazi B. A novel process configuration for co-production of NGL and LNG with low energy requirement. Chemical Engineering and Processing: Process Intensification. 2013;63(0):16-24.

[214] Kim S, Nam K, Byun WY. Selection Study on Natural Gas Liquid Extraction Processes in Offshore Plants. Proceedings of the 24th International Ocean and Polar Engineering Conference (ISOPE 2014). Busan, Korea: International Society of Offshore and Polar Engineers (ISOPE); 2014.

[215] Yoon S, Binns M, Park S, Kim J-K. Development of energy-efficient processes for natural gas liquids recovery. Energy. 2017;128:768-75.

[216] Mehrpooya M, Vatani A, Ali Mousavian SM. Introducing a novel integrated NGL recovery process configuration (with a self-refrigeration system (open–closed cycle)) with minimum energy requirement. Chemical Engineering and Processing: Process Intensification. 2010;49(4):376-88.

[217] Mak J. Configurations and Methods for Offshore NGL Recovery. U.S. Patent No. 20140060114 A1; 2014.

[218] Chen F, Ott CM. Lean Gas. LNG Industry. 2013(Jan/Feb).

[219] Ghorbani B, Shirmohammadi R, Mehrpooya M. A novel energy efficient LNG/NGL recovery process using absorption and mixed refrigerant refrigeration cycles – Economic and exergy analyses. Applied Thermal Engineering. 2018;132:283-95.

[220] Ghorbani B, Salehi GR, Ghaemmaleki H, Amidpour M, Hamedi MH. Simulation and optimization of refrigeration cycle in NGL recovery plants with exergy-pinch analysis. Journal of Natural Gas Science and Engineering. 2012;7:35-43.

[221] Svalheim S, King DC. Life of Field Energy Performance. Proceedings of Offshore Europe 2003. Aberdeen, UK: Society of Petroleum Engineers (SPE); 2003.